RETROFIT STRATEGY OF NON-SEISMICALLY DESIGNED FRAME SYSTEMS BASED ON A METALLIC HAUNCH SYSTEM

A Thesis
Submitted in Partial Fulfillment
of
the Requirements for the Degree
of
Master in Civil Engineering
at the
University of Canterbury
Christchurch
New Zealand

by

Te-Hsiu Chen

Supervisor
Dr. Stefano Pampanin
University of Canterbury

Co-Supervisor
Dr. Constantin Christopoulos
University of Toronto

2006

ABSTRACT

Due to the lack of capacity design principles as well as of appropriate structural details, most of the reinforced concrete building designed primarily for gravity loads as typical of pre-1970s code provisions, are expected and has been demonstrate to suffer sever damage or total collapse under the earthquake excitation. Due to the use of plain round bar and inadequate reinforcing details, critical shear failure in the joint connection region could occur, leading to sever damage when not total collapse of the building.

In this research project, a comprehensive experimental programme was carried to investigate the seismic performance of existing beam column joints prior and after retrofit intervention with a recently proposed low-invasive retrofit technique based on a metallic haunch system. The joint performance was evaluated in terms of the principal tensile stresses that caused the joint shear cracks in the joint panel zone. Quasi-static cyclic tests under uni-directional or bi-direction loading regime were carried out to record the response of a series of under-designed beam column joints (with either a wide-beam or a deep-beam solution, deformed or plain round bars with end hooks). The experimental results were used to investigate the effect of structural detailing and loading regime on the seismic performance.

To retrofit the potential deficiencies in the existing beam-column joints, the feasibility and efficiency of a low invasive retrofit solution based on a diagonal metallic haunch was investigated. The proposed haunch retrofit solution aims to provides an economic, ease of implementation alternative to protect the joint from the brittle shear failure by relocating the beam plastic hinge away form the joint panel zone. To achieve the desired capacity design (hierarchy of strength) and sequence of event, a simplified analytical formulation has been adopted to account for the joint shear strength in terms of principle tensile/compression stresses prior and after the retrofit intervention. A useful visualization tool based on a M-N (moment-axial load) performance domain can be adopted to evaluate the actual performance point and events, by comparing demand vs. capacity.

Designed charts are proposed based on displacement compatibility conditions to evaluate the efficiency of the haunch solution. In addition, a complete step-by step design procedure to implement the retrofit strategy and intervention to achieve the desired hierarchy of strength, by using the proposed diagonal metallic haunch solution, is derived and presented.

The effectiveness of the proposed haunch solution and reliability of the derived analytical design/assessment procedure, were validated through experimental tests of 2-D and 3-D subassemblies, shown in the first experimental part to have the most vulnerable behaviour in the joint panel zone. Conceptual issues related to the design of the retrofit intervention, when moving from a 2-D to a 3-D behaviour are discussed.

The experimental results showed an excellent performance of the proposed intervention, able to protect the panel zone region (by limiting the principle tensile stress demand), while enforcing the formation of a plastic hinge in the beam, far away from the joint interface. As a result, a much more stable inelastic response could be developed, confirming the high potential of such a low-invasive, low-cost retrofit intervention on under-designed frame systems.

In conclusion, a simple numerical model, based on a lumped plasticity approach, was developed and validated on the experimental results to capture the full response of the subassembly prior and after the retrofit intervention.

ACKNOWLEDGEMENTS

This research was reported in the Department of Civil Engineering, University of Canterbury, New Zealand. The researcher would like to give the thanks to the following people.

I wish to express my heartfelt emotion to my supervisors, Dr. Stefano Pampanin, University of Canterbury and Dr. Constantin Christopoulos, University of Toronto for their inspiration, guidance and enthusiasm.

I am thankful to Dr. James Mackechnie for his interest and advice.

Thanks are extended to Gary Harvey for his help with the experimental program.

Thanks are also given to my friends Eric Hertanto and Cong Liu for their friendship and discussions.

Also thanks to the technical support in the laboratory.

Special thanks to my parents and parents-in-law, for their unwavering support in spirit and livelihood.

TABLE OF CONTENTS

NOTATION

ε_s =strain of steel

v =poisons ratio of steel

Φ_i =safety factor or strength reduction factor

α =design angle between haunch and beam

α_{u1}, α_{u2} = unloading coefficient of Pampanin hysteresis rule of joint

α_{r1}, α_{r2}, = reloading coefficient of Pampanin hysteresis rule of joint

α_h =geometry coefficient for varying column axial load

β =shear transferring factor for the beam

β' =shear transferring factor for the column

θ_{beam} =total inter-storey drift caused by beam deformation

θ_{column}=total inter-storey drift caused by column deformation

θ_{joint} =total inter-storey drift caused by joint deformation

$\delta_{b,fle}$ =displacement caused by beam flexural deformation

$\delta_{b,rot}$ =displacement caused by beam fix-end rotation

$\delta_{bh,rot}$ =displacement caused by rotation of plastic hinge in the beam

$\delta_{c,fle}$ =displacement caused by column flexural deformation

$\delta_{c,rot}$ =displacement caused by column fix-end rotation

Δ_{beam} =displacement of column top caused by beam deformation

Δ_{column} =displacement of column top caused by column deformation

Δ_{end} =displacement of beam end caused by beam deformation

Δ_{tot} =total displacement of column top

Δ_g =deformation of grout

Δ_g =deformation of steel bar

Δ_{joint} =displacement of column top caused by joint deformation

A_b =section area of beam

A_c =section area of column

A_e =effective area of joint

A_{eh} =effective section area of haunch

A_g =gross area of joint

D_b =diameter of longitudinal bar

D_{bar} =diameter of haunch bar

D_{tube} =inside diameter ob tube

E_g =Young's modulus of grout

E_s =Young's modulus of steel

F_y =equivalent lateral force to M_y

FY_y = equivalent lateral force to MY_y

FY_z = equivalent lateral force to MY_z

F_z = equivalent lateral force to M_z

H_c =storey height between centrelines or column height

H_n =clear storey height between beam faces or column height of beam depth excluded

I_b =second moment inertia of beam

I_c =second moment inertia of column

K_d =design haunch stiffness

K_j =joint stiffness

K_{u1}, K_{u2} = unloading stiffness of Pampanin hysteresis rule of joint

K_{r1}, K_{r2} = reloading stiffness of Pampanin hysteresis rule of joint

L' =design haunch position measured from the column face

L_b =beam span length between centrelines

L_n =clear beam span length between column faces

M_{bc} =equivalent joint moment from beam

M_{bc}^* =equivalent joint moment from beam to cause joint failure or joint moment capacity

$M_{b(max)}$ =maximum bending moment in the beam

$M_{c(max)}$ =maximum bending moment in the column

M_{cb} =equivalent joint moment from column

M_y =interaction moment capacity of X-axis on failure surface

MY_y =moment capacity of principal X-axis

MY_z = moment capacity of principal Z-axis

M_z = interaction moment capacity of Z-axis on failure surface

N =column axial load

N_g =column axial force from design dead load

$P_{critical}$ =critical axial stress of haunch

P_g =normal pressure in the grout

P_s =normal pressure in the steel bar

V_b =shear force in the beam

V_c =inter-storey shear force in the column

V_{hx} =haunch-induced horizontal shear force in the column

V_{jh} =nominal horizontal shear force in the joint core

$\overline{V}_b$ =shear strength of beam

$\overline{V}_c$ =shear strength of column

$\overline{V}_{c,beam-hinge}$ = inter-storey shear force to cause beam flexural failure

$\overline{V}_{c,beam-shear}$ = inter-storey shear force to cause beam shear failure

$\overline{V}_{c,column-hinge}$ = inter-storey shear force to cause column flexural failure

$\overline{V}_{c,column-shear}$ = inter-storey shear force to cause column shear failure

$\overline{V}_{c,joint}$ =inter-storey shear force to cause joint failure

$\overline{M}_{by}$ =beam moment capacity

$\overline{M}_{cy}$ =column moment capacity

b_c =column width

b_j =effective joint width

b_w =beam width

d_b =beam depth

f_a =nominal vertical stress in the column and joint

f_{bu} =ultimate bond strength between concrete and steel bars

f_c' =compressive strength of concrete

f_g' =compressive strength of grout

f_{cu} =ultimate compressive strength of concrete

h_c, d_c =column depth

jd_b = lever arm between centres of compression and tension in the beam

k = coefficient for principal tensile stress

p_t =principal tensile stress

v_{jh} =nominal horizontal shear stress in the joint core

CHAPTER 1

INTRODUCTION

1.1 THE NEED FOR RETROFITTING

With great advance in understanding the post-elastic behaviour of structures, seismic design procedures for concrete structures have significantly developed since the 1970s around the world. Before the introduction of the capacity design philosophy in the 1970s, the as-built concrete structures in earthquake prone hazards designed with non-seismic oriented code may be deficient to resist the major earthquakes. The seismic vulnerability of these existing reinforced buildings designed with out-dated code has received attention after the catastrophic effects of recent earthquake events and a number of research program on retrofitting strategy have been carried out to improve the seismic performance of existing buildings.

The 1985 Mexico earthquake and recent Californian earthquake (the 1987 Whittier Narrows, the 1989 Loma Prieta and the 1994 Northridge) caused the serious damage and/or collapse of the existing reinforced concrete structures [Hakuto, 1995]. Many of these buildings that were designed for gravity-loads-only in pre-1970 without adequate reinforcing details did not have satisfactory performance under large earthquake. During the 1985 Mexico earthquake with unique ground motions, there were about 210 existing reinforced concrete buildings collapsed among 2300 damaged structures in Mexico city (Fig. 1.1) and thousands of lives were lost [Liu, 2001]. In the 1995 Hyogo-ken Nanbu Earthquake in Kobe city, the existing reinforced concrete buildings built before 1970 suffered much more sever damage than the buildings built after 1981 when the most recent Japanese seismic code was introduced (Table 1.1). The earthquake caused the minor or no damage to the most of reinforced concrete buildings built after 1981 [Okada, 1997].

Typically buildings designed for gravity-loads-only, before introduction of seismic-oriented design codes in the 1970s, suffered serious damage during sever earthquake (Fig. 1.2). Recent experimental and analytical investigation on the seismic performance of existing reinforced concrete building, designed for gravity loads only confirmed the expected inherent weaknesses of reinforced concrete beam-column connection. Because of the absence of capacity design philosophy and the use of plain round reinforcing bars, peculiar brittle failure

mechanisms were observed with low ductility capacity. The local damage of beam-column joint panel zones, through particularly brittle shear failure mechanisms, greatly impaired the overall structural performance of RC frame at the global level.

Therefore, several retrofit techniques to improve the seismic performance of existing structures have been developed and experimentally validated. To avoid devastating damage to vulnerable existing buildings, basically conventional retrofit scheme such as installation of new shear walls or steel framed braces into existing frames, and jacketing of existing columns with steel profiles have been applied. Further research of retrofit strategy is emphasized on developing more economic measures based on effectiveness and ease of installation.

Fig. 1.1 Collapse of the building during the 1985 Mexico earthquake

Fig. 1.2 Damage to corner joints of the existing structure (Izmit, Turkey earthquake 1999)

Table 1.1: Damage grade versus constructions years of reinforced concrete buildings in a part of Kobe City [Okada, 1997]

	Pre-1971	1971-1981	Post 1981
Collapse or Severe Damage	22(24%)	5 (5%)	3 (6%)
Medium Damage	8 (9%)	4 (4%)	2 (4%)
Minor Damage	12 (13%)	12 (13%)	6 (13%)
No Damage	51 (55%)	73 (77%)	34 (76%)
Total	93 (100%)	94 (100%)	45 (100%)

Since the column axial loads influence the bond performance of reinforcing bars, particularly in the plain bars, passing through the joint cores, the joint shear strengths will be significantly affected by the variation of the axial loads during earthquakes. Due to the limited information considering the variation of the column axial load in the previous beam-column joint tests, it could be dangerous in assessing the joint shear failure. Hence, it is important to take the worst condition of the joint core into account while applying the retrofitting strategies.

1.2 BACKGROUND OF THE RESEARCH PROJECT

Due to limited information on the vulnerability of existing reinforced concrete building, several research programs have been carried out at the University of Canterbury to investigate the cyclic loading behaviour of reinforced concrete components that would dominate the post-elastic seismic behaviour of the whole structure. As a result of the absence in capacity design philosophy and poor reinforcing detail, the joint shear failure were observed in the beam-column subassemblies designed prior to the 1970s in previous experimental tests. The experiments (Fig. 1.3) that were carried out at the University of Pavia on testing existing reinforced concrete frame designed before the introduction of seismic-oriented codes in the mid-1970 also revealed the deficiency of the brittle joint shear mechanism with respect of low ductility and inadequate strength degradation [Pampanin, Calvi and Moratti, 2002]. Following the previous study on existing beam-column joint subassemblies, more experimental investigation on the behaviour of the typical joints designed before 1970 in New Zealand were involved with interest.

Most of the previous tests on existing beam-column subassembly are based on using the deformed bars for longitudinal reinforcement; however, the plain round bars were still used in New Zealand until the deformed bars were generally available in the mid 1960s. According to

the research results, the bond strength of plain round bars developed between the reinforcement and concrete material is low compared with deformed reinforcement [Wilby, 1991]. As a result, the out-dated code on the basis of assumption of perfect bond strength between the longitudinal reinforcement and the surrounding concrete would lead to incorrect design in flexural and shear strength and affect the seismic performance. Therefore, the complete investigation and comparison on the beam-column joint behaviour by using the different types of reinforcement could provide useful information to assessing the seismic behaviour of existing buildings.

Since floor-to-ceiling heights are restricted and formwork economy is intended, shallow beam-column connections are often found in one-way concrete joist systems. To achieve the required flexural strength, the beams must be wider than their supporting columns and may be three times as wide as they are deep. Due to the beam bars anchored outside of the column core, stress of the longitudinal reinforcement in the beam can not be complete transferred to the column because of either losing bond stress or failing to transmit the induced stress of the outside beam element into the column core. Thus, the formation of an incomplete beam plastic hinge will result in the smaller flexural strength than the designer intended [Gentry and Wight, 1994]. Considering the effective joint area of wide beam-column joint, information in terms of joint principal tensile stress is required to assess the joint shear mechanism of the existing joint subassembly with the shallow beam.

Since the earthquake loadings, in reality, come from not only single direction, the two-way frame system with the spandrel beam is generally observed in the real structure while the general response of the structure under earthquake excitation is displayed in Fig. 1.4. From the small amount of the previous tests, the joint shear strength suggested to be higher for the corner joint of 3-D than exterior joint of 2-D by using deformed reinforcement only. However, the lack of information on the corner joint capacity with plain round bars that were generally used in pre-1970s may lead to incorrect seismic assessment of the as-built two-way structures. The interaction of the joint capacities in orthogonal directions is also expected since the joint shear stress in one direction will affect the stress capacity in the other direction. Hence, the as-built corner joint is designed to investigate the joint capacity interaction.

In addition, with lack of consideration in structural geometry, the zero or constant axial column loads were applied in the previous beam-column joint tests. Actually, the varying

axial load induced with the respect of structural geometry significantly influenced the column capacity and the joint seismic performance. Especially in using plain round bars, the presence of the compressive axial column load could increase the bond strength within the joint core and the introduced larger horizontal shear force may accelerate the joint shear failure [Liu, 2001]. Therefore, it is necessary to involve the real situation of column axial load in investigating the existing joint behaviour.

Following the investigation of retrofit schemes in protecting the welded connection of steel frames [Gross, Engelhardt, Uang, Kasai, and Iwankiw, 1999] and [Christopoulos and Filiatrault, 2000], a non-invasive retrofit solution shown as Fig. 1.5 for existing R.C. frame systems has been recently proposed by Pampanin and Christopoulos to protect the beam-column joint region from the brittle joint shear failure by relocating a plastic hinge in the beam [Pampanin and Christopoulos, 2003]. The main concept was based on appropriate capacity design to redistribute the stress flow that passed through the weak joint panel zone to the beam and migrate the plastic hinge some distance away form the face of the column in the beam. Recent analytical investigation numerically demonstrated the effectiveness of haunch retrofitting strategy by increasing the strength and ductility of local behaviour and improving the global seismic performance of the retrofitted frame system, particularly the avoidance of soft-storey mechanism. Although the haunch solution could provide a practical retrofit strategy of cost effective scheme and simple implementation, a reliable design procedure for R.C. frame system and further experimental validations of the proposed retrofit technique applied on the R.C. beam-column joints are needed to confirm the results from the numerical study.

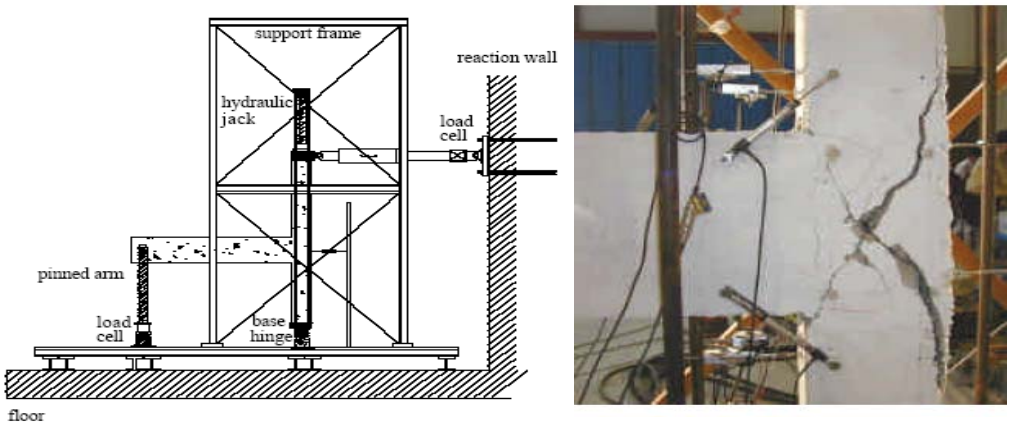

Fig. 1.3 Test set-up and joint shear failure of as-built subassembly [Pampanin, Calvi and Moratti, 2002]

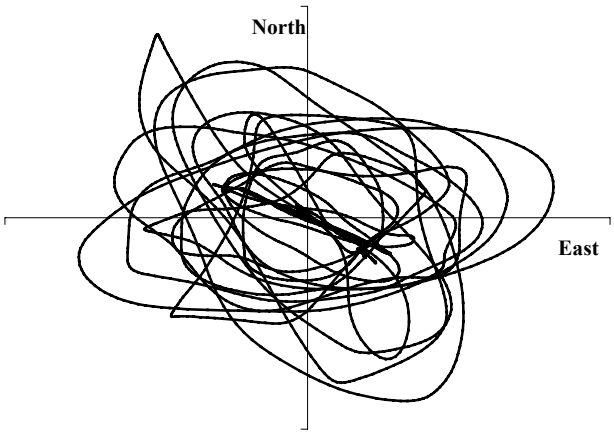

Fig. 1.4 Loading path during earthquake

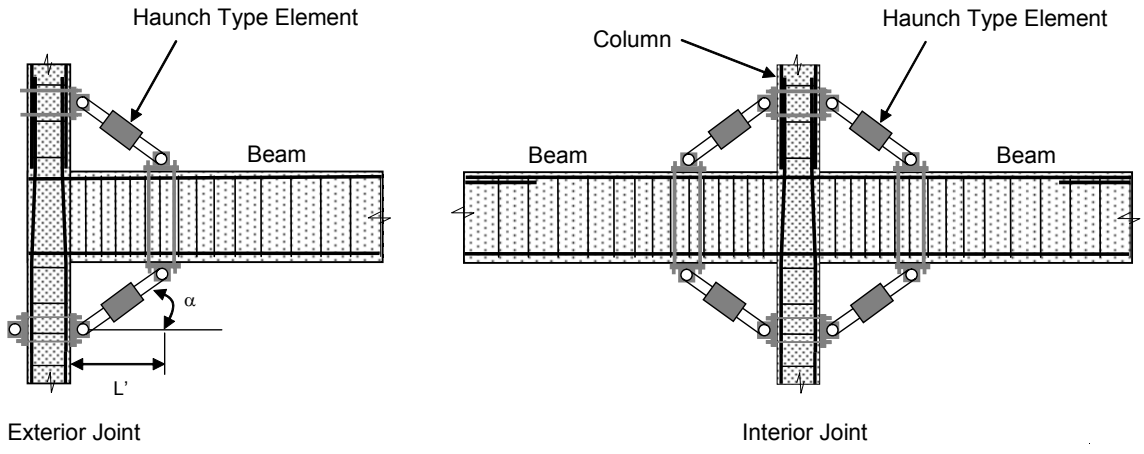

Fig. 1.5 Proposed haunch retrofit configuration for exterior and interior joints [Pampanin and Christopoulos, 2003]

1.3 OBJECTIVE OF THE RESEARCH PROJECT

As the more vulnerable feature of the exterior joint and more stable hysteretic behaviour with hardening after first cracking were observed, the existing beam-column joints of exterior typology are the main issues investigated in this research project. To understand the deficiency of the reinforced concrete structure designed with gravity-loads-only before the introduction of seismic design in New Zealand, several 2/3 scaled exterior beam-column joint subassemblies design in pre-1970s were tested. The experimental results would demonstrate the behaviour of reinforced concrete component with different reinforcing detail such as using plain round bars and deformed bars. By using one transverse reinforcing stirrup only in the

joint core, the effectiveness of joint shear reinforcement would be investigated. Additionally, the beam-column joints of the shallow beams that had the same flexural capacities with the deep beams were also tested to investigate how the longitudinal reinforcement anchored outside the column cores had effect on the joint principal tensile stresses. To investigate the bi-directional loading effect on the exterior beam-column joint, the 2/3 scaled as-built corner subassemblies were constructed for 3-D tests (Fig. 1.6). The behaviour of brittle joint shear mechanism under bi-directional-loading test will be extracted for comparison with the joint behaviour of 2-D tests in terms of principal tensile stress. The influence of using no transverse reinforcement in the corner joint for bi-directional test will be the point of the research. For all tests, emphasis would be placed on the influence of varying column axial load associated with the capacity design philosophy.

By installation of diagonal metallic haunch system into the as-built beam-column joint connection, the brittle shear mechanisms will be prevented in the existing both 2-D and 3-D subassemblies while inverting the hierarchy strength to form beam-hinging mechanism. On the basis of exterior beam-column joint, since it is recognized to have the most vulnerability, the proper design concept of haunch retrofit strategy would be introduced in this research project. In addition, the analytical formulation of internal force flow is developed to demonstrate a complete step-by-step design procedure on the basis of design theory and design charts that, according to the derived formula, could be simply illustrated. To experimental validate the haunch retrofit solution, the 2/3 scaled existing subassembly of the same reinforcing detail that suffers most sever joint shear failure in the previous test are chosen to be retrofitted with different types of haunch. The experimental results of retrofitted beam-column joint would be compared with those obtained in the as-built joint tests and used to evaluate the effectiveness of haunch solutions.

Finally, appropriate numerical models used to predict the seismic behaviour of existing and retrofitted beam-column joints would be established with proper pinching hysteric loop proposed by Pampanin for the under designed joint behaviour. Numerical validation of the experimental result is also the important part of the research project.

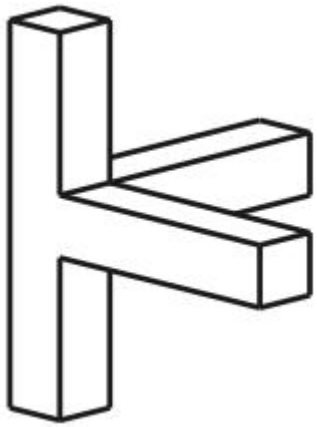

Fig. 1.6 Corner joint in 3-D test

1.4 ORGANIZATION OF THE THESIS

This thesis consists of 9 Chapters and classified into 5 parts including the research work, theory study, as-built test units, retrofitted test units, numerical study and conclusion

The review of the previous research is presented in Chapter 2 that describes the past contribution on the investigation of the as-built subassembly including the consideration of the deep beams, shallow beams and two-way corner joints. This chapter also describes the development of alternative retrofitting strategies.

In Chapter 3, the detail of theoretically accessing the beam-column joint performance is given as well as the introduction of the haunch retrofitting strategy. The step-by-step haunch retrofitting design procedure is also detailed in this chapter.

The part that consists of Chapter 4 and Chapter 5, about as built test units, describes the proposed test scheme in this project and the experimental results respectively. Emphasis is placed on studying the seismic behaviour of the as-built beam-column joint subassemblies and effects of using plain round bars and deformed bars.

Chapter 6 and Chapter 7 present the proposed test scheme and the experimental results respectively for the retrofitted test units. The effectiveness of haunch retrofitting solutions are validated and compared with predicted analysis while the effect of the haunch connections are also discussed in Chapter 7.

The feasible tool for numerical analysis is introduced and the comparisons between the experimental and numerical results, by using suitable model, are presented in Chapter 8.

Finally, the conclusions of this project are given in Chapter 9 while the recommendations on the future work are given as well.

CHAPTER 2

REVIEW OF RESEARCH INTO PRE-1970 R.C. BUILDINGS STRUCTURAL BEHAVIOUR AND RETROFIT STRATEGIES

2.1 INTRODUCTION

Before introducing the seismic design concept in pre-1970s, the reinforced concrete structures were designed for gravity-loads-only with using smooth bars, inadequate detailing of the reinforcement (i.e. total lack of transverse reinforcement in the joint region) and deficiencies in the anchorage (hook-ended bars). Due to the absence of capacity design principles, the weak joint strength caused the joint shear mechanism that had significant damage to the building structure. To understand the concept about capacity design, the basic idea is introduced in this chapter. In addition, according to New Zealand Concrete Structure Standard that was first published in 1982, plain round bars shall not be used for longitudinal (main) non-prestressed reinforcement. Without capacity design principle, however, the use of plain round bar was common before 1970s. The potential deficiencies of using plain round will be investigated in terms of bond strength.

To upgrade the seismic response of pre-1970 R.C. buildings, several strengthening/retrofit solutions have been studied in the past and have been adopted in practical applications, ranging from conventional techniques (i.e. braces, jacketing or infills) to more recent approaches including base isolation, supplemental damping devices or advanced non-metallic materials as Fibre Reinforced Polymers (FRP), or Shape Memory Alloys (SMAs). More understanding into different retrofit solutions will be achieved by reviewing the previous experimental or numerical verification in this chapter. To improve the issues of cost, invasiveness, and the ease of practical implementation, the proposed haunch solution was first numerically verified in the effectiveness of preventing joint shear failure. The numerical analysis that supported the feasible haunch solution will be also presented.

The summaries of the research study at the end of this chapter will be used to preliminarily understand the experimental results of this research and have appropriate comparison.

2.2 CAPACITY DESIGN PHILOSOPHY

Under an earthquake excitation, the structural elements of a building frame would behave in the post-elastic range. By locating the occurrence of such critical plastic regions (Fig. 2.1), the critical mechanisms of the structure could be simply treated as: (a) beam sidesway mechanism, (b) column sidesway mechanism and (c) joint shear sidesway mechanism. The desired beam sidesway mechanism that is also known as strong column-weak beam mechanism of a structure could lead to the appropriate energy dissipating performance without collapse of the structure while suffering the severe imposed deformations. On the other hand, the column sidesway mechanism, as known as soft-storey mechanism, and the joint shear sidesway mechanism would result in catastrophic collapse of the structure. Without consideration of capacity design, the joint brittle shear failure could potentially exist in the buildings designed before 1970s and cause the undesired joint shear sidesway mechanism that has low ductility and serious strength degradation.

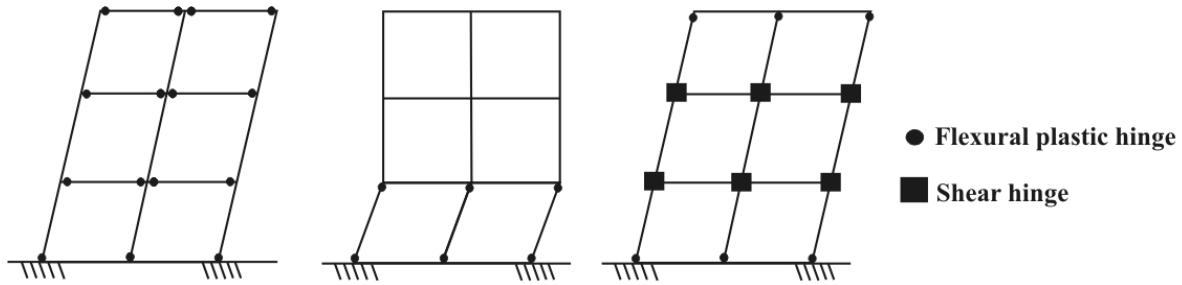

Fig. 2.1 Possible mechanisms of moment resisting frames [Paulay and Priestley, 1992]

For the last 30 years, the principles of capacity design of ductile structure originally introduced in New Zealand [Park and Paulay, 1975] were slowly and successfully adopted in other countries. The design philosophy demonstrates that chosen members of the primary lateral force resisting frames are suitably designed and detailed for energy dissipation at the critical regions under severe imposed deformations. These critical regions of inelastic flexural action could protect all other structural elements against actions that could cause undesired failure mode by providing greater strength in the elements than in the critical regions. The simple concept of capacity design philosophy could be illustrated by the reaction chain shown in Fig. 2.2. By comparing the adjacent brittle link, using the weakest link, a very ductile link that have less strength of involved strain hardening effect, could achieve the adequate ductility for the entire chain with the specified strength. As a result, the ductile failure of the

weakest link would guarantee to protect the other brittle links by concentrating the ductility on the particular ductile link.

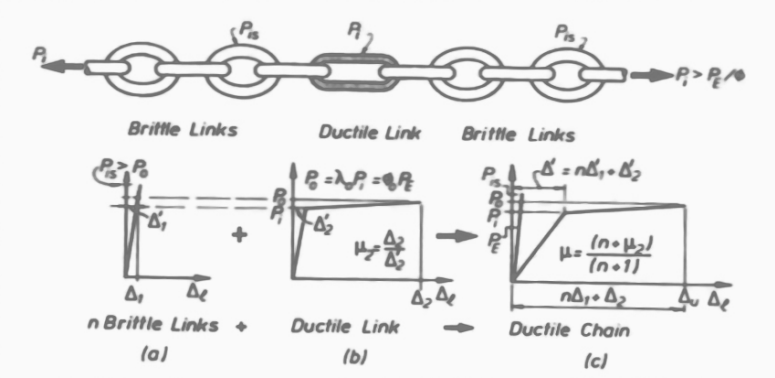

Fig. 2.2 Principle of strength limitation illustrated with ductile chain [Paulay and Priestley, 1992]

2.3 USE OF PLAIN ROUND BARS

As shown in the example of typical reinforcing detail designed in pre-1970s (Fig. 2.3), the plain round bars with hooked end were generally used around the world for the longitudinal reinforcement in the reinforcement concrete structure designed with the old practice. According to the commentary on New Zealand building code of the 1950's (Fig. 2.4), the plain round bars with hooked end could be commonly found in the RC buildings designed in pre-1970's around New Zealand. Due to the low bond strength provided between the plain round steel and the concrete, the bar slippage occurs and causes the development of the premature strength combined with the serious strength degradation and the reduced ductility of the local element. In addition, the concentrated compressive force at the end-hook combined with the bar slippage within the joint region could cause the "concrete wedge" and lead to poor structural performance by brittle joint shear damage [Pampanin 2003c].

Bond stress consists of firstly an adhesive resistance and then a frictional resistance [Wilby 1991]. A pull-out test of a steel rod from a concrete block shows an illustration as Fig. 2.5. The pull force, P is gradually transmitted to the concrete by frictional resistance in the portion of the graph AB. At the point B, the force still in the bar is equal to the adhesive resistance of the remainder of the bar. Therefore, the force in BC is insufficient to overcome the adhesive resistance and is gradually transmitted to the concrete by adhesion. During increasing the load from P to P', the length of the bar slipping is increasing which means the A'B' is the new

frictional stage and B'C' is the new adhesive stage. According to the experimental tests, the design ultimate bond stress f_{bu} is given as:

$$f_{bu} = B\sqrt{f_{cu}} \tag{2.1}$$

where B is the coefficient for the different types of reinforcement as given in Table. 2.1. Compared with deformed bars, it is obvious that the plain round bars provided relatively lower bond stress by smaller values of B. The use of plain round bars, therefore, could lead to the development of the premature strength in the local elements due to the undesired lower bond strength being reached.

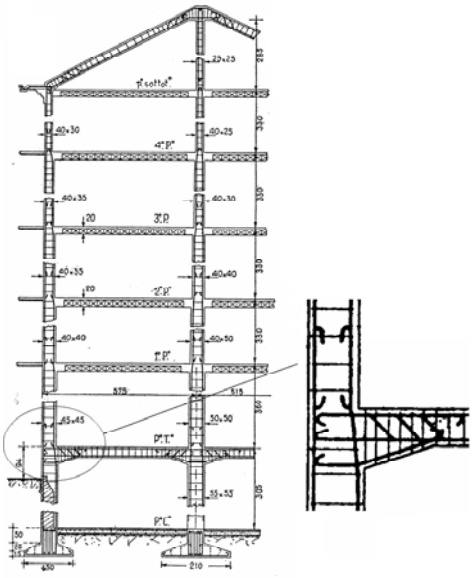

Fig. 2.3 Typical section elevation of a reinforced concrete building designed in Italy in late 1950s [Pampanin, Calvi and Moratti, 2003c]

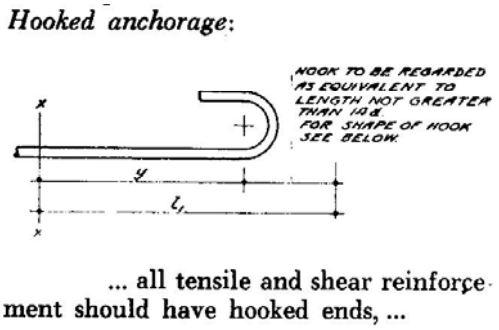

Fig. 2.4 Reinforcement detail from the New Zealand Code of 1950's

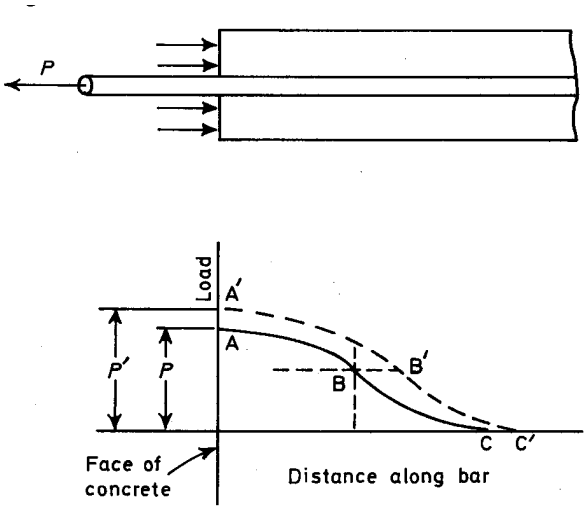

Fig. 2.5 Pull-out test of reinforcing bars [Wilby, 1991]

Table 2.1 Coefficient for the bond strength [Wilby, 1991]

Designation	f_y	B	
		Tension	Compression
Plain hot rolled mild steel	250	0.38	0.35
Square-twisted bars (deformed type1)	460	0.4	0.5
High-yield ribbed bars (deformed type 2)	460	0.5	0.63

2.4 PREVIOUS EXPERIMENTAL RESEARCH ON THE BEHAVIOUR OF EXISTING BEAM-COLUMN JOINTS

2.4.1 Research by Hakuto, 1995

One full-scale beam exterior column joint subassembly with beam bar end anchorages that were bent away the joint core was constructed while the other subassembly was also constructed with the ends of beam bars bent into the joint core. These two specimens, referred to each other, were used to investigate the effect of such different configurations of the end hooks on the performance of the beam-column joint typical of the 1950's reinforced concrete building frames. One stirrup was used in the joint core of each specimen that was corresponding to the lack of joint transverse reinforcement for the as built RC structure while the deformed reinforcing bars were used for the longitudinal reinforcement of both specimens. Fig. 2.6 and Fig. 2.7 show the reinforcing detail and the experimental response for the subassemblies of the bent into and bent away anchorages respectively. Due to insufficient shear reinforcement in the joint core, the shear cracks were observed in the as-built joint regions for both anchorage types. In addition, the result demonstrated that, with anchorage bent away from the joint core, the poor joint performance accompanied with the serious joint strength degradation occurred due to the knock out of the concrete wedge. However, the better performance was observed in the subassembly with anchorage bent into the joint core due to the provided node points for the development of efficient compression strut mechanism.

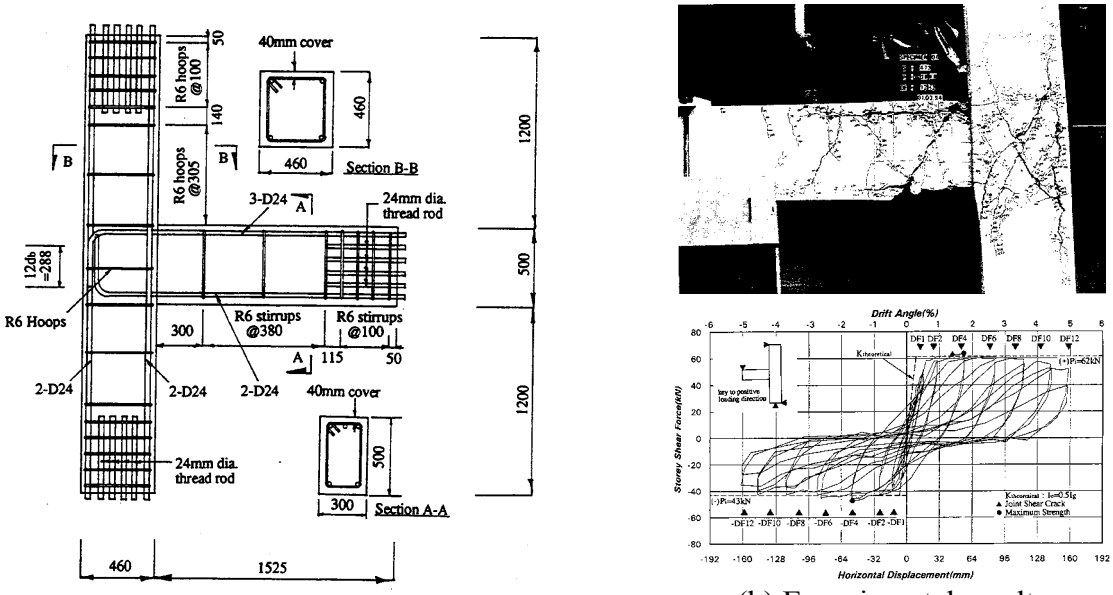

(a) Reinforcing detail (b) Experimental result

Fig. 2.6 Specimen with end hook bent into joint core [Hakuto, 1995]

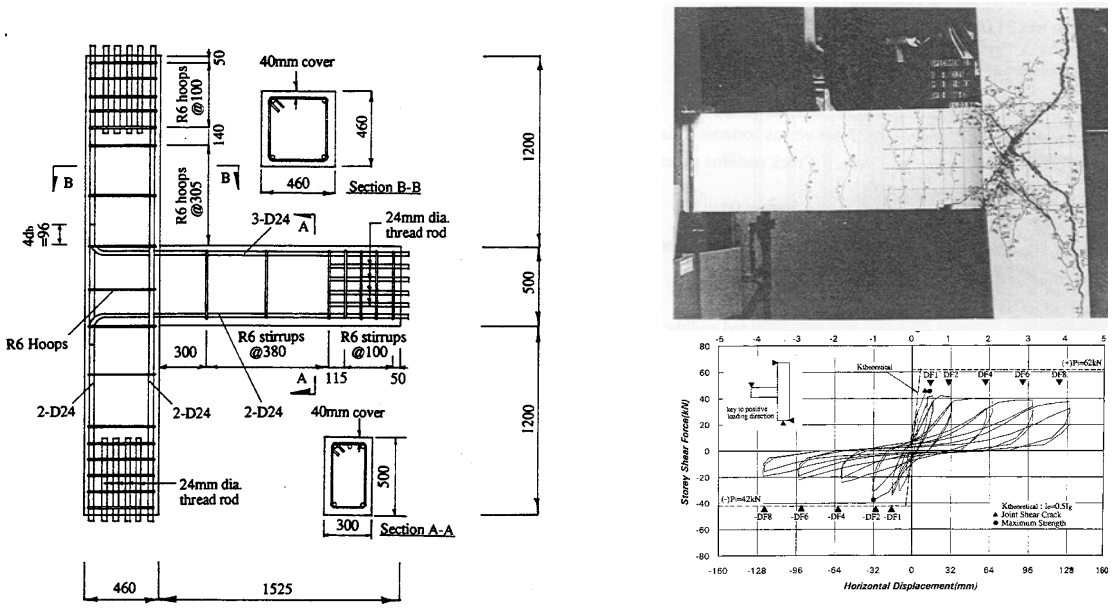

(a) Reinforcing detail (b) Experimental result

Fig. 2.7 Specimen with end hook bent away joint core [Hakuto, 1995]

2.4.2 Research by Pampanin et al. 2002

The experimental test on 2/3 scaled exterior beam-column joints typical in Italy before introduction of seismic oriented codes in the mid-70s was performed at the Laboratory of the Department of Structural Mechanics of the University of Pavia. The smooth bars with end-hook anchorage were used for the beam longitudinal reinforcement while no shear transverse reinforcement was presented in the joint core as shown in Fig. 2.8. Under the quasi-static push-pull loadings, the brittle joint shear mechanism with concrete wedge was observed during the test. Since the inadequate reinforcing detail, the experimental results confirmed that the vulnerability of the joint panel zone underlined the low ductility and sever strength degradation of the as-built joint performance and the marked "pinching" hysteretic behaviour appeared after the first diagonal shear crack in the joint. The principal tensile stress that caused the joint first diagonal crack was proposed to be $p_t = 0.2\sqrt{f_c'}$ for the exterior joint with end hook and smooth bars.

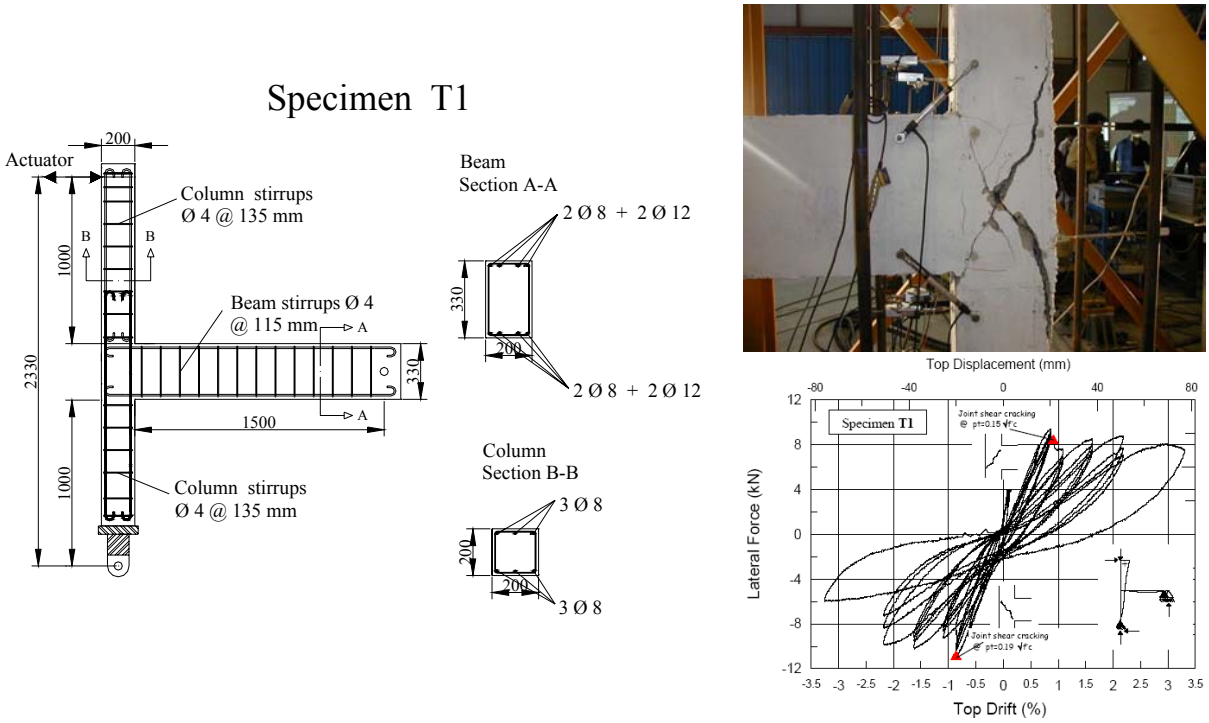

(a) Reinforcing detail (b) Experimental result

Fig. 2.8 The exterior joint specimen using smooth bars [Pampanin, Calvi and Moratti, 2002]

2.4.3 Research by Gentry et al. 1994

Since part of the beam longitudinal reinforcement passes outside of the confined column core in wide beam-column connections, the shear and moment of this part will be transferred through the side face of the column. Under the earthquake excitation, loss of the bond stress of the beam bars anchored outside of the column and thus loss of stiffness may cause the tension of these bars could not be transferred to the column core. This will result in the formation of an incomplete beam plastic hinge with a smaller beam moment strength than the designer intended, which in turn reduces the lateral force required form a collapse mechanism for the concrete frame.

Four 3/4-scale subassemblies were tested to explore the behaviour of exterior wide beam-column connections as shown in Fig. 2.9a and Fig. 2.9b. Depend on the primary variables of the designed configuration, the experimental results were exploited to investigate the effect of (1) the beam width to the column width, (2) fraction of the total longitudinal reinforcement anchored in the column core, (3) the column moment strength to beam moment strength ratio, and (4) the shear stress applied to the joint, on the performance of the wide beam-column connections. The pinching behaviours were observed in all specimens even if the strength did

not decrease with increasing drift level in Specimen 2 and 3. However, the reduced moment strengths of the beams, smaller than the calculated values were observed in Specimen 1 and 4; the loss of strength at the higher drift level coincided with the formation of a wrapping, torsional cracks on the back face of the connection. It was demonstrated that the longitudinal bar anchored outside of the column core became ineffective if the torsional cracks occurred at the rear face of the wide beam and thus the beam lost the stiffness (Fig. 2.10). Since the longitudinal bars that were anchored within the crack surface retained their anchorage and continued to act as par of the plastic hinge, the designed strength of the wide beam could be fully developed if the fraction of the total longitudinal reinforcement anchored outside of the column was appropriate determined.

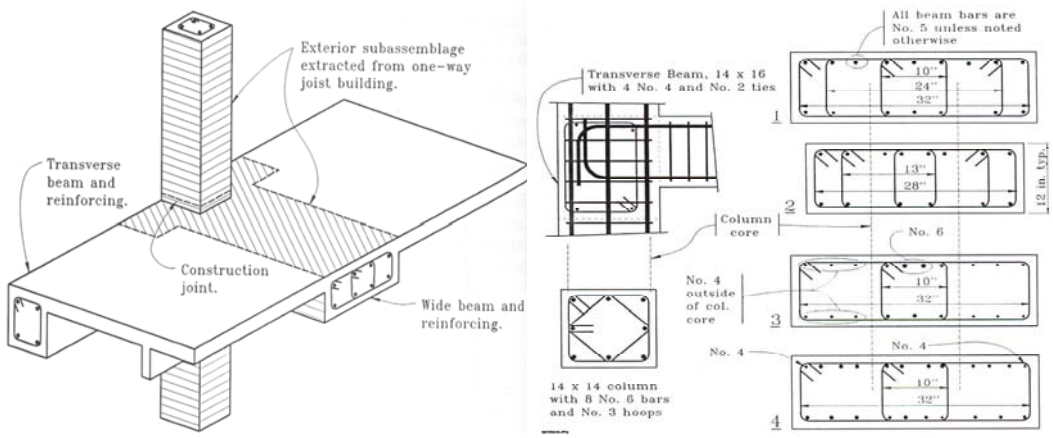

(a) Reinforcing detail

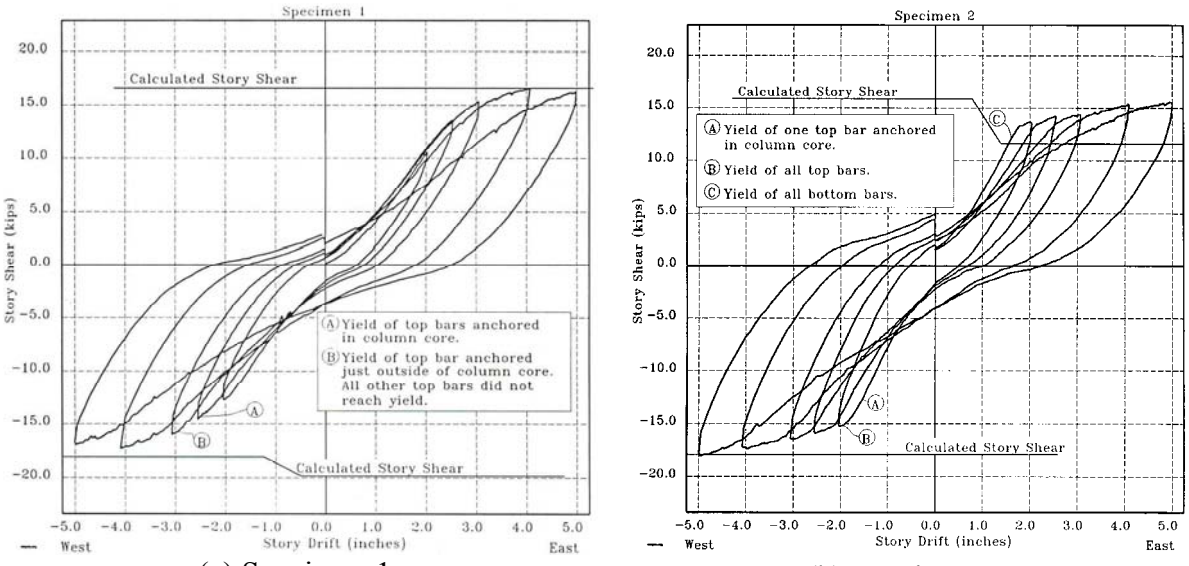

(a) Specimen 1 (b) Specimen 2

Fig.2.9a Exterior wide-beam column connection [Gentry and Wight, 1994]

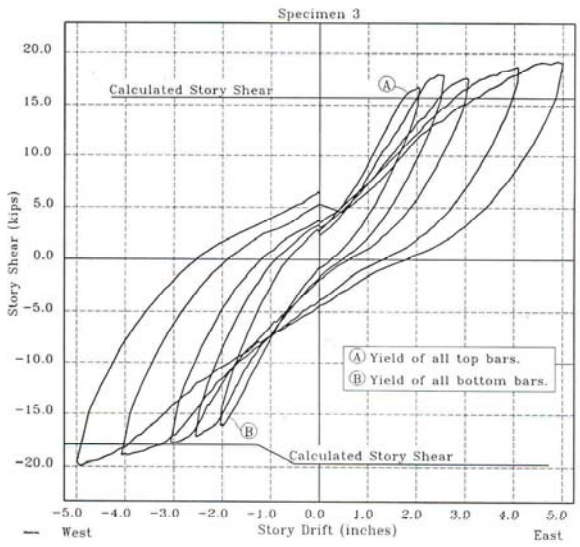

(c) Specimen 3

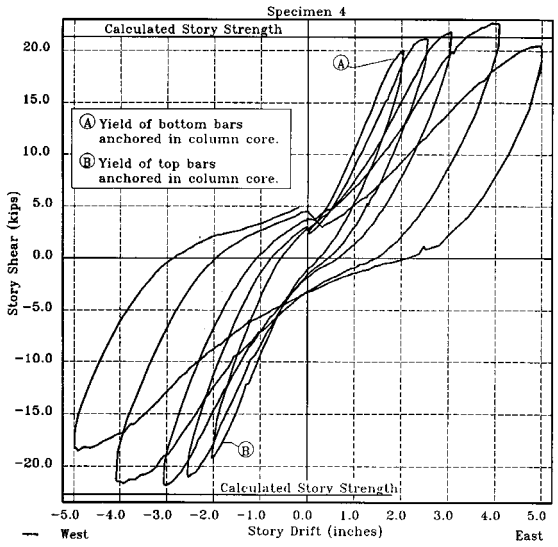

(d)Specimen 4

Fig. 2.9b Exterior wide-beam column connection [Gentry and Wight, 1994]

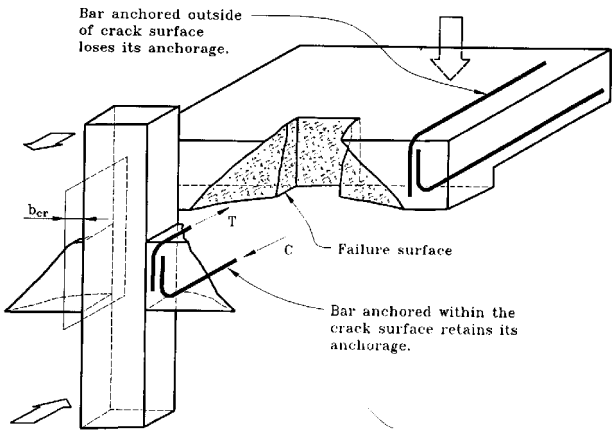

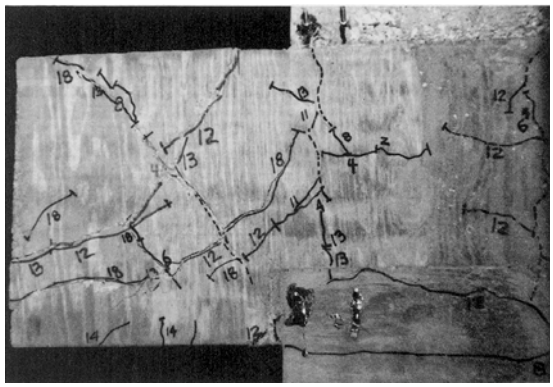

Fig. 2.10 Shear crack patterns on the rear face of the beam [Gentry and Wight, 1994]

2.4.4 Moment Interaction under Biaxial Loading

Due to the interaction of the moments along two orthogonal axes in biaxial loading tests, the column capacity is reduced to be less than the expected value in uniaxial loading tests. According to the previous research [Furlong 1961], the failure surface of the square column was proposed by applying axial load and moments on both principal axes. From two given interaction column capacity estimated with a principal axis, the failure surface is presented in Fig. 2.11 that shows the square column has a lower moment capacity about a non-principal axis. This failure surface was further proposed in a generalized expression as the interaction of principal axis moment capacity on a plane with a constant axial load (as given in Eq. 2.2).

$$\left(\frac{M_y}{MY_y}\right)^{\alpha}+\left(\frac{M_z}{MY_z}\right)^{\alpha}=1.0 \tag{2.2}$$

where M_y and M_z is the coordinates of any point along the edge of the plane and α determines the curve of the plane. However, the derived interaction relationship is for column flexural strength but joint shear capacity. Within analysing the joints of a frame, it is a non-conservative assumption that the biaxial interaction does not occur. Hence, the bi-directional capacity surface has also been adopted to evaluate the beam-column joint strengths. Much research has been done to investigate the behaviour of reinforced concrete in space frames. Based on the experiments done by Leon and Jirsa on a series of reinforced beam-column joint subassemblies [Leon and Jirsa,1986], preliminary work to derive α for the inter-storey shear at the corresponding failure point of the plane was performed by Trowland and α= 1.3-1.4 was suggested to be used for the square column [Trowland, 2004].

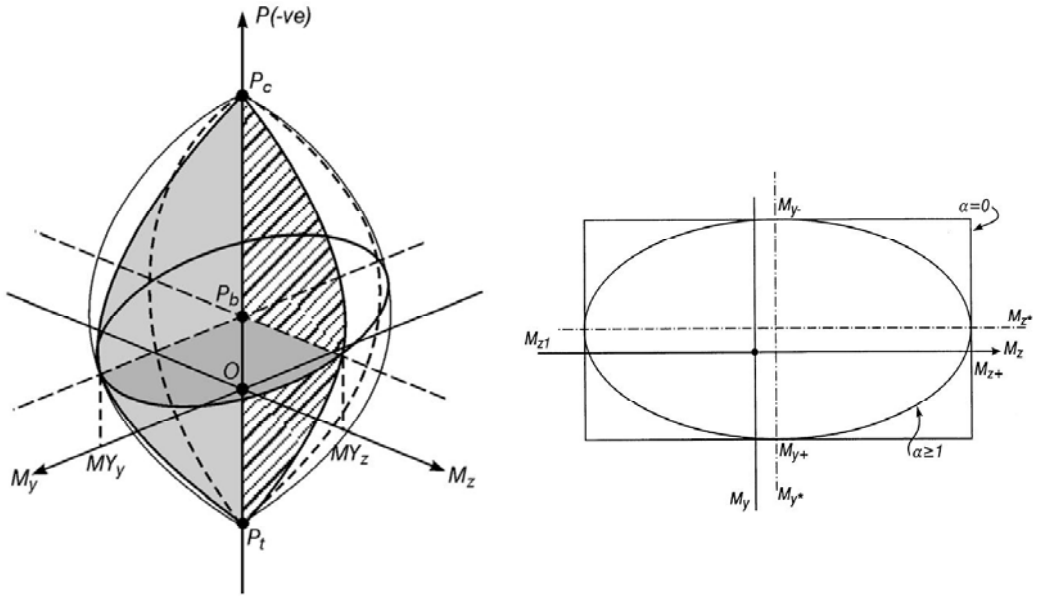

Fig. 2.11 Interaction surface of the reinforced concrete column in two-way frames [Carr, 2003]

2.5 DEVELOPMENT OF AN ALTERNATIVE LOW-INVASIVE RETROFIT SOLUTION

2.5.1 Fibered Reinforced Polymers, FRP

In the past decade, the use of advanced of non-metallic materials such as Fibre Reinforced Polymers, FRP [fib 2006] was given more attention on. To validate the FRP as an applicable retrofit solution, the experimental investigations were carried out on the feasibility and efficiency of externally bonded FRP composites as a retrofit solution [Nassi, 2002]. The 2/3-scaled beam-column joint subassemblies researched by Pampanin in the above paragraph were retrofitted on the basis of hierarchy strength considerations to achieve the desired performance [Pampanin, Bolognini, Pacese, Magenes and Calvi, 2004]. The expected sequence of events can be visualized through demand-capacity curves within M-N performance domain. The as-built and retrofitted configurations are illustrated in Fig. 2.12(a) where uni-directional carbon fibre laminates were adopted in the retrofit configurations. Vertical FRP laminates were used on the external face of the column in the exterior joints (2 layers per side) in order to increase the column flexural capacity as well as the joint shear strength (Fig .2.12(b)). In addition, in the exterior joint specimen, a U-shape horizontal laminate, wrapped around the exterior face of the specimen at the joint level, was used to increase the joint shear strength as well as prevent the expulsion of a concrete wedge. From the experimental results presented in Fig. 2.12(c), the efficiency of the adopted retrofit solution was confirmed with that the formation of a brittle shear hinge mechanism was avoided and the beam plastic hinge mechanism was developed. This would enforce a more desirable hierarchy of internal strength and sequence of events to be achieved.

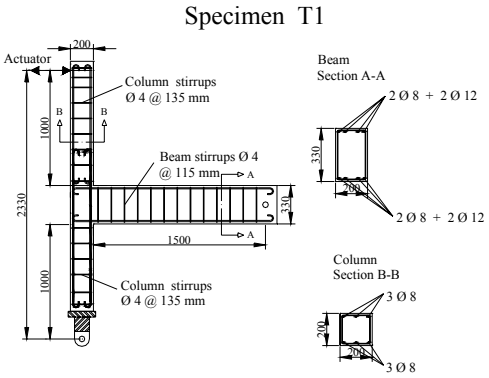

(a) As-built specimen

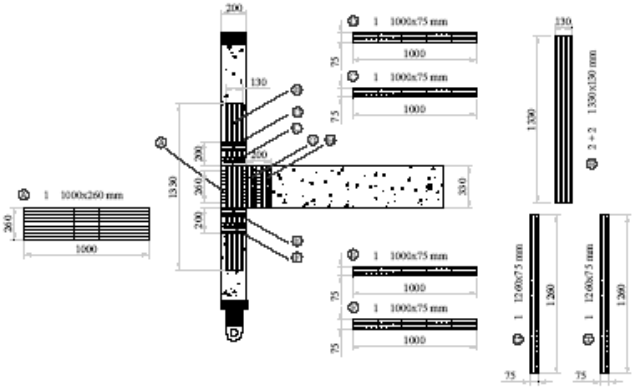

(b) FRP retrofit solution

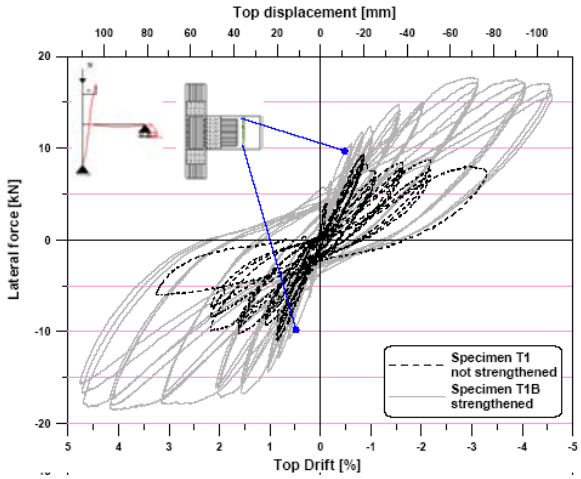

(c) Comparison of experimental results

Fig. 2.12 Applied FRP retrofit solution [Pampanin, Bolognini, Pacese, Magenes and Calvi, 2004]

2.5.2 Non-Invasive Energy Dissipation Devices

An alternative redesign approach based on the local installation of energy dissipation devices was proposed by Martinez [Martinez R., 1998]. By installation of friction or yielding devices assembled in the vicinity of beam-column joints as illustrated in Fig. 2.13, a non-invasive redesign technique was developed to have additional energy dissipation around regions with anticipated high rotation ductility demands. The proposed technique cooperating friction or yielding devices dissipates energy by rotational deformation induced moment. Due to the high rotation ductility demands being required in the enclosed member regions, the desirable mechanism of a redesigned subassembly for effective energy dissipation is illustrated in Fig. 2.13(b) while the inefficient mechanisms in dissipating energy is also presented in Fig. 2.13(c).

The analytical study is presented in Fig. 2.14 where the fatter hysteric behaviour and higher shear strength without strength degradation were observed at a certain displacement level within the up-graded subassembly. The proposed techniques succeeded to numerically upgrade the performance of the beam-column joint.

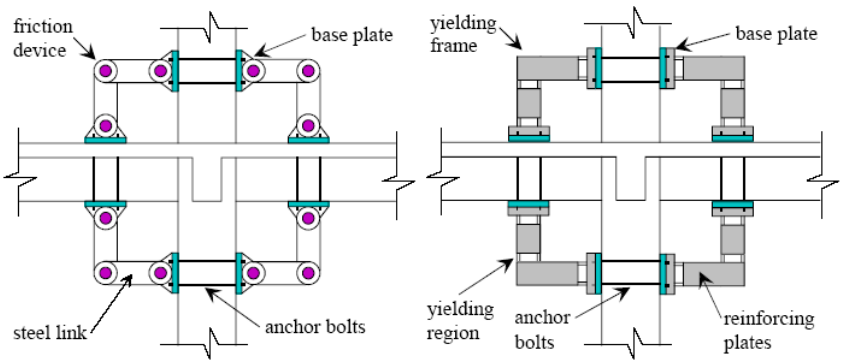

(a) at interior joint

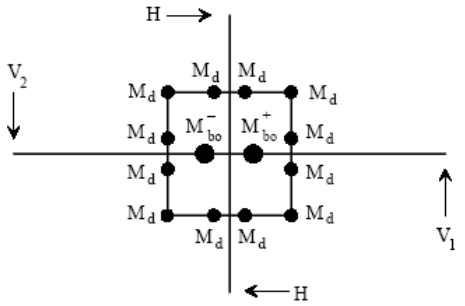

(b) Desirable beam-sway mechanism

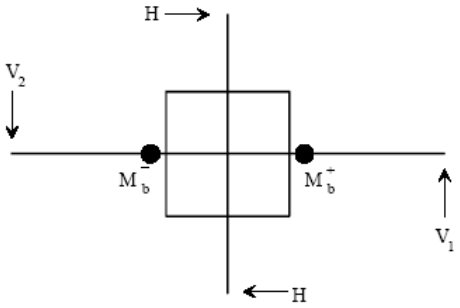

(c) Undesirable beam-sway mechanism

Fig. 2.13 Local incorporation of hysteretic devices around beam-column regions [Martinez R., 1998]

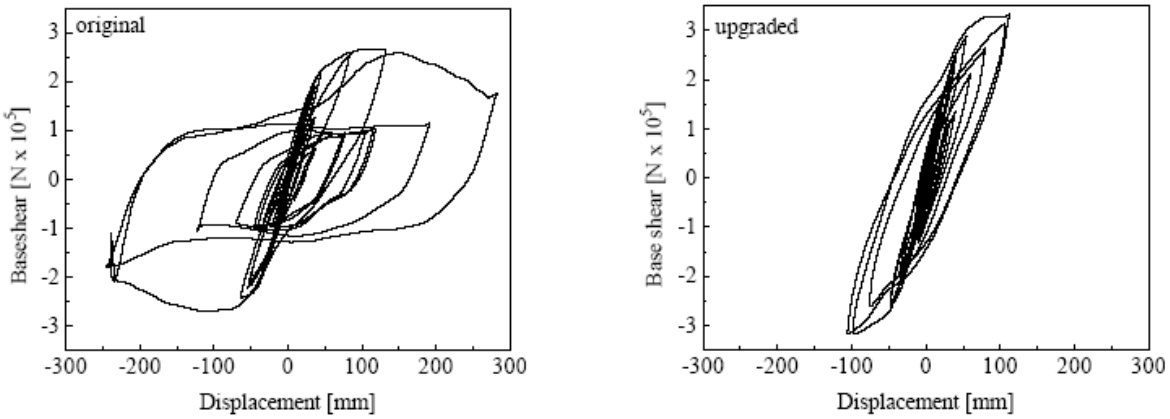

(a) Original (b) Upgraded

Fig. 2.14 Comparison of seismic response [Martinez R., 1998]

2.5.3 Haunch Solution for Steel frames

After the 1994 Northridge California earthquake caused the damage in connections of steel moment-resisting frames as well as the reduced strength, a repaired method by adding haunches on either the bottom side of the beam to protect the connections was proposed and verified experimentally [Uang and Lee, 1997]. The basic concept of the repair is to reinforce the steel moment frame connection with a triangular haunch at the beam bottom flange as illustrated in Fig. 2.15.

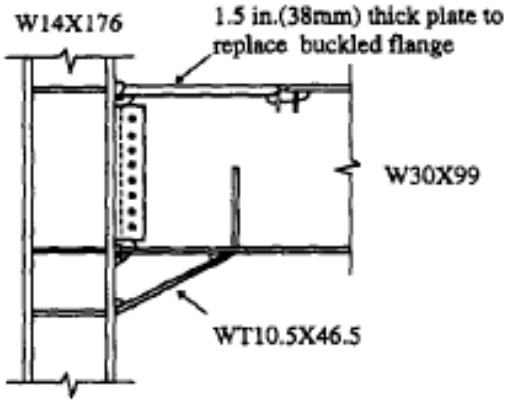

Fig. 2.15 Configuration of haunch solution for steel frames [Uang and Lee, 1997]

It is exploited to shift the plastic hinging away from the critical region where the force demand on the complete joint penetration welds is then reduced by increase in the effective depth of the section. Therefore, the brittle failure of the connection is avoided. Compared with the behaviour Fig. 2.16(a), Fig. 2.16(b) presented that the plastic region was effectively relocated away from the face of the column and the stress in the groove welds at the column face was thus reduced by repairing the damaged steel frame.

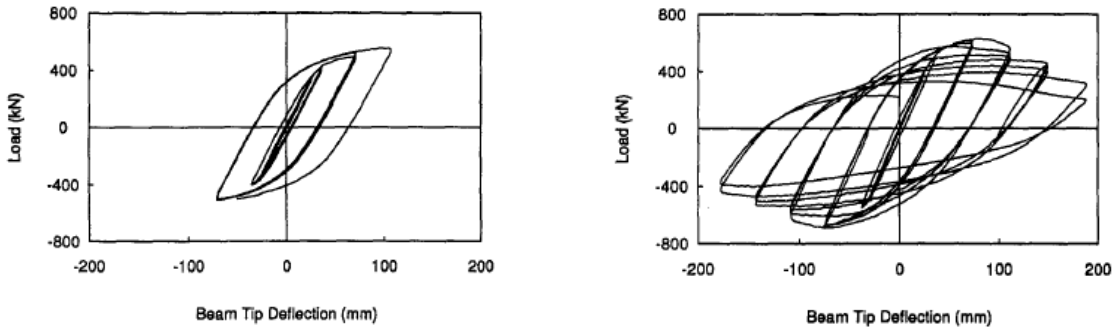

(a) before repair (b) after repair

Fig. 2.16 Haunch solution for steel frames [Uang and Lee, 1997]

2.5.4 Numerical Study of Haunch Solution on RC Frames

Due to the poor performance of the existing reinforce concrete frame building where the brittle joint shear failure was observed, a non-invasive retrofit solution that introduce the haunch device was proposed by Pampanin as illustrated in Fig. 2.17(a) [Pampanin and Christpoulos, 2003]. The basic concept of the haunch retrofitting strategy is to relocate the plastic hinge in the beam and away from the critical joint region that is protected through haunch straining to reduce the principal tensile stress. The numerical study was investigated to confirm the effectiveness of the haunch retrofitting solution. As illustrated in Fig. 2.17(b), the retrofitted subassembly, compared with the as built subassembly, performed a higher strength with desired beam hinging mechanism. In addition, the numerical investigation on the frame system demonstrated that the desired beam sidesway mechanism was observed in the haunch-retrofitted frame while the joint shear sideway mechanism could cause the soft storey and serious strength degradation in the as-built frame (Fig. 2.18).

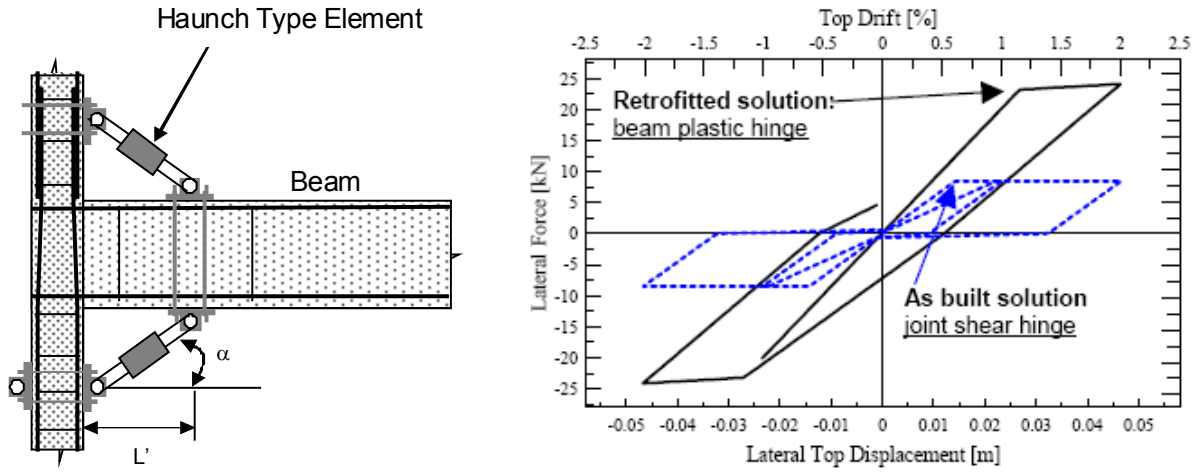

(a) Haunch configuration (b) Comparison of numerical results

Fig. 2.17 Haunch solutions for exterior RC joint [Pampanin and Christpoulos, 2003]

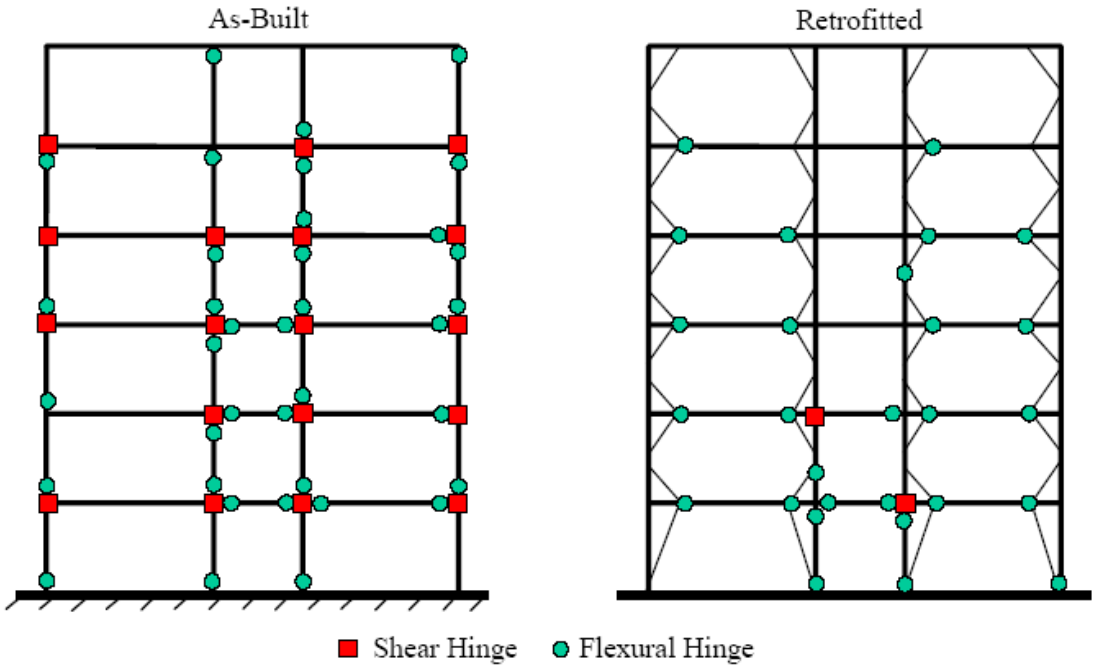

Fig. 2.18 Comparison seismic response [Pampanin and Christpoulos, 2003]

2.6 STRENGTH DEGRADATION CURVES

Since investigating into the results of the previous research, Hakuto et al. and Priestley suggest that the shear strength are still developed in the joints of insufficient shear reinforcement if there are no shear cracks observed in the joint core. It is suggested that the probable horizontal joint shear strength without shear reinforcement presented in the joint core can be given by:

$$V_{jh} = k\sqrt{f_c'}\sqrt{1+\frac{N}{A_g k\sqrt{f_c'}}}b_j h_c \le 1.5\sqrt{f_c'}b_j h_c \qquad (2.3)$$

where $p_t = k\sqrt{f_c'}$. According to the equation, the column axial load is taken into account for evaluating the horizontal shear strength which relationship between internal forces is illustrated in Fig. 2.19.

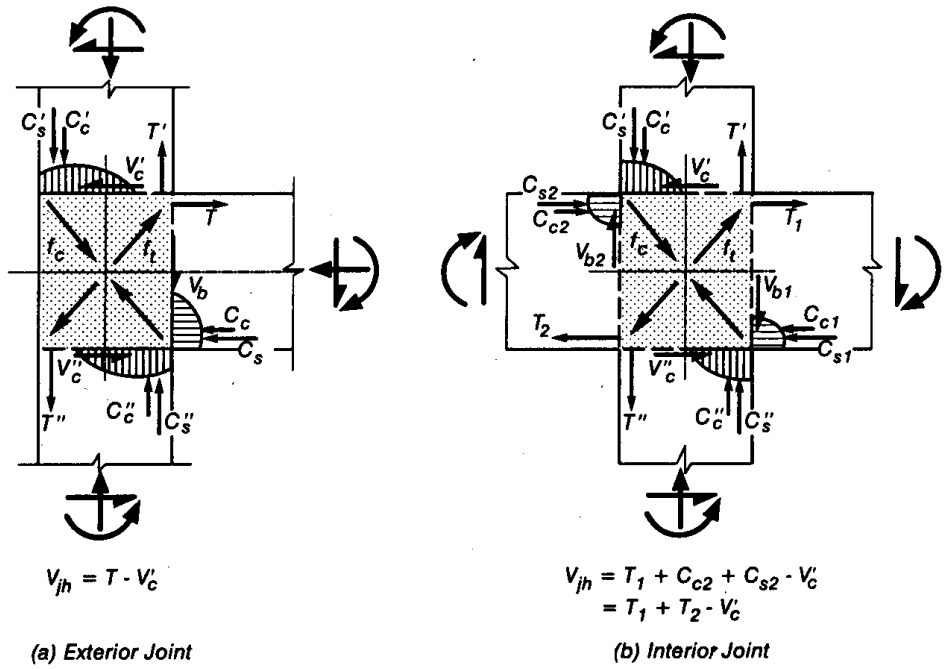

Fig. 2.19 Forces in beam-column joints and calculation of horizontal shear force acting on joint core [Park, 1997]

According to what typically recognized in literature [Priestley, 1997], it is classified within different possible damage mechanisms depending on the reinforcement detailing of the exterior beam-column joints (Fig. 2.20).

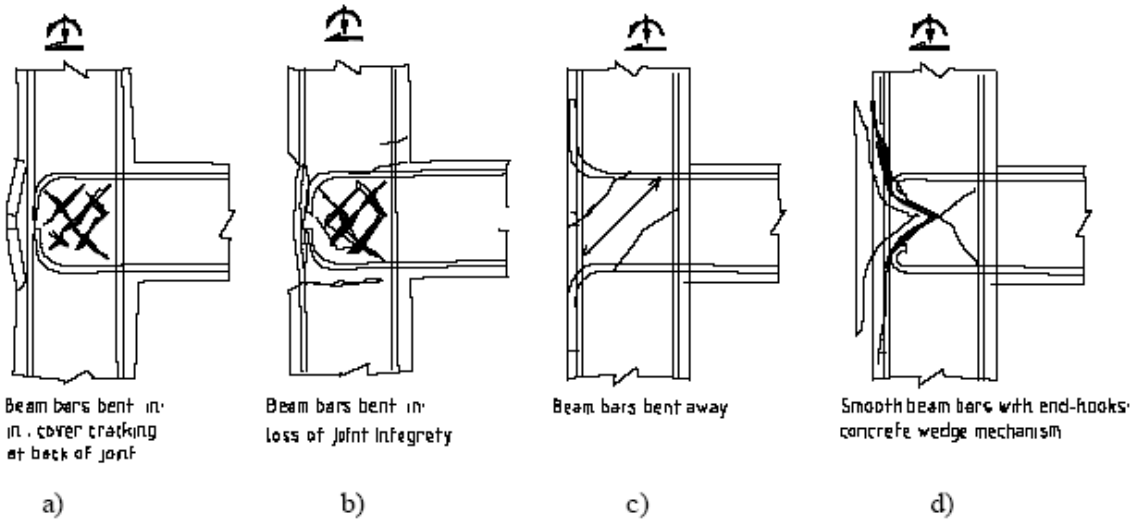

Fig. 2.20 Alternative damage mechanism for exterior tee-joints [Pampanin, Calvi and Moratti, 2003c]

On the basis of the previous research of experimental tests, the principal tensile stress p_t was suggested for different reinforcing detail without sufficient transverse reinforcement. For first

crack in the joint core, p_t is defined as $0.2\sqrt{f'_c}$ and $0.29\sqrt{f'_c}$ for exterior joint (with end-hooks and smooth bars) and interior joint respectively. After first cracking occurs, hardening behaviour until p_t=$0.42\sqrt{f'_c}$ is assumed for interior joint or exterior joint if appropriate strut mechanism can be developed. The suggested value of the principal tensile stress is illustrated in Fig. 2.21(a) and Fig. 2.21(b) with respect of joint deformation γ and inter-storey drift respectively

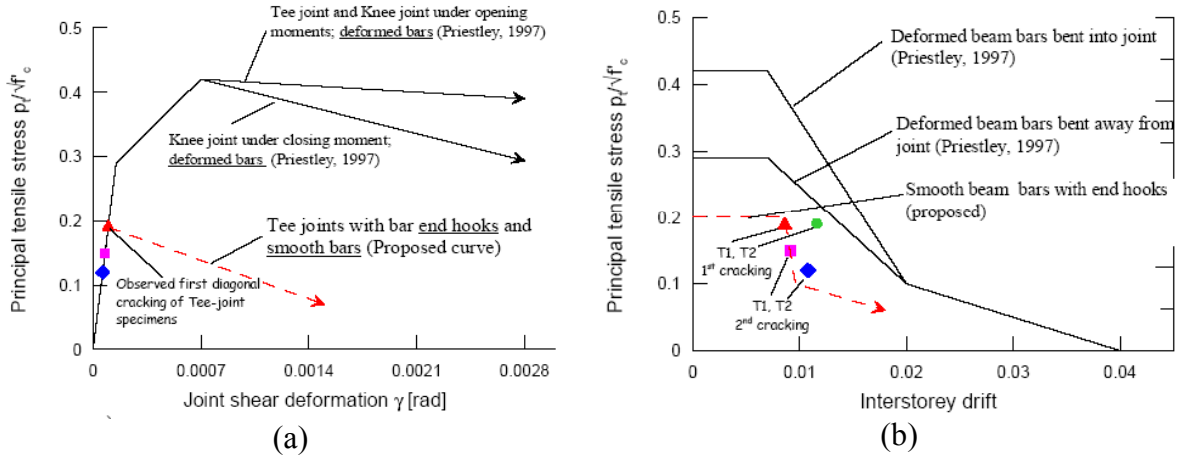

Fig. 2.21 Strength degradation for exterior joint [Pampanin, Calvi and Moratti, 2003c]

Since the spandrel beam in the two-way joint behaves as external joint transverse reinforcement, the principal tensile stress of the corner joint is higher than the exterior tee joint while the same uniaxial load is applied (Fig. 2.22). The obtained principal tensile stress p_t =$0.58\sqrt{f'_c}$ for joint shear failure on the corner joint is based on using deformed reinforcement, thus the advanced investigation of the principal tensile stress for joint shear failure in the corner joint reinforced with smooth bars is necessary.

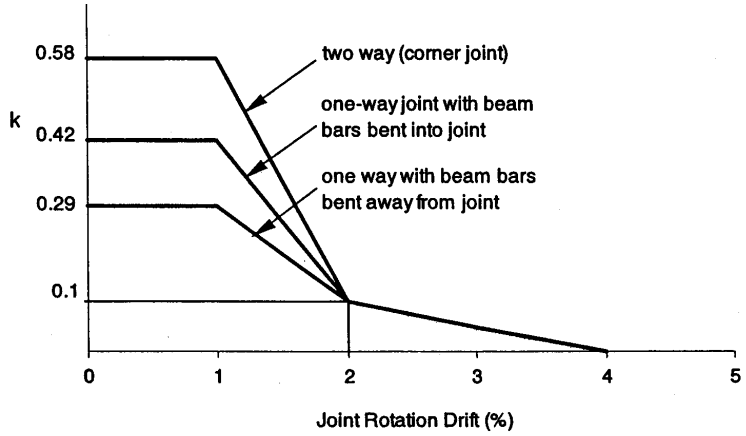

Fig. 2.22 Strength degradation of one-way and two-way joint [Liu, 2001]

CHAPTER 3

HIERARCHY STRENGTH DESIGN CONCEPT AND THEORY OF HAUNCH RETROFIT STRATEGIES

3.1 INTRODUCTION

As investigation of previous study, principal stresses are the more reliable criteria than horizontal shear stresses to predict the joint response since they present the actual stress state of the joint by considering a combination of the nominal shear force V_{jh} (or corresponding stress, v_{jh}) with the column axial load N (or corresponding stress, f_a). Since the more venerable feature of the exterior joint compared with the interior joint is expected, the design concept of evaluating hierarchy strength of elements, based on the exterior beam-column joint, is introduced in this chapter to assess the sequence of events by applying the equivalent yielding capacity of joint for first cracking or extensive damage. The variation of column axial load caused by the frame geometry, particularly in exterior beam-column joints, should be properly identified while estimating the actual stress level. By comparing the capacity and demand of joint subassembly, the equivalent yielding of the existing joint region would be expected prior to hinging of the beam and column and cause the joint shear failure. Through modifying the hierarchy strength, the retrofitted beam-column joint could present the desired weak-beam strong-column mechanism of the beam hinging prior to the column and joint failure. Therefore, based on the capacity design philosophy, appropriate retrofitting strategies that provide adequate protection to the joint region are proposed to up-grade the joint capacity and improve the seismic response of existing structures.

Following the investigation on brittle fracture of moment connections in steel moment-resisting frames caused in the 1994 Northridge earthquake, a variety of improved moment connection details were proposed. To enhance the seismic performance of damaged steel connection and retrofit the existing steel moment-resisting frames (SMRFs) where the connection failure was potentially fundamental deficiencies, the use of a hunch on the bottom side of the beam had been proposed and demonstrated with the respect of effectiveness [Uang,, Bondad and Lee, 1998] and [Uang, Yu, Noel and Gross, 2000].

According to the effective performance of the haunches in retrofitting the steel moment connection, a similar retrofit strategy for significant cost saving was introduced to retrofit the existing R.C. beam-column joint designed with gravity-loads-only [Pampanin, Calvi and Moratti, 2002]. The concept of protecting the peculiar brittle joint is based on redirecting the stress-flow around the joint region and re-positioning the plastic hinge in the beam away from the face of column through axial straining of the haunch. The strength hierarchy of designed elements is modified with respect to capacity deign principles that the strong-column weak-beam mechanism is introduced to prevent the brittle joint behaviour and the development of soft-storey mechanism by properly reviewing the geometry and stiffness of haunches. Consequently, the higher strength and stiffness of global frame system is also expected to reduce the inter-storey drift demand. Following the numerical analysis that supported the respect of effectiveness in retrofitting R.C. frame system with haunches [Pampanin and Christopoulos, 2003], it is required to investigate into more detail of haunch retrofit strategy and derive a set of design principles for the simplified retrofit scheme. When applying this retrofit solution to existing reinforced concrete frame buildings without considering capacity design philosophy, however, additional challenges that the desired beam flexural hinge mechanism develops before other failure mechanism (e.g. shear failure and column flexural failure) should be guaranteed by introducing appropriate safety factors during design procedure.

In this chapter, the basic concept of protecting exterior joint panel zone by haunches as well as the detail of design formula would be described and the effectiveness of essential designed parameter, β-factor (shear transferring coefficient), that was first introduced in the retrofit model of steel connection [Yu, Uang and Gross, 2000] is discussed and numerically validated in the following section. The concept of simple deign chart in the respect of designed parameters would be introduced while a complete step-by-step design procedure is also suggested as feasible tool to achieve the desired strength hierarchy for the haunch retrofit strategy of exterior beam-column joints.

3.2 ASSESSMENT OF HIERARCHY STRENGTH

3.2.1 Introduction of Equivalent Yielding Capacity of Exterior Joint

As mentioned in Chapter 2, the critical principal tensile stresses for the exterior joint of different reinforcing details are identified from the experimental results for different limit states as shown in Table 3.1. To compare the bearing capacity of the joint with capacity of the adjacent beam and column member, the equivalent yielding moment of first cracking or extensive damage for the joint is introduced by considering the equilibrium on the bending moment of adjacent elements. Due to the more significant effect of the beam depth, the equivalent joint moment is supposed to take into account the imposed moment from the beam member. From the free body diagram in Fig. 3.1(a) and (b), the applied inter-storey shear force on the top of column V_c causes the joint moment M_{bc} while a horizontal shear force immediately induced by M_{bc} is given by M_{bc}/jd_b. Therefore, the nominal horizontal shear force in the joint V_{jh} is given by (Fig. 3.1(c)):

$$V_{jh} = \frac{M_{bc}}{jd_b} - V_c \tag{3.1}$$

According to the Mohr's circle of stress, the principal tensile stress of the joint is determined by the horizontal shear stress v_{jh} and vertical normal stress f_a in the joint core:

$$p_t = \frac{f_a}{2} + \sqrt{\left(\frac{f_a}{2}\right)^2 + \left(v_{jh}\right)^2}$$
$$\text{where } v_{jh} = \frac{V_{jh}}{A_e}, f_a = \frac{N}{A_g} \tag{3.2}$$

The effective joint area A_e is specified to safeguard the core concrete against excessive diagonal compression stresses. The horizontal shear stress corresponding with the shear force V_{jh} is based on the effective joint area $A_e=b_jh_c$ as defined in Fig. 3.2 that consider the difference of effective joint core between the deep beam and wide beam connection [NZS3101:1995]. Consequently, with a given column axial force N and specified principal tensile stress p_t of the particular joint limit state, the nominal horizontal shear force in the joint could be simplified as the expression:

$$V_{jh} = A_e \sqrt{p_t^{\,2} - \frac{p_t N}{A_g}} \tag{3.3}$$

Since the relationship between the induced joint moment M_{bc} and inter-storey shear force V_c is established as followings:

$$M_{bc} = V_c \frac{H_c}{(1 + d_c / L_n)} \tag{3.4}$$

where $L_n = L_b - d_c$

The horizontal inter-storey shear V_c could be described as the function of V_{jh} by solving the Eq. 3.1 while M_{bc} is replaced with the expression in Eq. 3.4. As a result, the critical inter-storey shear $\overline{V}_{c,joint}$ corresponding to the occurrence of a defined level of principal tensile stress p_t in the joint can be evaluated as well as the corresponding moment capacity $M_{bc}^{\,*}$ of the exterior joint by substituting $\overline{V}_{c,joint}$ into Eq. 3.4.

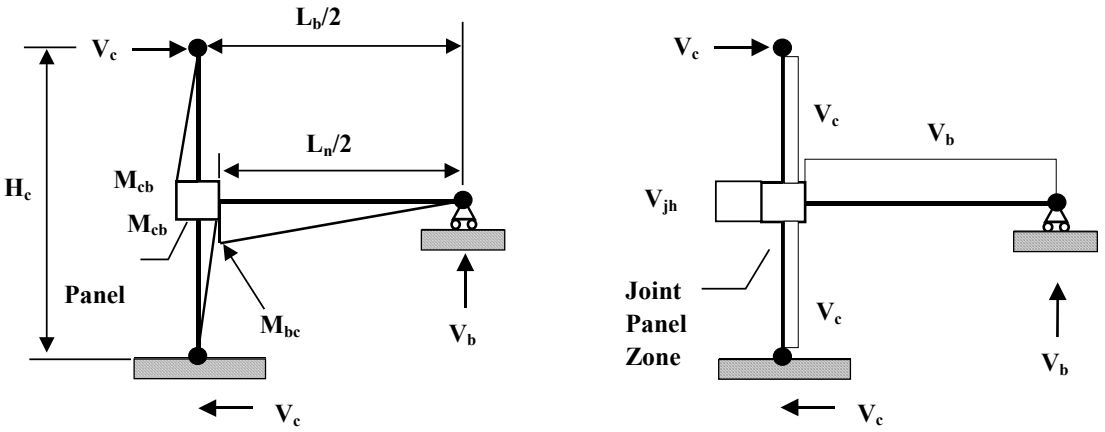

(a) Bending moment distribution

(b) Internal shear force diagram

(c) Induced nominal horizontal shear force in the joint

Fig. 3.1 Free body diagram of as-built subassembly and column shear force distribution

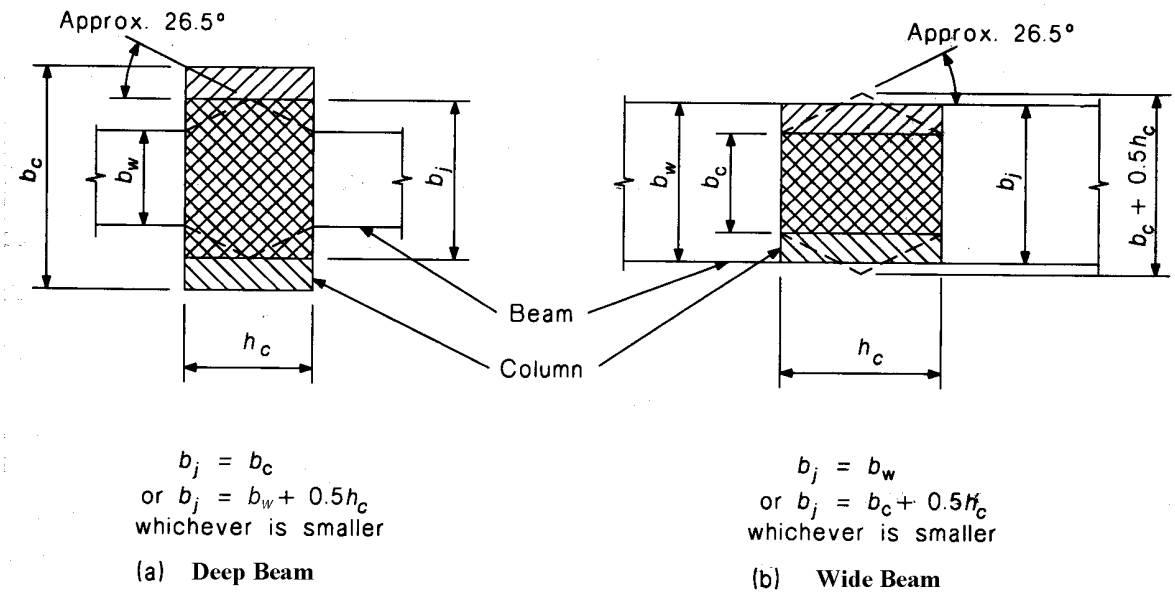

Fig. 3.2 Effective joint area [NZS3101:1995]

Table. 3.1 Limit states for exterior joint based on principal tensile stress

Limit State	Plain Round Bar with End Hooks	Deformed Bars with Hooks Bent into Joint
First Diagonal Shear Cracking	$p_t=0.2\sqrt{f_c'}$	$p_t=0.29\sqrt{f_c'}$
Extensive Damage	Nil	$p_t=0.42\sqrt{f_c'}$

3.2.2 Considerations on The Effects of The Variation of The Column Axial Load Due to Lateral Loading

Due to the geometry of the frame system, the varying axial load of the column caused by the imposed lateral force results in the varying column and joint capacity that are both axial-force dependent during the closing and opening action. Thus, the inadequate consideration of column axial load would lead to the incorrect assessment of the sequence event as well as the inappropriate and not necessarily conservative design of the retrofit alternatives. More detail of the varying column axial load is given in Chapter 4.

3.2.3 Hierarchy Strength And Sequence of Events

A simple procedure that determines the sequence of events by comparing the internal hierarchy strengths within a beam-column joint has been proposed by Pampanin [Pampanin, Bolognini, Pacese and Magenes and Calvi, 2004]. From the previous introduced concept, the

column, beam and joint capacity curve, referred to the beam-column connection could be plotted together with the appropriate demand curve where the moment demand of the beam-column connection M_{bc} is derived from the imposed lateral shear force V_c by Eq. 3.3 while the particular column axial force is presented by $N = N_g + \alpha_h V_c$ (N_g is the constant dead load and α_h is a geometry coefficient). By comparing the capacity and demand curves through the loading history, the expected sequence of events could be evaluated within this *M-N* (moment-axial load) performance domain. As the example illustrated in Fig. 3.3, the sequence of events for exterior joint TDP2 (designed in Chapter 4) with the specified damage level (i.e. p_t=0.2$\sqrt{f_c'}$) is displayed and listed in Table 3.2. The joint shear hinge mechanism is predicted to be the failure mode in the as-built subassembly TDP2 because the brittle joint shear failure occurs before the other events of beam and column yielding.

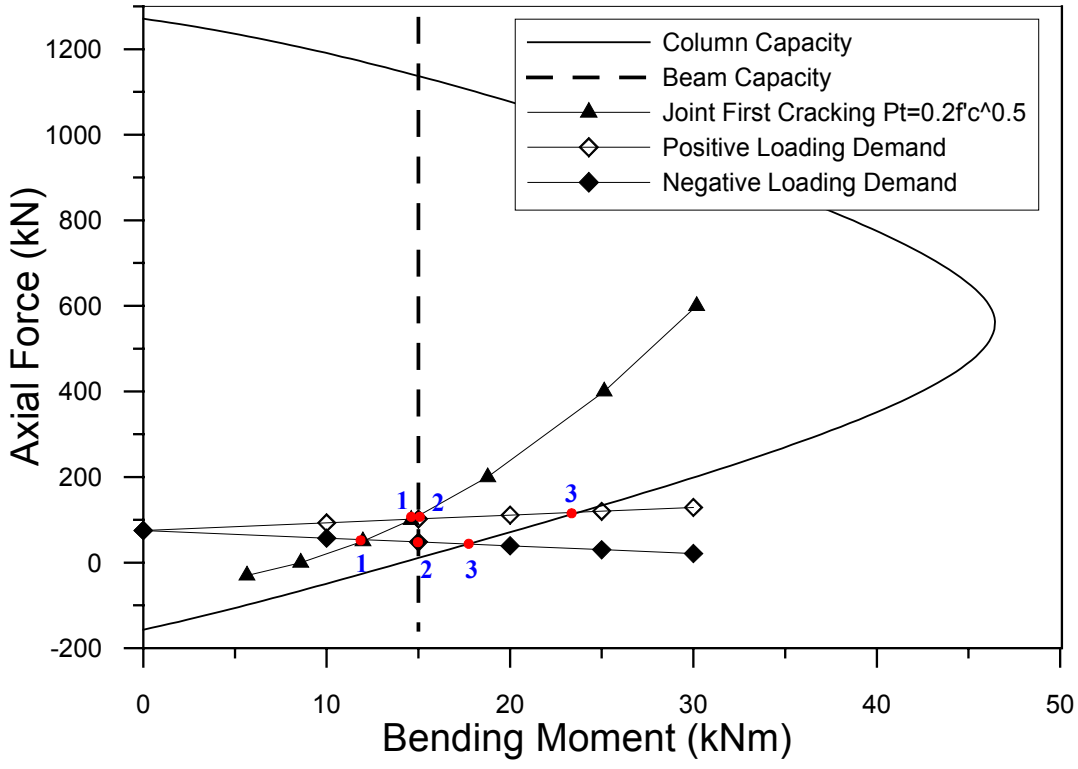

Fig. 3.3 Hierarchy strength diagram of beam-column joint and evaluation of event sequence in M-N performance domain (with TDP2 configuration)

Table 3.2 Sequences of events for exterior joint TDP2

Lateral Force Direction	No.	Specimen TDP2 (As-Built) Event
Positive Loading	1	Joint First Diagonal Cracking and Deterioration Starting
	2	Beam Yielding
	3	Column Yielding
Negative Loading	1	Joint First Diagonal Cracking and Deterioration Starting
	2	Beam Yielding
	3	Column Yielding

3.3 HAUNCH RETROFIT STRATEGY

3.3.1 General

The design concept of haunch retrofit strategy in existing buildings is based on modifying the strength hierarchy of structure element by relocating the plastic hinge in the beam, through the axial straining of the haunch, to avoid the undesired joint failure mechanism that has low ductility and significant strength degradation with high damage level. Fig. 3.4(a) illustrates the basic configuration of haunch retrofit strategy and it is obvious that, from Fig. 3.4(c), the internal forces of the beam-column subassembly are significantly altered when haunch type elements are introduced at a distance *L'* from the face of column and connected at an angle α above and below the beam. The effectiveness of haunch elements is to reduce the designed joint moment M_{bc} and protect the joint panel zone from brittle shear failure without reaching the critical value of equivalent principal tensile stress level that depend on the joint typology (exterior or interior) and reinforcing detail (i.e. plain round or deformed, anchorage solutions).

3.3.2 Effect of Haunch Elements on Retrofitted Exterior Joint

Assuming the inflection points are located at mid spans of the beam and column, the free body diagram of the exterior beam-column subassembly is illustrated as Fig. 3.4(b) while the inter-storey shear, V_c, is applied on the top of column. The designed joint moment M_{bc} at the face of column causes the brittle shear failure of existing joint when M_{bc} reaches the joint capacity that is equivalent to the critical value of principal tensile stress. To produce the joint moment M_{bc} in the as-built subassembly, the inter-storey shear V_c can be evaluated by Eq. 3.5.

$$V_c = M_{bc}\frac{(1+d_c/L_n)}{H_c} \qquad (3.5)$$
$$\text{where } L_n = L_b - d_c$$

When haunch type elements are introduced and connected above and below the beam at a distance *L'* with an angle α, as illustrated in Fig. 3.4(a), the beam and column moments at the joint panel zone interface can be significant reduced. The moment diagram of the exterior joint subassembly is modified such that the maximum moment in the beam and in the column is relocated away from the original critical sections. Through significantly reducing the joint moment $M_{bc,}$ this migration of the maximum moment in the beam, if designed adequately, can properly develop the flexural hinge at a distance *L'* from the face of column before critical failures occur. Meanwhile, according to the maximum moment in the beam $M_{b(max)}$, the inter-storey shear V_c for the haunch retrofitted subassembly can be given by:

$$V_c = M_{b(\max)}\frac{\left(1+\left(d_c+2L'\right)/\left(L_n-2L'\right)\right)}{H_c} \qquad (3.6)$$

The design concept of the haunch retrofit strategy consists of properly selecting the geometry (distance from the column interface *L'* and angle α) as well as the axial stiffness K_d of the haunch elements. According to the deformation compatibility of structural element, the chosen geometry and stiffness of haunches determines the subsequent effects of redirecting beam shear forces to the column through the induced internal axial force in haunches. As a result, the redistributed joint moment reduces the principal tensile stress in the joint panel zone to save the beam-column joint while the beam flexural hinge is enforced to occur at a distance *L'* from the column face that could be a preferred weak beam/strong column mechanism. The effects of the haunch retrofit solution and the detail of moment and shear force diagrams in an exterior beam-column joint subassembly subjected to lateral loads with inflection points assumed at mid-span of the beam and mid-height of the column are illustrated in Fig. 3.5.

Due to the axial straining of haunch, the total haunch-induced shear force in the beam is equally contributed by two haunches and is expressed as a function of the beam reaction βV_b where β factor is a shear transferring coefficient determined by the selection of the three

haunch design parameters L', α and K_d. Therefore, as illustrated in Fig. 3.5, once βV_b is determined, the moment and shear diagrams of the beam and column from the point of inflection to the face of the joint connection are known. Because of the symmetry of the top and bottom haunches, the equivalent free body diagram demonstrate that no axial load is introduced in the beam and the concentrated moment reduction, $\Delta M_H = [\beta \mathrm{V_b}(\frac{d_b}{2})]/\tan\alpha$, caused by the eccentric force of haunches at the points where the haunches are connected to the beam (Fig. 3.6).As a result, the reduced joint moment in the beam at the face of the column is expressed by the following equation:

$$M_{bc} = M_{b(\max)}\left[1 - \frac{\beta d_b}{2L\tan\alpha} + \frac{(1-\beta)L'}{L}\right] \qquad (3.7)$$
$$\text{where } L = (L_n/2) - L'$$

Similarly, the reduced column moment at the beam interface M_{cb} can be expressed as:

$$M_{cb} = M_{c(\max)}\left[1 - \frac{\beta' d_c \tan\alpha}{2H} + \frac{(1-\beta')L'\tan\alpha}{H}\right] \qquad (3.8)$$
$$\text{where H} = (H_n/2) - L'\tan\alpha$$

where $\beta' = \beta \cdot \left(\frac{H_c}{L_b \tan\alpha}\right)$ and H_c is the total inter-storey height (from centreline to centreline of beams). The maximum column moment developed at the level of the haunch connection can be also expressed as the function of the maximum moment in the beam:

$$M_{c(\max)} = M_{b(\max)} \frac{\left(H_c/2 - d_b/2 - L'\tan\alpha\right)\left(1 + \left(d_c + 2L'\right)/\left(L_n - 2L'\right)\right)}{H_c} \qquad (3.9)$$

Considering the moment diagram presented in Fig. 3.5, the negative shear force estimated by β-factor greater than 1 is desirable for more efficiently protecting the beam-column joint. The derivation of the factor β based on displacement compatibility and investigation of design parameter on factor β (L', α and K_d) are discussed in detail in a subsequent section.

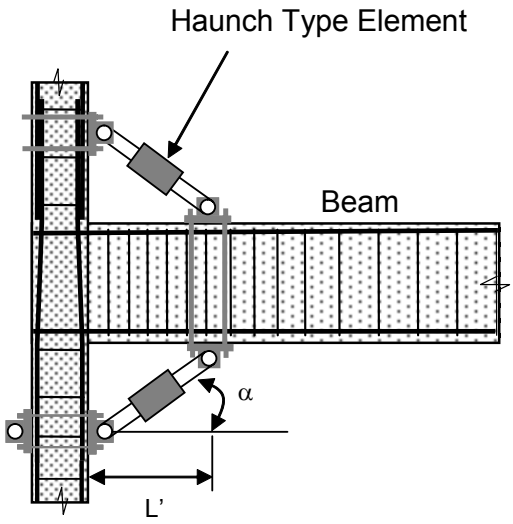

(a) Proposed haunch retrofit configuration

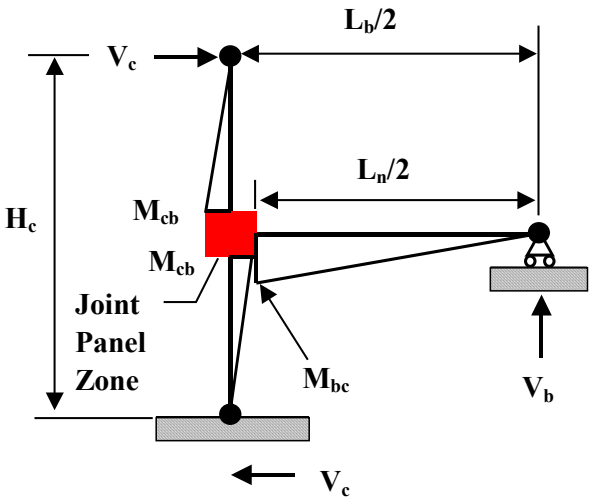

(b) Joint shear hinge without haunches

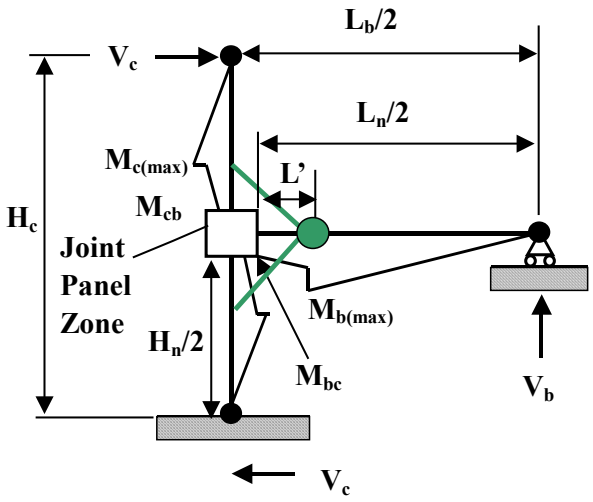

(c) Beam flexural hinge with haunches

Fig. 3.4 Haunch configuration for exterior joints; free body and moment diagram of the as-built/retrofitted exterior joint

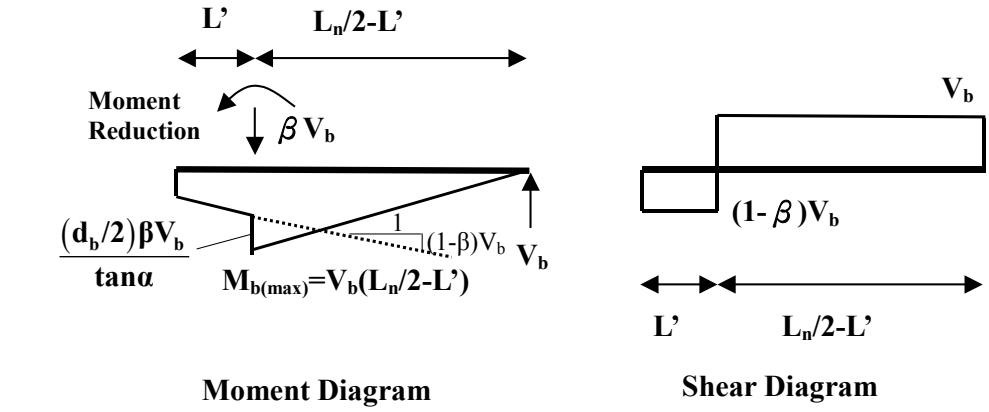

(a) Beam

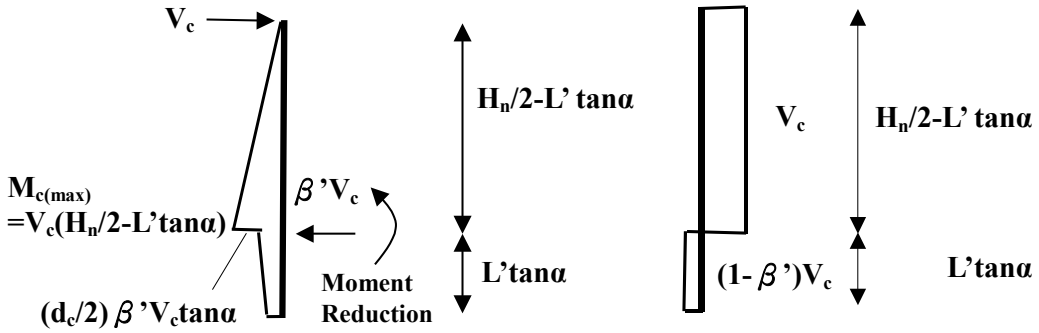

(b) Column

Fig. 3.5 Shear and moment diagram of the beam and column

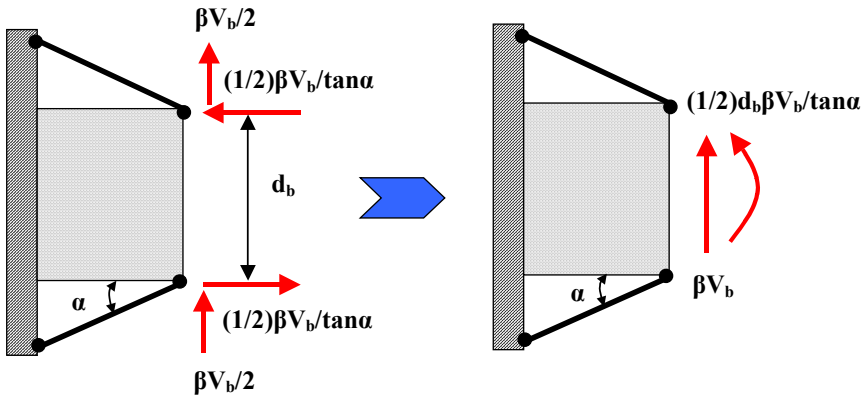

Fig. 3.6 Eccentric force due to haunch strut action on the beam

3.4 DESIGN PHILOSOPHY AND PROCEDURE

3.4.1 General

To eliminate the damage in the joint panel zones of non-seismically designed RC frames while enhancing the global response, the primary aim of proposed haunch retrofit strategy is to assure the reversal of the strength hierarchy through forcing plastic hinge at the haunch-connected point of the beam. Furthermore, through capacity design considerations, the shear failure mechanisms must be avoided in both beams and columns when the beam flexural hinge occurs before column flexural failure. To achieve this purpose, a proper hierarchy strength is developed. Since the haunch retrofit alters the moment distribution in the beam-column subassembly, the equivalent inter-storey shears V_c corresponding to the development of the failure mechanism are introduced. Through designing the haunch solution (choice of L', α and K_d), the comparison of the capacity and demand curve within the V_c-N (lateral shear-axial load) performance domain are exploited to guarantee that the beam flexural mechanism develops before undesirable critical mechanisms. This also means the inter-storey shear of causing beam flexural failure mechanism is lower than those corresponding to undesirable critical mechanisms; these mechanisms, from the least sever to the most severe response of the overall structural damage are: i) column hinging, ii) joint shear failure, iii) beam shear failure and iv) column shear failure. Therefore, the target hierarchy strength for the whole design can be summarized as:

$$\overline{V}_{c,beam-hinge} \le \Phi_1 \overline{V}_{c,col-hinge} \le \Phi_2 \overline{V}_{c,joint} \le \Phi_3 \overline{V}_{c,col-shear} \le \Phi_4 \overline{V}_{c,beam-shear} \tag{3.10}$$

where Φ_i are design safety factors (or as known strength reduction factor). These factors are important to representing the acceptable "margin" between two subsequent mechanisms to consider the material uncertainties and some undesired factors (i.e. labour work or strain hardening effect).

3.4.2 Modified Hierarchy Strengths with Effect of Haunch

Since the haunch retrofit solution alters the moment distribution in the beam-column joint subassembly, the concept of equivalent inter-storey shear capacity that cause the critical failure mechanisms is introduced to modify the hierarchy strengths for comparing the

capacity-demand curve in V_c-N performance domain. The proposed equivalent inter-storey shear is aimed to express the force that can derive the expected value at critical parts of the element. To produce $M_{b(max)}$ in the beam, as illustrated in Fig. 3.7(a), the inter-storey shear V_c is derived as given in Eq. 3.6 and the following equation express V_c with having $M_{c(max)}$ in the column.

$$V_c = \frac{M_{c(\max)}}{\left(H_c/2 - d_b/2 - L'\tan\alpha\right)} \tag{3.11}$$

As shown in Fig. 3.7(c), the nominal horizontal shear force in the joint V_{jh} can be expressed as a function of the moment in the beam at the joint interface:

$$V_{jh} = \frac{M_{bc}}{jd_b} - \left(V_c - V_{hx}\right) \tag{3.12}$$

where (V_c-V_{hx}) is the actual shear value in the column at the panel zone interface and V_{hx} is the horizontal shear force introduced into the column from the haunch:

$$V_{hx} = \frac{2\beta V_c H_c}{2\tan\alpha\left(L_n + d_c\right)} \tag{3.13}$$

By substituting Eq. 3.6, Eq. 3.7 and Eq. 3.14 into Eq. 3.12, the inter-storey shear V_c having a defined horizontal joint shear force V_{jh} is given by:

$$V_c = \frac{A_e\sqrt{p_t^{\,2} - \dfrac{p_t N}{A_g}}}{\left(1 - \dfrac{\beta H_c}{(L_n + d_c)\tan\alpha} - \dfrac{H_c(L_n - 2L')}{jd_b(L_n + d_c)}\left(1 - \dfrac{\beta d_b}{2L\tan\alpha} + \dfrac{(1-\beta)L'}{L}\right)\right)} \tag{3.14}$$

where the numerator also represents the joint nominal shear force $V_{jh} = A_e\sqrt{p_t^{\,2} - \dfrac{p_t N}{A_g}}$ as displayed in Eq. 3.3 (A_g being the column gross section and A_e being the effective joint area).

Alternatively, according to Eq. 3.12, a relationship between a given beam moment at the joint interface M_{bc} and corresponding inter-storey shear V_c can be written as:

$$V_c = \frac{M_{bc}/jd_b}{\left(2 - \frac{2\beta H_c}{(L_n + d_c)\tan\alpha} - \frac{H_c(L_n - 2L')}{jd_b(L_n + d_c)}\left(1 - \frac{\beta d_b}{2L\tan\alpha} + \frac{(1-\beta)L'}{L}\right)\right)} \tag{3.15}$$

As a result, the modified hierarchy strength could be plotted within V_c-N performance domain when the critical values of limit states are properly defined. The appropriate step-by step-design procedure, based on the modified hierarchy strength, is discussed in the following section.

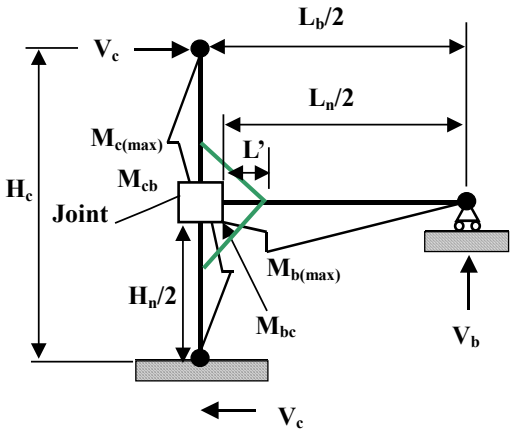

(a) Bending moment distribution

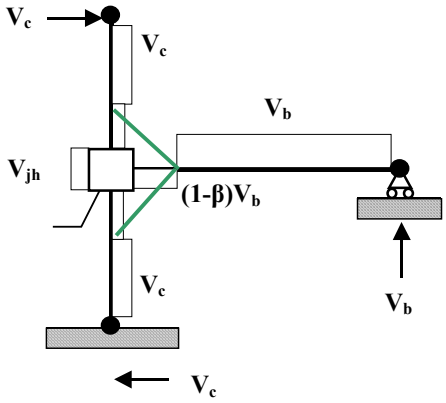

(b) Internal shear force diagram

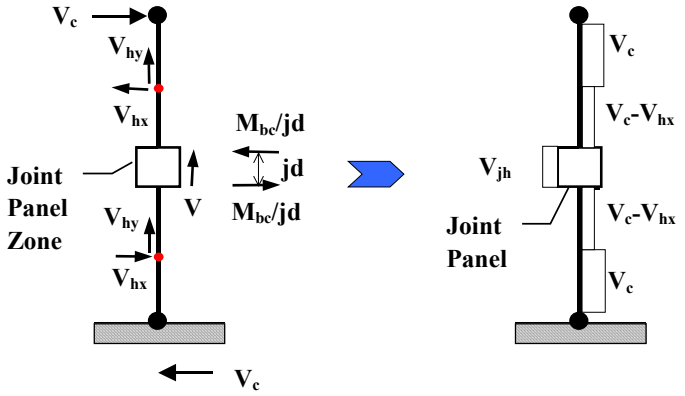

(c) Induced nominal horizontal shear force in the joint

Fig. 3.7 Free body diagram of haunch retrofitted subassembly and column shear force distribution

3.4.3 Step-by-step Design Procedure

The following steps present the proposed design procedure that utilizes the iterations on selecting haunch-designed parameter to achieve the retrofitting purpose.

Step 1: Preliminary choice of haunch properties. A preliminary selection of the design parameters of the haunch retrofitting scheme L', α and K_d is first required. Practically speaking, higher values of α are suggested to be more effective choices for quicker convergence to feasible solutions. In addition, the lowest value of L' is preferred to reduce the invasiveness of the retrofit strategy. Since the value of K_d is determined by the choice of the haunch element sections and materials, more than one combination of the haunch properties may achieve the designed value and it is suggested to investigate a number of possible combinations.

Step 2: Definition of acceptable damage/limit states in the joint. Since principal stresses are the more reliable criteria than nominal shear stresses to predict the joint response, similar to assessing the joint capacity of as-built assemblies, the starting point of the design scheme is to define the acceptable stress level in the joint on the basis of principal tensile stress p_t or principal compression stress p_c. With substituting the given critical principal tensile stress at different limit state level (Table 3.1) into Eq. 3.14, the inter-storey shear capacity $\overline{V}_{c,joint}$ corresponding to the occurrence of a defined level of shear or principal tensile stress demand (i.e. damage) is given by:

$$\overline{V}_{c,joint} = \frac{A_e\sqrt{p_t^{\,2} - \dfrac{p_t N}{A_g}}}{\left(1 - \dfrac{\beta H_c}{(L_n + d_c)\tan\alpha} - \dfrac{H_c(L_n - 2L')}{jd_b(L_n + d_c)}\left(1 - \dfrac{\beta d_b}{2L\tan\alpha} + \dfrac{(1-\beta)L'}{L}\right)\right)} \tag{3.16}$$

Alternatively, if the joint moment capacity $M_{bc}^{\,*}$ corresponding to the given principal tensile stress p_t is available by solving Eq. 3.12, the inter-storey shear capacity can also be expressed as:

$$\overline{V}_{c,joint} = \frac{M_{bc}^{*} / jd_b}{\left(2 - \frac{2\beta H_c}{(L_n + d_c)\tan\alpha} - \frac{H_c(L_n - 2L')}{jd_b(L_n + d_c)}\left(1 - \frac{\beta d_b}{2L\tan\alpha} + \frac{(1-\beta)L'}{L}\right)\right)} \tag{3.17}$$

Step 3: Force the development of a plastic hinge in the beam. To force the beam hinge occur, the maximum moment at the haunch connection $M_{b(max)}$ is required to reached the yielding moment capacity of the beam $\overline{M}_{by}$. In this situation, the corresponding moment in the beam at the joint interface M_{bc} is obtained simply by substituting $M_{b(\max)} = \overline{M}_{by}$ into Eq. 3.7. Similarly, through substituting $M_{b(\max)} = \overline{M}_{by}$ into Eq. 3.6, the equivalent inter-storey shear corresponding to the development of a plastic hinge in the beam is given by:

$$\overline{V}_{c,beam-hinge} = \overline{M}_{by}\frac{\left(1 + \left(d_c + 2L'\right)/\left(L_n - 2L'\right)\right)}{H_c} \tag{3.18}$$

In order to assure that the development of a plastic hinge in the beam occurs before a predefined level of damage is suffered by the joint, the following capacity design equation must be met:

$$\overline{V}_{c,beam-hinge} \le \Phi_1 \cdot \Phi_2 \overline{V}_{c,joint} \tag{3.19}$$

Step 4: Check column is not hinging prior to beam or joint. To avoid undesired column flexural failure, it is important to recall that the development of the plastic hinge in the beam should occur before the maximum moment in the column $M_{c(max)}$ reaches the column yielding capacity $\overline{M}_{cy}$ by ensuring that:

$$\overline{V}_{c,beam-hinge} < \Phi_1 \overline{V}_{c,column-hinge} < \Phi_2 \overline{V}_{c,joint} \tag{3.20}$$

where $\overline{V}_{c,\ col-hinge}$ is the equivalent inter-storey shear (subassembly lateral force) corresponding to the development of a plastic hinge in the column and given by:

$$\overline{V}_{c,col-hinge} = \frac{\overline{M}_{cy}}{\left(H_c/2 - d_b/2 - L'\tan\alpha\right)} \tag{3.21}$$

Step 5: Final check of shear capacity in members and control of global hierarchy strength and sequence of event. To satisfy Eq. 3.10, the final check is required to ensure the shear capacities of beam and column are strong enough to resist the shear demand that develops in these elements of the retrofitted subassembly when the beam flexural mechanism occurs. It is important to understand that the chosen beam elements used to check the shear capacity is β-dependent since the greater shear demand in the beam is located at one side of haunch close to the beam end if β<2 and the other side of haunch close to the joint connection if β>2. The equivalent inter-storey shear capacity $\overline{V}_{c,beam-shear}$ causing the beam shear failure is given as:

$$\text{If } \beta<2$$
$$\overline{V}_{c,beam-shear} = \frac{\overline{V}_b(L_n + d_c)}{2H_c} \tag{3.22}$$

and

$$\text{If } \beta > 2$$
$$\overline{V}_{c,beam-shear} = \frac{\overline{V}_b(L_n + d_c)}{2H_c(\beta - 1)} \tag{3.23}$$

where $\overline{V}_b$ is the shear strength of the designed beam section where the haunch is located. Moreover, it is understood that the inter-storey shear force $\overline{V}_{c,col-shear}$ of causing column shear failure is treated to be equal to the shear strength $\overline{V}_c$ of the designed column section. Through reviewing the typical code provisions of either design or assessment, it is also noted that concrete contribution should be neglected when evaluating the shear capacity within a plastic hinge region as for the retrofitted example in beams. To increase the shear capacity of beam and column during the design procedure, using fibered reinforce polymers FRP as given in section 2.5.1 is a practicable solution.

Step 6: Iteration process. With a set of design parameter in Step1, the design procedure is supposed to be followed in sequence. Once either one of Step 2-4 are not satisfied, iteration process that consists of redefining the design parameter (Step1) is reviewed until the whole design procedure is achieved. If certain parameters of the system make it unfeasible for all the

steps to be met, alternative hybrid retrofit can be combined with the proposed haunch to meet the design requirements. In the existing under-designed column or beam that the shear capacity is not sufficient to guarantee a proper inversion of the hierarchy strength with the formation of a flexural hinge in the beam, for example, FRP composite materials in the form of strips, sheets, or rods as well as other forms of local jacketing (i.e. steel plates) could be a simple solution, Furthermore, vertical post-tensioned bars or externally mounted surface could be adopted to increase the shear (as well as flexural) capacity of the column (as well as joint). More practical design details that follow the step-by-step design procedure are described in Chapter 6.

3.4.4 Energy Dissipating Elasto-plastic Haunch Element

Considering the haunch element with a designed yielding or slipping strength F_s, the haunches will exhibit an elasto-plastic hysteresis as extra energy dissipating devices and improve the global behaviour of buildings by absorbing earthquake energy. Assuming that the given F_s reaches before the beam plastic hinge occurs, up to this point, the moment and shear distribution in the beam follows the distribution presented in Fig. 3.7 but $\overline{M}_{by}$ is not achieved yet. The joint subassembly still remains elastic so that the internal forces increase with increasing inter-storey shear V_c even if the elasto-plastic behaviour with a certain energy-dissipating pattern is observed in the haunch devices. The beam flexural hinge occurs while the increased V_c causes the $\overline{M}_{by}$ being reached. Therefore, F_s must be chosen carefully such that joint moment M_{bc} would not reach the critcal value M_{bc}^* (or p_t is lower than the critical value of limit state level) before the beam yielding such that the joint damage is guaranteed to be avoided.

3.5 DEFORMATION COMPATIBILITY: EVALUATION OF THE β-VALUE

3.5.1 General

The shear transferring coefficient, β-factor, is fist introduced in the analytical model of retrofitting the steel moment connection with one welded haunch [Yu, Uang and Gross, 2000]. To completely define moments and shears in beams and columns, as illustrated in Fig. 3.5, the

critical factor β is required to be properly determined. The value of β is estimated by writing deformation compatibility equations that describe the compatible axial deformation of the haunch with the local displacement between points in the column and beam where the haunch is connected. The axial, flexural and shear deformations in both beams and columns as well as joint elastic shear deformations would be involved to completely formulate the deformation compatibility equations. According the relative stiffness of elements and relative contribution of these deformations to the total local deformation, the equations are simplified by neglecting some of these contributions. First derivation of the β-factor of the proposed model with a (single) haunch retrofit solution, considering the beam flexural deformation only for simplicity, has been presented by Yu [Yu, Uang and Gross, 2000]. This concept is extended to consider the column and joint deformation in obtaining the value of β-factor while the configuration of two haunches on the top and bottom is the proposed retrofit solution in this research. The effectiveness of β-factor derived with different models is discussed in the following section when the influence of variables such as haunch stiffness and haunch geometry in the formulas is also investigated and described in the design charts.

3.5.2 Development of Deformation Compatibility Conditions for Steel Frame with Haunch Systems

On the basis of one welded haunch on the bottom of the beam, the analytical method to derive the β-factor with deformation comparability theory is proposed with the model of the steel moment connection as shown in Fig. 3.8 and Fig. 3.9 [Yu, Uang and Gross, 2000]. The horizontal and vertical component of the beam deformation at the haunch tip (Point B) that is influenced by haunch stiffness K could be computed with given V_{pd}. With the bending moment diagram in Fig. 3.5 similar to that introduced previously with two haunch elements, the beam bending moment in the haunch region could be expressed in x defined as the distance of the beam section measuring from the haunch tip toward the column face.

$$M(x) = (L'/2 + x)V_{pd} - x(\beta V_{pd}) - (\beta V_{pd} / \tan\theta)\frac{d}{2} \tag{3.24}$$

According the mechanics of materials, the compressive stress in the beam bottom flange is derived by the bending moment together with the beam axial force ($\beta V_{pd}/tan\theta$ in Fig. 3.9) and given as follows:

$$\sigma(x) = \frac{(L'/2 + x)V_{pd}}{I_b}\left(\frac{d}{2}\right) - \frac{x(\beta V_{pd})}{I_b}\left(\frac{d}{2}\right) - \frac{(\beta V_{pd}/\tan\theta)}{I_b}\left(\frac{d}{2}\right)^2 - \frac{\beta V_{pd}/\tan\theta}{A_b} \quad (3.25)$$

The horizontal component u_B of the beam deformation at the haunch tip is equal to the axial shortening of the beam bottom flange in the haunch region.

$$u_B = \int_0^a \frac{\sigma(x)}{E_s}dx = \left(\frac{L'/d - (\beta/\tan\theta)}{E_s I_b}\left(\frac{d}{2}\right)^2 a + \frac{(1-\beta)a^2}{2E_s I_b}\left(\frac{d}{2}\right) - \frac{\beta a/\tan\theta}{E_s A_b}\right)V_{pd} \quad (3.26)$$

The moment-area method, where the moment along the beam is expressed in Fig. 3.9, is used to estimate the vertical component v_B of the beam deformation at the haunch tip.

$$v_B = \int_0^a \frac{xM(x)}{E_s I_b}dx = \left(\frac{L'/d - (\beta/\tan\theta)}{E_s I_b}\left(\frac{d}{4}\right)a^2 + \frac{(1-\beta)a^3}{3E_s I_b}\right)V_{pd} \quad (3.27)$$

Based on the components u_B and v_B of the haunch tip displacement, the shortening of haunch δ_h can be determined by:

$$\begin{aligned} \delta_h &= \sqrt{(a-u_B)^2 + (b-v_B)^2} - l_h \approx u_B\cos\theta + v_B\sin\theta \\ l_h &= \sqrt{a^2+b^2} \end{aligned} \quad (3.28)$$

where l_h is the original length of haunch and higher-order terms for the small deformation theory is ignored to simplify the equation. By taking the haunch as a free body, the axial shortening of haunch δ_h can be estimated by the haunch axial force that is equal to $\beta V_{pd}/\sin\theta$. As a result, the relationship of haunch axial deformation is given by:

$$\delta_h = u_B\cos\theta + v_B\sin\theta = \frac{\beta V_{pd}/\sin\theta}{E_s A_h}l_h \quad (3.29)$$

By solving the above equation, β is obtained in the following expression:

$$\beta = \frac{b}{a}\left(\frac{3L'd + 3ad + 3bL' + 4ab}{3d^2 + 6bd + 4b^2 + \frac{12I_b}{A_b} + \frac{12I_b}{A_h\cos^3\theta}}\right) \quad (3.30)$$

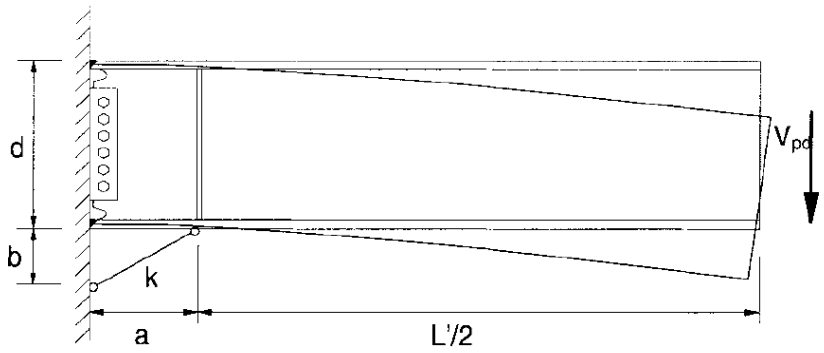

Fig. 3.8 Deformation model of the haunch by a given V_{pd} [Yu, Uang and Gross, 2000]

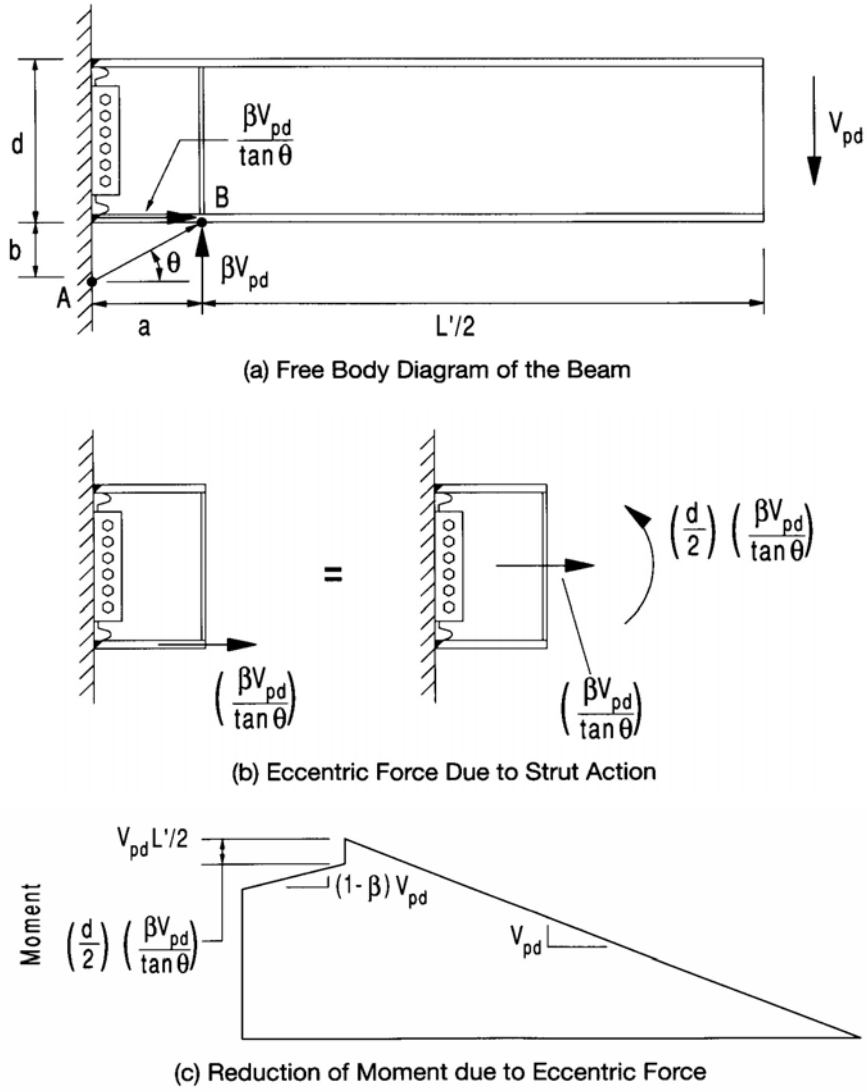

Fig. 3.9 Free body and moment diagrams of haunch reinforced beam [Yu, Uang and Gross, 2000]

3.5.3 Derivation of β-factor by Considering The Exterior Concrete Joint Retrofitted with Two Haunches

To investigate β-factor for the exterior reinforced concrete beam-column subassembly, the similar models considering different contribution of elastic deformation are developed with two haunch retrofitting assumption. Adapting the above concept of the beam flexural deformation only, the expression of β-factor for RC frames can be derived [Pampanin and Christopoulos, 2003]:

Assumption: Beam flexural deformation only 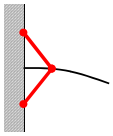

$$\beta = L'\left(\frac{-6Ld_b\sin\alpha\cos\alpha - 3L'd_b\sin\alpha\cos\alpha - 6L'L + 6L'L\cos^2\alpha - 4L'^2 + 4L'^2\cos^2\alpha}{-3\cos^2\alpha d_b^{\,2}L' - 6d_bL'^2\sin\alpha\cos\alpha - 4L'^3\cos^2\alpha - 12EI_b/(2K_d)}\right) \quad (3.31)$$

According to the retrofit configuration in Fig. 3.6, a simpler expression obtained by substituting $a=L'$ and $b=L'\tan\alpha$ in Eq. 3.31 can be given as Eq. 3.32 that considers only the beam flexural deformation to trigger the haunches.

$$\beta = \left(\frac{b}{a}\right)\cdot\frac{6Ld_b + 3ad_b + 6bL + 4ab}{3d_b^{\,2} + 6bd_b + 4b^2 + \dfrac{12EI_b}{2K_d a\cos^2\alpha}} \quad (3.32)$$

Although this equation is adequate for the frames where column deformations are smaller, column flexural deformations and joint shear deformations are more significant for existing pre-1970s frame systems where columns and joints were designed only considering gravity loads. The similar simulated model is illustrated in Fig. 3.10 where the top and bottom haunches are proposed to be symmetrical and have the same stiffness. Therefore, the total shear force βV_b is equally provided by the top and bottom haunches and no axial load caused by the haunch is introduced in the beam while the elastic deformation is assumed in the beam, column and joint panel. The refined versions of the β-formulation derived for different assumptions are shown as followings where the additional terms (when compared to Eq. 3.31) related to the column flexibility and joint deformation are highlighted in boxes (terms in □)

and parentheses (terms in $\{\ \}$). When the column deformation is included, the β-factor is derived as Eq. 3.33.

Assumption: Beam and column flexural deformation 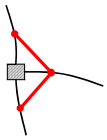

$$\beta = \left(\frac{b}{a}\right) \cdot \frac{6Ld_b + 3ad_b + 6bL + 4ab + \boxed{\frac{2I_bL_bb^3}{I_caH_c} + \frac{3I_bHL_bb^2}{I_caH_c} + \frac{3I_bd_cL_bb^3}{2I_ca^2H_c} + \frac{3I_bd_cHL_bb^2}{I_ca^2H_c}}}{3d_b^{\,2} + 6bd_b + 4b^2 + \frac{12EI_b}{(2K_d a\cos^2\alpha)} + \boxed{\frac{6I_bb^2}{a^2A_c} + \frac{2I_bb^3}{I_ca} + \frac{3I_bd_cb^2}{I_ca^2} + \frac{3I_bd_c^{\,2}b^3}{2I_ca^3}}} \quad (3.33)$$

When the joint flexibility is also included, the complete formulation of the β-factor is given as Eq. 3.34.

Assumption: Elastic deformation is assumed for the beam, column and joint 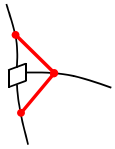

$$\beta = \left(\frac{b}{a}\right) \cdot \frac{\begin{array}{l} 6Ld_b + 3ad_b + 6bL + 4ab + \boxed{\frac{2I_bL_bb^3}{I_caH_c} + \frac{3I_bHL_bb^2}{I_caH_c} + \frac{3I_bd_cL_bb^3}{2I_ca^2H_c} + \frac{3I_bd_cHL_bb^2}{I_ca^2H_c}} + \\ + \left\{\frac{12EI_b}{K_ja}(b + \frac{d_b}{2})(a + \frac{d_c}{2} + L)\right\} \end{array}}{\begin{array}{l} 3d_b^{\,2} + 6bd_b + 4b^2 + \frac{12EI_b}{(2K_d a\cos^2\alpha)} + \boxed{\frac{6I_bb^2}{a^2A_c} + \frac{2I_bb^3}{I_ca} + \frac{3I_bd_cb^2}{I_ca^2} + \frac{3I_bd_c^{\,2}b^3}{2I_ca^3}} + \\ + \left\{\frac{12EI_bb}{K_ja}(b + \frac{d_c}{2})(1 + \frac{d_b}{2b} + \frac{d_c}{2a})\right\} \end{array} \quad (3.34)$$

where $K_j = G\left(\frac{jd_bH_c}{H_c - jd}A_c\right)$ (Joint Rotational Stiffness)

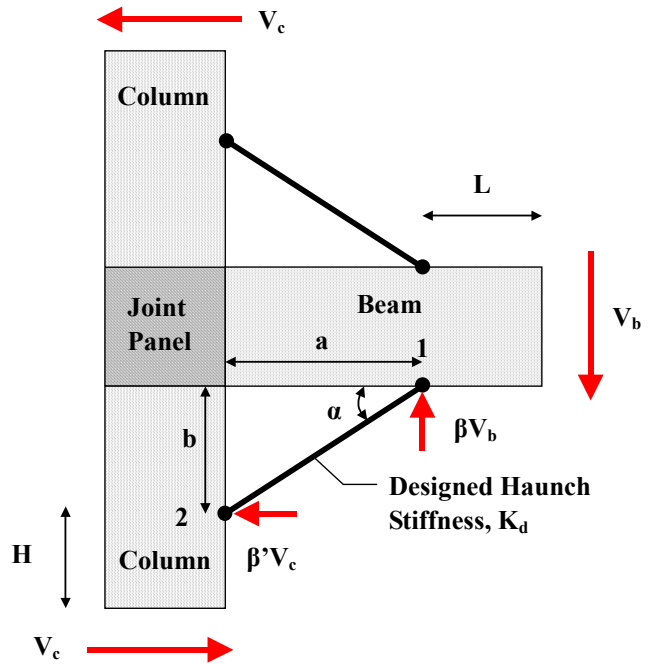

Where $V_c=V_bL_b/2H_c$ $\beta=\beta'(\tan\alpha)L_b/H_c$ $L=L_n-2a$ $H=H_n-2b$

Fig. 3.10 Deformation compatibility model for exterior joint retrofitted by two symmetrical haunches

3.5.4 Investigation of Designed Variables

To evaluate the effectiveness of formulations for β-factor, a comparison between theoretical predictions using equations (through Eq. 3.31 to Eq. 34) and numerical results from SAP2000 where the analytical model of the retrofitted beam-column joint is established to simulate the beam, column and joint elastic deformation. The comparison is carried out in three cases: (1) β-factor vs. angle α with fixed L' and K_d, (2) β-factor vs. haunch stiffness K_d with fixed α and L' and (3) β-factor vs. haunch position L' with fixed α and K_d and the properties of the beam-column joint for formulating and modelling in Sap2000 are detailed in Table 3.1.

Table 3.3 Properties of the beam-column joint used in β-factor formulation and SAP2000

E: 28.7Gpa, E_s: 200Gpa, L_b:3000mm, H_c: 2000mm					
Beam (200x330)		**Column (230x230)**		**Joint**	
d_b(mm)	330	d_c(mm)	230	K_j(kNm/rad)	236000
A_b(mm^2)	66000	A_c(mm^2)	52900		
I_b(mm^4)	1.38x10^8	I_c(mm^4)	0.8x10^8		
L_b(mm)	2770	H_c(mm)	1670		
Case1: L'=200, K_d=100000kN/m					
Case2: L'=400, α=45˚					
Case3: α=45˚, K_d=100000kN/m					

Note: I_b and I_c present the effective second moment inertia of beam and column respectively

Figure. 3.11 illustrates the comparison between the different formulations of the β-factor when the numerical results from Sap2000 are also presented to validate the effectiveness of the derived formulations. It is interesting to note that the values of β evaluated from a beam-only-flexibility tend to be lower (up to 15-20%) than the corresponding values calculated including the column deformability, thus underestimating the efficiency of the added haunch in protecting the panel zone (conservative) as well as the shear forces developed in the structural elements (not conservative). However, the values of β obtained from different formulations with the column or the column and joint deformation included are very close the values obtained using the SAP2000 model. It can also been seen that neglecting the joint deformation in predicting values of the β-factor is practicable when the column deformations are included. From case 1, it is noted that there is more difference between the value of β obtained by formulation assuming the beam deformation only and numerical results with increasing design angle α. The reason for this phenomenon is that the neglected column deformations involved in evaluating β-factor have more impact with increasing design angle α while the haunch location in the beam is fixed. On the other hand, as shown in case 2, changing haunch stiffness K_d would not significant affect the efficiency of formulation with beam deformations only to predict values of β. Similarly, since the column deformations compared with beam deformations have less impact on beam-deformation-only formulation with increasing haunch location L' and fixed α, the smaller difference of values obtained between the formulation and SAP2000 is presented with larger L'.

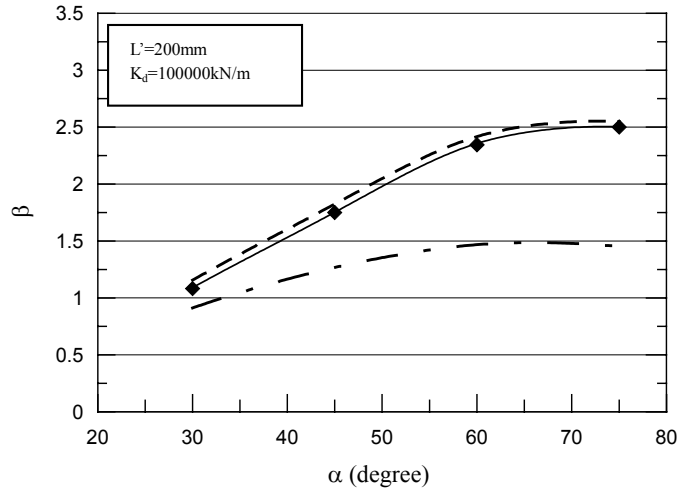

(a) Case 1: β-factor versus angle α with fixed L' and K_d

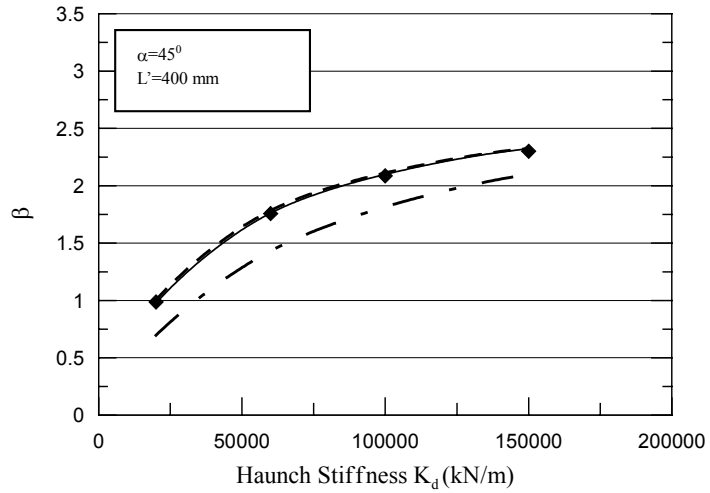

(b) Case 2: β-factor versus. haunch stiffness K_d with fixed α and L'

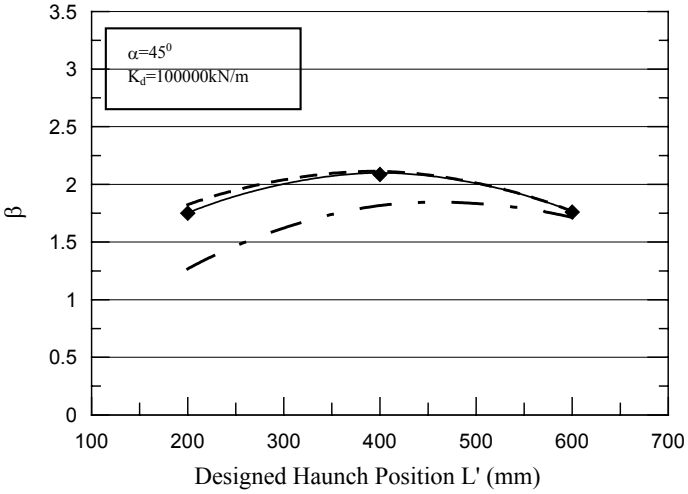

(c) Case 3: β-factor versus haunch position L' with fixed α and K_d

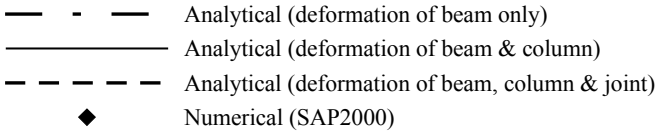

Fig. 3.11 Comparison between alternative formulations of the haunch β-factor

3.6 UTILIZATION OF THE DESIGN PROCEDURE BY SIMPLE DESIGN CHARTS

By evaluating the equivalent horizontal shear capacity V_c for different failure mechanism, the full step-by-step design procedure can be simplified and followed through the visualization of accessing the hierarchy strength similar to the described methodology in accessing as-built subassemblies. This practical design procedure utilized the visualization of the hierarchy strength can be achieved by availability of sufficient design charts before starting design procedure. To target the designed haunch, the appropriate design charts are exploited with capacity design philosophy.

While reviewing Step1 in Section 3.4.3, the design charts with different design values of the haunch parameters position *L'* and design angle α, as illustrated in Fig. 3.12, are available with a guessing value of β by plotting the hierarchy strength in V_c-N performance domain through Eq. 3.17, Eq. 3.18 and Eq. 3.21 (i.e. using the properties given in Table 3.1). By comparing the proposed demand curve plotted on the performance domain with $\overline{V}_{c,beam-hinge}$, a proper *L'* can be selected to achieve the goal in Step 3. Within that design chart of the selected *L'*, the goal of Step 2 and Step 4 that check the column and joint capacity is reached by determining the adequate α value while the comparison between the capacity and demand curve is exploited again. After checking Step 5 in the design procedure, the proper haunch retrofit design can be completed by determining the haunch stiffness K_d through checking the formulated curve of β-factor vs. K_d in Fig. 3.13. Since the values of β, α and *L'* are selected in the previous steps, the haunch stiffness K_d is already determined by the formulation (Eq.3.31).

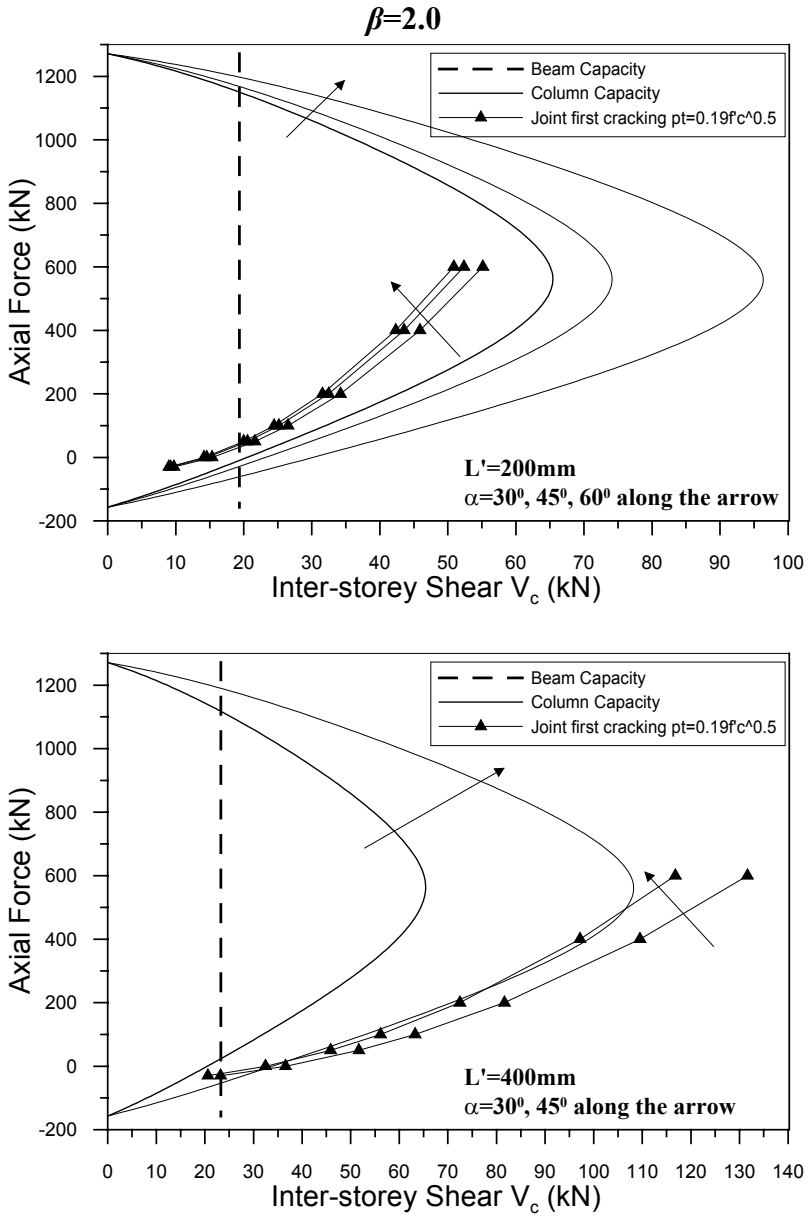

Fig. 3.12 Design charts with different values of design parameters as β=2.0

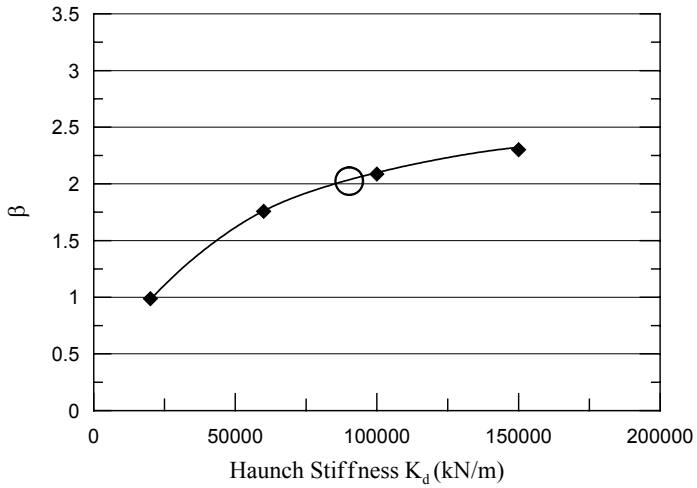

Fig. 3.13 Design of haunch stiffness by using β-factor versus K_d design chart (β=2.0)

CHAPTER 4

EXPERIMENTAL PROGRAM OF THE AS-BUILT SPECIMEN

4.1 INTRODUCTION

Because of inadequate reinforcing details and lack of capacity design principles, the typical structure deficiencies of existing buildings designed with gravity-loads-only have been emphasized on the joint shear failure that caused the brittle mechanism of low ductility and inadequate strength degradation for the local and global performance. Due to the scarce information regarding the seismic behaviour of the existing beam-column joints, more experimental investigation of the beam-column joint subassemblies that commonly existed in New Zealand before introduction of seismic-oriented code in pre-1970s were required. Several exterior beam-column joint subassemblies of the existing buildings typical in New Zealand were constructed in 2/3 scales and experimentally tested under simulated quasi-static loading in the laboratory of Canterbury University (Fig. 4.1).

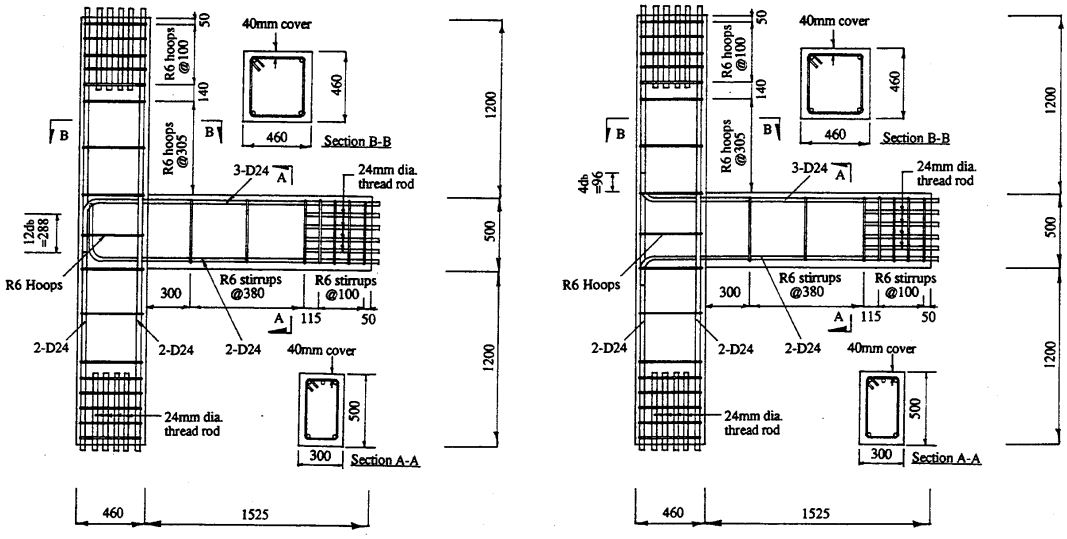

Fig. 4.1 Typical pre-1970s reinforced concrete beam-column joint in New Zealand [Hakuto, 1995]

In order to investigate the behaviour of the reinforced concrete beam-column joints built in the 1970s in New Zealand, several 2/3 scaled beam-column joint subassemblies were constructed in the laboratory. The reinforcing detail of the test specimens and experimental

configuration are illustrated in this chapter. One or no stirrup in the joint cores were used to present the feature of poor shear reinforcement in the existing beam-column joint. Based on the same beam capacity, the subassemblies with deep or shallow beams were constructed to investigate the effect of shallow beams on the joint behaviour in 2-D level. The bi-directional loading was also applied on the corner joint to evaluate the impact of the spandrel beam to the corner joint in 3-D level. The purpose of investigation on biaxial 3-D test was to compare the difference of seismic response in the corner joint between one-way and two-way frame systems. According to the hierarchy strength diagram together with considering the varying axial load in the column, the expected sequence of events was evaluated through the comparison of capacity and demand curve.

4.2 TEST SPECIMENS

Experimental tests of seven as-built subassemblies were carried out in the laboratory. These specimens as named in Table 4.1 will be detailed with the reinforcing arrangement, configurations and material properties in the following sections.

Table 4.1 Description of specimens

Abbreviation	Description of Specimens
TDP1	2-D subassembly with a deep beam of unbalanced reinforcement by using plain bars
TDD1	2-D subassembly with a deep beam of unbalanced reinforcement by using deformed bars
TDP2	2-D subassembly with a deep beam of balanced reinforcement by using plain bars
TDD2	2-D subassembly with a deep beam of balanced reinforcement by using deformed bars
TSP1	2-D subassembly with a shallow beam of unbalanced reinforcement by using plain bars
TSD1	2-D subassembly with a shallow beam of unbalanced reinforcement by using deformed bars
DD2	3-D subassembly with two spandrel beams of symmetric reinforcement by using plain bars

4.2.1 Specimen Detail of Beam-column Joint Subassemblies

2-D Unit:

Six 2/3-scaled existing beam-column joint subassemblies, referred to the typical design in New Zealand before pre-1970s, were experimentally investigated into the seismic response of different reinforcing detail (i.e. use of plain round or deformed reinforcement) and beam typology (i.e. deep beam or shallow beam). All exterior beam-column joint subassemblies of

the same designed column capacity have the identical features of beam span length, column storey height and one shear reinforcement in the joint core while the longitudinal reinforcement details are different for each specimen. Table 4.2 summarizes the test specimens and Fig. 4.2 to 4.7 show the dimensions and reinforcement details of all specimens. Grade300 steel was used for all longitudinal reinforcement of 10mm diameter and transverse reinforcement of 6mm diameter while the longitudinal deformed bars were used in TDD1, TDD2 and TSD1 but the longitudinal plain round bars were used in TDP1, TDP2 and TSP1. The columns in all specimens had the same cross section of 230mm deep and 230mm wide while the deep beams presented in TDP1, TDD1, TDP2 and TDD2 had the cross section of 330mm deep and 200mm wide but the shallow beams presented in TSP1 and TSD1 had the cross section of 133mm deep and 533mm wide. The transverse reinforcement was spaced at 133mm in the beams and 100mm in the columns where all first stirrups were located at 50mm from the face of columns and beams. A single stirrup corresponding to the insufficient shear reinforcement was placed in the middle of each joint core and investigated into the influence on the joint response. The designed concrete compressive strength for the 2-D as-built specimens was 23MPa with normal weight.

Table 4.2 Summary of test specimen

Specimen		**TDP1**	**TDD1**	**TDP2**	**TDD2**	**TSP1**	**TSD1**
Beam	**Size**	200x330	200x330	200x330	200x330	533x133	533x133
	Top Bars	4-R10 (ρ'=0.52%)	4-D10 (ρ'=0.52%)	4-R10 (ρ'=0.52%)	6-D10 (ρ'=0.79%)	12-R10 (ρ'=1.64%	12-D10 (ρ'=1.64%
	Bottom Bars	2-R10 (ρ=0.26%)	2-D10 (ρ=0.52%)	4-R10 (ρ=0.52%)	4-D10 (ρ=0.52%)	6-R10 (ρ=0.82%)	6-D10 (ρ=0.82%)
	Stirrups	2-R6@133	2-R6@133	2-R6@133	2-R6@133	2-R6@133	2-R6@133
Column	**Size**	230x230	230x230	230x230	230x230	230x230	230x230
	Main Bars	6-R10 (ρt=0.89%)	6-D10 (ρt=0.89%)	6-R10 (ρt=0.89%)	6-D10 (ρt=0.89%)	6-R10 (ρt=0.89%)	6-D10 (ρt=0.89%)
	Stirrups	2-R6@100	2-R6@100	2-R6@100	2-R6@100	2-R6@100	2-R6@100
Joint	**Stirrups**	2-R6@Middle	2-R6@Middle	2-R6@Middle	2-R6@Middle	2-R6@Middle	2-R6@Middle
Cover to Longitudinal Bar =25mm							

Note: $\rho = A_s/bd$, $\rho' = A_s'/bd$, $\rho t = A_{st}/A_g$, where A_s=area of longitudinal tension reinforcement of beam, A_s'=area of longitudinal compression reinforcement of beam, A_{st}=total area of longitudinal reinforcement of column, b=width of beam, d=distance from extreme compression fibre of concrete to centroid of tension reinforcement of beam, and Ag=gross area of column

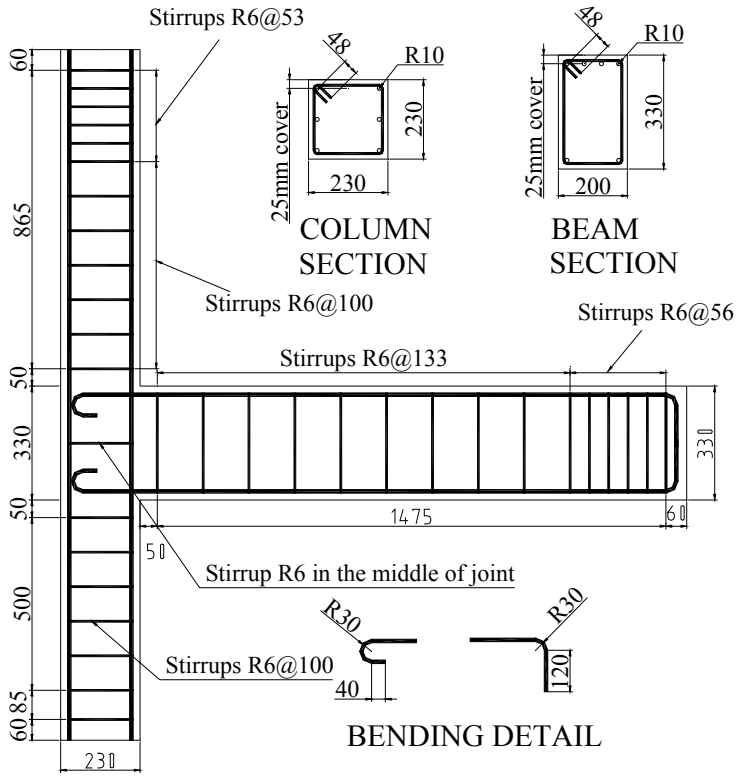

Fig. 4.2 Dimensions and reinforcement details of the as-built specimen TDP1

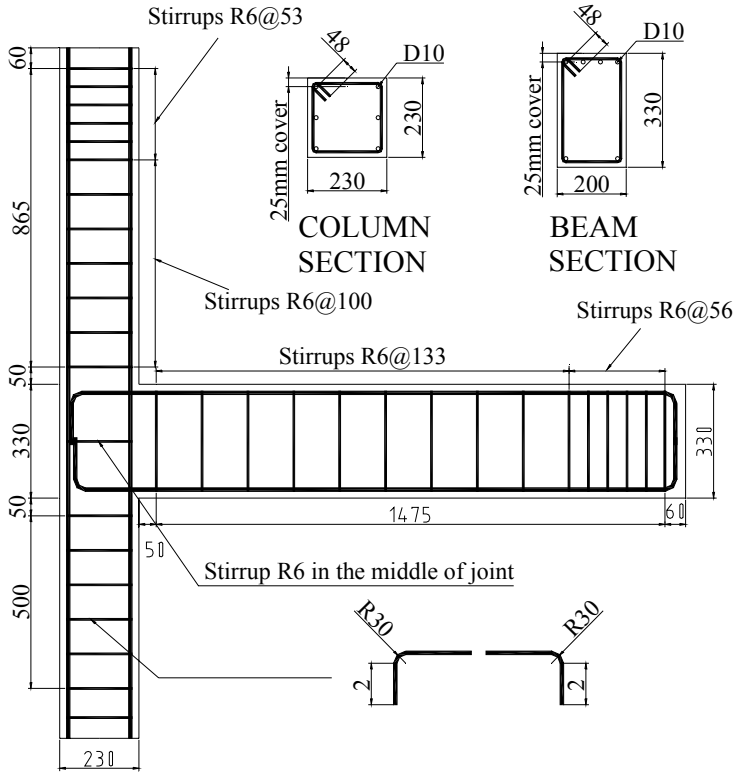

Fig. 4.3 Dimensions and reinforcement details of the as-built specimen TDD1

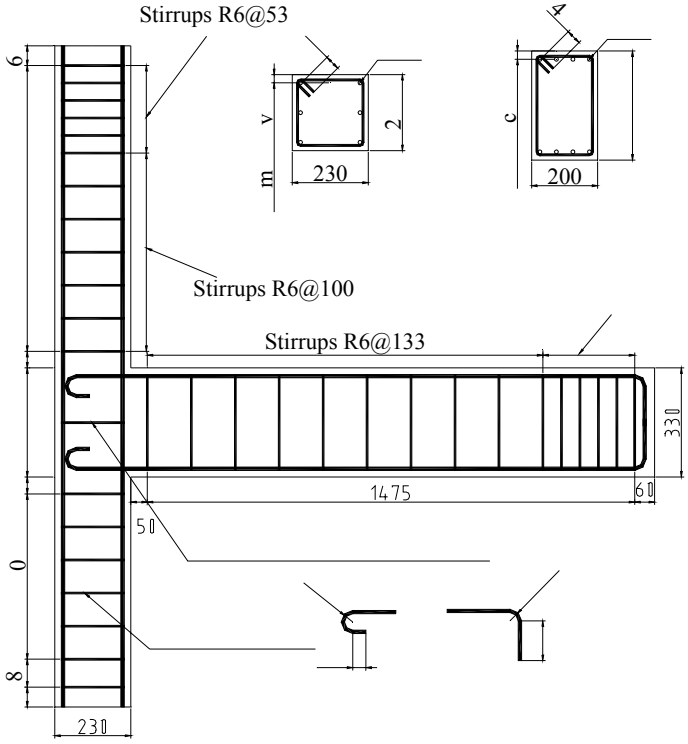

Fig. 4.4 Dimensions and reinforcement details of the as-built specimen TDP2

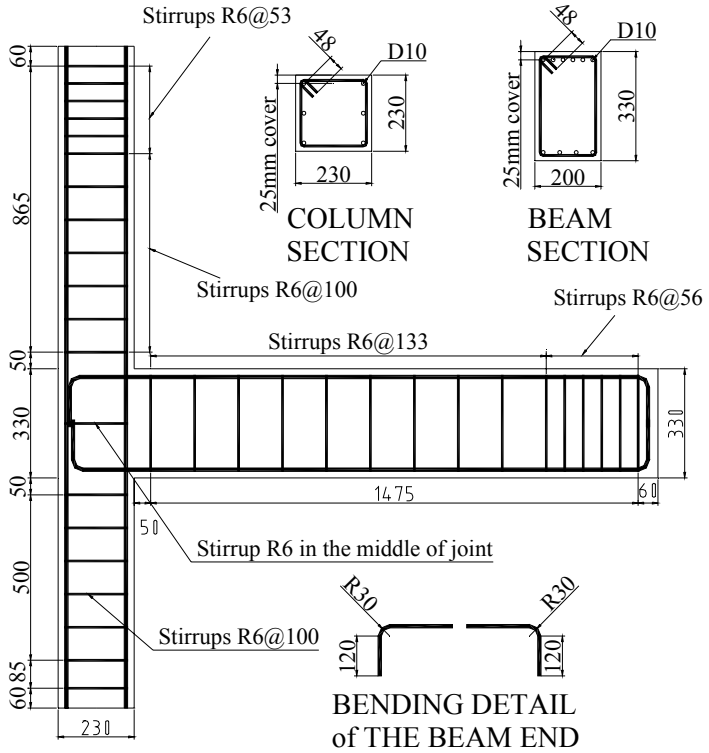

Fig. 4.5 Dimensions and reinforcement details of the as-built specimen TDD2

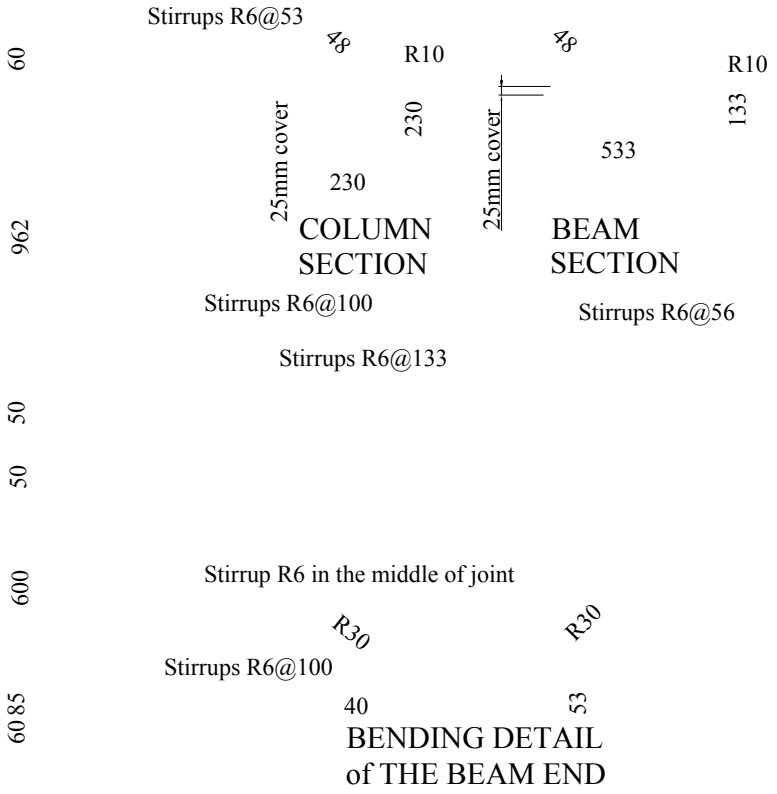

Fig. 4.6 Dimensions and reinforcement details of the as-built specimen TSP1

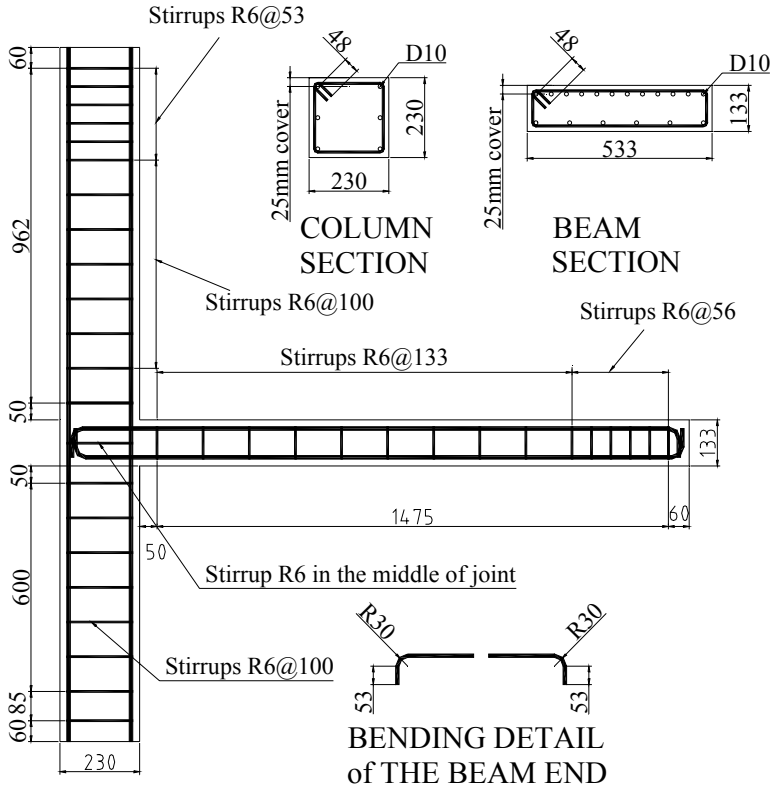

Fig. 4.7 Dimensions and reinforcement details of the as-built specimen TSD1

3-D Unit:

One 3-D existing beam-column joint subassembly, as a spandrel beam connected to the TDP2, is proposed to investigate the response of the corner joint designed with non-seismic practice. The 2/3-scaled beam-column joint subassembly, referred to DD2, has the same beam and column dimensions and similar reinforcing detail with TDP2. As shown in Table 4.3, the cross sections of the beams are both 330mm deep and 200mm wide for the X-direction face and Y-direction face with the column cross section of 230mm deep and 230mm wide. The reinforcing detail of DD2 that is the same for both beams in X and Y-direction faces has transverse reinforcement spacing at 133mm in the beam and 100mm in the column while the first stirrups are located at 50mm away from surfaces of beam and column (Fig. 4.8). It is noted that, unlike TDP2, no shear reinforcement in the joint is applied to decrease joint capacity for the biaxial loading direction test. The plain round bar with Grade300 is used for both longitudinal and transverse reinforcement and 23MPa compressive strength is required for the designed concrete strength.

Table 4.3 Summary of test specimen DD2

Specimen		**DD2**		
		X-direction Face	**Y-direction Face**	**Configuration**
Beam	**Size**	200x330	200x330	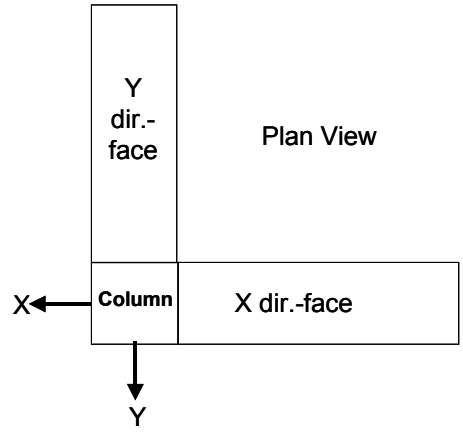
	Top Bars	4-R10 (ρ '=0.52%)	4-R10 (ρ '=0.52%)	
	Bottom Bars	4-R10 (ρ =0.52%)	4-R10 (ρ =0.52%)	
	Stirrups	2-R6@133	2-R6@133	
Column	**Size**	230x230		
	Main Bars	6-R10 (ρ t=0.89%)		
	Stirrups	2-R6@100		
Joint	**Stirrups**	Nil		
Cover to Longitudinal Bar =25mm				

Note: $\rho = A_s/bd$, $\rho' = A_s'/bd$, $\rho t = A_{st}/A_g$, where A_s=area of longitudinal tension reinforcement of beam, A_s'=area of longitudinal compression reinforcement of beam, A_{st}=total area of longitudinal reinforcement of column, b=width of beam, d=distance from extreme compression fibre of concrete to centroid of tension reinforcement of beam, and Ag=gross area of column

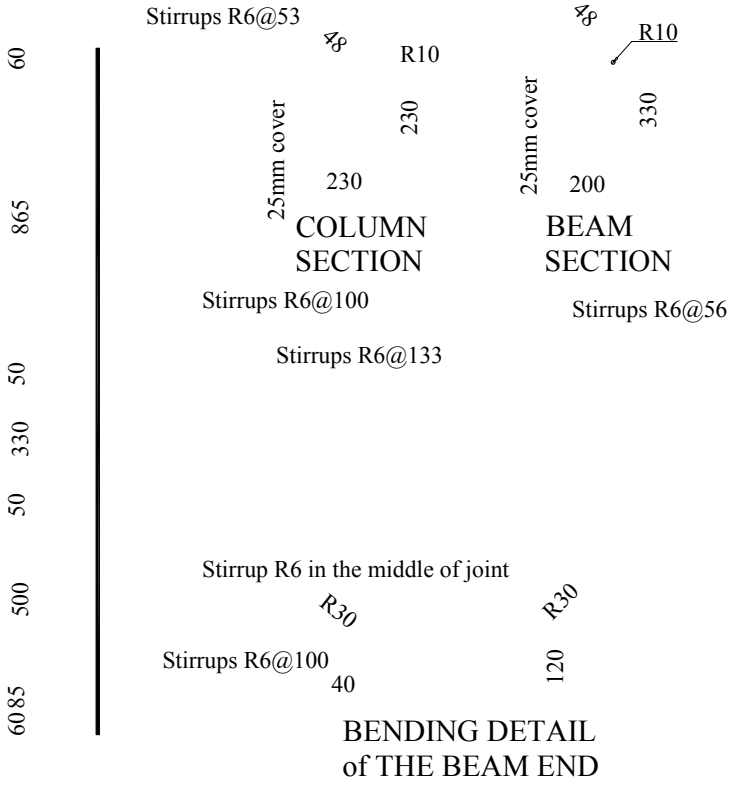

X-DIRECTION FACE

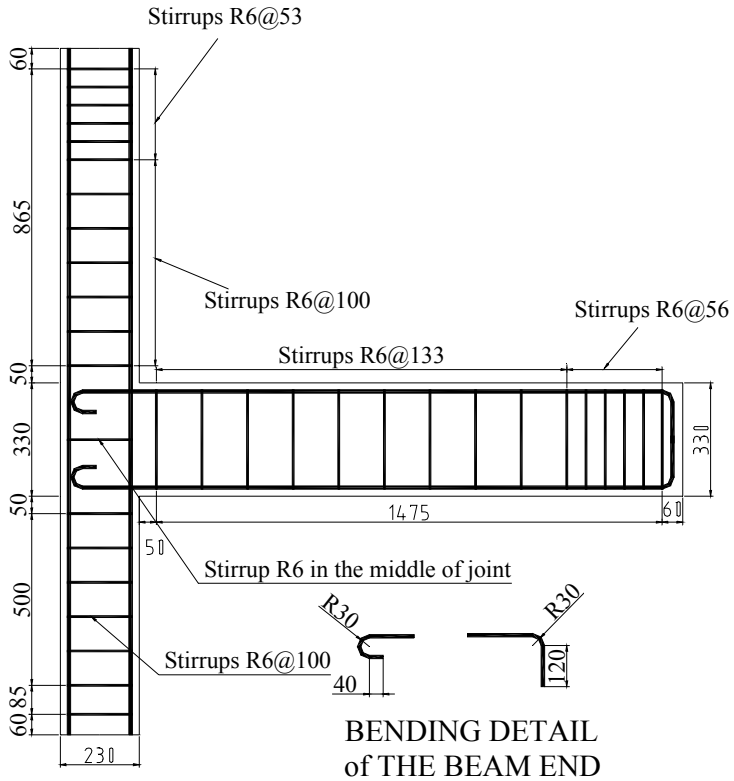

Y-DIRECTION FACE

Fig. 4.8 Dimensions and reinforcement details of the as-built specimen DD2

4.2.2 Material Properties

Reinforcing steel:

Through the monotonic loading tests by an Avery Universal Testing Machine, the measured tensile properties of the reinforcing steel used in the specimens are listed in Table 4.4 where the average value obtained from three samples was presented. The measured yield strengths were larger than the specified values up to 18% for 10mm diameter bars and 40% for 6mm diameter bars respectively.

Table 4.4 Measured reinforcing steel propertied used for specimens

Unit	TDP1, TDD1, TSP1, TSD1			TDP2, TDD2			DD2	
Steel Grade	Grade300			Grade300			Grade300	
Bar Size	R6	R10	D10	R6	R10	D10	R6	R10
Yield Strength f_y(MPa)	424	348	324	408	333	354	396	341
Yield Strain ε_y	2400	1750	1700	2140	1520	1720	2000	1560
Strain Hardening ε_{sh}	25300	23000	25000	22000	21000	21000	10700	26000
Ultimate Strength, f_u(MPa)	495	464	457	482	467	481	485	480
Young's Modulus E_s(GPa)	177	199	191	191	219	206	198	218

Note: R6=plain round bar of 6mm diameter

R10=plain round bar of 10mm diameter

D10=deformed bar of 10mm diameter

Compressive test of concrete cylinder:

Several 100mm diameter x 200mm concrete cylinders were prepared for the compressive test. The test cylinders were cured in a fog room and tested at twenty eight days to obtain the standard compressive strength of the concrete while three cylinders were tested for each specimen just before the experimental testing to obtain the compressive concrete strength f_c' of the tested specimen. The average values for all specimens are listed in Table 4.5. By reviewing the concrete strength test for DD2, the concrete compressive strength obtained at twenty-eight days was a little higher than the value obtained before testing. Because there were only 40 days between two tests, it was reasonable by expecting the experimental tolerance of the obtained value. The higher slump concrete was used to improve workability in casting the 3-D subassembly.

Table 4.5 Measured concrete properties by compressive test specimens

	Slump (mm)	28 days fc'(MPa)	Before Testing fc'(MPa)
TDP1	90	21.3	22.9 (45days)
TDD1	90	21.3	23.3 (50days)
TSP1	90	21.3	23.8 (56 days)
TSD1	90	21.3	24 (59days)
TDP2	75	23.3	25 (51days)
TDD2	75	23.3	24.7 (59days)
DD2	150	28.9	27.4 (40days)

Note: Each value was obtained from the average of three specimens

f_c'=compressive strength of 100mm dia. x 200mm concrete cylinder

E_c=28.7Gpa (Concrete Young's Modulus obtained from the average measured value of three specimens)

4.2.3 Specimen Fabrication

The formwork was made from plywood that could be easily dimensioned. To diminish the buckling and deformation of the formwork, the steel angled and timber blocks were used to stiffen the constructed moulds (Fig. 4.9a). The moulds were sealed along the edge to prevent leaking of the water. Water based and oil based painting was applied in turn on inside-moulds to preclude water penetration and concrete sticking on the formwork.

All the longitudinal reinforcement and the stirrups were cut to length and bent in the factory. The stirrups were tied to the longitudinal bars with steel wires at the proper position (Fig. 4.9b). Through the proper procedure of attachment, the 120ohm electrical strain gauges (Tokyo Sokki FLA-5-11-3L in Fig. 4.9c) were firmly attached on the side of the bar in the critical regions (Fig. 4.9d) to measure the strain in the reinforcement. After drying the waterproof glue covering the strain gauges, the constructed cages were carefully placed in the moulds and fixed at the correct position before casting the concrete (Fig. 4.9e and f).

The concrete was mixed and provided by the commercial plant. The designed 28-day compressive strength was 23MPa and the specified maximum aggregate size was 19mm for all test specimens. During casting concrete, the electrical vibrators were used to well distribute the concrete in the moulds (Fig. 4.8g and h). Before placing the cover for curing, the concrete surface was smoothed by timber strips.

a. Specimen formwork

b. Caging the specimen

c. Strain gauge type

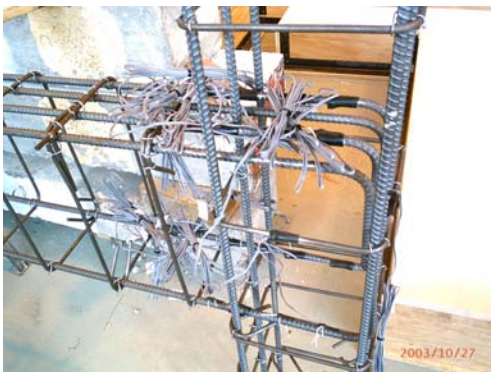

d. Attachment of strain gauges

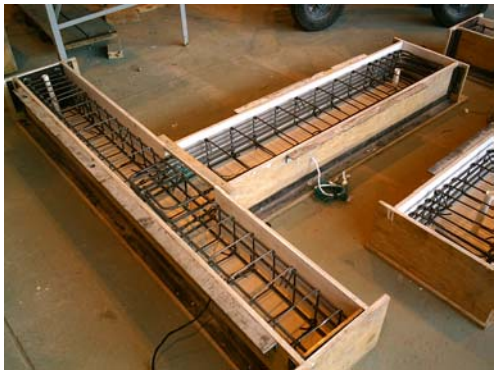

e. The specimen ready for casting

f. Zoom of the critical joint region

g. Concrete casting

h. Vibrating concrete of specimens

Fig. 4.9 Construction of the test specimen for 2-D subassembly

The fabrication procedure of 3-D beam-column joint subassembly was similar to the detail described above for 2-D subassembly. In addition, the vertical close formwork was constructed for vertical casting of concrete (Fig. 4.10). To ensure the concrete well distributed, the electrical vibrators were also used through the pre-opened holes on the top-side formwork of the beam during casting the concrete.

a. Formwork Construction

b. Concrete Casting

Fig. 4.10 Construction of the test specimen for the 3-D subassembly

4.3 TEST SET-UP

4.3.1 Loading System

In 2-D experimental tests, the loading system is designed for simulating quasi-static push-pull experiment as shown in Fig. 4.11. A hinge was simulated at the base of column to allow free rotation while a roller was simulated at the end of beam to allow horizontal displacement and hold against vertical displacement. A rigid reaction frame was set-up on the strong floor. Two actuators were used to simulate the lateral shear force and the varying axial force of column respectively during loading sequence. The bolted tendon was used to clamp and activate the actuator. The load cell of 200kN capacity was placed on the top of column while two 50kN-capacity load cells were connected to the lateral force actuator and the support of beam end respectively. Two transducers were used to measure the travelling distance of the column top and beam end.

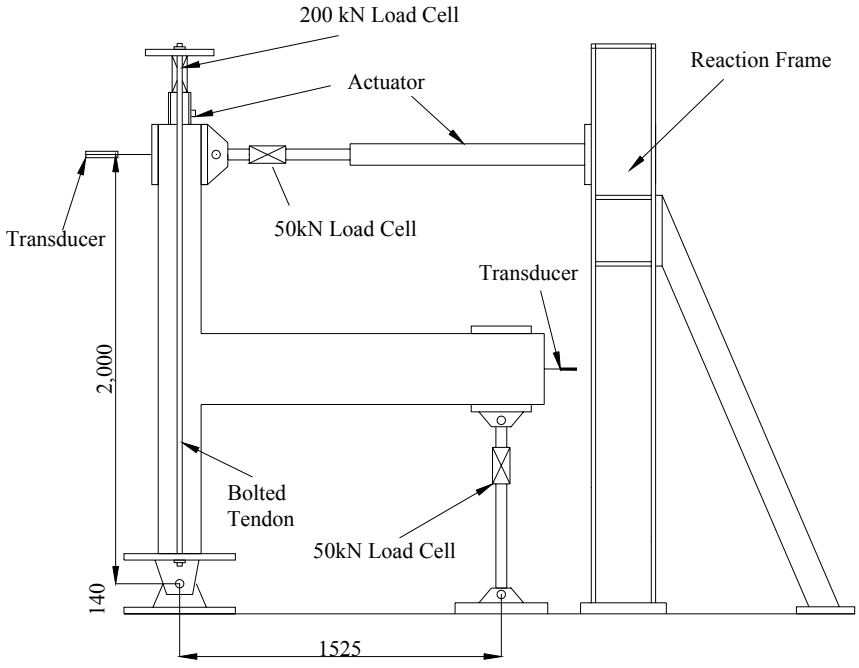

Fig. 4.11 The loading system for 2-D tests

To simulate bi-directional loading system for 3-D test, two orthogonal reaction frames were established in the laboratory (Fig. 4.12). Since the limit of strong floor, the reaction frame for Y-direction face was modified by bracing with hollow box section toward the bottom of column. The universal beam was also bolted on the top of two reaction frames to avoid fame

rotation caused by torque. The loading system was similar to the 2-D set-up except that all pins in 3-D set-up were capable to rotate in both directions and sustain enough rotation, especially for the hinges at the bottom of column and the both ends of lateral actuators connected between reaction frames and the columns.

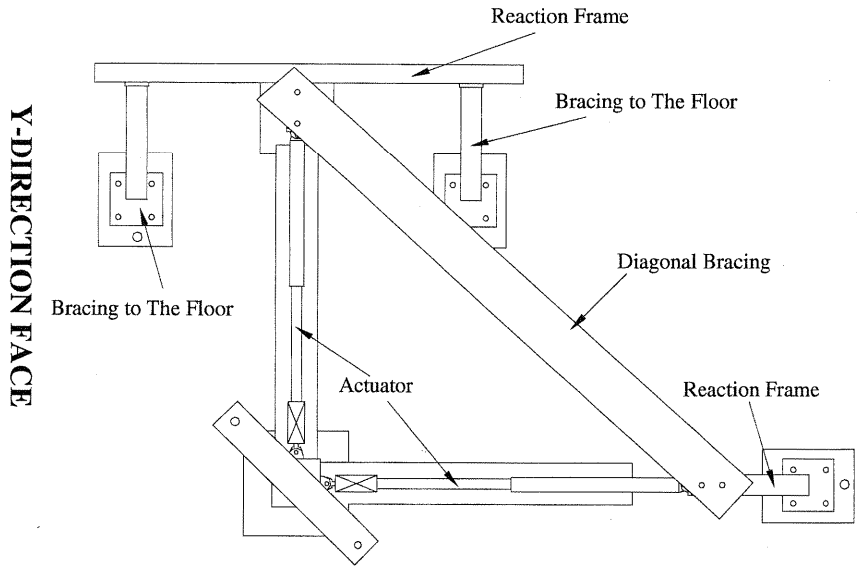

(a) Plan view

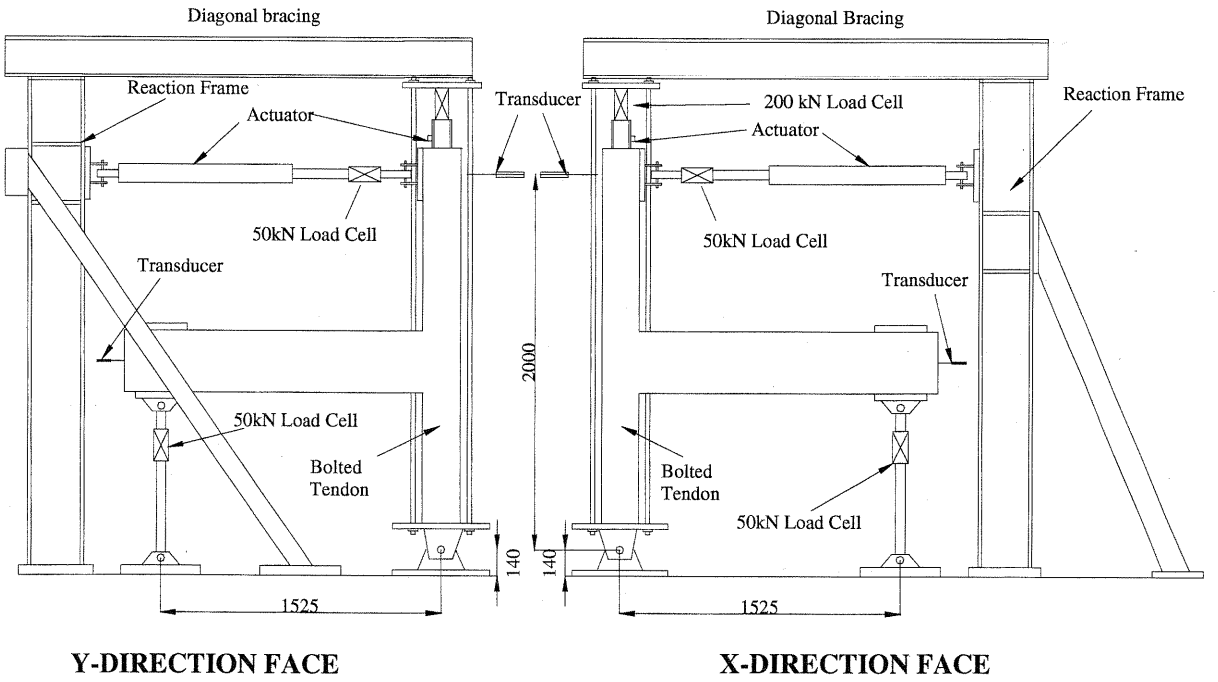

(b) Elevation view

Fig. 4.12 The loading system for the 3-D test

4.3.2 Testing Regimes

In 2-D tests, the specimens were loaded under quasi-static simulated seismic load. The displacement controlled loading system was used by applying the lateral force to the top of column until the lateral drift of column top reached the particular drift level. The loading history corresponding to the simulated storey drift level of the column top is shown in Fig. 4.13. The test specimens were subjected to two cycles loading for each drift level of 0.1%, 0.2%, 0.5%, 1.0%, 1.5%, 2.0%, 2.5%, 3.0%, 4.0%. The sequence was initiated in small increment of 0.1% and had an increment of 0.5% finally in increasing the lateral displacement. After 0.5% testing drift level, as required by the current code for the plastic region, a small cycle of 0.2% drift following each main drift level was applied to close the gaps between aggregates in the concrete.

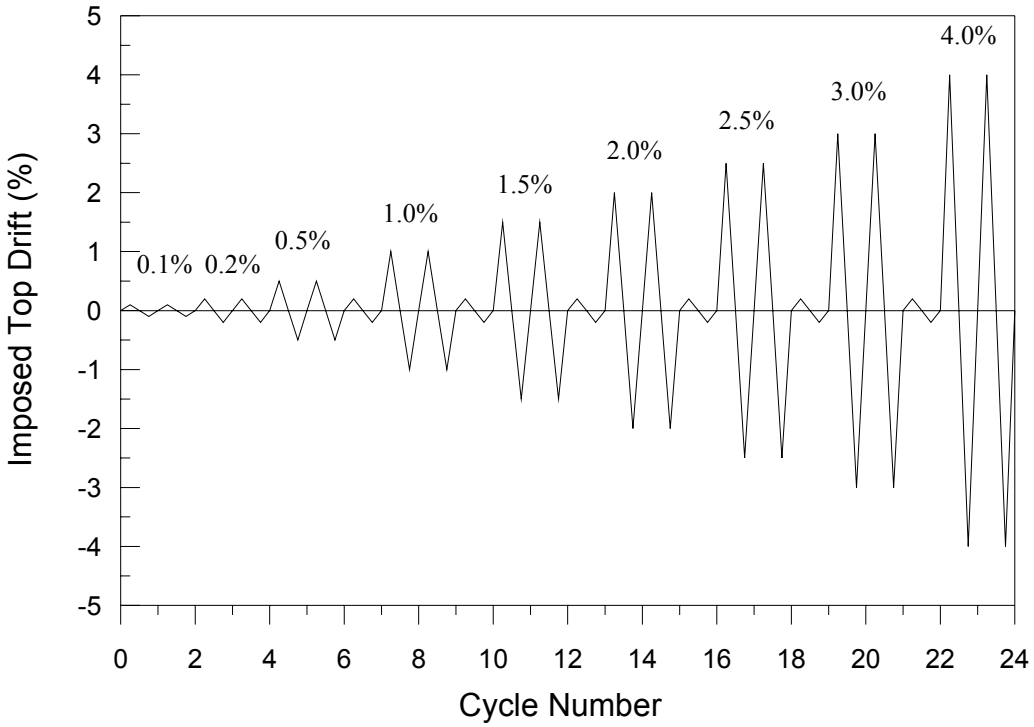

Fig. 4.13 Loading history in 2-D tests

For bi-directional loading experiment, the displacement control was also used in simulating the quasi-static loading history that the combination of two loading direction was more realistic situation during earthquake. The loading path of X and Y loading directions is illustrated as Fig. 4.14 where the sequence is directed from quadrant one to quadrant four, referred to Q1 to Q4, and the arrow is presented as the loading direction. The target drift level that was the resultant drift of the independent X and Y directions and was in a sequence of

0.1%, 0.2%, 0.5%, 1.0%, 1.5%, 2.0%, 2.5%, 3.0%, 4.0% while the a small cycle of 0.2% drift following each main drift level was also applied after 0.5%. Because the fully loading period of the 3-D joint was two times the period of loadings in X or Y direction, the loading path could in X-Y plan could be described as:

$$P(R,\theta) = R\sin(2\theta) \tag{4.1}$$

Where R was the target displacement of the column top to the origin at the particular drift level and θ was the measured angle of any points to the principal axes along the loading path. Then the resultant drift could be estimated from the resultant displacement R and the movement of the joint in X or Y direction could also be determined by defining the coordinates of the loading path as below:

$$\begin{aligned} X &= \cos P(R,\theta) \\ Y &= \sin P(R,\theta) \end{aligned} \tag{4.2}$$

As the displacement control in 2-D test, two cycles of fully running four quadrants were designed for each drift level and the loading histories of X and Y loading direction (from Eq. 4.2) is illustrated in Fig. 4.15 and Fig. 4.16 respectively.

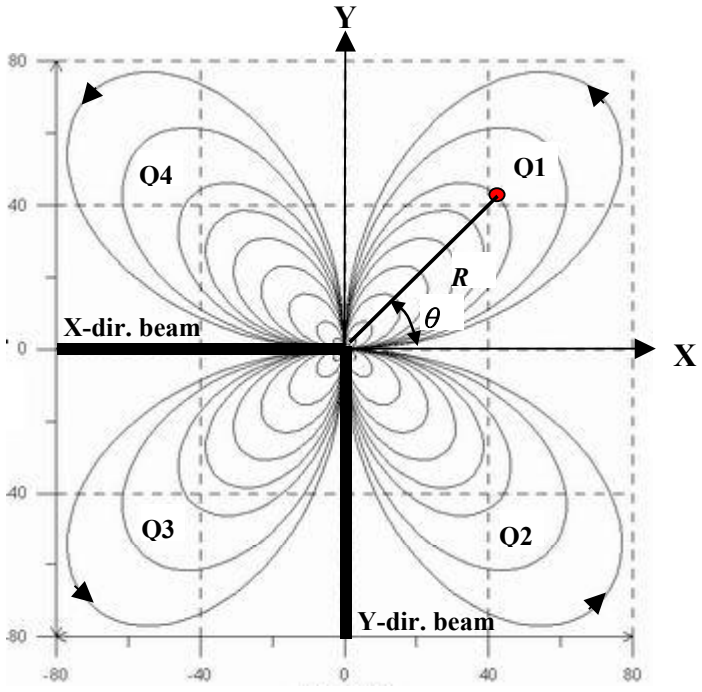

Fig. 4.14 Plane view of the loading path in the 3-D test

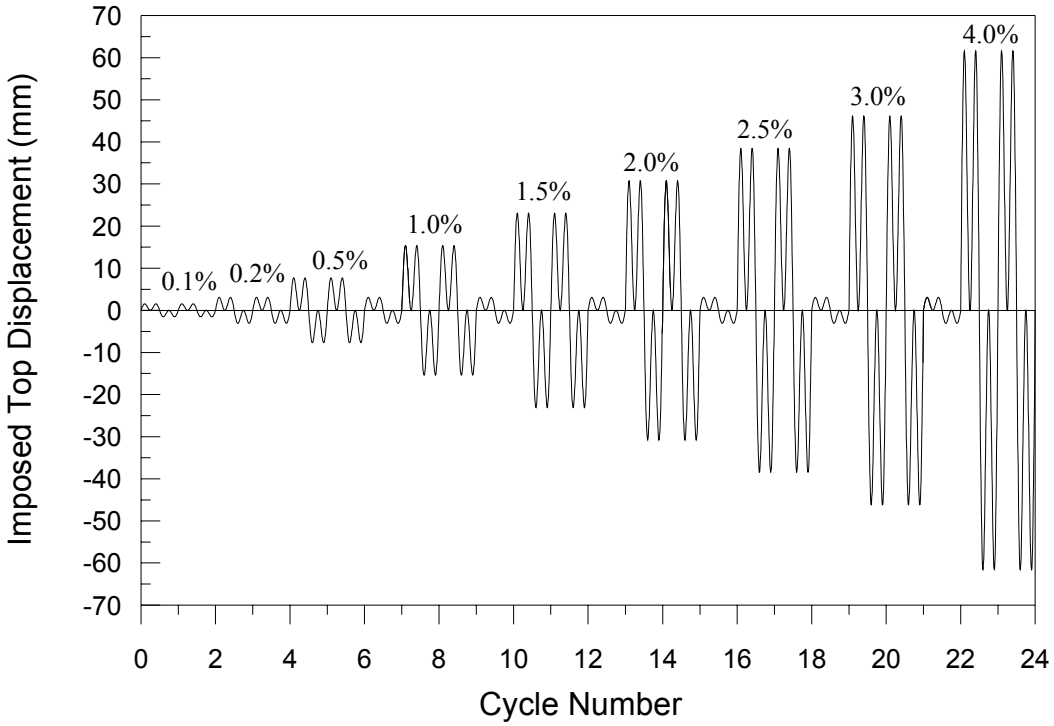

Fig. 4.15 Loading history of the 3-D test in X-direction

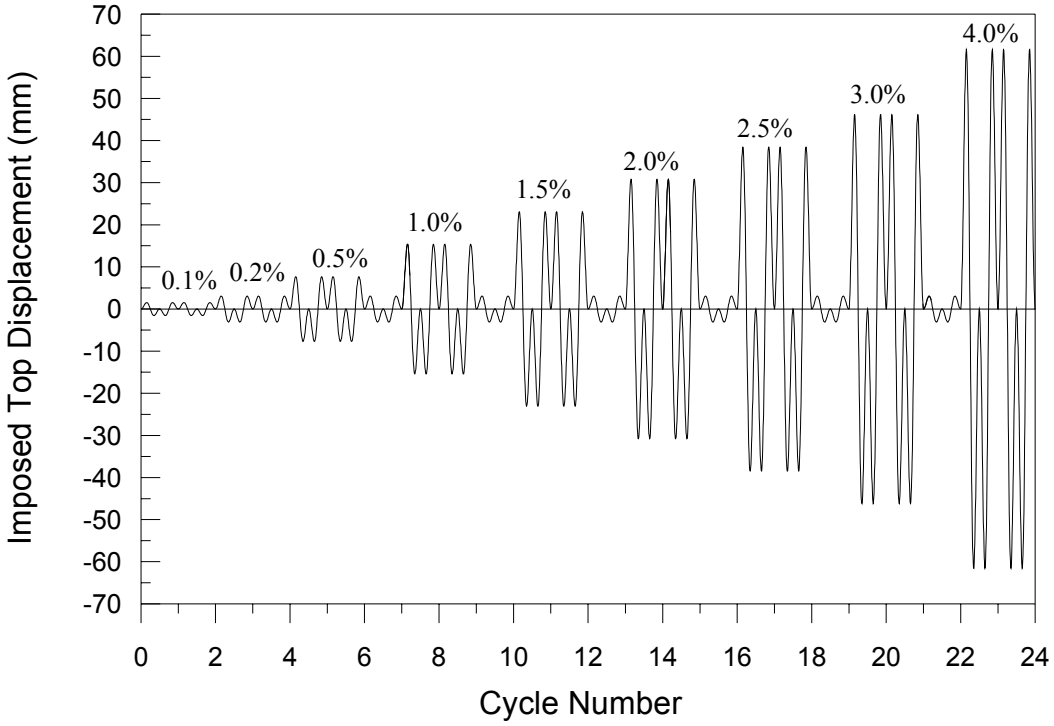

Fig. 4.16 Loading history of 3-D test in Y-direction

4.3.3 Loading Direction And Varying Column Axial Load

Due to the structural geometry, an induced column axial force $\Delta N=\alpha_h V_c$ was applied to the exterior beam-column joint subassembly as circled in Fig. 4.17 while the building suffered a equivalent seismic loading V_c. Because of this asymmetric effect on the exterior joint, the varying axial load in the column was expected during the experiments and described as a function of the lateral load. Eq. 4.3 describes the total column axial load $N_{2\text{-}D}$ for 2-D test while equation 4.4 describes the total column axial load $N_{3\text{-}D}$ for 3-D test.

$$N_{2-D} = N_g \pm \alpha_h V_c \tag{4.3}$$

$$N_{3-D} = N_g \pm \alpha_{hx} V_{cx} \pm \alpha_{hy} V_{cy} \tag{4.4}$$

The constant dead load and lateral inter-storey shear force are presented as N_g and V_c respectively as coefficient α_h is evaluated from the structural geometry. Since the same structural geometry is assumed in both direction frames of 3-D test, $\alpha_{hx}=\alpha_{hy}$ is expected in this research. To evaluate these coefficients, the preliminary analysis of the R.C. frame system was necessary in deriving the linear relationship between column axial load and inter-storey shear for the specific joint. By using the computer program, SAP2000 to simulate the pushing triangle loadings on the selected frame (Fig.4.17), the plot of column axial load versus inter-storey shear, as well as the α coefficient, were determined as given in Fig. 4.18 (i.e. $\alpha_{h,}$ α_{hx} and α_{hy} equal to 1.8 for both 2-D and 3-D tests). Table 4.6 summarizes the values of coefficient used for each test. To clearly describe the experimental result, it was important to define the loading directions in the tests. Fig. 4.19 and 4.20 define the loading directions and deformed shape for 2-D and 3-D tests.

Triangle loadings on the analysed frame	Dimensions of the frame
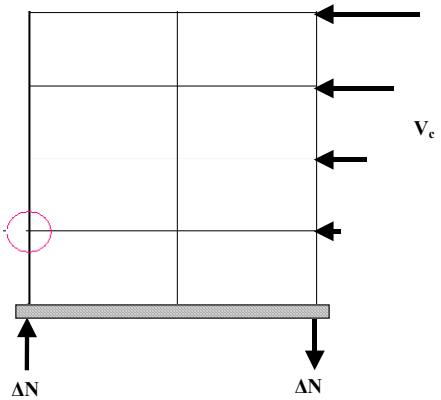	Level height: 3m Span length: 5m 1st column section: 350mm*350mm 2nd, 3rd and 4th column section: 300mm*300mm Beam section: 300mm*500mm

Fig. 4.17 The selected frame used for determining α coefficient of the critical joint

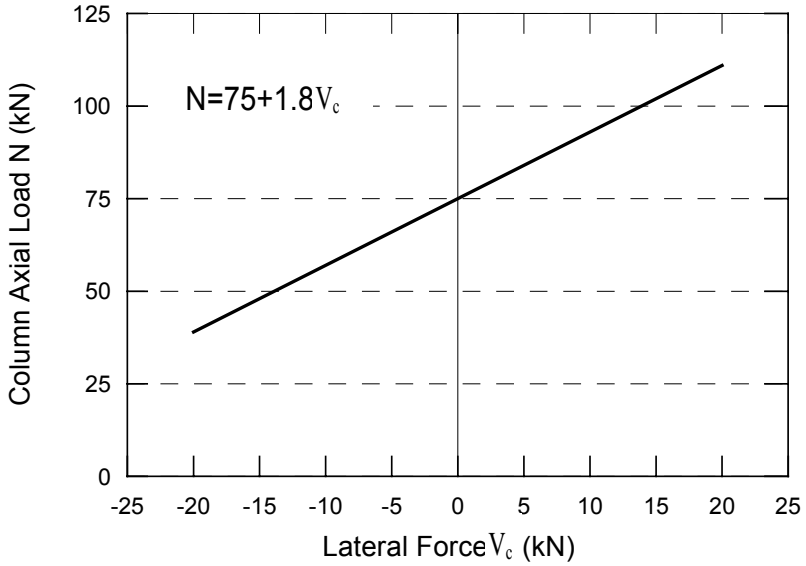

Fig. 4.18 Column axial load versus inter-storey shear force for the exterior joint

Table 4.6 Loading coefficient used in the experiments

Specimen	N_g	α_h	
TDP1, TDD1, TSP1, TSD1, TDP2, TDD2	75	1.8	
Specimen	N_g	α_{hx}	α_{hy}
DD2	75	1.8	1.8

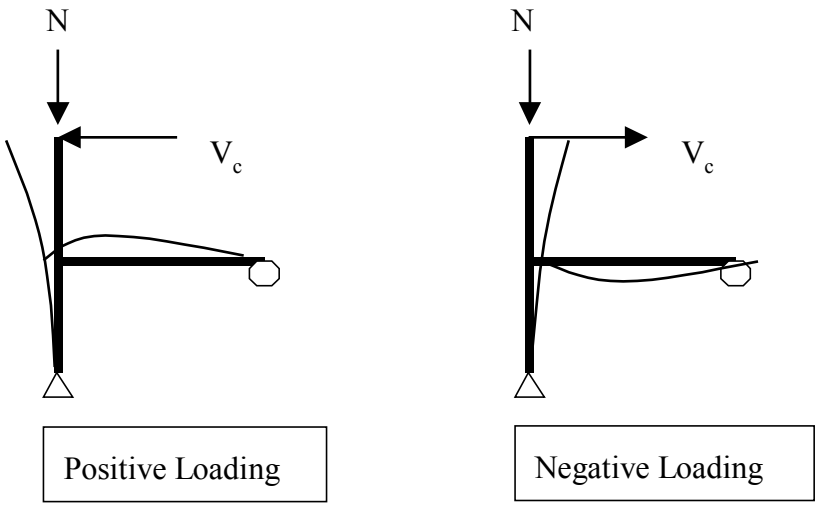

Fig. 4.19 Definition of loading direction and deformed shape for 2-D tests

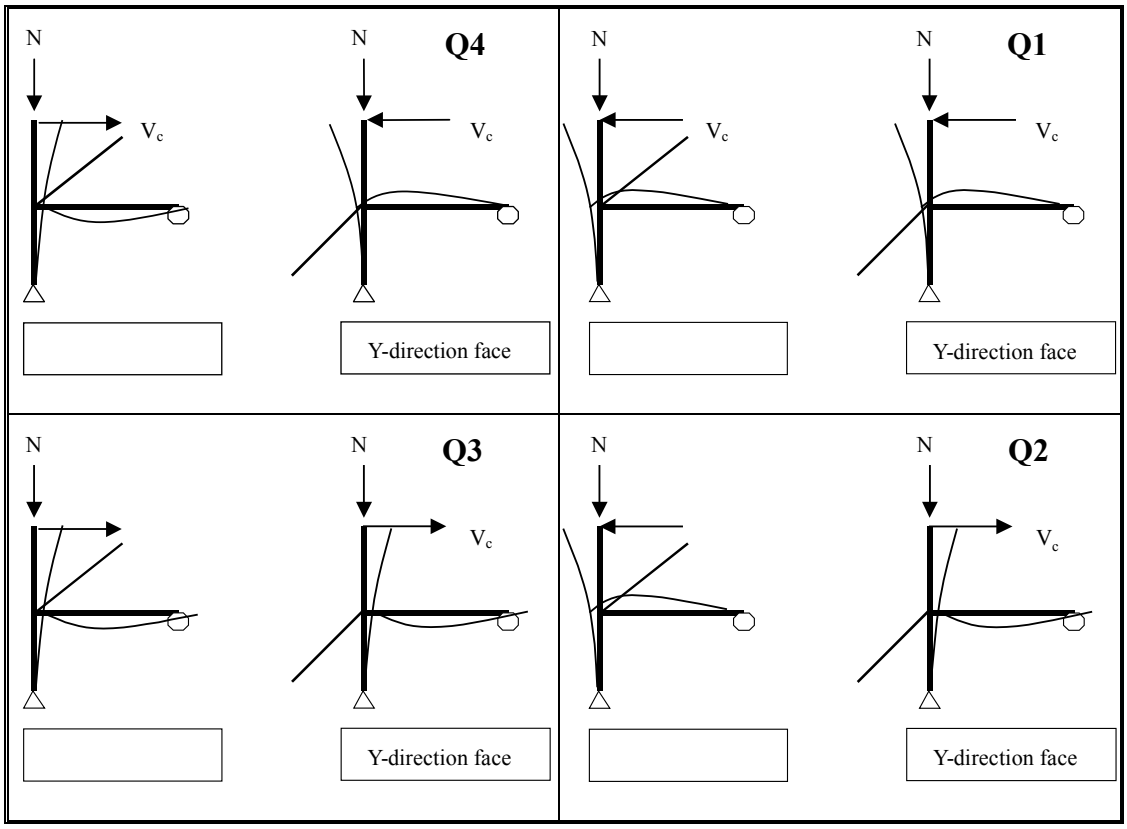

Fig. 4.20 Definition of loading direction and deformed shape for 3-D tests

4.3.4 Instrumentation

Measurement of loads: 50kN load cells were used to measure the applied horizontal load and reaction force at the beam end while a 200kN load cell was used to measure the vertical axial load in the column. The applied horizontal load was simulated as storey shear force and vertical axial load was treated as gravity loads plus earthquake-induced axial forces. The load cells were calibrated in compression by Avery Universal Testing Machine and the obtained calibration number was assumed to be effective for the particular load cell in tension as well.

Measurement of drift: Two linear potentiometers were used as transducers to measure the horizontal displacement of the column top and the beam end. By using linear potentiometer of 200mm and100mm travelling capacity for the column top and the beam end respectively, the satisfactory 5% maximum drift level was available during the test where only 4% drift level was required.

Measurement of element deformation: Twelve small linear potentiometers with 30mm travelling capacity were located at one side of the joint panel region to measure the element

deformation. Each pair of potentiometer connected between the joint and beam/column members was used to estimate the rotation of fixed end while the potentiometers attached to the joint were used to estimate the joint shear distortion by reading the horizontal, vertical and diagonal displacement in the joint. The details of potentiometers position are presented in Fig. 4.20 and in Fig. 4.21 for 2-D subassemblies and 3-D subassemblies respectively.

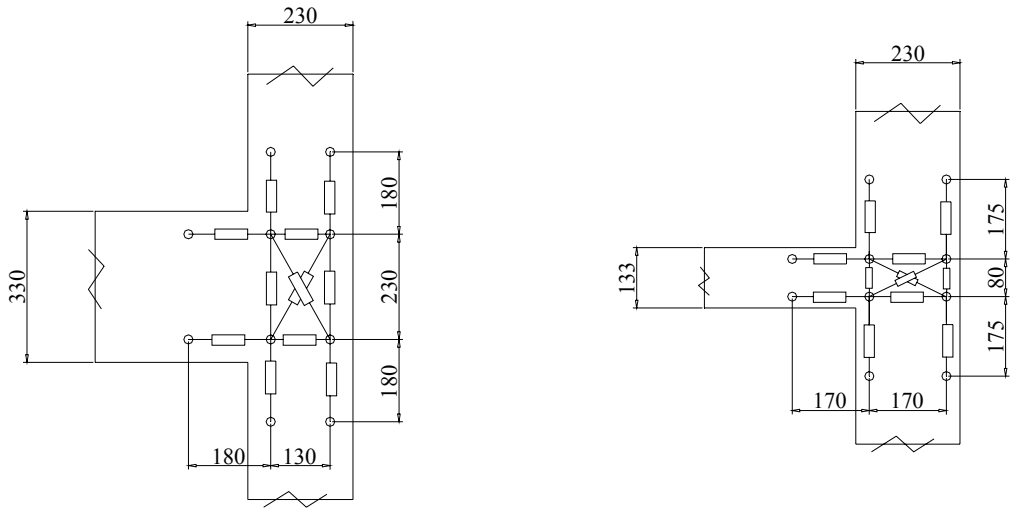

(a) TDP1, TDP2, TDP3, TDP4 (b) TSP1, TSP2

Fig. 4.20 Location of potentiometers for 2-D test

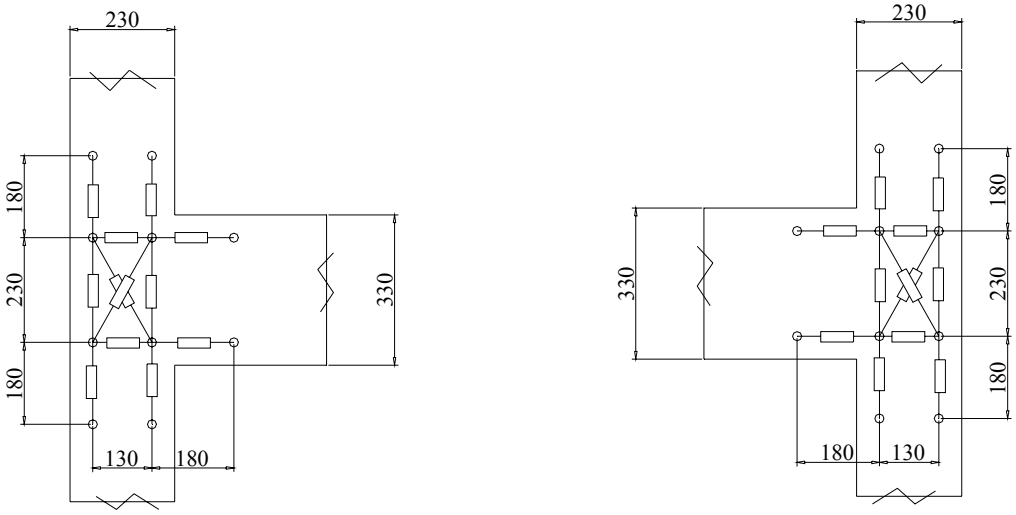

(a) X-direction face (b) Y-direction face

Fig. 4.21 Location of potentiometers for 3-D test

Measurement of strain in reinforcing bars: Strain gauges were used to measure the local strains of the reinforcing bars and the stirrups in the critical regions of beams and joints. The strain gauges were attached on the side of reinforcing bars along the bending neutral axis to

minimize the effect of bending. Twenty strain gauges were used in each specimen and, due to the different longitudinal reinforcement of the beam for each specimen, the strain gauge arrangement was not identical as shown from Fig. 4.22 to Fig. 4.24.

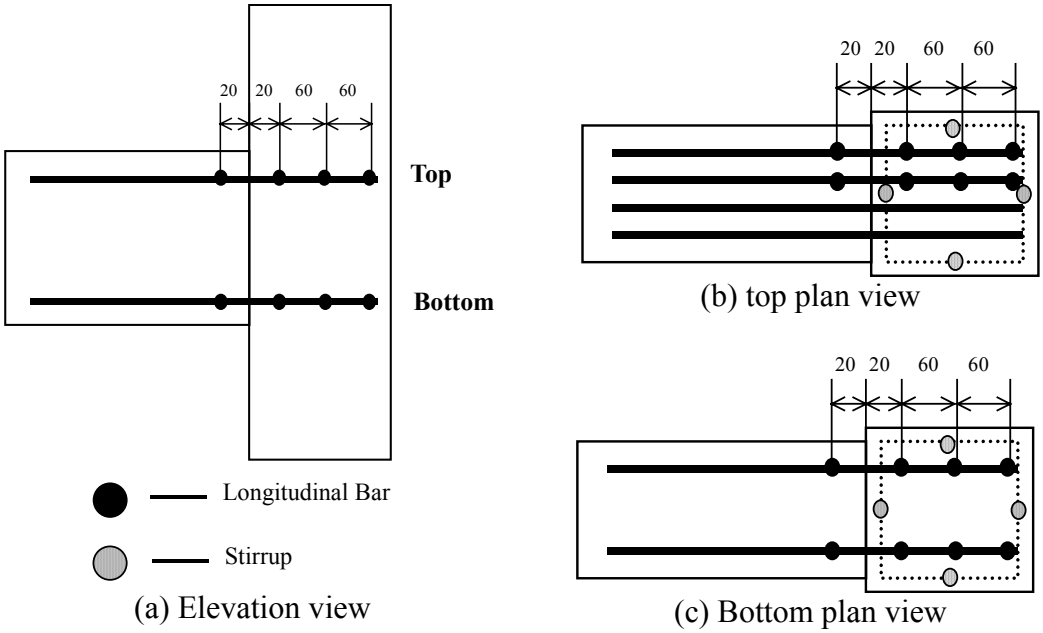

Fig. 4.22 Location of strain gauges for TDP1, TDD1

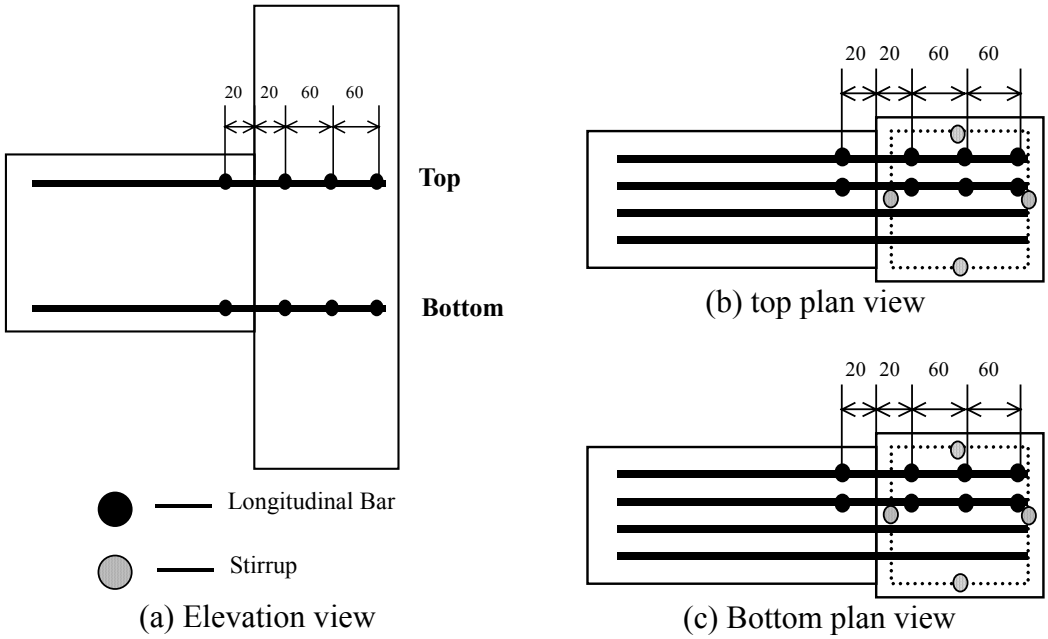

Fig. 4.23 Location of strain gauges for TDP2, TDD2 and DD2

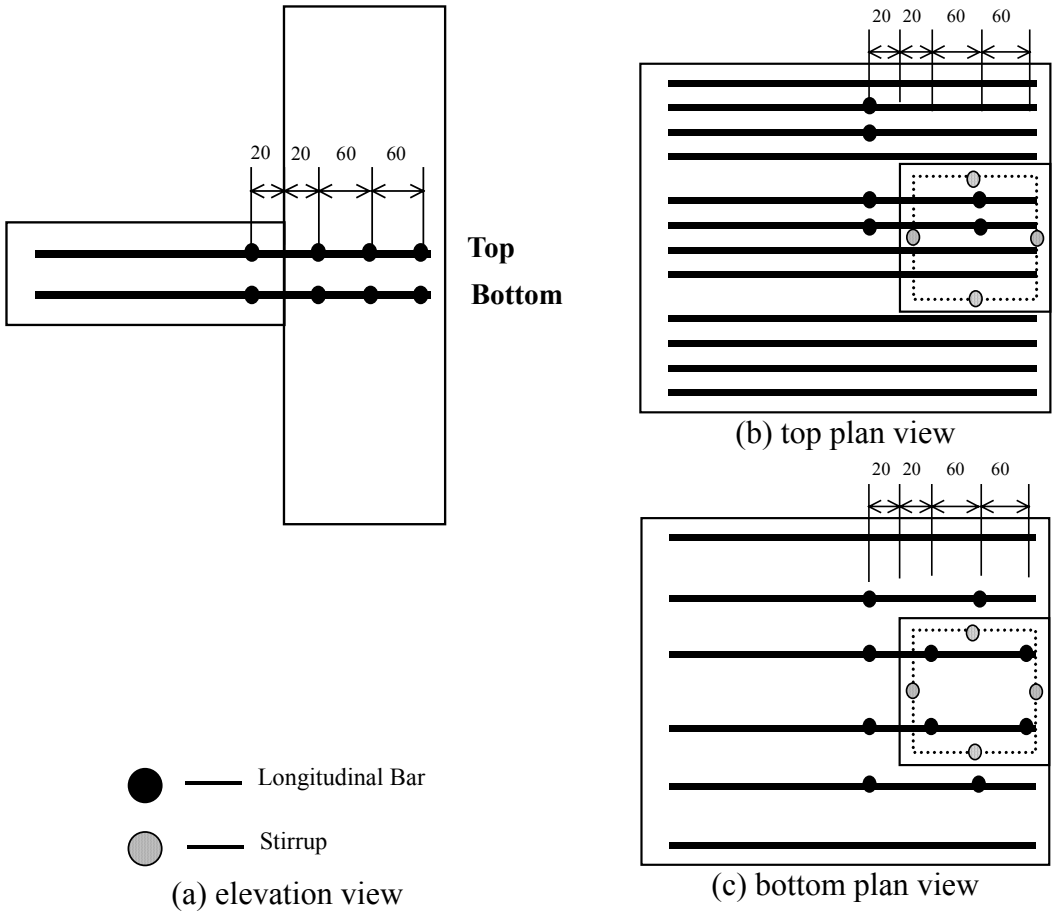

Fig. 4.24 Location of strain gauges for TSP1, TSD1

4.4 DEFORMATION ESTIMATION AND CRACK OBSERVATION

4.4.1 Estimation of Average Rotation for The Fix End

Due to the bar slippage and tensile strain of longitudinal bar, the fix end rotation of members adjacent to the joint could happen. Referred to Fig. 4.25, a pair of linear displacements that could be obtained form readings of the potentiometers attached to the beam and column elements was required to estimate the fix end rotation in the beam and column by following formulas.

Fix end rotation of beam:

$$\theta_b = (\delta_{t\_} \delta_b) / Dv \tag{4.5}$$

Fix end rotation of column:

$$\theta_c = (\delta_{r\_} \delta_l) / Dh \tag{4.6}$$

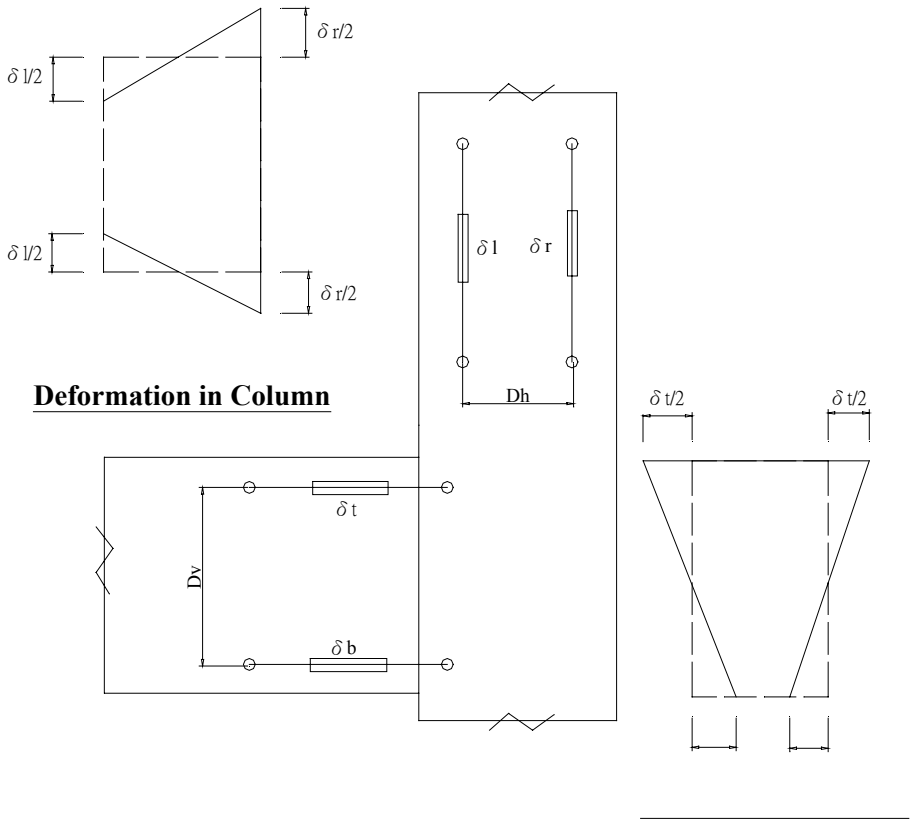

Fig. 4.25 Estimation of fixed-end rotation of the column

4.4.2 Estimation of Shear Distortions for the Joints

Six potentiometers were used to estimate the shear rotation of the joint. Either one of diagonal potentiometer was used as dummy reading for the reservation purpose. Referred to the linear potentiometers' locations, the rotation value was estimated by the following formulas with Fig. 4.26.

Shear distortion of joint:

$$\gamma_j = \Delta_s / Dv$$

$$\text{where } \Delta_s = \frac{|\delta_{ds}|}{\cos R}$$

$$\delta_{ds} = \delta_d - \delta_{dh} - \delta_{dv} \tag{4.7}$$

$$\delta_{dh} = \frac{\delta_{jt} + \delta_{jb}}{2} \cos R$$

$$\delta_{dv} = \frac{\delta_{jl} + \delta_{jr}}{2} \sin R$$

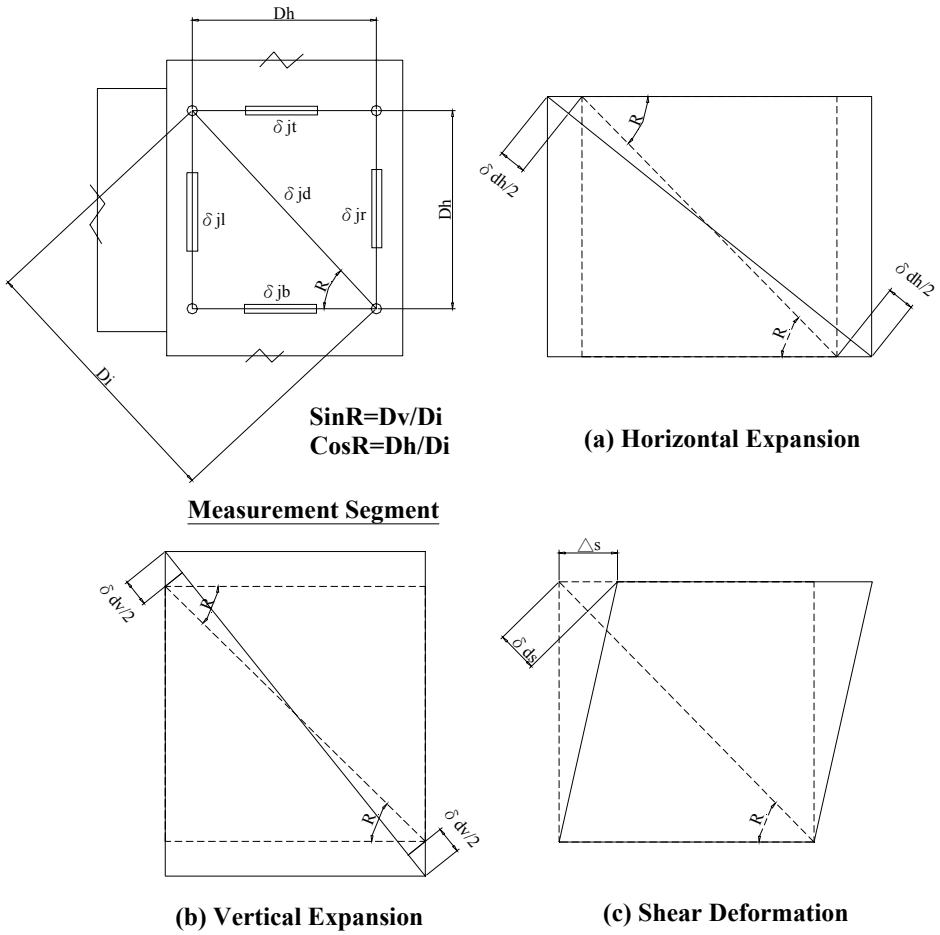

Figure.4.26 Estimation of the joint shear rotation

4.4.3 Crack Observation

The critical region of beam column subassembly was painted in white colour and all observed cracks in the critical region were marked with the blue and red colour that were representative of the positive and negative loading respectively. The photos were taken after marking the cracks at the peak drift of each loading cycle.

4.5 COMPONENT OF HORIZONTAL DISPLACEMENT

4.5.1 General

The total horizontal displacement of the top column Δ_{tot} was composed of the horizontal displacements caused by the deformation of the beam, column and joint as illustrated in Fig. 4.27. The beam and column deformations were both contributed by the elastic deformations and fix end rotation of the elements while the joint deformation was estimated by the shear deformation only. The components of the total horizontal displacement for the beam, column and joint, referred to Δ_{beam}, Δ_{column} and Δ_{joint}, are detailed below while types of inter-story drifts θ_{beam}, θ_{column}, θ_{joint} are introduced to understand the corresponding inter-storey displacement as given below:

$$\begin{aligned} &\Delta_{tot} = \Delta_{beam} + \Delta_{column} + \Delta_{joint} \\ &\theta_{tot} = \theta_{beam} + \theta_{column} + \theta_{joint} \\ &\text{where } \theta_i = \frac{\Delta_i}{H_c} \end{aligned} \tag{4.8}$$

4.5.2 Horizontal Displacement Component of The Beam

The displacement at the beam end Δ_{end} was composed of the displacements caused by the flexural deformation along the beam element and the fix-end rotation at the joint connection and this can be given by:

$$\Delta_{end} = \delta_{b,fle} + \delta_{b,rot} \tag{4.9}$$

where $\delta_{b,fle}$ and $\delta_{b,rot}$ were the displacement caused by the flexural deformation and fix-end rotation respectively. Once the displacement at the beam end Δ_{end} was obtained, the horizontal contribution of the beam deformation could be estimated by:

$$\Delta_{beam} = \frac{\Delta_{end} H_c}{L_n} \tag{4.10}$$

4.5.3 Horizontal Displacement Component of The Column

Similarly, the horizontal contribution of the column deformation Δ_{column} could be directly estimated by the flexural deformation along the column element and the fix-end rotation at the joint connection as given:

$$\Delta_{column} = \delta_{c,fle} + \delta_{c,rot} \tag{4.11}$$

where both top and bottom columns were involved to evaluate the values of $\delta_{c,fle}$ and $\delta_{c,rot}$.

4.5.4 Horizontal Displacement Component of The Joint

The inter-storey drift θ_{joint} that was equal to the joint shear rotation γ_j as given in Eq. 4.7 was used to evaluate the horizontal contribution of the joint deformation by the equation:

$$\Delta_{joint} = \theta_{joint} H_n \tag{4.12}$$

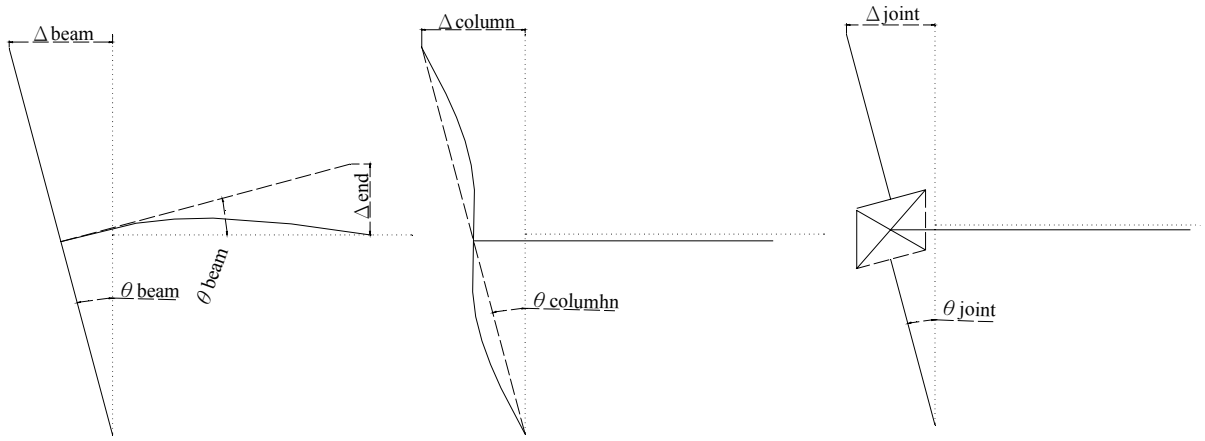

Fig. 4.27 Component contribution to the total horizontal displacement

4.6 SEISMIC ASSESSMENT OF AS-BUILT TEST UNITS

4.6.1 General

The performance under quasi-static loading of the beam-column joint subassembly were assessed theoretically to predict the behaviour of specimen during the testing. The assessment includes the element properties of the subassembly and the failure mechanism by hierarchy strength diagram. The transverse reinforcement detail was also investigated and compared with current design code.

4.6.2 Theoretical Strength and Stiffness

The theoretical flexural properties of beams and columns were estimated by the computer program (Table . From the plotted moment-curvature diagram by giving the section information to the computer, the flexural strength and stiffness could be determined. The flexural capacity ratio of the column strength to the beam strength was used to predict the ease of plastic hinge occurring in the beam. The greater number presented that the beam hinge more easily occurred in the beam than in the column. To estimate the joint stiffness K_j, the formula was derived (Appendix A) as given below:

$$K_j = G_c \left(\frac{j d_b H_c}{H_c - j d_b} \right) A_e \tag{4.13}$$

In order to investigate the amount of transverse reinforcement in the subassemblies, the maximum imposed shear force with the occurrence of plastic hinge in the beam was compared with available shear strength of members. The transfers reinforcement for the concrete confinement and anti-buckling was also investigated by comparing the actual amount with the required amount (Table 4.8). From the results, the greater value of imposed shear force than shear capacity in the joint of TDP1, TSP1, TSD1, TDP2, TDD2 and DD2 implied that the joint shear failure might occur. Moreover, greater spacing and less area of actual transverse reinforcement might lead to the failure in concrete confinement and anti-buckling. The obtained value were estimated on the basis of NZS3101:1995, except the joint shear capacity that was estimated by the limit state of equivalent principal tensile stress. An example of all calculating procedures could be found in Appendix A.

Table 4.7 Theoretical flexural properties of members of subassemblies

Specimen		Flexural strengths M (kN-m)	Flexural stiffness EI (kN-m^2)	Capacity Ratio $\Sigma M_{column}/\Sigma M_{beam}$	Joint Stiffness (kNm)
TDP1	Beam negative	31.2	3850	1.46(-)	
	Beam positive	15.4	2160	2.95(+)	236000
	Column	22.7	2000		
TDD1	Beam negative	30.0	3850	1.45(-)	
	Beam positive	14.8	2160	1.45(+)	236000
	Column	21.7	2000		
TSP1	Beam negative	29.0	1000	1.57(-)	
	Beam positive	16.7	600	2.72(+)	103000
	Column	22.7	2000		
TSD1	Beam negative	27.2	1000	1.60(-)	
	Beam positive	15.9	600	2.73(+)	103000
	Column	21.7	2000		
TDP2	Beam negative	30.1	3900	1.47(-)	
	Beam positive	30.1	3900	1.47(+)	236000
	Column	22.1	2000		
TDD2	Beam negative	46.8	5500	1.0(-)	
	Beam positive	31.9	3900	1.47(+)	236000
	Column	23.5	2000		
DD2	Beam negative	31.5	3900	1.47(-)	
	Beam positive	31.5	3900	1.47(+)	236000
	Column (X-dir)	22.7	2000		
	Column (Y-dir)	22.5	2000		

Note: 75kN column axial load present

Table 4.8 Shear, concrete confinement and anti-buckling of members of subassemblies

		Shear Strength Requirement		**Concrete Confinement And Anti-buckling**			
Specimen	**Parts of Units**	**Maximum Imposed Shear (kN)**	**Shear Force Capacity (kN)**	**Required Amount**		**Actual Amount**	
				Spacing (mm)	Area (mm^2)	Spacing (mm)	Area (mm^2)
TDP1	Beam	22.1	54.0	60	17.8	133	28.3
	Column	16.9	48.0	51	10	100	28.3
	Joint	94.5	82.2	100	16.5	165	28.3
TDD1	Beam	21.3	54.0	60	16.6	133	28.3
	Column	16.0	48.0	51	9.4	100	28.3
	Joint	91.1	107.9	100	15.5	165	28.3
TSP1	Beam	20.6	54.0	27	53.6	133	28.3
	Column	15.5	48.0	51	10	100	28.3
	Joint	306.7	123.4	100	6.7	66.5	28.3
TSD1	Beam	19.3	54.0	27	49.8	133	28.3
	Column	14.5	48.0	51	9.4	100	28.3
	Joint	287.7	161.8	100	6.3	66.5	28.3
TDP2	Beam	21.3	52.0	60	17.8	133	28.3
	Column	16.0	46.1	51	10	100	28.3
	Joint	91.5	82.2	100	16.5	165	28.3
TDD2	Beam	33.2	52.0	60	18.9	133	28.3
	Column	24.9	46.1	51	10.6	100	28.3
	Joint	142.2	107.9	100	17.5	165	28.3
DD2	Beam	31.5	52.0	60	18.7	133	28.3
	Column	17	46.1	51	10.5	100	28.3
	Joint	96.5	82.2	100	17.5	Nil	Nil

Note: Maximum imposed shear forces are calculated assuming that the plastic hinges formed n the columns of specimens and the specimens reach their flexural strengths at the plastic hinges. In order to eliminate the shear failure in the beam and column, the concrete shear contribution is ignored by assuming v_c=0 at both PPHZ and non-PPHZ. The shear capacity values are estimated by using current New Zealand code method of NZS3101: 1995.

4.6.3 Hierarchy Strength Analysis

The hierarchy strength diagrams were used to visually access the failure mechanism of the beam column subassembly. According the preliminary study on the hierarchy strength (Appendix A), the sequence of events for each test is summarized in Table 4.9. The procedure in plotting hierarchy is also described in Appendix A.

From the preliminary work, the joint shear failure of both loading directions will be found in TDP2, TDD2, TSP1, TSD1 and DD2. For TDP1, the joint shear failure will only be observed only in positive loading direction while the beam flexural failure will be found during the negative loading. However, without any joint shear failure, the pure flexural failure will occur in TDD1 in both loading directions because the higher principal tensile strength is expected in the joint by using deformed bars.

Table 4.9 Preliminary study on sequence of events for each specimen

	Lateral Force Direction	No.	Event
TDP1	**Positive Loading**	1	Joint First Diagonal Cracking and Deterioration Starting
		2	Beam Yielding
		3	Column Yielding
	Negative Loading	1	Beam Yielding
		2	Joint First Diagonal Cracking and Deterioration Starting
		3	Column Yielding
TDD1	**Positive Loading**	1	Beam Yielding
		2	Joint First Diagonal Cracking
		3	Column Yielding
	Negative Loading	1	Beam Yielding
		2	Joint First Diagonal Cracking
		3	Column Yielding
TDP2	**Positive Loading**	1	Joint First Diagonal Cracking and Deterioration Starting
		2	Beam Yielding
		3	Column Yielding
	Negative Loading	1	Joint First Diagonal Cracking and Deterioration Starting
		2	Beam Yielding
		3	Column Yielding

TDD2	**Positive Loading**	1	Joint First Diagonal Cracking and Deterioration Starting
		2	Beam Yielding
		3	Column Yielding
	Negative Loading	1	Joint First Diagonal Cracking and Deterioration Starting
		2	Beam Yielding
		3	Column Yielding
TSP1	**Positive Loading**	1	Joint First Diagonal Cracking and Deterioration Starting
		2	Beam Yielding
		3	Column Yielding
	Negative Loading	1	Joint First Diagonal Cracking and Deterioration Starting
		2	Beam Yielding
		3	Column Yielding
TSD1	**Positive Loading**	1	Joint First Diagonal Cracking and Deterioration Starting
		2	Beam Yielding
		3	Column Yielding
	Negative Loading	1	Beam Yielding
		2	Joint First Diagonal Cracking and Deterioration Starting
		3	Column Yielding
DD2	**Quadrant 1**	1	Joint First Diagonal Cracking and Deterioration Starting
		2	Beam Yielding
		3	Column Yielding
	Quadrant 3	1	Joint First Diagonal Cracking and Deterioration Starting
		2	Beam Yielding
		3	Column Yielding
	Quadrant 2, 4	1	Joint First Diagonal Cracking and Deterioration Starting
		2	Beam Yielding
		3	Column Yielding

CHAPTER 5

EXPERIMENTAL RESULTS OF THE AS-BUILT SPECIMENS

5.1 INTRODUCTION

The beam-column joint subassemblies discussed in Chapter 2 were tested. The experimental results of using plain round and deformed bars respectively were compared and discussed. The principal tensile strength at different limit state was estimated to validate the proposed value in the previous research. The effectiveness of horizontal joint shear stress was investigated on the respect of predicting joint shear failure. The joint shear contribution to the total drift was also illustrated for different failure mechanisms.

5.2 TEST OF TDP1

5.2.1 Specimen

Due to the unbalanced reinforcement in the beam, the beam flexural strength was expected two times greater for the negative reinforcement than positive reinforcement. The experimental results presented that joint shear failure with the first shear crack was observed in the positive loading direction and beam flexural failure occurred in the negative loading direction. After the beam hinging, the first joint shear crack was still marked with strength degradation at 2.5% drift level in the negative loading direction.

5.2.2 General Behaviour

The final crack pattern and the measured hysteric response are illustrated in Fig. 5.1 and 5.2 respectively. Fig. 5.3 illustrates the sequence of observed crack patterns at each critical drift level.

It is worth noting that an accidental crack occurred in the bottom beam before the experiment and it would certainly decrease the stiffness of subassembly in the negative loading direction. The accidental crack in the bottom beam began propagating further when loading to negative 0.5% drift level during which the flexural of the beam occurred. In the positive loading

direction, the joint was elastic until first crack happened at 1.33% with 16.3kN lateral resistance. The lateral resistant force suddenly dropped, once joint cracked then recover a little force to 1.5% drift level. However, the lateral resistant force decreased at positive higher drift level because of brittle joint shear crack occurred in the positive loading direction. The subassembly remained as beam flexural failure in the negative loading direction until 2.5% drift level. The new joint shear crack initiated in the loading to –3.0 drift level and the lateral resistant force at peak drift level decreased acting as brittle joint shear failure. Even if the beam ductile failure existed, the joint brittle failure still happened at higher drift level.

Fig. 5.1 Final crack of TDP1

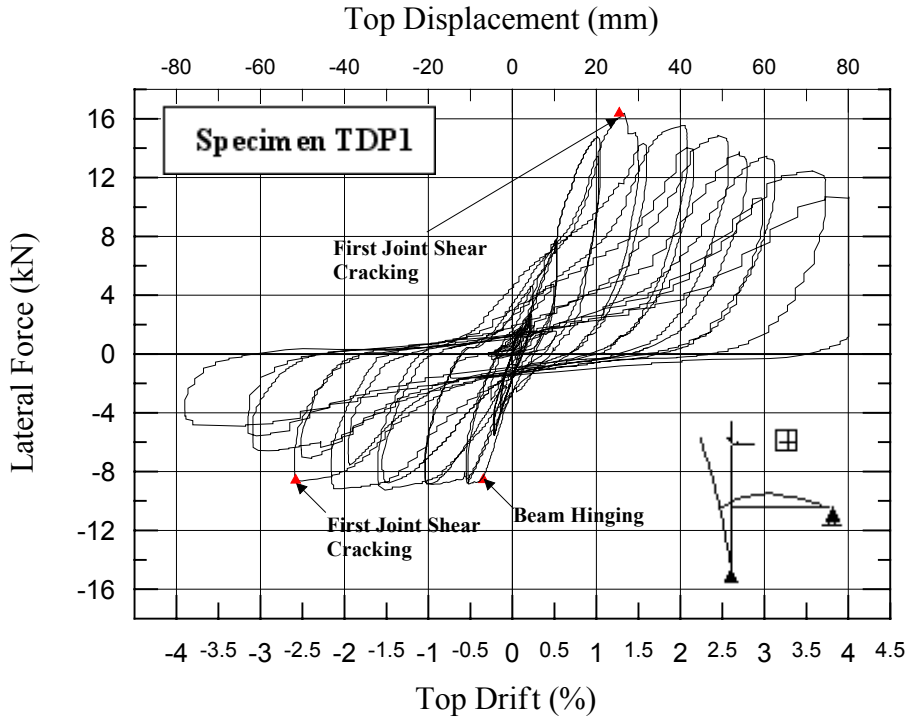

Fig. 5.2 Storey-shear force versus horizontal relationship of specimen TDP1

a) Minor cracks in bottom beam at –0.2% drift

b) Minor crack in top beam at +0.5% drift

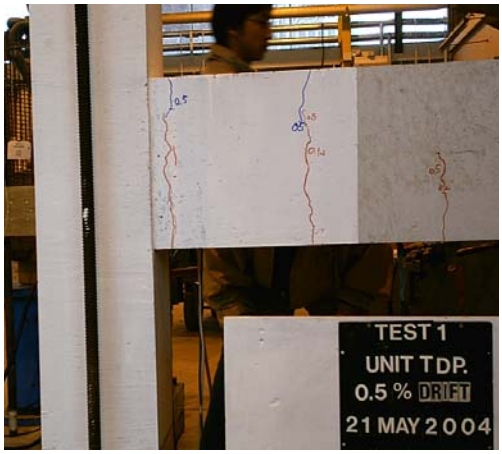

c) Beam yielding crack at –0.5% drift

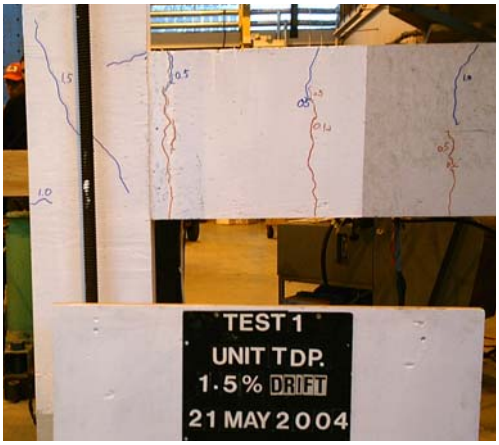

d) First joint shear crack at +1.5% drift

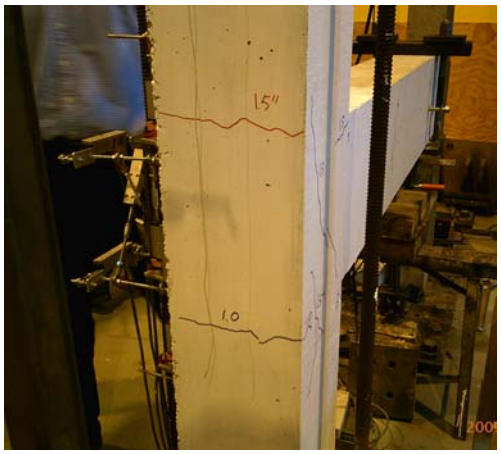

e) Minor cracks in back of column at 1.0% and –1.5% drift respectively

f) Major joint shear crack at –3.0% drift and bigger crack in bottom beam at higher drift

Fig.5.3 Sequence of Observed Cracks

5.2.3 Joint Behaviour

From Fig. 5.3, the joint first crack was observed at p_t=0.185$\sqrt{f'_c}$ in the positive loading direction while the beam hinging was observed in the negative loading direction as expected. The joint strength degradation occurred once the first joint shear crack was observed. After beam hinging, the joint crack still performed in the negative loading direction when the higher drift level, 2.5%, was achieved. The principal tensile stress at this level decreased to 0.085$\sqrt{f'_c}$ for the joint crack. The joint rotation was observed to be 0.00136 while the pure joint shear failure occurred as illustrated in Fig. 5.5. The horizontal joint shear stress was 1.65MPa for the first joint crack in the positive loading direction (Fig. 5.6). The experimental results showed that the first joint shear crack occurred at not only the peak of principal tensile stress, which meant the expected limit state of the joint, also the higher drift level.

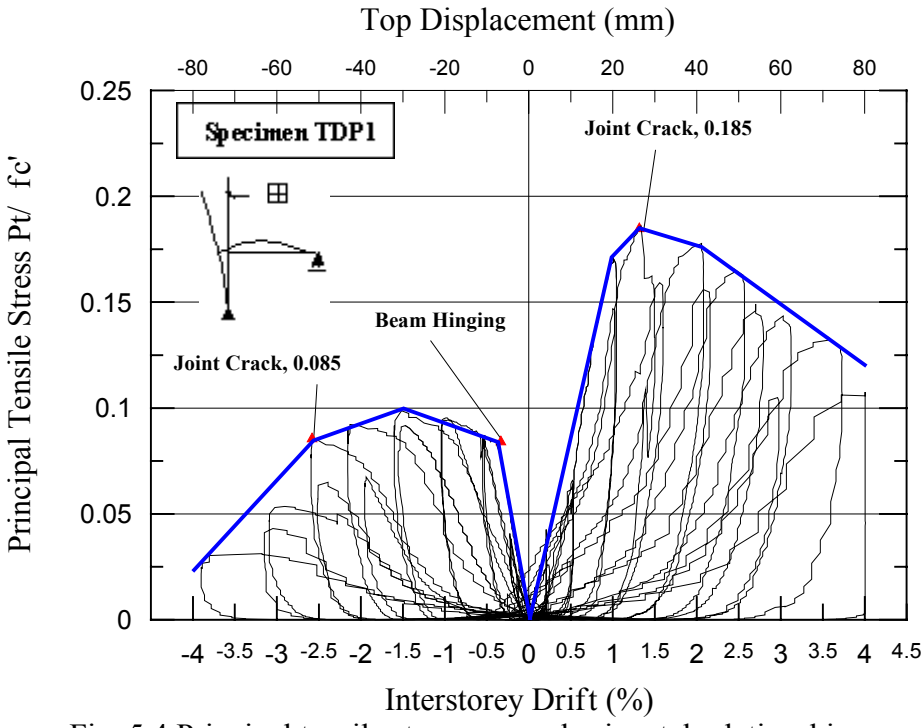

Fig. 5.4 Principal tensile stress versus horizontal relationship

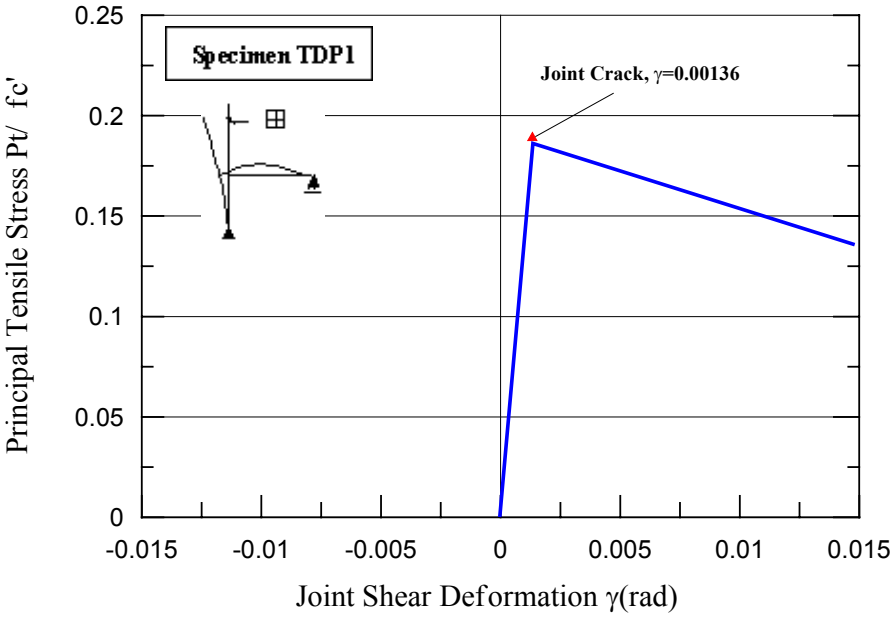

Fig. 5.5 Principal tensile stress versus joint rotation

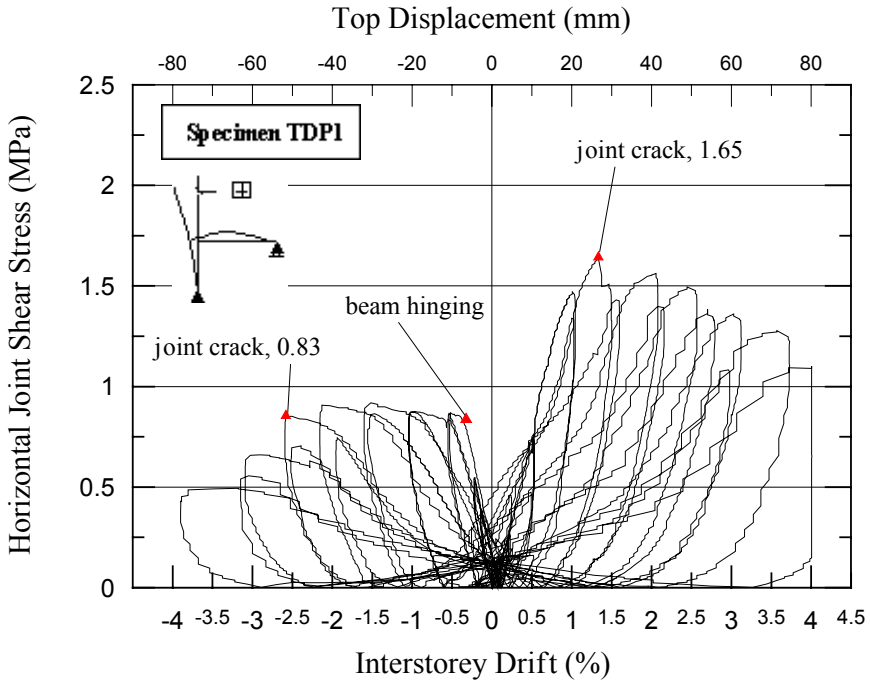

Fig. 5.6 Horizontal joint shear stress versus horizontal relationship

5.2.4 Decomposition of Horizontal Displacement

Due to the accident of the beam before the test, the joint contribution to the total horizontal drift was not significantly observed as illustrated in Fig. 5.7. However, it is till also observed that the joint contribution increased after first joint crack at 1.5% drift level in the positive loading direction and after 2.5% drift level in the negative loading direction.

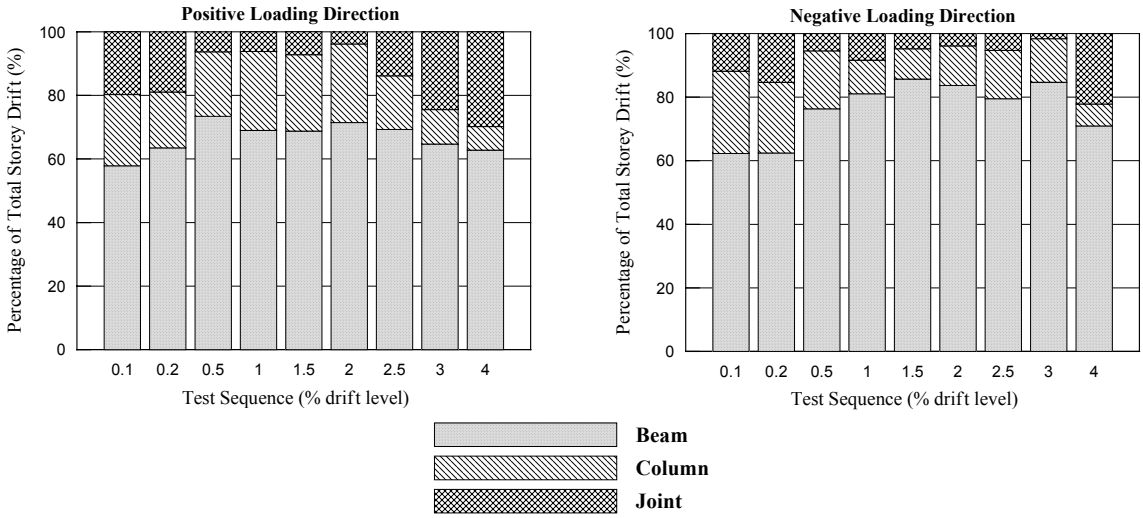

Fig. 5.7 Contributions to subassembly drift of beam, column and joint in TDP1

5.3 TEST OF TDD1

5.3.1 Specimen

From the hierarchy strength diagram, the joint became stronger because of using deformed bar. The greater joint shear capacity enforced the beam to have flexural failure before brittle shear failure. Although the beam flexural strength was two times in positive loading direction than in the negative one, the pure flexural failure in the beam was expected in both directions.

5.3.2 General Behaviour

The final crack pattern and the measured global hysteretic loops are shown in Fig. 5.8 and 5.9 respectively. Fig. 5.10 illustrates the sequence of observed crack patterns at each critical drift level.

During the small drift of 0.2% drift, several minor cracks occurred in the beam along both positive and negative flexural sides. During the loading procedure of 0.5% drift level, the beam remain elastic with widening minor cracks in the positive flexural side while the beam began flexural yielding in the negative loading direction due to the smaller flexural strength. Although the minor crack appeared on the back of column, the beam have pure flexural failure with increasing strength caused by the strain hardening in the beam bars before loading to 2.0% drift level. In the loading to positive 2.5% drift, the big crack was observed cross the part of joint region and formed a concrete wedge. Once concrete wedge occurred, the slippage

of the bars was observed from the hysteretic loop even the subassembly could still reached the strength. However, the spalling off from the column back during 3.0% drift loading and the longitudinal reinforcement of column was buckling during the loading to -3.0% drift. The strength degradation was observed from the hysteretic loop due to buckling of column reinforcement although the joint seemed integral. The testing was stopped at first cycle of 3.0% drift level rather than designed 4.0% level due to safety reason. Because pure flexural beam failure in both positive and negative loading direction, the lateral resistant forces of subassembly were about 16.0kN and 8.0kN respectively which was at a ratio of 2:1 corresponding to the beam reinforcing arrangement in the positive and negative sides.

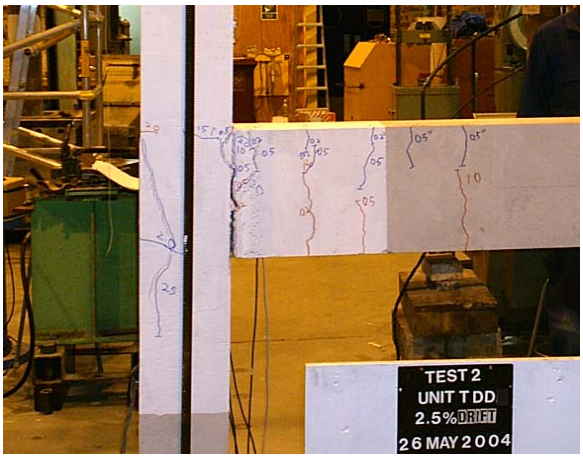

Fig. 5.8 Final crack of TDD1

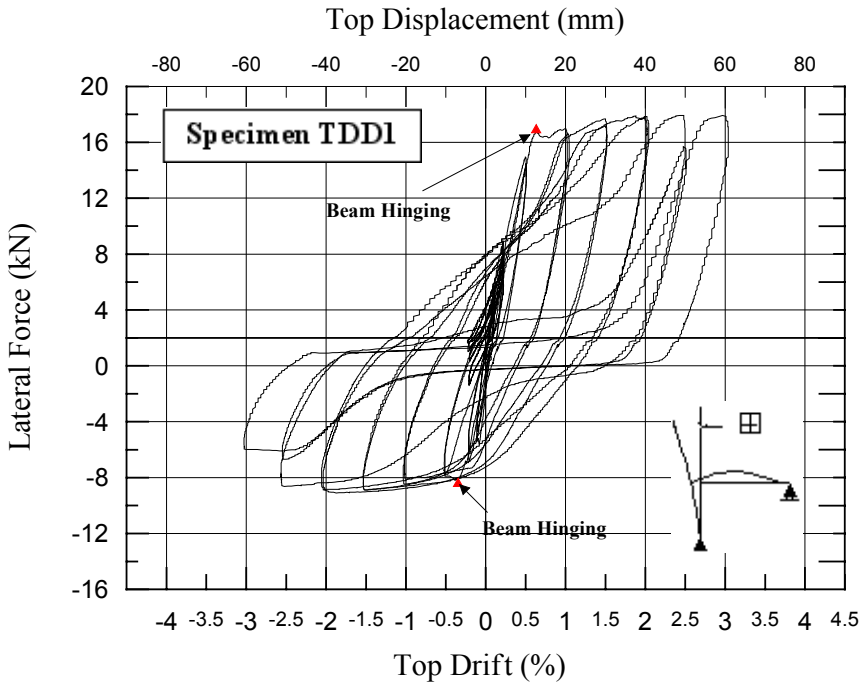

Fig. 5.9 Storey-shear force versus horizontal relationship of specimen TDD1

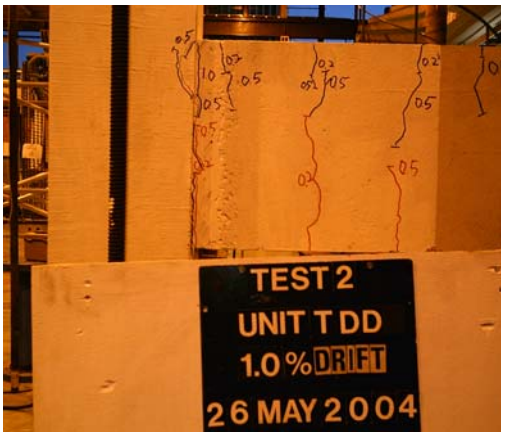

a) Flexural cracks along the beam to 1.0% drift

b) Major flexural crack opening along the beam-column intersection in –0.5% drift

c) Minor cracks on column during 2.0% drift

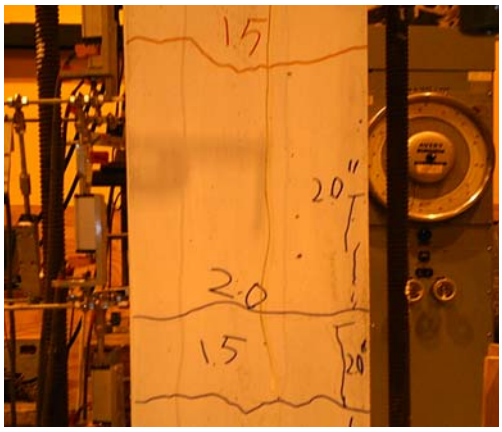

d) Minor flexural cracks appeared on column back

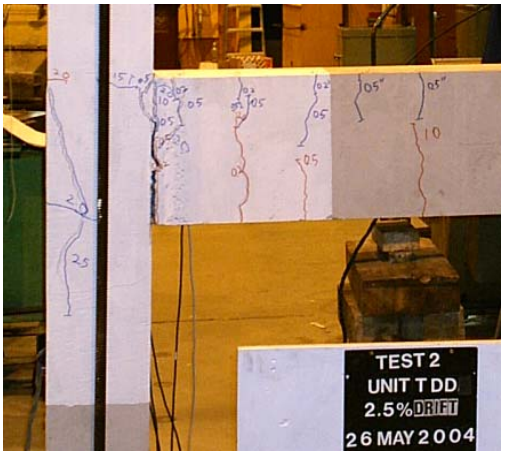

d) Big cracks cross the column back to form concrete wedge during 2.5% drift

e) Several cracks appeared on the column back

f) Concrete wedge spalling off during 3.0% drift

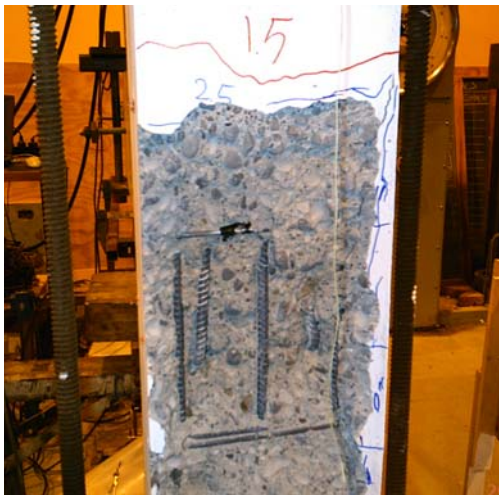

g) Column reinforcement was buckling at the concrete spalling region

Fig. 5.10 Sequence of observed cracks

5.3.3 Joint Behaviour

From Fig. 5.11, the principal tensil stress p_t=0.2$\sqrt{f'_c}$ was reached while the beam hinged in the positive loading direction. Since the critical principal tensile stress of joint failure p_t=0.29 $\sqrt{f'_c}$ for using deformed bars was not reached, the beam flexural failure was observed in both loading directions. However, the occurrence of column bar buckling and concrete spalling off the column caused the principal tensile stress in the joint decreasing after 2.5% and 1.5 % for the positive loading and negative loading respectively. It was noted that the peak value of horizontal joint shear stress was 1.75MPa (Fig. 5.12) and higher than the value obtained in the test of TDP1. Therefore, horizontal joint shear stress is not effective to predict the joint shear failure.

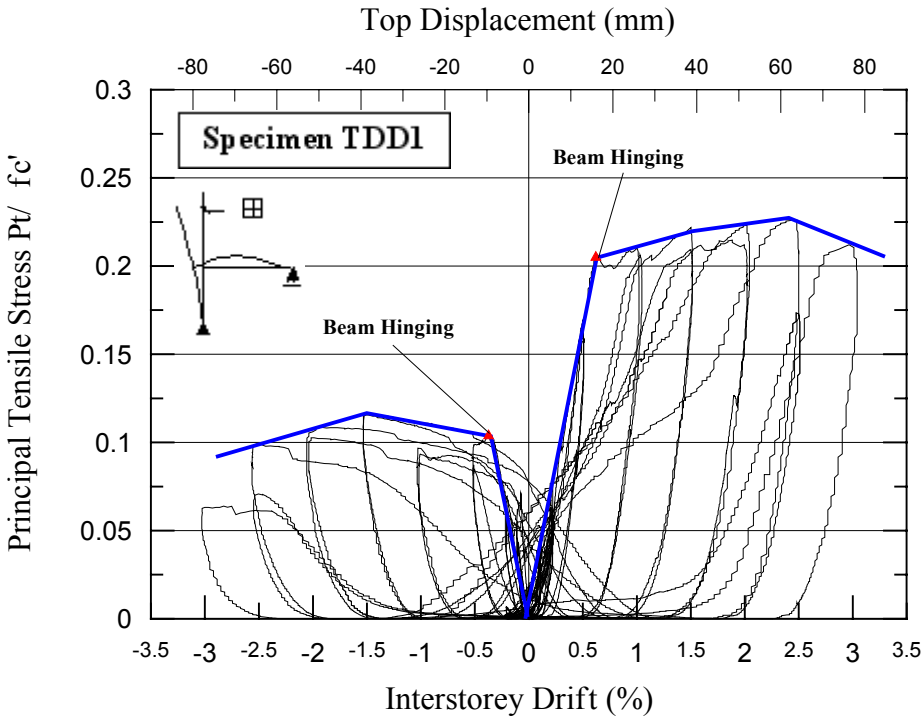

Fig. 5.11 Horizontal joint shear stress versus horizontal relationship

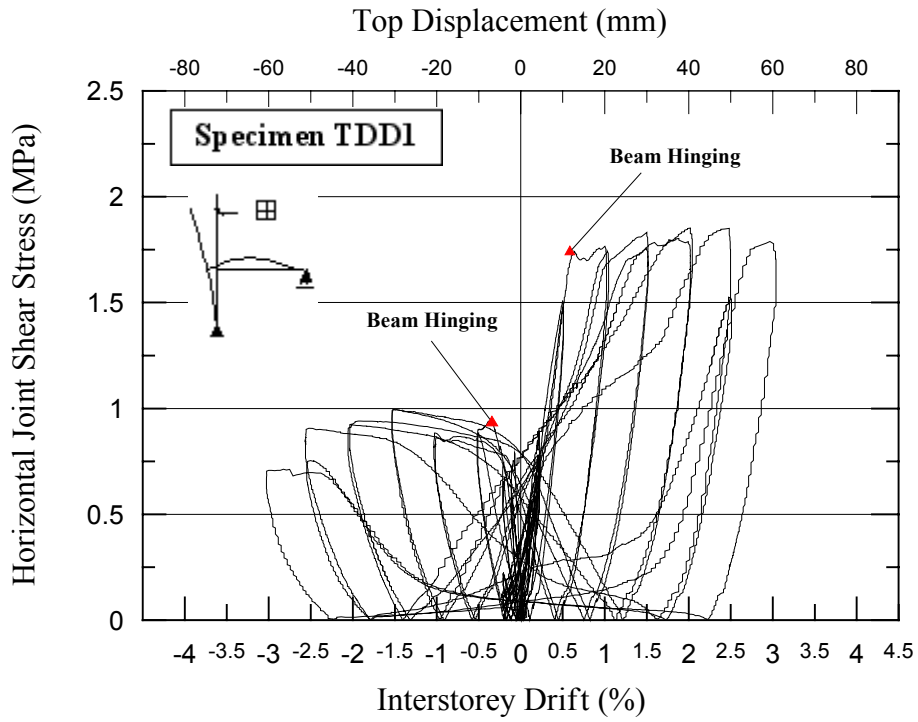

Fig. 5.12 Horizontal joint shear stress versus horizontal relationship

5.3.4 Decomposition of Horizontal Displacement

As illustrated in Fig. 5.13, the joint deformation was small and contributed a little to the total horizontal displacement. Due to occurrence of the beam hinging, the contribution of the beam flexural deformation to the horizontal storey drift increased gradually and became the main source of inter-storey drift.

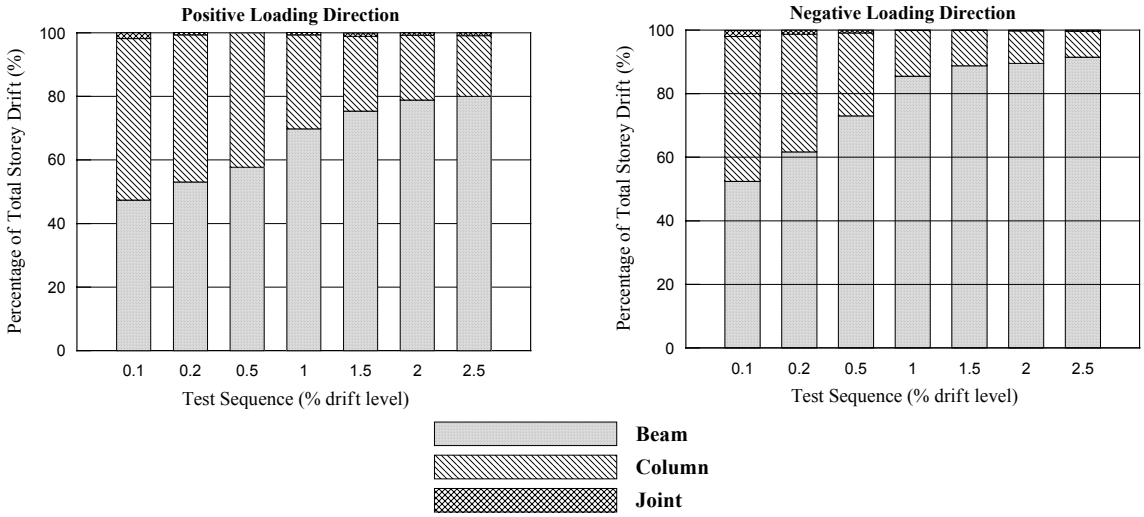

Fig. 5.13 Contributions to subassembly drift of beam, column and joint in TDD1

5.4 TEST OF TDP2

5.4.1 Specimen

The joint brittle shear failure was expected to happen in both positive and negative loading directions although the joint strength was still close to the beam flexural capacity in the positive loading.

5.4.2 General Behaviour

The final crack pattern and the measured global hysteretic loops are shown in Fig. 5.14 and 5.15 respectively. Fig. 5.16 illustrates the sequence of observed crack patterns at each critical drift level.

The first crack in positive loading happened at 0.73% during loading to 1.0% drift level and the lateral resistant force dropped down suddenly. The lateral force at 1.0% level was smaller

than that at first crack level. The lateral resistant force increased to the maximum value, 16.18kN, at 1.5% drift in positive loading direction and the peak value at each drift level began to decrease dramatically. In the negative loading direction, the first crack happened at 0.46% drift which was smaller than that in the positive loading direction and the lateral shear force at this drift was 12.4kN. The peak value of lateral shear force at each drift level after 0.5% in the negative loading direction kept increasing until 2.0% drift and began to decrease dramatically. The sequence of crack patterns was presented in Fig. 5.16.

Fig. 5.14 Final crack of TDP2

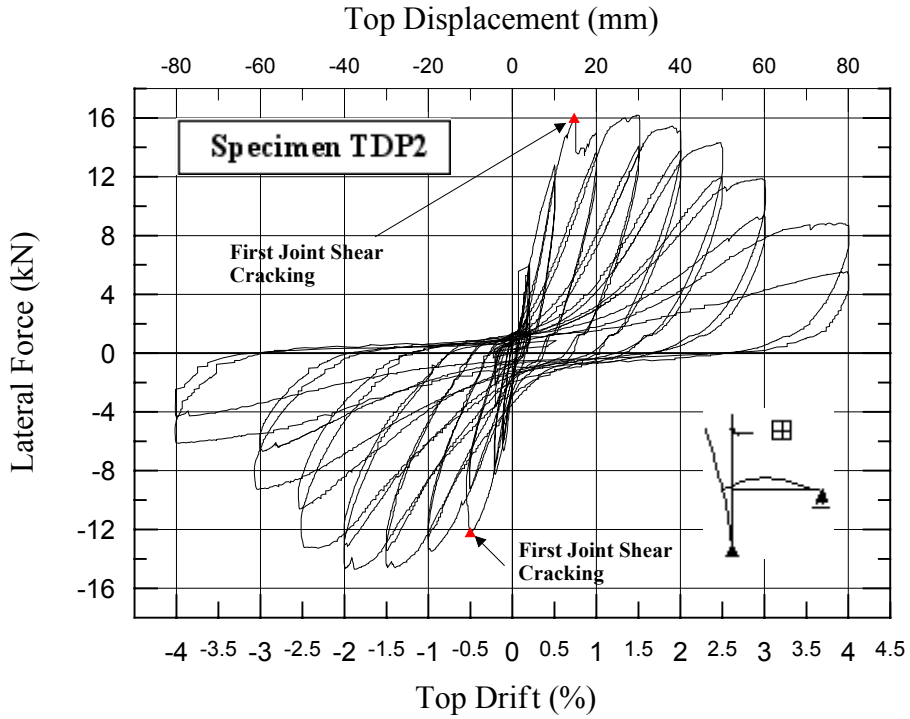

Fig. 5.15 Storey-shear force versus horizontal relationship of specimen TDP2

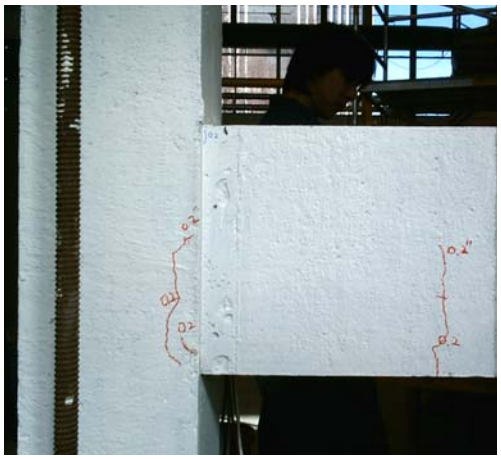

a) Minor cracks occurred in the beam at small drift level

b) First joint shear crack at -0.5% drift level in the negative loading direction

c) First joint shear crack at 1.0% drift level in the positive loading direction

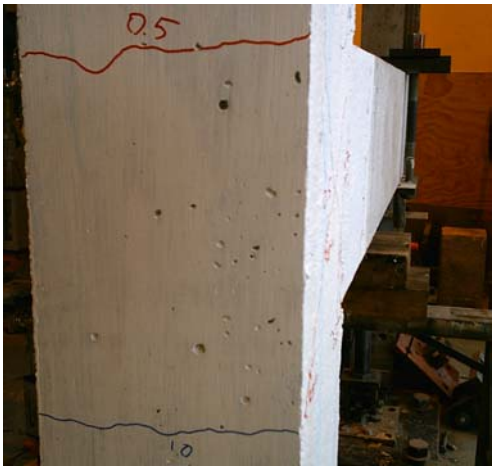

d) Crack in the back of column at first joint shear crack level

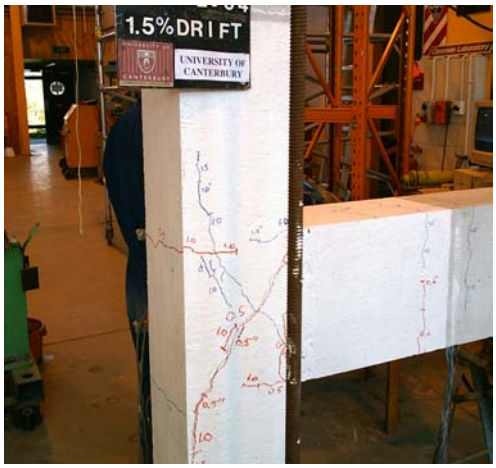

e) The original joint shear crack extended longer at 1.5% drift level

f) The joint shear crack become bigger and opening at 2.0% drift level

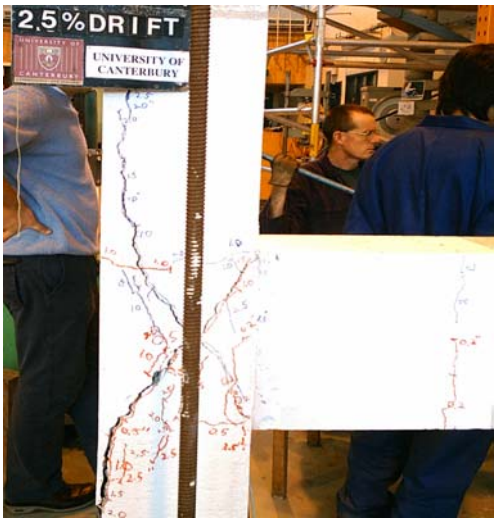

g) The brittle joint formed a concrete wedge by the crack opening at 2.5% drift level

h) The column back had serious crack by concrete spalling off

i) The opening of the concrete wedge become bigger at 3.0 level drift level

j) The concrete in the joint panel zone started falling down at final stage

Fig. 5.16 Sequence of observed cracks

5.4.3 Joint Behaviour

The joint shear crack were observed in both positive and negative loading direction with p_t=0.195$\sqrt{f'_c}$ and p_t=0.175$\sqrt{f'_c}$ respectively (Fig. 5.17). Since the providence of a single transverse reinforcement in the joint core, the principal tensile stress increased after first shear crack. The joint strength degradation occurred after loading to 1.5% drift level in both loading

directions. The joint shear deformation at the first crack was 0.001 and 0.0013 for the positive and negative loading respectively (Fig. 5.18). As illustrated in Fig. 5.19, the horizontal joint shear stresses at the first joint crack state were observed of 1.7MPa and 1.25MPa for each loading direction.

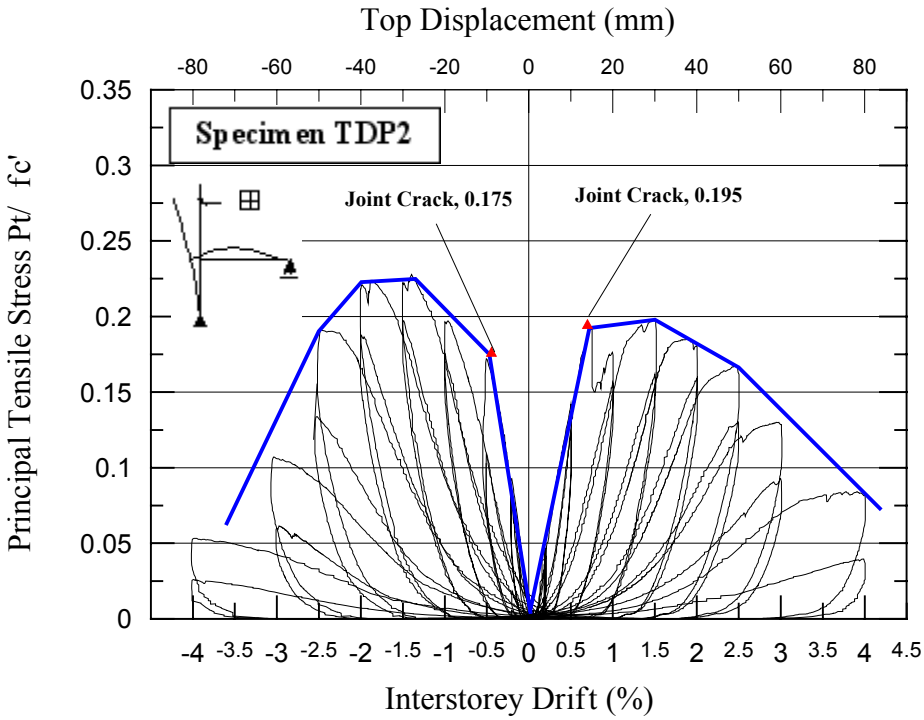

Fig. 5.17 Principal tensile stress versus horizontal relationship

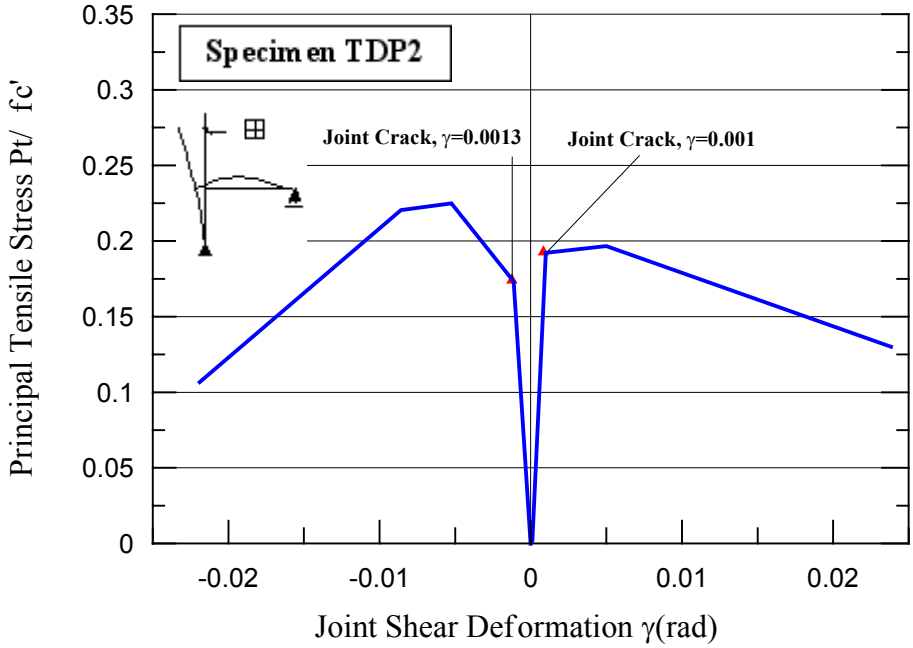

Fig. 5.18 Principal tensile stress versus joint rotation

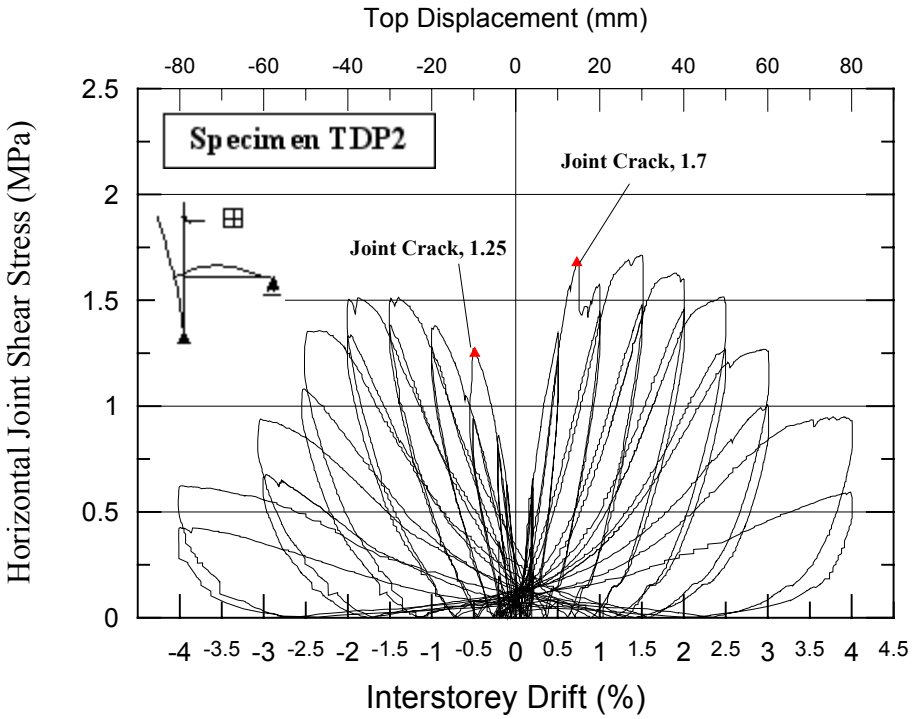

Fig. 5.19 Horizontal joint shear stress versus horizontal relationship

5.4.4 Decomposition of Horizontal Displacement

Fig. 5.20 illustrated that the great deformation of the joint after first shear crack contribute the most of the total horizontal displacement. It was also noted that the joint contribution dramatically increased after the joint shear failure was observed while the contribution of the beam to the drift angle decreased after the critical drift level.

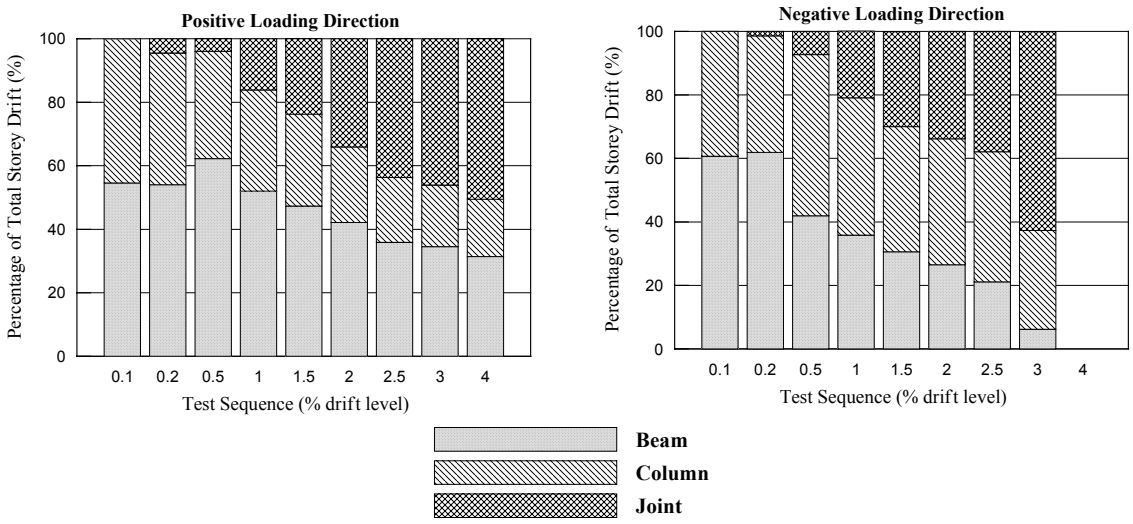

Fig. 5.20 Contributions to subassembly drift of beam, column and joint in TDP2

5.5 TEST OF TDD2

5.5.1 Specimen

From the hierarchy strength diagram, the joint first crack capacity increased because of using deformed bar. The joint shear crack was expected to be observed in both loading directions before the flexural failure in the beam by the increased positive flexural strength of the beam in TDD2.

5.5.2 General Behaviour

From Fig. 5.21, the joint failure mechanism was observed during the test. The first crack of the positive loading occurred at 0.65% during the loading to 1.0% drift level and then, the lateral resistant force dropped down suddenly (Fig. 5.22). The lateral force at 1.0% level was smaller than that at the first crack. The lateral resistant force increased to the maximum value, 23kN, at 1.0% drift in the positive loading direction and the peak value at each drift level began to decrease dramatically. In the negative loading direction, the first crack occurred at 0.65% drift with 15.9kN lateral shear force and dropped suddenly after the crack. The peak lateral force reached the maximum value, 16kN, at –1% drift and decreased significantly at the higher drift level. The sequence of crack pattern was presented in Fig. 5.23.

Fig. 5.21 Final crack of TDD2

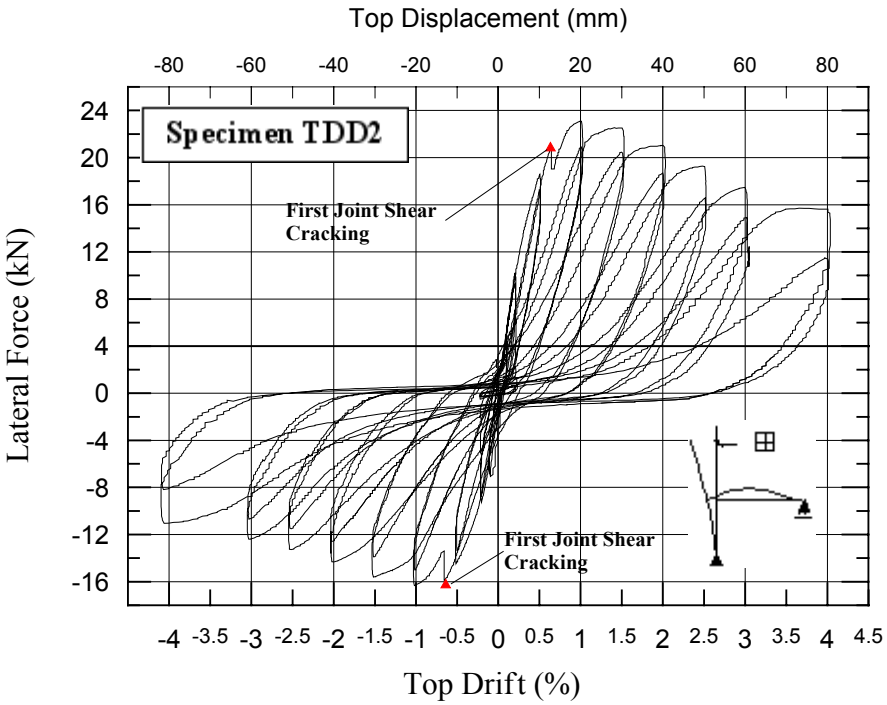

Fig. 5.22 Storey-shear force versus horizontal relationship of specimen TDD2

a) Minor cracks evenly distributed in the beam at small drift level

b) Some minor cracks appeared in the column back at small drift level

c) First joint shear crack at 1.0% drift level in the positive loading direction

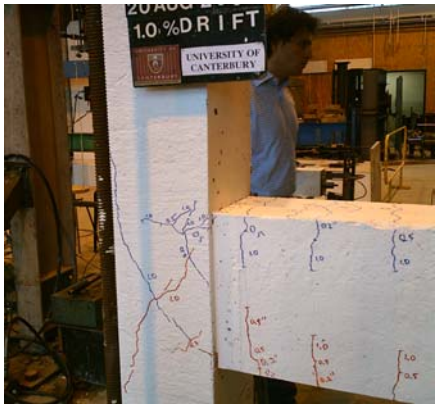

d) First joint shear crack at –1.0% drift level in the negative loading direction

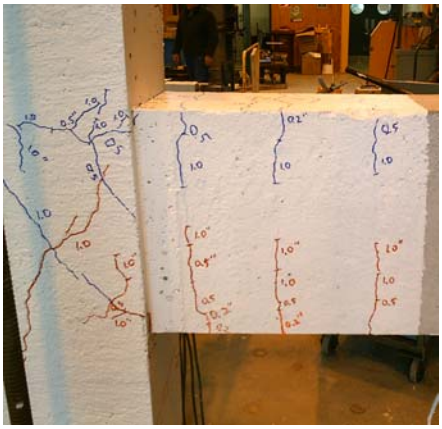

e) New extended cracks in the beam in the second cycle of 1.0% drift level

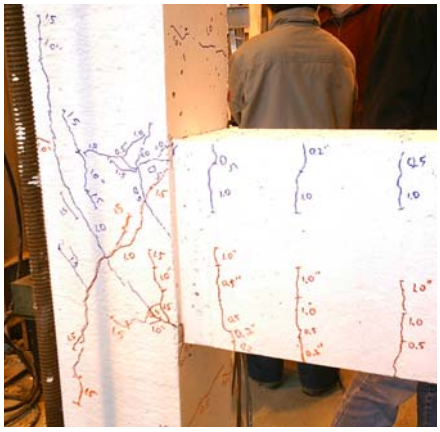

f) New cracks concentrated on joint panel zone in 1.5% drift level in both loading directions

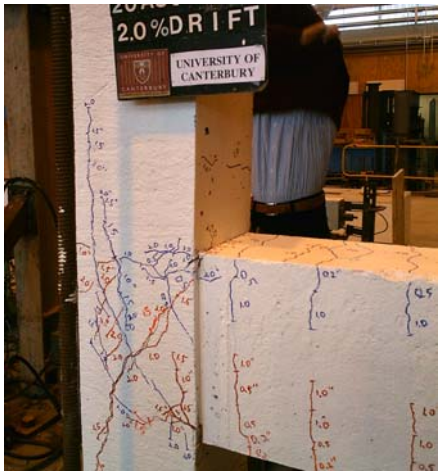

g) New cracks in the joint panel zone and major joint shear crack extended at 2.0% drift level

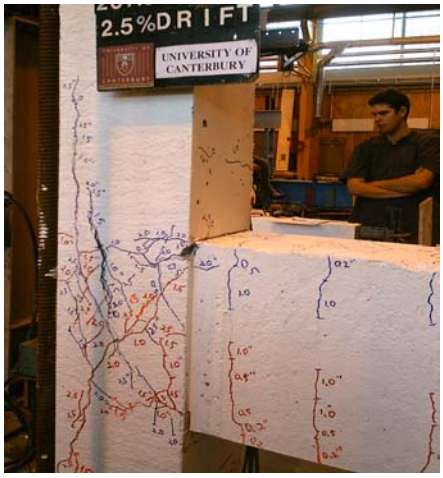

h) The major shear cracks began opening at 2.5% drift level

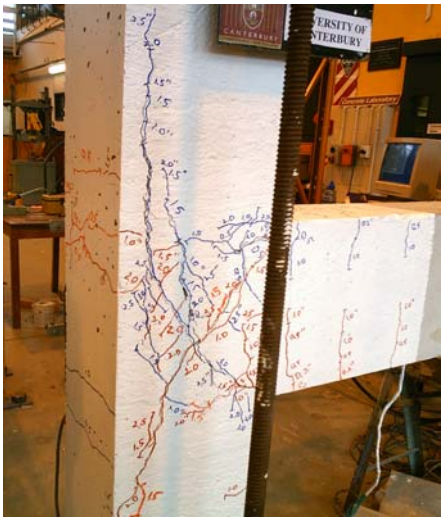

i) The concrete wedge was formed by the shear cracks opening at 3.0% drift level

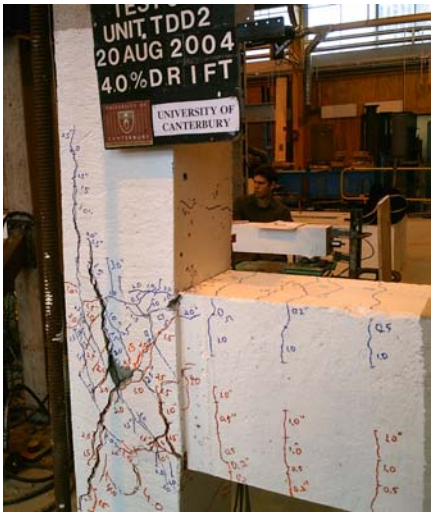

j) Concrete began to spall off from the brittle joint region

Fig. 5.23 Sequence of observed cracks

5.5.3 Joint Behaviour

From Fig. 5.24, the first joint crack occurred at p_t=0.29$\sqrt{f'_c}$ and p_t=0.26$\sqrt{f'_c}$ for the positive and negative loading directions respectively. The principal tensile stress of the joint kept increasing till the extensive damage was achieved at p_t=0.33$\sqrt{f'_c}$ and p_t=0.265$\sqrt{f'_c}$ for the positive and negative loading respectively. The joint strength in terms of principal tensile stress for the extensive damage was lower than the expected value. The joint rotations at the first shear crack were observed as 0.0029 and 0.0025 in each loading direction (Fig. 5.25). The horizontal joint shear strength was 2.45MPa in the positive loading direction that was much higher than 1.65MPa in the negative loading direction (Fig. 5.26). The great difference of horizontal joint shear stresses to cause the joint shear failure demonstrated the unreliability of them in predicting the joint response.

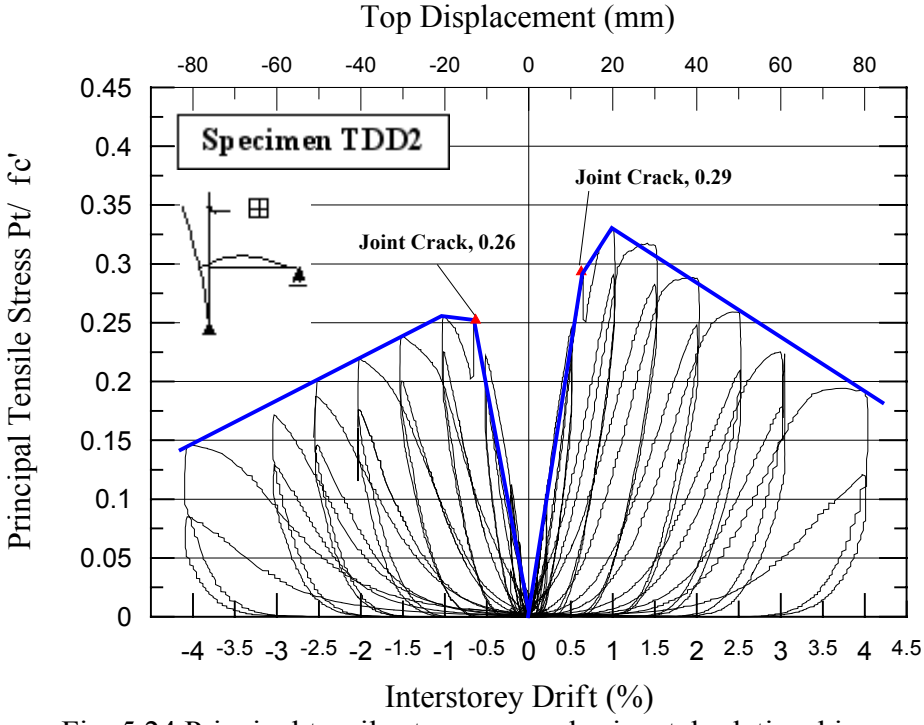

Fig. 5.24 Principal tensile stress versus horizontal relationship

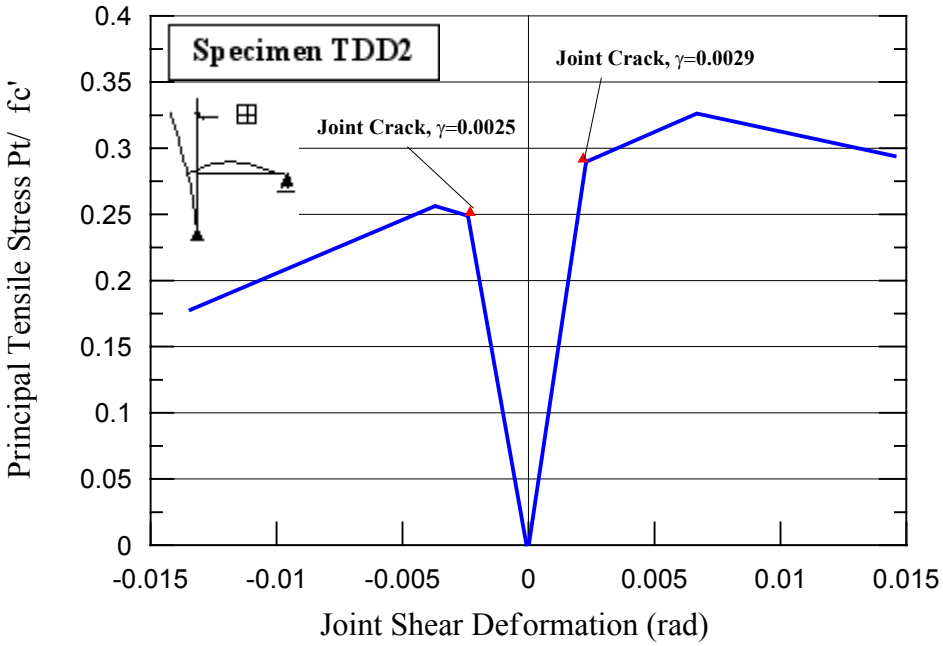

Fig. 5.25 Principal tensile stress versus joint rotation

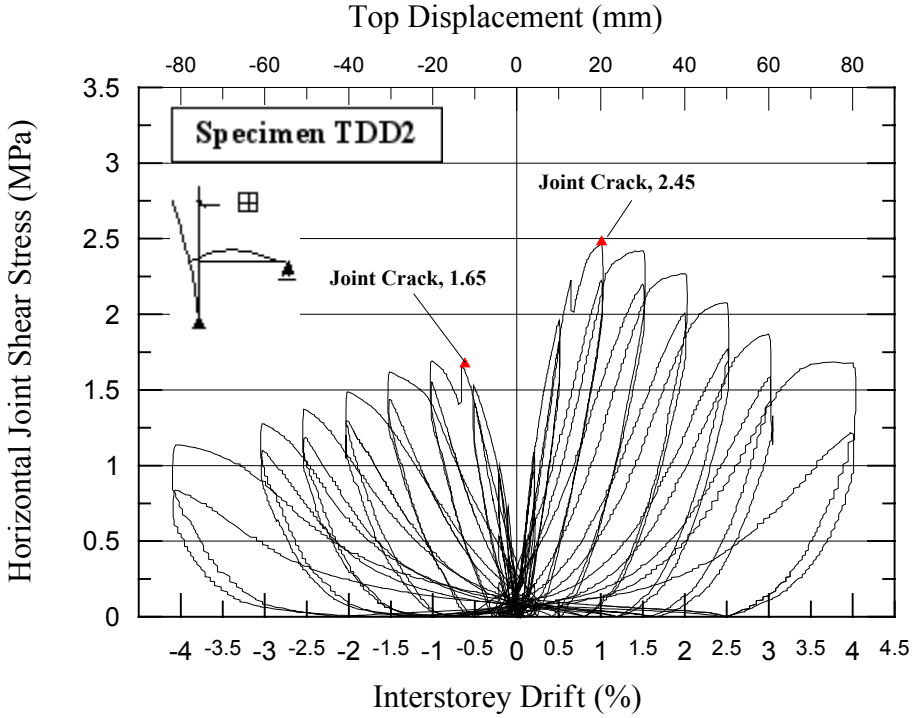

Fig. 5.26 Joint horizontal shear stress versus hotizontal relationship

5.5.4 Decomposition of Horizontal Displacement

Due to the occurrence of the joint shear failure, the contribution of the joint deformation to the total horizontal drift increased dramatically after the first crack in the positive loading

direction (Fig. 5.27). As result of cracks in the joint panel zone, the potentiometers used to measure the joint deformation were not well fixed to the column surface and the recorded values were not reasonable for the negative loading direction after the first joint crack.

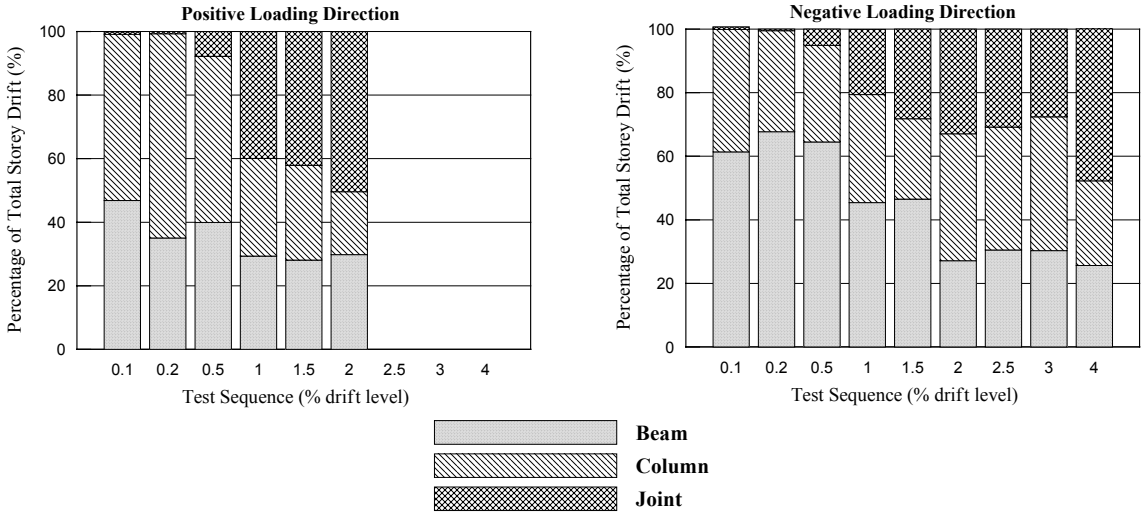

Fig. 5.27 Contributions to subassembly drift of beam, column and joint in TDD2

5.6 TEST OF TSP1

From the hysteretic loop illustrated in Fig. 5.28, the beam flexural hinges were observed in both loading directions. Due to the incomplete development of the beam flexural strength, the inter-storey shear force was smaller than the expected value. Instead of the joint shear failure mechanism, a rare shear failure observed in the rear face of the beam. With this shear cracks appearing, the beam bar anchored outside the joint core began sliding and the remarkable pinching seismic response was observed in the hysteresis loop after the first cracks at 1.5% drift level. The sever shear crack at the back of the beam was presented in Fig. 5.29

Since the intact joint panel zone was observed during the test, the small joint contribution to the horizontal total drift was presented. Due to the beam flexural failure, most of the horizontal total displacements came from the beam deformation (Fig. 5.30). However, the greatly increased contribution of the column deformation to the horizontal drift after 2.0% drift level was caused by accounting the beam shear cracks at the back of the beam into the column deformation.

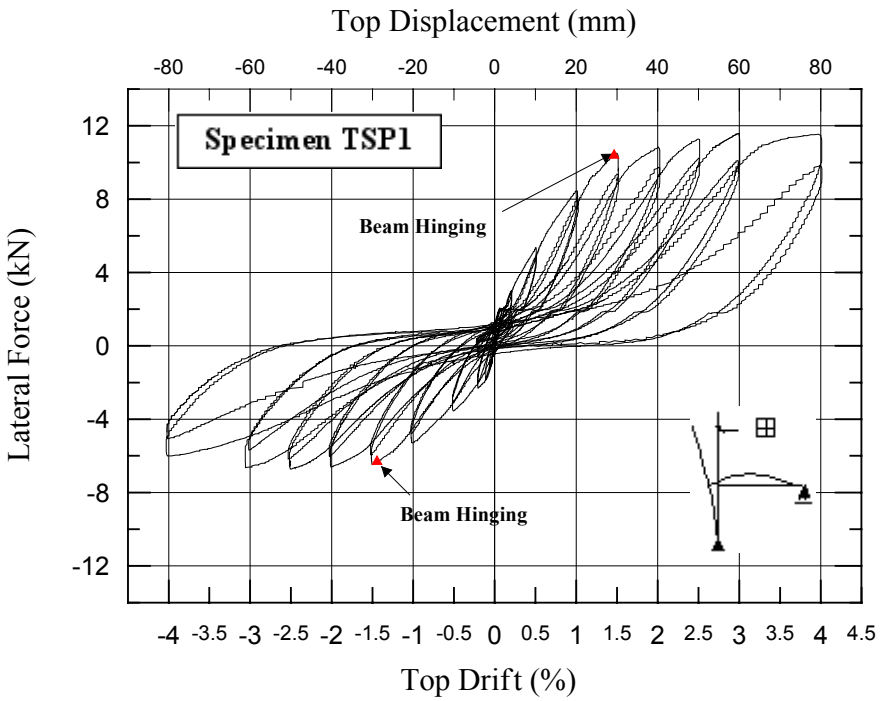

Fig. 5.28 Storey-shear force versus horizontal relationship of specimen TSP1

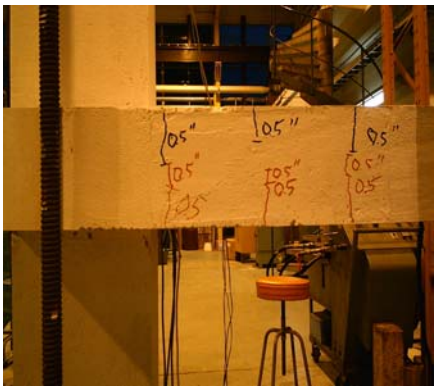

a) Minor cracks in the beam at 0.5% drift level

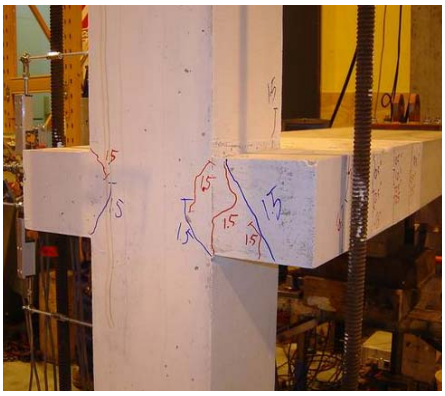

b) Shear cracks at the rear face of the beam at 1.5% drift level

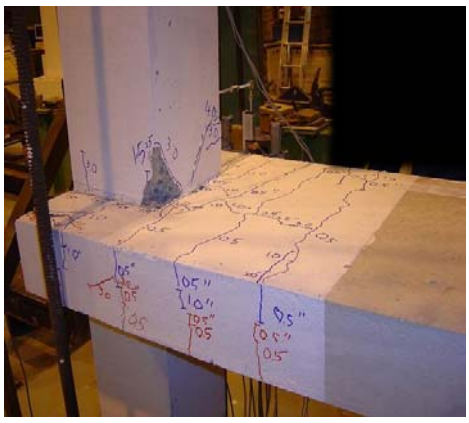

c) Final crack pattern ain the beam

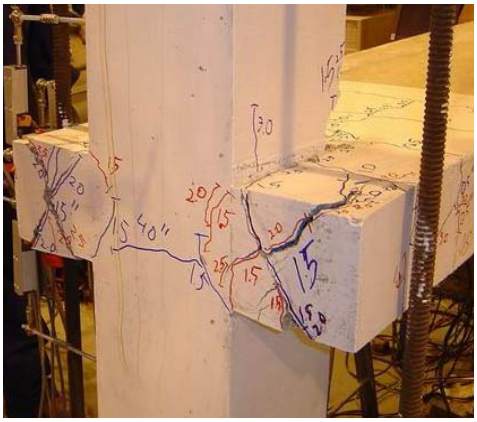

d) Final crack pattern at the rear face of the beam

Fig. 5.29 Sequence of observed Cracks

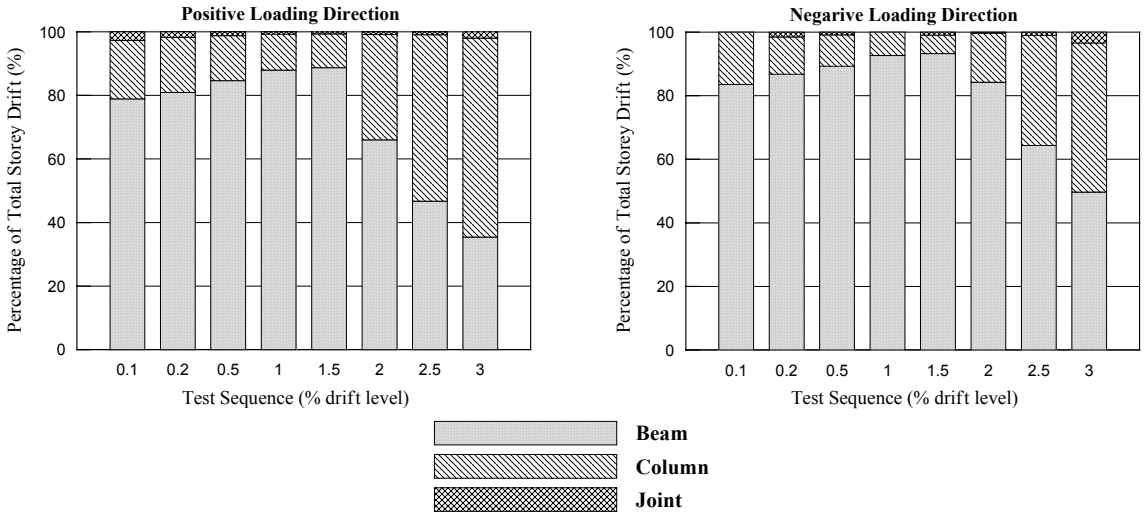

Fig. 5.30 Contributions to subassembly drift of beam, column and joint in TSP1

5.7 TEST OF TSD1

From the hysteretic loop illustrated in Fig. 5.31, the beam flexural hinges were also observed in both loading directions. Since the fully flexural strength of the beam could not be developed, the inter-storey shear force was lower than expected value. Instead of joint shear failure mechanism, a rare shear failure observed in the rear face of the beam. Although the pinching seismic response still occurred once the shear crack appeared in the rear face of the beam after 1.5%, the less slippage was observed in the test compared with TSP1 test. This was because the use of deformed bar in this subassembly could provide the better bond stress to resist the bar slippage. However, by using deformed bars, the stronger bond strength between the reinforcement and concrete material may cause serious concrete deterioration (Fig. 5.32).

Form Fig. 5.33, the beam had the most contribution to the horizontal total displacement before 1.5% drift level. Once the shear crack occurred in the back of the beam, the column contribution increased significantly. This was because the shear crack of the beam could be counted into the deformation of the column.

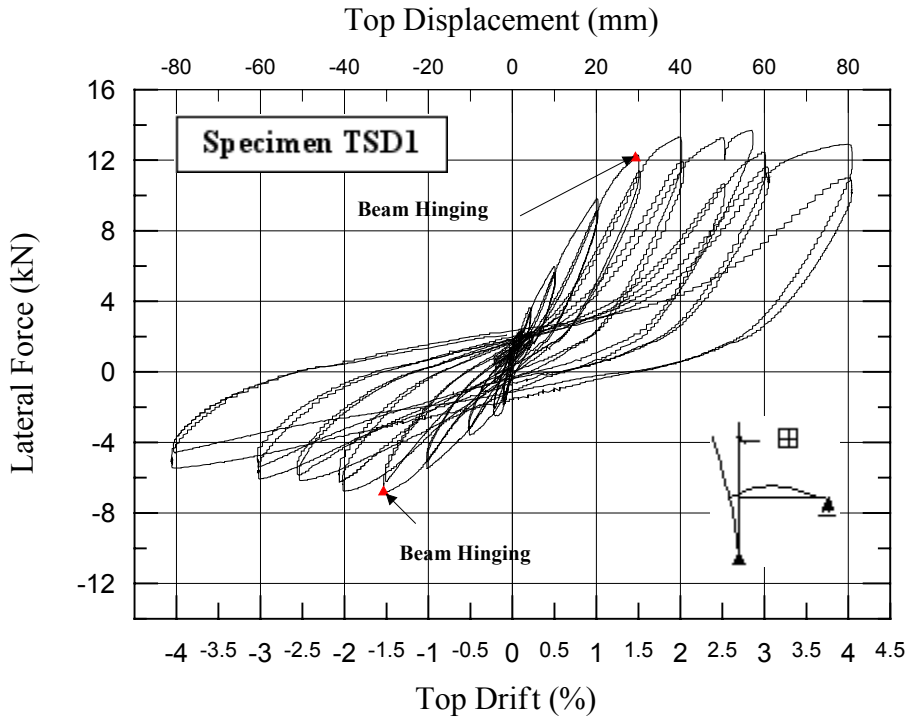

Fig. 5.31 Storey-shear force versus horizontal relationship of specimen TSD1

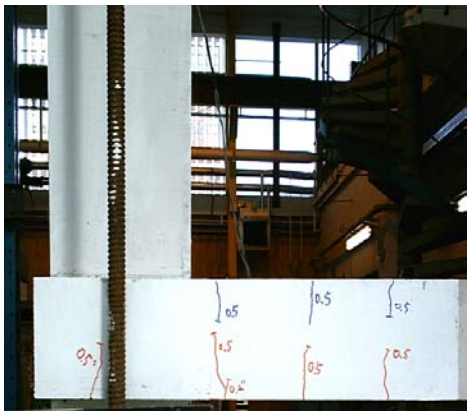

a) Minor cracks in the beam at 0.5% drift level

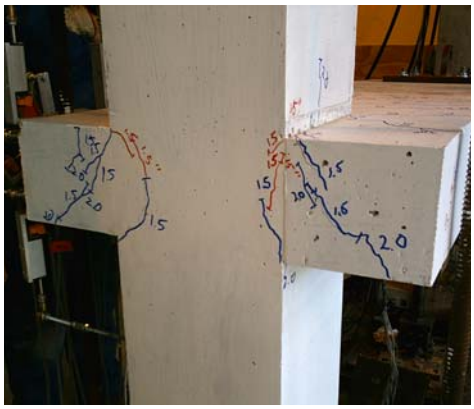

d) Final crack pattern at the rear face of the beam

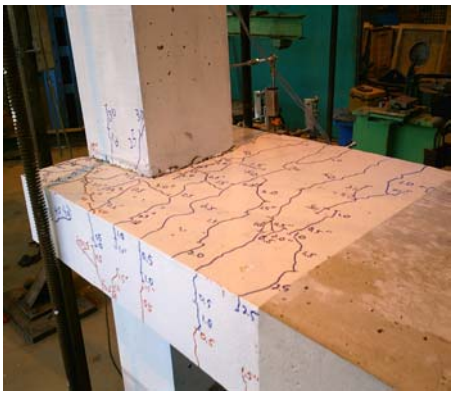

c) Final crack pattern ain the beam

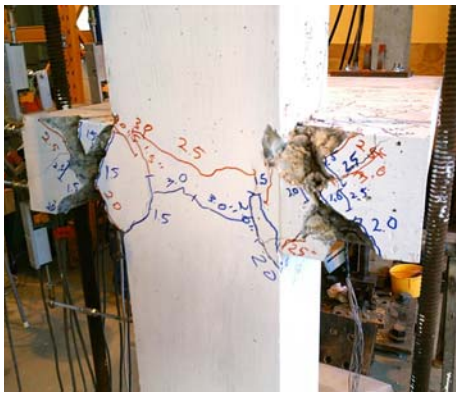

d) Final crack pattern at the rear face of the beam

Fig. 5.32 Sequence of observed Cracks

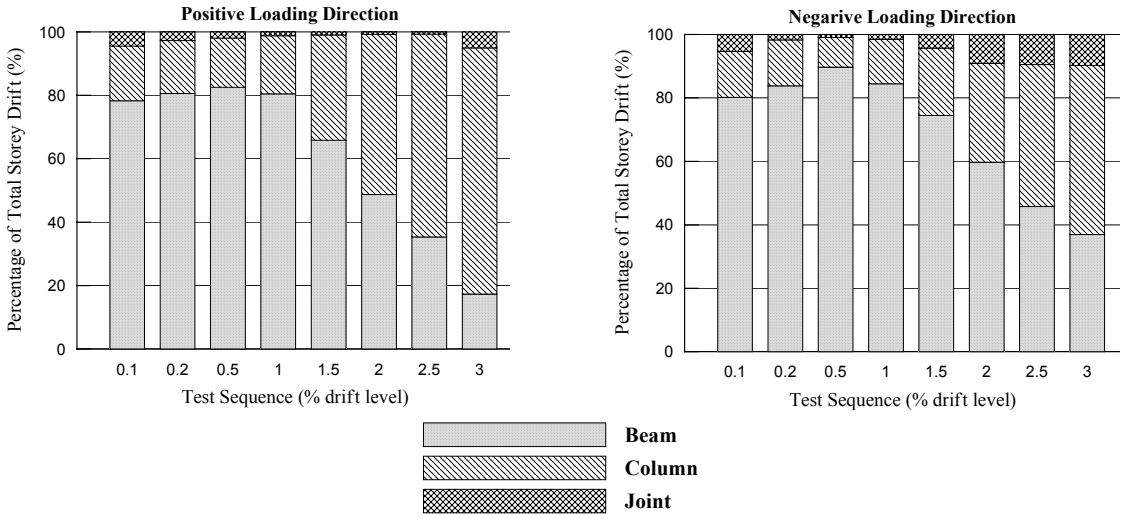

Fig. 5.33 Contributions to subassembly drift of beam, column and joint in TSD1

5.8 TEST OF DD2

5.8.1 Specimen

The existing corner joint, named DD2, was tested in 3-D experimental configuration to investigate the joint response under the biaxial loadings. Without providing the transverse reinforcement in the joint core, the strength degradation was expected after the first joint shear crack. Due to the difficulties in measuring the joint deformation, some data was not available after cracks occurring in the joint region. To investigate the joint behaviour during the bi-directional loadings, the principal tensile stress was also discussed for the specimen DD2 and considered with the interaction of capacities in principal axes.

5.8.2 General Behaviour

Due to the safety consideration, the loadings were applied to 3.0% resultant drift only and the potentiometers were taken off after 2.5% resultant drift to avoid being damaged. As shown in Fig. 5.34, the final damage of the subassembly presented the joint shear failure in DD2. There were some minor cracks observed in the beam during the loading to 0.2% drift. The first joint diagonal joint crack occurred during the cycle of loadings to 1.0% drift level and the joint deterioration started in the following drift level. Because no transverse reinforcement was used in the joint core, the column reinforcing bars through the joint panel zone were buckling and the concrete over this region was spalling off seriously after test. Due to the relative

weakness of the joint, beams maintained elastic without occurrence of flexural hinge even if there were some minor cracks in them.

Fig. 5.34 Final crack of DD2

5.8.3 Joint Behaviour

X-direction face:

The final crack pattern and the measured global hysteretic loops are illustrated in Fig. 5.35 and Fig. 5.36 respectively. The serious joint shear damage was observed after the test with the buckling of the column reinforcement in the joint core. The seismic response of DD2 also had a remarkable pinching behaviour in the X-direction loading. Compared with TDP2 where the strength kept up a little after the joint shear cracks, the sudden strength degradation was observed after the first diagonal shear crack in the joint panel zone. The possible reason was that absence of the transverse reinforcement in the joint could lead to more serious joint damage with buckling column bars. The first crack was observed at about 0.75% drift in both positive and negative loading directions and the peak strength of 17.5kN and 15.2kN at these points. In the following drift level accompanied with the propagated and widened cracks, the strength decreased dramatically and reached about 8.0kN and 4.0kN for the positive and negative loadings respectively.

Fig. 5.35 Final crack of DD2 for X-direction face

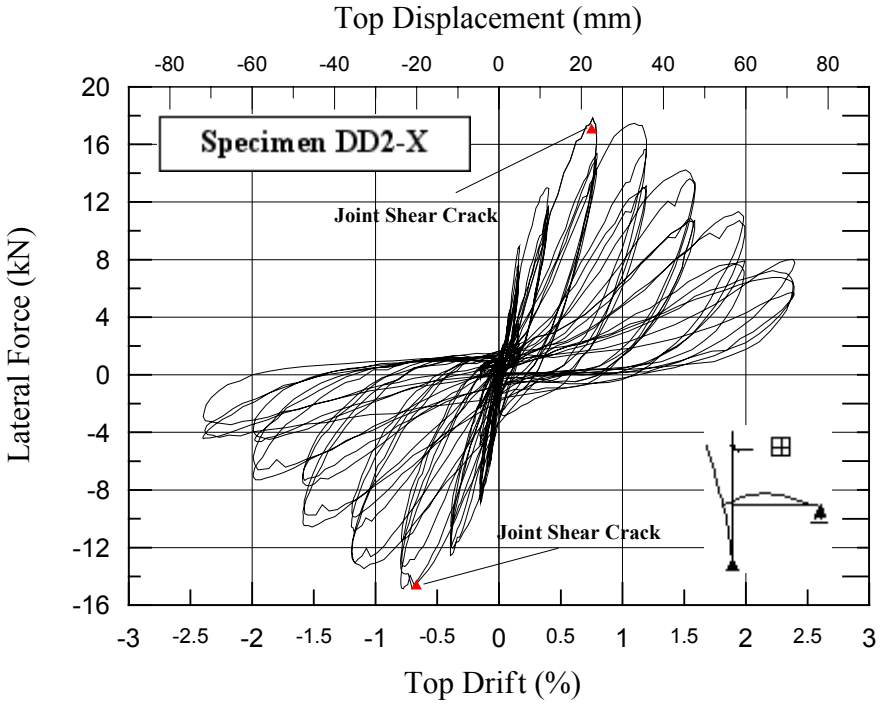

Fig. 5.36 Storey-shear force versus horizontal relationship of specimen DD2 for X-direction face

From Fig. 5.37, the first joint shear crack was observed with principal tensile stress of $0.175\sqrt{f'_c}$ and $0.21\sqrt{f'_c}$ in the positive and negative loading direction respectively. There was a little increase of principal tensile stress after first shear crack. However, without transverse reinforcement presented in the joint core, the strength degradation of the joint was severe. Compared with the 2-D test of TDP2, the principal tensile strength seemed not to increase in the corner joint under bi-directional loadings.

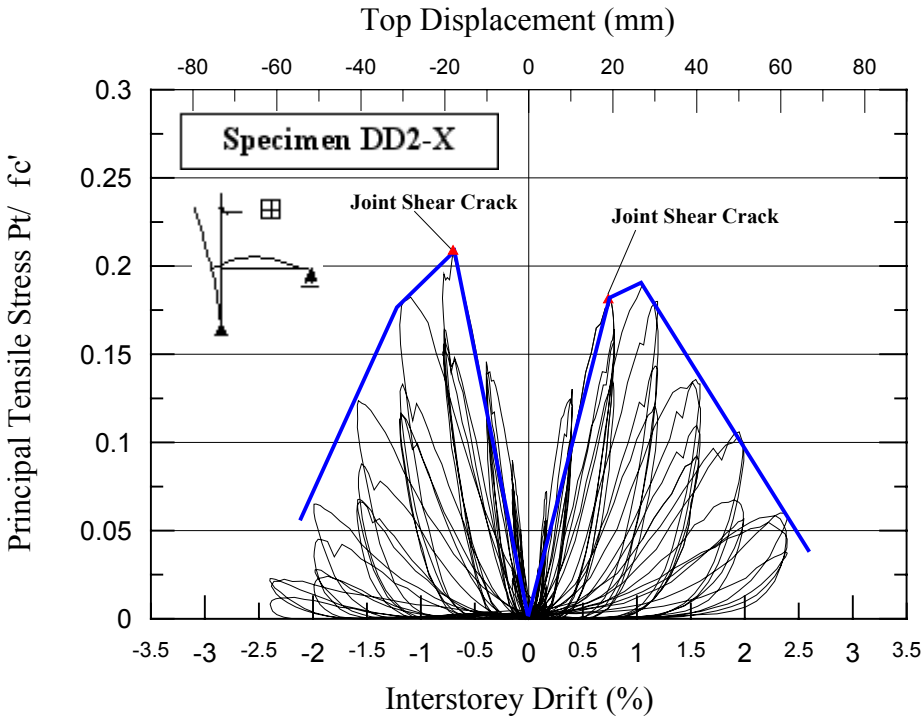

Fig. 5.37 Principal tensile stress versus horizontal relationship for X-direction face

Y-direction Face:

Similar behaviour of joint shear brittle mechanism was observed in the Y-direction face. The seismic response of loading on Y-direction was illustrated in Fig. 5.38 and the final crack pattern was presented in Fig. 5.39. It was also observed again that the strength degradation occurred after the joint shear cracks were initiated at 0.75% o drift for both positive and negative loading directions. The peak strengths at first joint cracks were 16.2kN and 17.8kN for the positive and negative loadings respectively and the propagated cracks in the joint panel zone caused the strength decreases to about 6kN for both directions of final drift level.

Fig. 5.38 Final crack of DD2 for Y-direction face

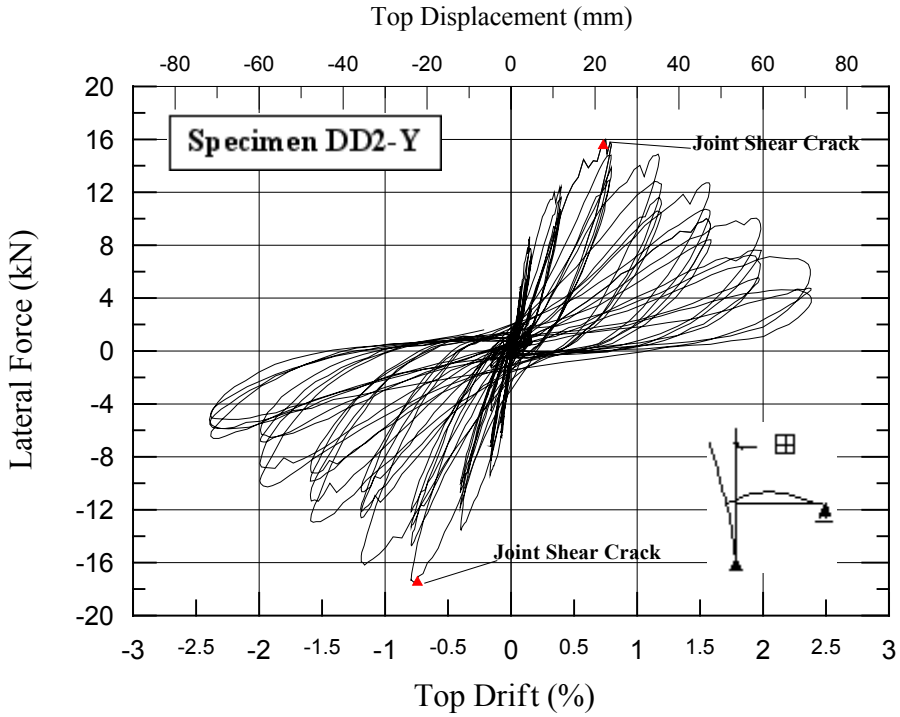

Fig. 5.39 Storey-shear force versus horizontal relationship of specimen DD2 for Y-direction face

The principal tensile stress obtained in the Y-direction loading is illustrated in Fig. 5.40. It was observed that the first joint shear crack occurred when the value of the principal tensile stress reached $0.15\sqrt{f'_c}$ and $0.24\sqrt{f'_c}$ for the positive and negative loadings. The strength almost degraded right away after the joint shear crack. The great difference of tensile strength between positive and negative loadings was probably cased by the great difference of the column axial loads while the joint cracks were first observed. As illustrated in Fig. 5.41, while the joint cracks were observed in the first and third quadrants for the positive and negative loadings of Y-direction face, the measured column axial loads were 125kN and 62kN respectively. With similar lateral forces of 16.0kN and 17.0kN in positive and negative Y-directions, the horizontal joint shear forces V_{jh} were also similar. According to Eq. 3.3, the greater column axial load resulted in the smaller principal tensile stress that was critical in causing the joint shear crack.

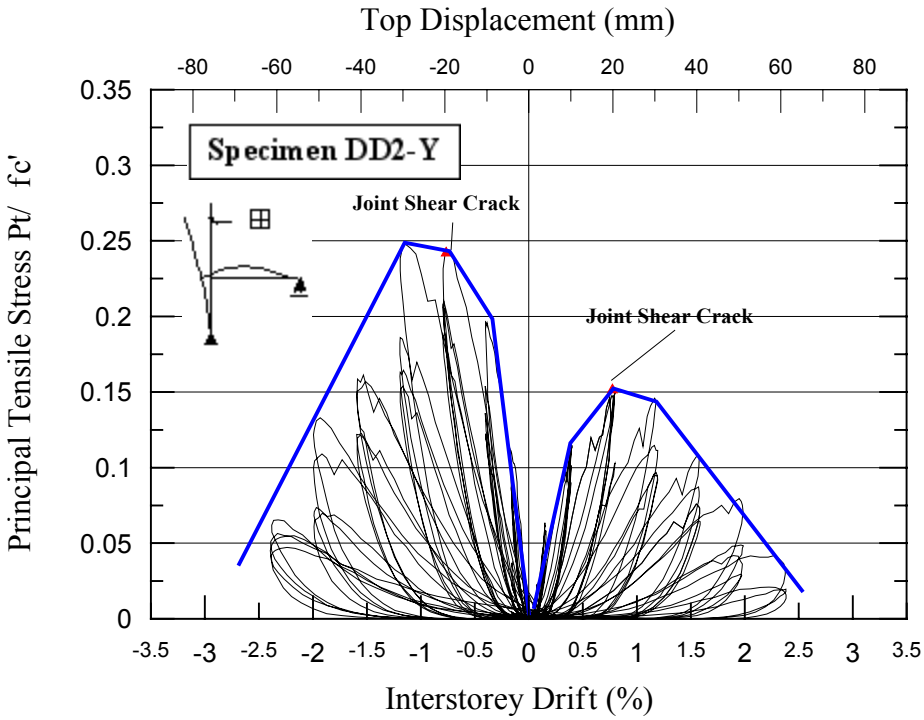

Fig. 5.40 Principal tensile stress versus horizontal relationship for X-direction face

5.8.4 Interaction of The Corner Joint under Biaxial Loadings

According to the previous investigation Chapter 2, the principal tensile strength of the corner joint was supposed to be $0.58\sqrt{f'_c}$ that was based on using deformed reinforcement and uni-directional loadings. Because the bi-directional loadings were applied in this test, according to the review in section 2.4.4, the obtained principal tensile strength under bi-directional loadings would be less than the joint strength about principal axes. In other words, due to the interaction of the bi-directional loadings, the corner joint became weaker in resisting the horizontal joint shear forces while it suffered bi-directional loadings. Therefore, it is interesting to estimate the principal tensile strength about the principal axis while the corner joint was reinforced in plain round bars.

As illustrated X-Y loading domain of Fig. 5.41, the marked points revealed the lateral forces applied on the joint in X or Y-directions while the first joint crack occurred. Due to the structural geometry, the column axial loads that could affect the joint capacity were also varied for each point. Because the bi-directional capacity surface was supposed to be adopted in evaluating the beam-column joint strengths, Eq. 2.2 could be generally expressed as:

$$\left(\frac{F_y}{FY_y}\right)^{\alpha}+\left(\frac{F_z}{FY_z}\right)^{\alpha}=1.0 \tag{5.1}$$

where FY_y and FY_z were the lateral strengths about principal X and Y axes and F_y and F_z were lateral strengths of any points along failure surface. Assume that the lateral strength are equal about principal X and Y axis (i.e. FY_y=FY_z) and α=1.4, the value of FY_y and FY_z which caused the joint shear crack under the uni-directional loading on the corner joint could be estimated by a given value of any failure point. Once the lateral strength was determined, the principal tensile strength could be obtained by the procedure described in Chapter 3. The evaluated results of each point as shown in Fig. 5.41 are given in Table 5.1. Although the much higher value of principal tensile strength about the principal axis was obtained in the negative loading of Y-direction face, generally speaking, $0.26\sqrt{f'_c}$ could be proposed to be the principal tensile strength of the corner joint under uni-directional loadings. Compared with $0.2\sqrt{f'_c}$ for 2-D joint, the spandrel beam in the corner joint provided better confinement to the joint and the joint could have higher shear strength consequently.

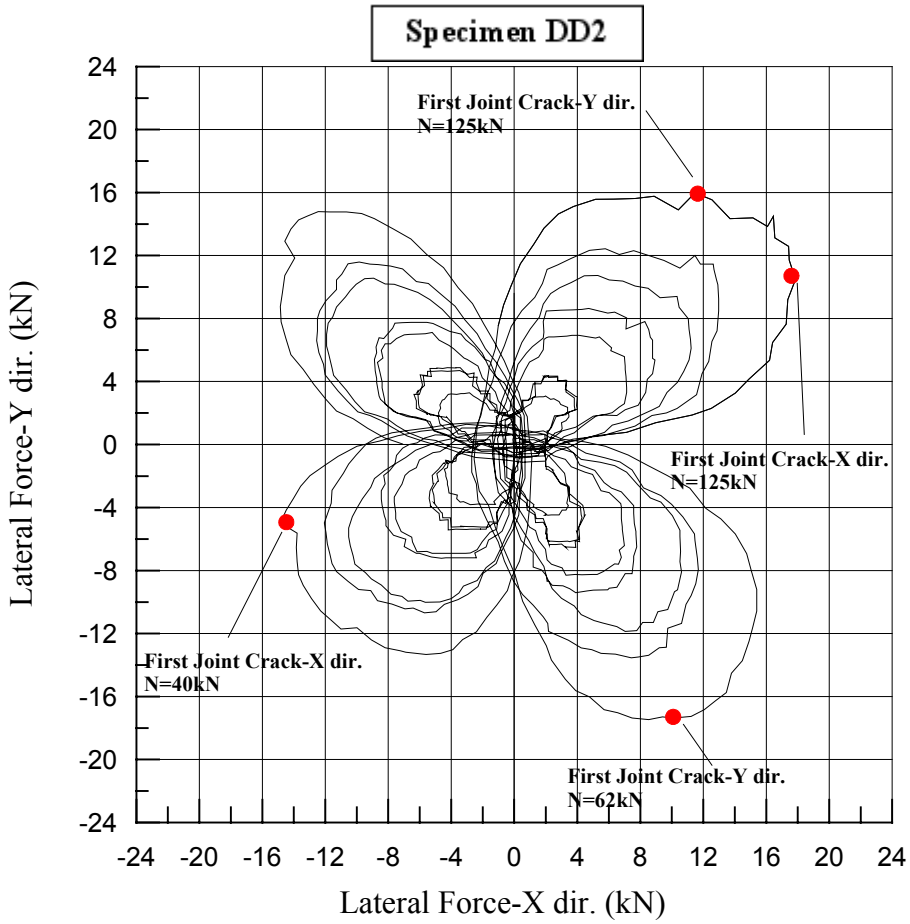

Fig. 5.41 Inter-storey Forces in X-Y Plane

Table 5.1 Proposed principal tensile strength of first joint crack about principal axes

Condition	**Column axial load N (kN)**	**Column lateral force of joint shear crack**		**Column lateral strength about principal axis**	**Joint strength about principal axis**
		F_x **(kN)**	F_y **(kN)**	$FY_y=FY_z$ **(kN) if** α**=1.4**	**Proposed** p_t
Q1: Positive in Y-dir. face	**125**	12	16	23	$0.26\sqrt{f'_c}$
Q1: Positive in X-dir. face	**125**	17	11	23.2	$0.26\sqrt{f'_c}$
Q2: Negative in Y dir. face	**62**	10	17	22.4	$0.31\sqrt{f'_c}$
Q3: Negative in x-dir. face	**40**	15	5	17.2	$0.26\sqrt{f'_c}$

CHAPTER 6

EXPERIMENTAL PROGRAM OF RETROFIT SOLUTION

6.1 INTRODUCTION

According to the investigation of experimental results, the existing beam-column joint subassemblies TDP2 and DD2 designed under old practices without seismic design considerations confirmed that the pure brittle shear failure occurred in the joint. To avoid the undesired joint failure mechanism, the proper haunch solutions were required to retrofit the exterior beam-column joint subassemblies TDP2 and DD2. Regarding the capacity design philosophy with hierarchy strength design considerations, the target of proposed haunch retrofitting solution was to guarantee the strong column/weak beam mechanism by forcing the flexural hinge in the beam before other undesired failure mechanism.

In this chapter, different haunch solutions designed with the proposed design procedure in Chapter 3 are exploited to retrofit the existing beam-column joint subassemblies that had the same reinforcing details of TDP2 and DD2. Due to the biaxial loading effect on the varying axial load of the column, the specific considerations of the reduced column and joint capacity should be underlined in retrofitting the corner joint DD2 with haunch solutions and the external post tension on the column is suggested to achieve the designed capacity. The proper construction method of connecting the proposed haunch to the beam and column is suggested by considering the combination of the anchorage resistance and clamping force. Since the effectiveness of the haunch is stiffness-sensitive, the types of connection between the retrofitted subassemblies and haunches (i.e. hinge connection or fix connection) are investigated.

6.1.2 Design of The Haunch Elements

The design of the haunch retrofit solution system for all specimens was carried out following the conceptual procedure outlines in Chapter 3 and the descriptions of test specimens displayed in Table 6.1.

Table 6.1 Description of specimens

Abbreviation	Description of Specimens
THR1	Rebuilt 2-D subassembly TDP2 retrofitted with hinged haunches of elastic design
THR2	Rebuilt 2-D subassembly TDP2 retrofitted with hinged haunches of elasto-plastic design
THR3	Rebuilt 2-D subassembly TDP2 retrofitted with welded haunches of elastic design
THR3D	Rebuilt 3-D subassembly DD2 retrofitted with welded haunches of elastic design

Due to several uncertainties that were expected in the actual implementation of the haunch device, the haunch elements of THR1 and THR2 were first designed to target the stiffness of 10000kN/m with the tolerance by introducing the safety factors (saying Φ_1 and Φ_2 about 0.7 and 0.85 respectively). As a result, assuming L'=400 and $\alpha=45^o$ were suggested to achieve K_d=100000kN/m. The conservative design was aimed to protect the joint panel zone even if the significantly reduced stiffness of the haunch devices may be expected by using the hinge connection. THR3 then was designed to verify the effectiveness of the weld connection in the haunch device. The yielding properties acting like a fuse was designed in THR2 test to investigate the performance of the haunch element as an external energy dissipater. The additional biaxial test of THR3D was carried out to investigate effectiveness of the haunch solution on retrofitting the existing corner joint. To achieve the desired hierarchy strength in THR3D test, additional column axial load was added to simulate the external tendon force that was exploited to increase the column and joint strength.

6.2 TEST SPECIMENS

6.2.1 Specimen Detail of Beam-column Joint Subassemblies

2-D Unit:

Since the pure joint shear failure observed in TDP2, was representative of an as-built configuration in pre-1970s, the subassemblies of THR1, THR2 and THR3 retrofitted by the proposed haunch elements had the same specimen detail with TDP2. The specimen dimensions and reinforcing detail are given in Table. 6.2.

3-D Unit:

Experimental results of the corner beam-column joint DD2 in 3-D test were investigated to have critical joint shear failure. To compare the observed damage and performance of the retrofitted joint, THR3D was rebuilt with the same specimen detail of DD2 (Table 6.3) and retrofitted with the proposed haunch solutions.

Table 6.2 Summary of specimens in 2-D tests

Specimen		**THR1, THR2, THR3**	
Beam	**Size**	200x330	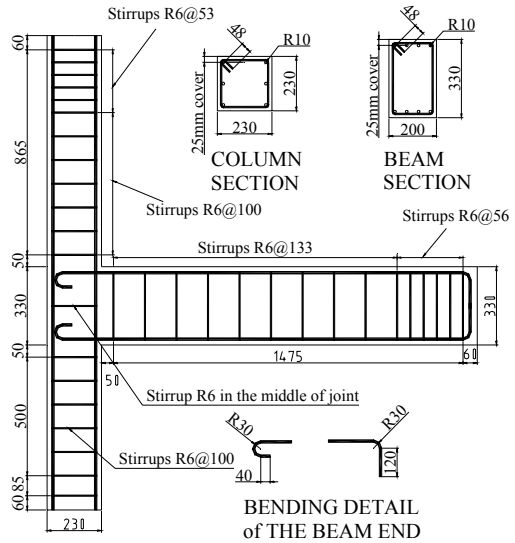
	Top Bars	4-R10	
		(ρ '=0.52%)	
	Bottom Bars	2-R10	
		(ρ =0.26%)	
	Stirrups	2-R6@133	
Column	**Size**	230x230	
	Main Bars	6-R10	
		(ρ t=0.89%)	
	Stirrups	2-R6@100	
Joint	**Stirrups**	2-R6@Middle	

Table 6.3 Summary of specimens in 3-D tests

Specimen		THR3D		
		X-direction Face	Y-direction Face	Configuration
Beam	Size	200x330	200x330	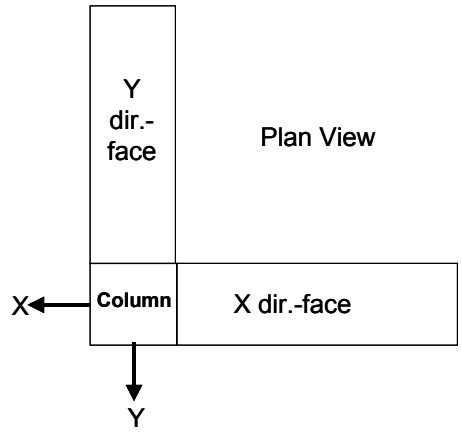
	Top Bars	4-R10 (ρ '=0.52%)	4-R10 (ρ '=0.52%)	
	Bottom Bars	4-R10 (ρ =0.52%)	4-R10 (ρ =0.52%)	
	Stirrups	2-R6@133	2-R6@133	
Column	Size	230x230		
	Main Bars	6-R10 (ρ t=0.89%)		
	Stirrups	2-R6@100		
Joint	Stirrups	Nil		
Cover to Longitudinal Bar =25mm				

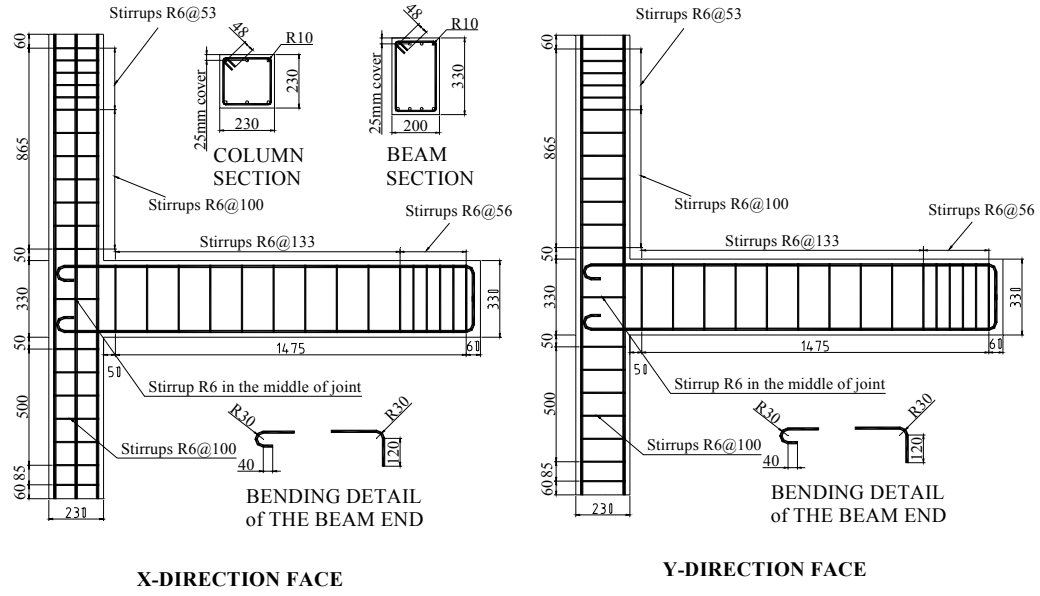

6.2.2 Haunch Detail for Retrofitted Beam-column Joint Subassemblies

For all testing specimens, the haunch stiffness K_d of the elements was designed as 100000kN/m. Since the hinge connections of haunches were presented in THR1 and THR2, the solid bars with specific configurations were used to satisfy the requirements such as stiffness and yielding strength. However, the buckling of the steel bars was a problem and had

to be avoided during the tests, the proper designed tube with infilled grout was proposed to prevent the buckling of haunch elements in THR1 and THR2. The steel tubes in THR1 and THR2 are used to provide the confinement of grout only without any contribution to the haunch strength. The suggested design idea, as illustrated in Fig. 6.1, was based on estimating the buckling force to crush the grout at ultimate strain.

When a steel bar suffers an axial compression, the steel bar is shortened longitudinally and expended horizontally. Since the horizontal expanding stresses (P_s and P_g), as well as the displacement (Δ_s and Δ_g), of the steel bars and grout respectively are the same at any critical points around the surface of steel bars, the relationship can be given:

$$\begin{aligned} P_s &= P_g \\ \Delta_s &= \Delta_g \end{aligned} \tag{6.1}$$

Therefore, the displacement of grout Δ_g at the critical point can be determined by the definition of the strain in the steel bar. Due to the grout limiting the steel bar to expand, a horizontally unknown strain which is induced by the confining pressure of grout is assumed $X\varepsilon_s$:

$$\Delta_g = \Delta_s = (\nu\varepsilon_s - X\varepsilon_s)D_{bar} \tag{6.2}$$

where ν is poisons ratio and 0.3 for steel. Assume the tube used to confine the grout to be not deformed. According to Hooke's Law, $P_s = P_g$ can be written as:

$$X\varepsilon_s E_s = \frac{\Delta_g}{(D_{tube} - D_{bar})} E_g \tag{6.3}$$

Then, the unknown ration X can be solved by subsisting Δ_g in Eq. 6.2 into Eq. 6.3. Once P_g reach the value of grout strength f_g' with a certain haunch axial force, the grout can not provide horizontal resistance anymore and the buckling occurs. At this critical situation, the haunch critical axial stress $P_{critical}$ can be derived by:

$$P_{critical} = \varepsilon_s E_s = \frac{f_g'}{X} \tag{6.4}$$

Therefore, the buckling force of the haunch can also be obtained by $A_{eh}P_{critical}$ where A_{eh} present the effective cross-section area of the haunch

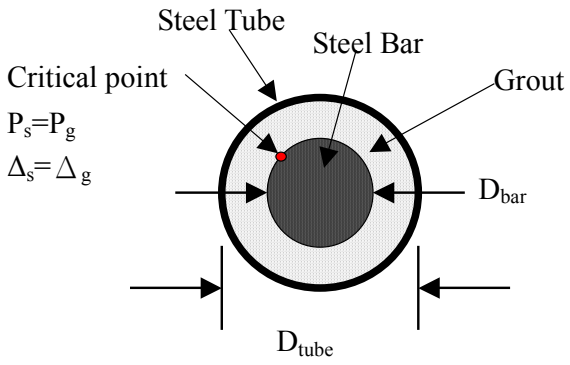

Fig. 6.1 Suggested method to estimate the buckling force

By using the weld connections in THR3 and THR3D, the manufacture procedure of haunches is much simplified. The hollow steel tubes are used to reach the desired stiffness and bucking force by estimating the effective steel area and tube diameter. The designed haunch details are given as below.

THR1 (K_d=100000kN/m):

The haunch was designed for elastic performance during active process. Therefore, the steel bars of Grade 430 were used to machine down for desired stiffness. The hinges were used for connection between haunches and beam/column elements to allow rotations such that the free moments existed in the connections. The haunches composite of the machined bars and steel tubes infilled with grout were locked to the hinges with nuts to complete whole haunch devices. The details of haunch devices are illustrated in Fig. 6.2.

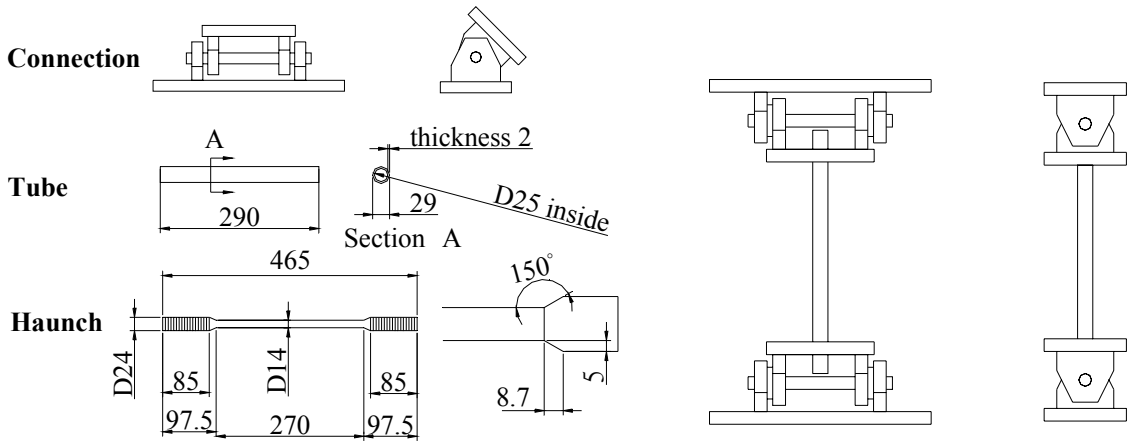

(a) Components of the haunch device (b) Full device set-up

Fig. 6.2 Haunch device configuration of THR1

THR2 (K_d=100000kN/m):

The haunch bar was designed to have elasto-plastic behaviour that can dissipate energy during the experiment. Compared with the steel bar in THR1, Grade300 steel and smaller cross section area (fuse) of 10mm length in the middle were designed to have the plastic behaviour after reach the strength F_s. The haunch fuses were also locked between the hinges used in THR1 as illustrated in Fig. 6.3

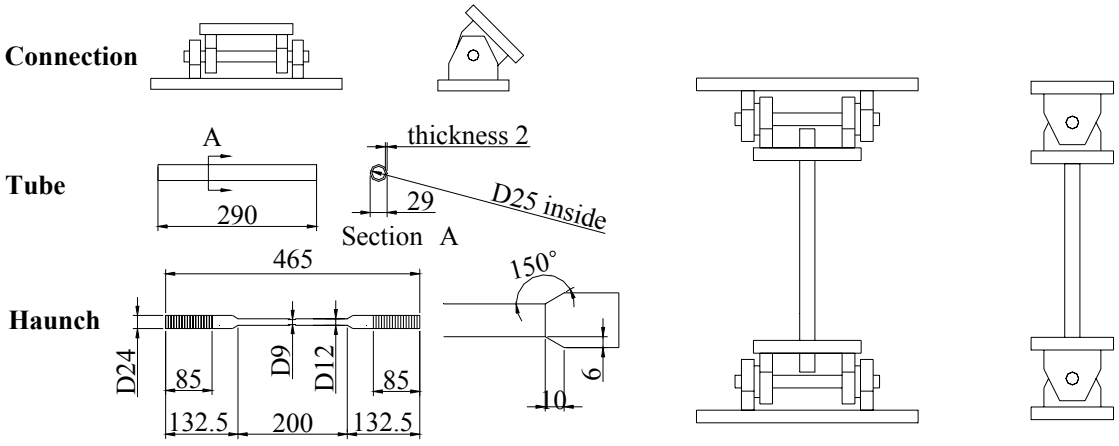

(a) Components of the haunch device (b) Full device set-up

Fig. 6.3 Haunch device configuration of THR2

THR3 (K_d=100000kN/m):

Since the gaps in the hinge significant reduce the haunch stiffness, the effectiveness of protecting the joint panel zone was lower than predicted one. To verify the haunch effect of the designed stiffness, the fix-end haunch device was proposed to be the other solution. Although small rotation between haunch locations of the beam and column was expected, according to numerical analysis in SAP2000, the induced moments in the haunch of fixed ends to the beam/column were little enough to be ignored. Therefore, the haunch elements were directly welded to the steel plates such that the potential displacement in the haunch device can be discarded. The steel tubes, instead of the steel bars, are designed to be elastic haunch elements with anti-buckling cross section. The detail of device configuration is illustrated in Fig. 6.4.

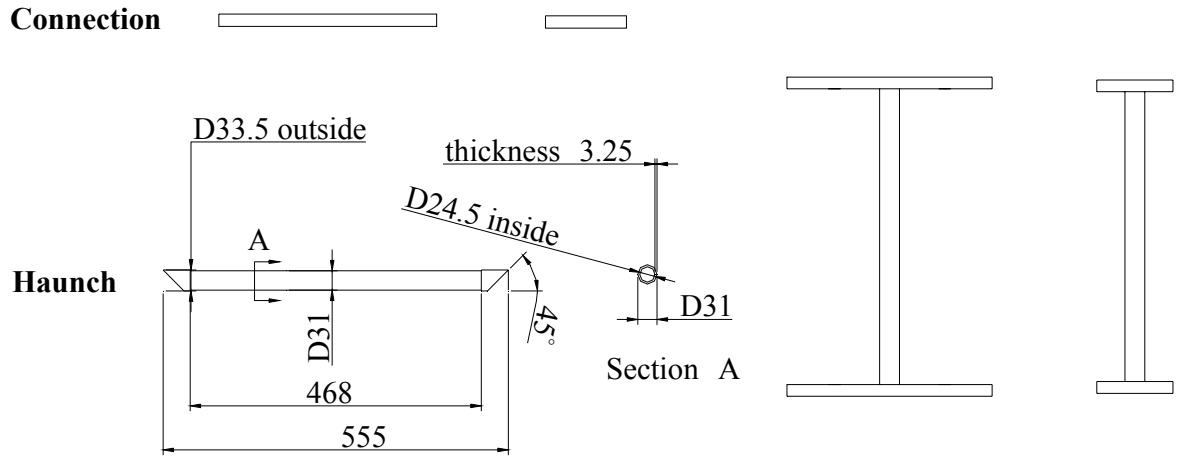

(a) Components of the haunch device (b) Full device set-up

Fig. 6.4 Haunch device configuration of THR3

THR3D (K_d=100000kN/m):

The configuration of the haunch device for THR3 was also used in THR3D except that the steel plate connections were modified a little to suit the two-direction set-up in 3-D test (Fig. 6.5).

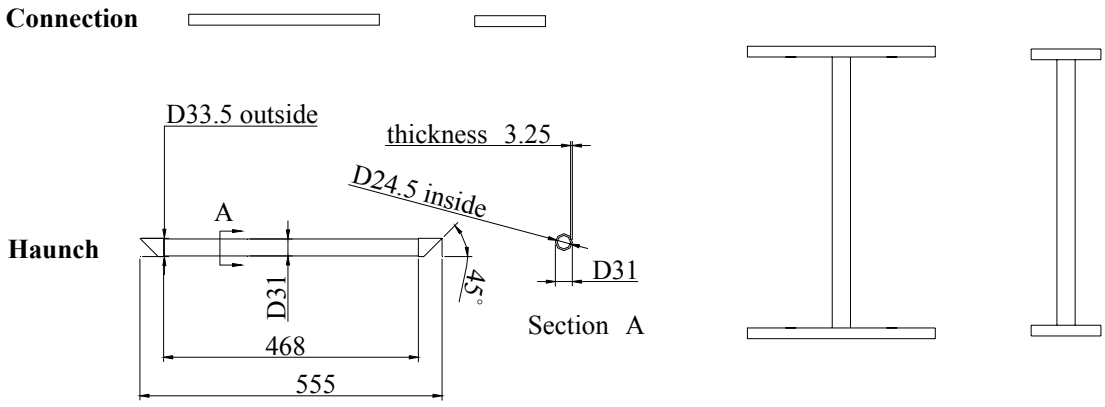

(a) Components of the haunch device (b) Full device set-up

Fig. 6.5 Haunch device configuration of THR3D

6.2.3 Material Properties

The procedure used to test the material properties of the reinforcing steel and concrete was the same with that introduced in Chapter 4. Besides, the properties of haunches could also be obtained by using Avery Universal Testing Machine of larger loading capacity.

Reinforcing steel:

Table 6.3 provides the testing properties of the reinforcing steel and the results obtained are the averaged value of three samples. The measured yield strengths were larger than the specified values up to 15% for 10mm diameter bars and 32% for 6mm diameter bars respectively.

Table 6.3 Measured reinforcing steel propertied used for retrofitted specimens

Unit	THR1		THR2		THR3		THR3D	
Steel Grade	Grade300		Grade300		Grade300		Grade300	
Bar Size	R6	R10	R6	R10	R6	R10	R6	R10
Yield Strength f_y(Mpa)	396	344	396	341	352	347	396	341
Yield Strain ε_y	2860	1510	2860	1560	1570	1580	2000	1560
Strain Hardening ε_{sh}	17000	24000	17000	27000	15000	25000	10700	26000
Ultimate Strength, f_u(Mpa)	485	478	485	480	436	474	485	480
Young's Modulus E(Gpa)	198	228	198	218	224	219	198	218

Note: R6=plain round bar of 6mm diameter

R10=plain round bar of 10mm diameter

D10=deformed bar of 10mm diameter

Compressive test of concrete cylinder:

Table 6.4 displays the average compressive concrete strengths of retrofitted specimens by testing 100mm diameter x 200mm concrete cylinders. The test cylinders were cured in a fog room and tested at twenty eight days to obtain the standard compressive strength of the concrete and three cylinders were tested for each specimen just before the experimental testing to obtain the compressive concrete strength f_c' of the tested specimen. The higher slump concrete was used to improve workability in casting the 3-D subassembly.

Table 6.4 Measured concrete properties by compressive test for retrofitted Specimens

	Slump (mm)	28 days fc'(MPa)	Before Testing fc'(MPa)
THR1	110	24.8	25.9 (56days)
THR2	110	24.8	25.9 (83days)
THR3	90	22.1	26.8 (56 days)
THR3D	190	27.5	30.3 (190days)

Note: Each value was obtained from the average of three specimens

f_c'=compressive strength of 100mm dia. x 200mm concrete cylinder

E_c=28.7Gpa (Concrete Young's Modulus obtained from the average measured value of three specimens)

Haunch material properties:

The steel solid bars of Grade430 and Grade300 were used for THR1 and THR2 respectively while the steel hollow tubes of Grade300 were used for THR3 and THR3D. The haunch elements in different configurations (i.e. solid bars of hollow tube) were tested by Avery Universal Testing Machine and the obtained results are given in Table 6.5.

Table 6.5 Measured material properties of haunch for retrofitted Specimens

Unit	THR1	THR2	THR3	THR3D
Haunch Steel Grade	Grade430	Grade300	Grade300	Grade300
Yield Strength f_y(Mpa)	498	340	325	325
Yield Strain ε_y	2970	1770	1380	1380
Strain Hardening ε_{sh}	29350	22900	NIL	NlL
Ultimate Strength, f_u(Mpa)	650	484	NIL	NIL
Young's Modulus E_s(Gpa)	176	195	235	235

6.2.4 Haunch Device Test

The push-pull tests of full haunch devices (with hinged or welded connections) were carried out in the laboratory to predict their behaviour in retrofitting as-built subassemblies. The set-up configurations of the tests were different depend on the devices with hinged or welded connections Fig. 6.6. As illustrated in Fig. 6.6(a) two potentiometers, P1 and P2 were used to measure the displacements between two points. The measured value from P1 excluded the gaps and deformations of hinges while the measure value from P2 took these uncertainties into account. In Fig. 6.6(b), the potentiometer P1 measured the relative displacement between two points which presented the pure deformation of the haunch. Strain1 and Strain2 were the strain gauges used to monitor the haunch stress during the tests.

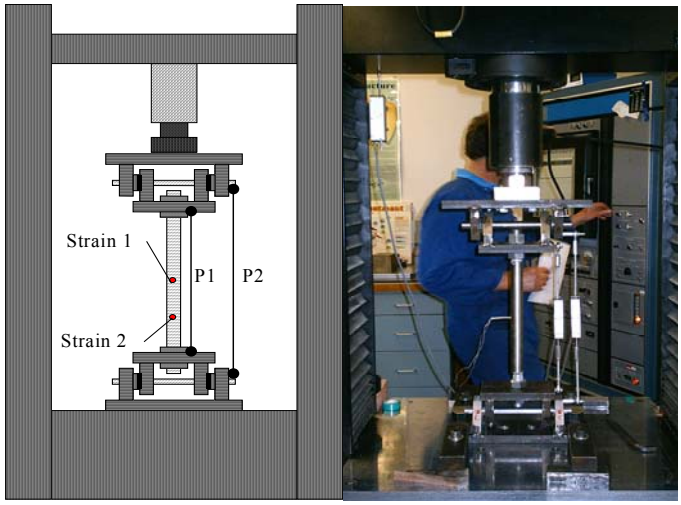

(a) THR1 & THR2

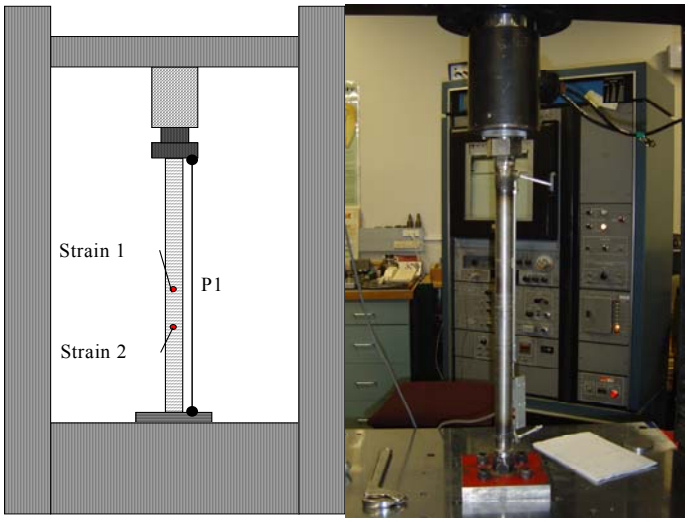

(b) THR3 & THR3D

Fig 6.6 Haunch device test

From the results given in Table 6.6, the axial stiffness of haunch element was close to the designed value, 100000kN/m. However, if the gaps and hinge deformations in whole haunch devices which were presented in THR1 and THR2 were considered, the haunch stiffness would be much lower than the designed value. Therefore, the haunch devices in retrofitting the specimens of THR1 and THR2 was expected to be less effective.

Table 6.6 Results of haunch device test

Unit	THR1	THR2	THR3	THR3D
Haunch Steel Grade	430	300	300	300
Young's Modulus E(Gpa)	176	195	235	235
Yield Strength f_y(Mpa)	498	340	325	325
Fuse Area (mm^2)	154	63	283	283
Yield Force F_y(kN)	76	22	90	90
Axial Stiffness (kN/m) (without hinge)	107000	109000	110000	110000
Axial Stiffness (kN/m) (with hinge)	33000	25000	Nil	Nil

6.2.5 Specimen Construction

The construction detail of the retrofitted subassemblies was similar to the as-built ones which could be found in Chapter 4. Before set up the specimens to the experimental loading system, the joint subassemblies had to be retrofitted by haunches. With combination of the clamping force and anchorage resistance, the fasteners were used to connect the haunch devices to the beam/column and provided enough anchorage strength if the fasteners could be designed and chosen appropriately.

The fasteners used in this project were offered by HILTI, which was a professional manufacturer to provide the reliable and strong fastening technology. According to the manual, HVU adhesive with has rod was the chosen fastening method to satisfy the strength and convenience requirement. With selected sizes of fasteners, the required drilled dimensions and depths could also be found in the manual. The labour work had to be complete to achieve the targeted strength by totally following the instruction in the manual. The complete haunch set-up are illustrated in Fig. 6.7

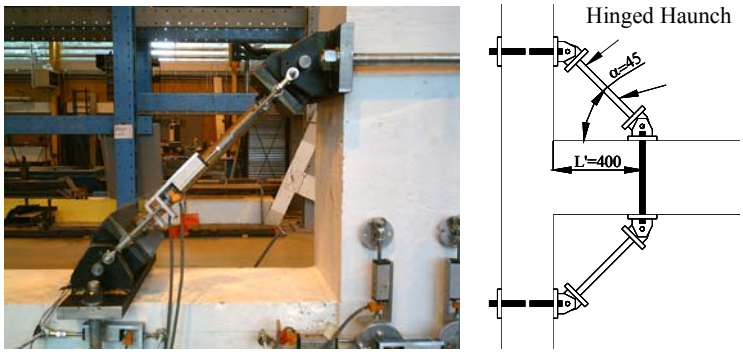

(a) Hinged connection

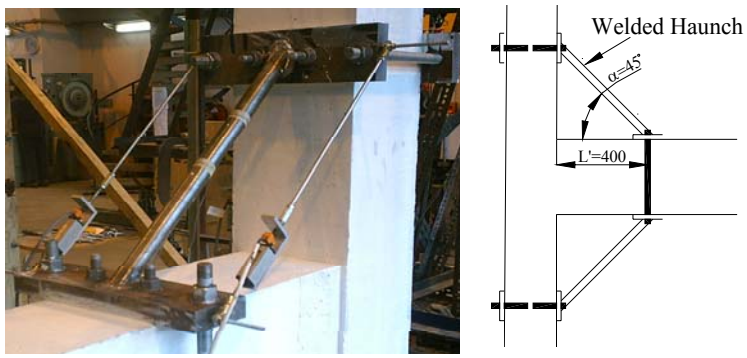

(b) Welded connection

Fig. 6.7 Haunch set-up

6.3 TEST SET-UP

6.3.1 Loading System

The loading system of 2-D tests for as-built specimens was repeated. The simulating quasi-static push-pull experiment as shown in Fig. 6.8. was presented to test the retrofitted subassemblies. A hinge was simulated at the base of column to allow free rotation while a roller was simulated at the end of beam to allow horizontal displacement and hold against vertical displacement. A rigid reaction frame was set-up on the strong floor. Two actuators were used to simulate the lateral shear force and the varying axial force of column respectively during loading sequence. The bolted tendon was used to clamp and activate the actuator. The load cell of 200kN capacity was placed on the top of column while two 50kN-capacity load cells were connected to the lateral force actuator and the support of beam end respectively. Two transducers were used to measure the travelling distance of the column top and beam end. The subassemblies were retrofitted the haunch devices located 400mm from

the column face with 45 degree of design angle for both hinge connected haunches and weld connected haunches. The haunch devices were clamped by the steel plated on the beam and column.

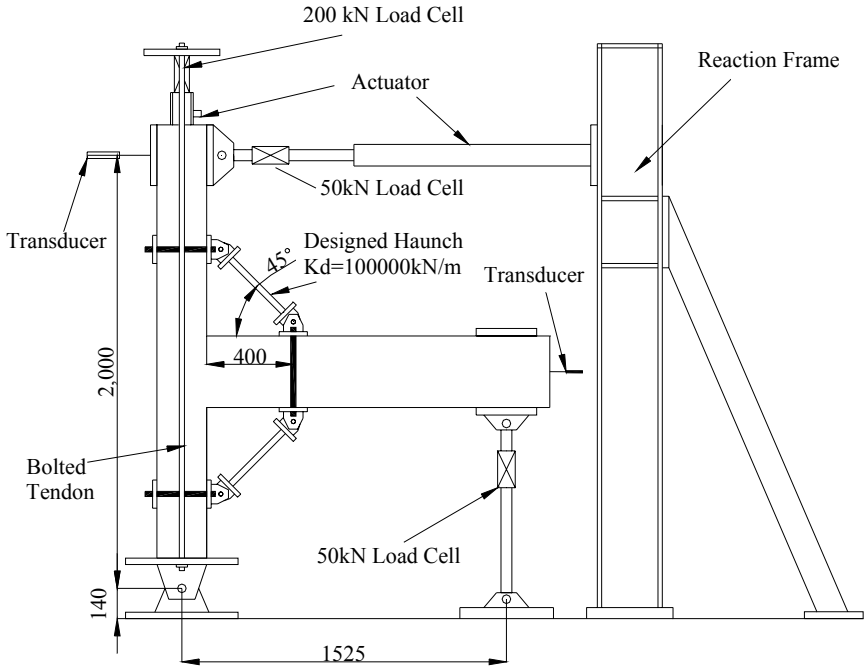

(a) Hinged haunch connection

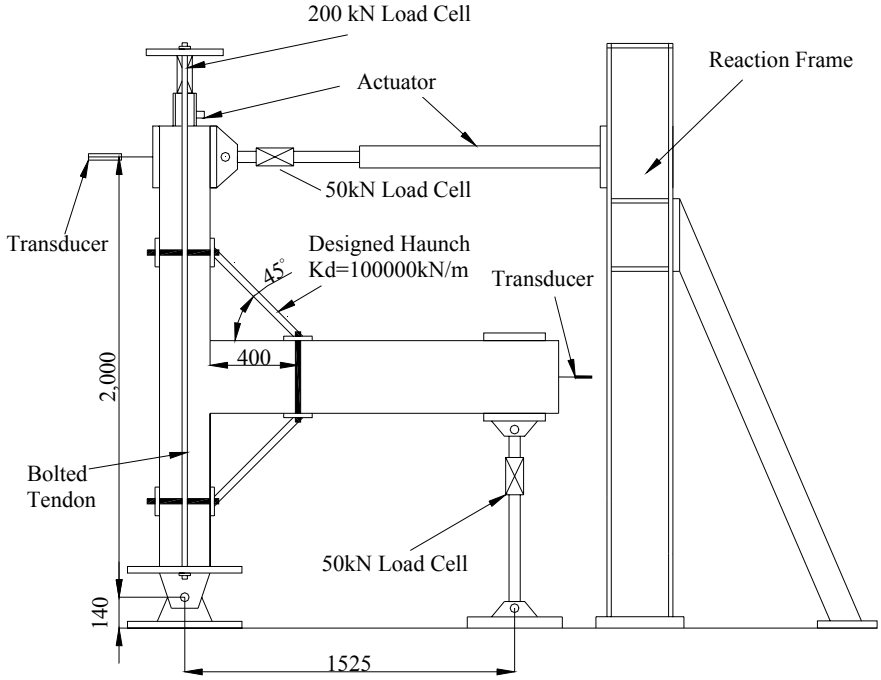

(b) Welded haunch connection

Fig. 6.8 The loading system for retrofitted 2-D Test

For the 3-D test of the retrofitted subassembly THR3D, the same set-up in testing DD2 was reconstructed. The haunch devices were applied on subassembly in both X and Y directions with the desired angle and location (Fig.6.9).

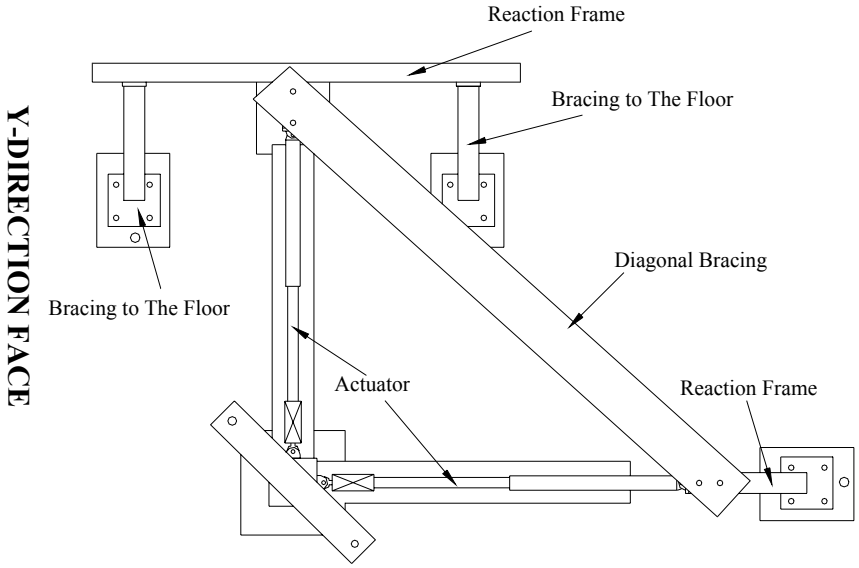

(a) Plan view

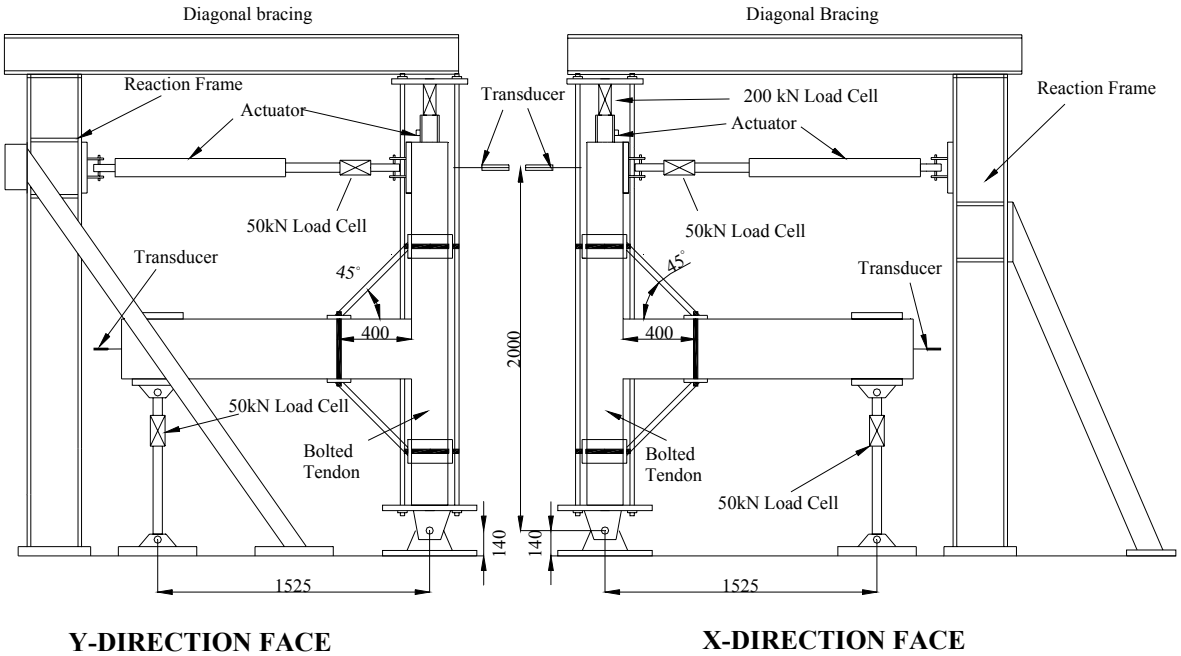

(a) Elevation view

Fig.6.9 The Loading system for retrofitted 3-D Test

6.3.2 Testing Regimes

The loading regimes used to test the retrofitted units of 2-D and 3-D tests were the same with the previous description for testing as-built subassemblies in chapter 4. The same detail of loading history for retrofitted 2-D and 3-D tests could be found in Section 4.4.2.

6.3.3 Loading Direction And Varying Column Axial Load

Due to the effect of the inter-storey shear and structural geometry, the varying axial loads, as described in Chapter 4 were still applied on the top of column. The coefficient used for the retrofitted test was similar to the value for the as-built test except that the greater dead load was accepted in THR3D test to guarantee the desired hierarchy strengths (Table 6.7). The increased dead load could be achieved by external post tendon force in real structure.

Table 6.7 Loading coefficient used in the experiments

Specimen	**N_g**	**α_h**	
THR1, THR2, THR3	75	1.8	
Specimen	**N_g**	**α_{hx}**	**α_{hy}**
THR3D	130	1.8	1.8

6.3.4 Instrumentation

As presented in Section 4., the instrumentation used in the as-built test was repeated in the retrofitted test. More potentiometers were used to measurement the displacement of the haunch and the deformation of the beam where the haunches were connected. In addition, the strain gauges used to measure the local strain of the beam bars were attached properly at the expected hinging region. The detail of the additional instrumentation for the haunch-retrofitted test is described in the following paragraph.

Measurement of element deformation: With original twelve potentiometers in the joint panel zone, two additional potentiometers were used to measure the displacement between the points where the haunches were connected on the beam and column while another three potentiometers were attached to the critical region where the beam hinging was expected. The potentiometer at the middle of critical region of the beam was used for reservation and

curvature estimation. The location detail of potentiometers is presented in Fig. 10 and applicable for all retrofitted specimen.

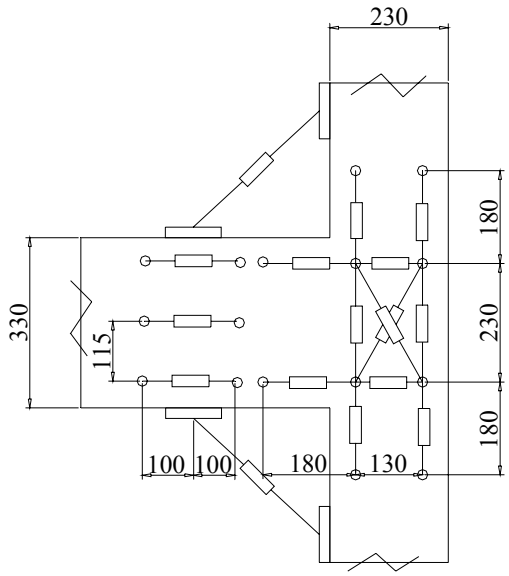

Fig. 6.10 Location of potentiometers for retrofitted subassemblies

Measurement of strain in reinforcing bars: Due to the effect of haunch axial force on the beam, the hinge was expected to occur in the beam where the haunch was connected. To investigate the beam behaviour, additional twelve strain gauges were attached to the longitudinal beam bars at the critical region and the locations of them are presented in Fig. 6.11.

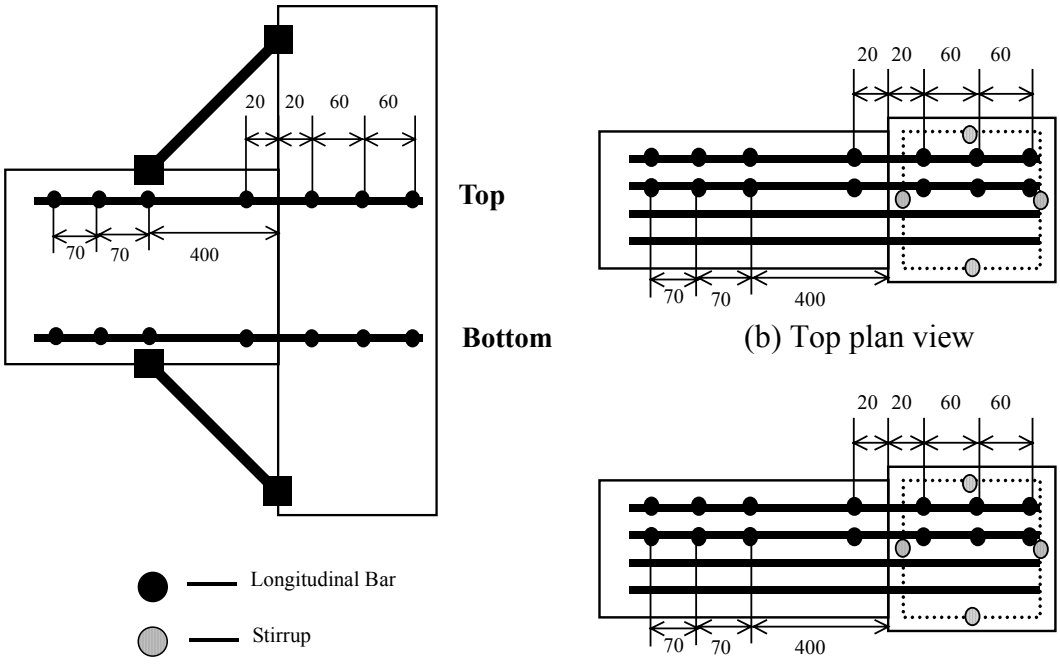

(a) Elevation view (b) Top plan view (c) Bottom plan view

Fig. 6.11 Location of strain gauges for retrofitted subassemblies

Measurement of loads: 50kN load cells were used to measure the applied horizontal load and reaction force at the beam end while a 200kN load cell was used to measure the vertical axial load in the column. The applied horizontal load was simulated as storey shear force and vertical axial load was treated as gravity loads plus earthquake-induced axial forces. The load cells were calibrated in compression by Avery Universal Testing Machine and the obtained calibration number was assumed to be effective for the particular load cell in tension as well.

Measurement of drift: Two linear potentiometers were used as transducers to measure the horizontal displacement of the column top and the beam end. By using linear potentiometer of 200mm and100mm travelling capacity for the column top and the beam end respectively, the satisfactory 5% maximum drift level was available during the test where only 4% drift level was required.

Measurement of element deformation: Twelve small linear potentiometers with 30mm travelling capacity were located at one side of the joint panel region to measure the element deformation. Each pair of potentiometer connected between the joint and beam/column members was used to estimate the rotation of fixed end while the potentiometers attached to the joint were used to estimate the joint shear distortion by reading the horizontal, vertical and diagonal displacement in the joint. The details of potentiometers position are presented in Fig. 4.20 and in Fig. 4.21 for 2-D subassemblies and 3-D subassemblies respectively.

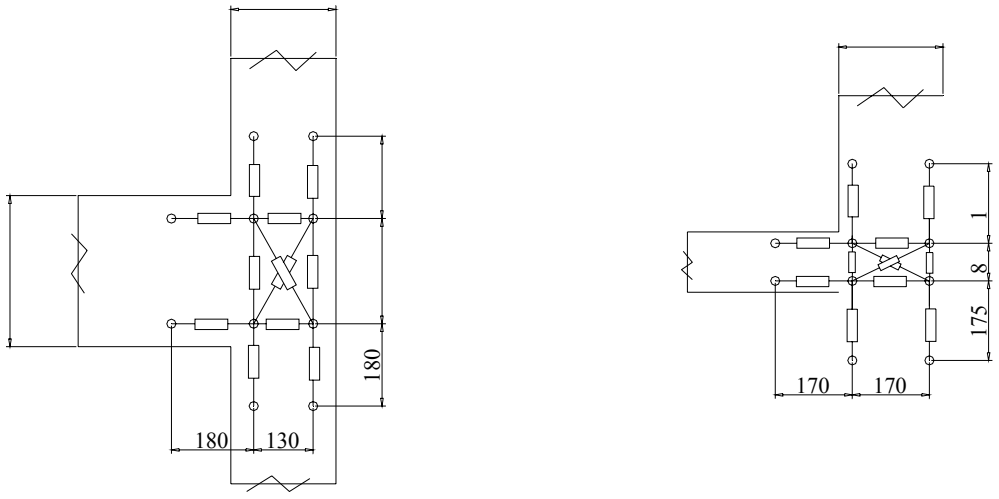

(a) TDP1, TDP2, TDP3, TDP4 (b) TSP1, TSP2

Fig. 4.20 Location of potentiometers for 2-D test

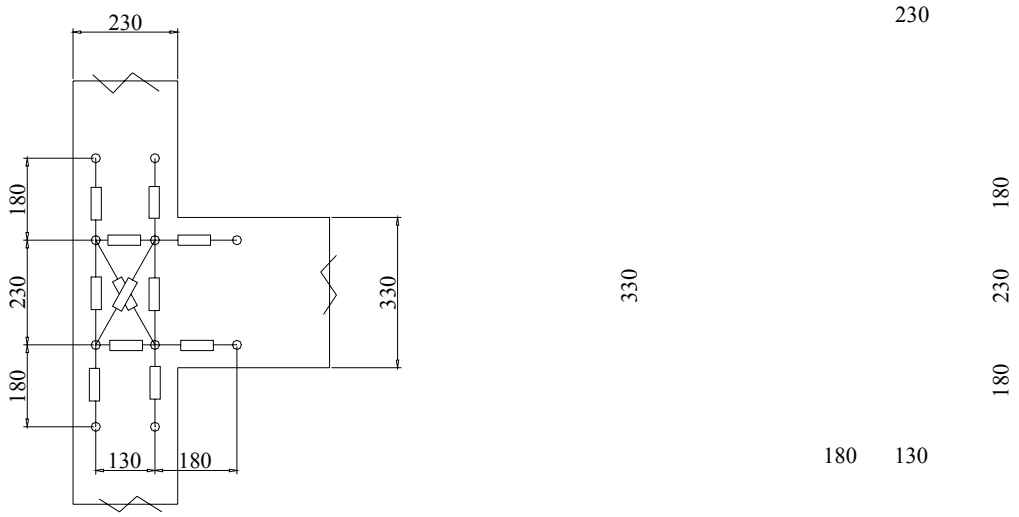

(a) X-direction face (b) Y-direction face

Fig. 4.21 Location of potentiometers for 3-D test

Measurement of strain in reinforcing bars: Strain gauges were used to measure the local strains of the reinforcing bars and the stirrups in the critical regions of beams and joints. The strain gauges were attached on the side of reinforcing bars along the bending neutral axis to minimize the effect of bending. Twenty strain gauges were used in each specimen and, due to the different longitudinal reinforcement of the beam for each specimen, the strain gauge arrangement was not identical as shown from Fig. 4.22 to Fig. 4.24.

6.4 DEFORMATION ESTIMATION AND CRACK OBSERVATION

6.4.1 Estimation of Average Rotation for The Hinge in The Beam

Due to the flexural hinge forming in the beam around haunch-connected region, the rotation of the hinge had to be included in counting the deformation of the beam. The methods for estimating deformation for the fix end and joint in the retrofitted subassemblies were the same with the description for as-built subassemblies in Chapter 4. To consider the effect of hinge deformation in the beam, Fig. 4.22 and following equation illustrate the method to estimate the rotation of beam hinge.

Hinge rotation of beam:

$$\theta_{bh} = (\delta_{th} - \delta_{bh}) / Dv \tag{6.5}$$

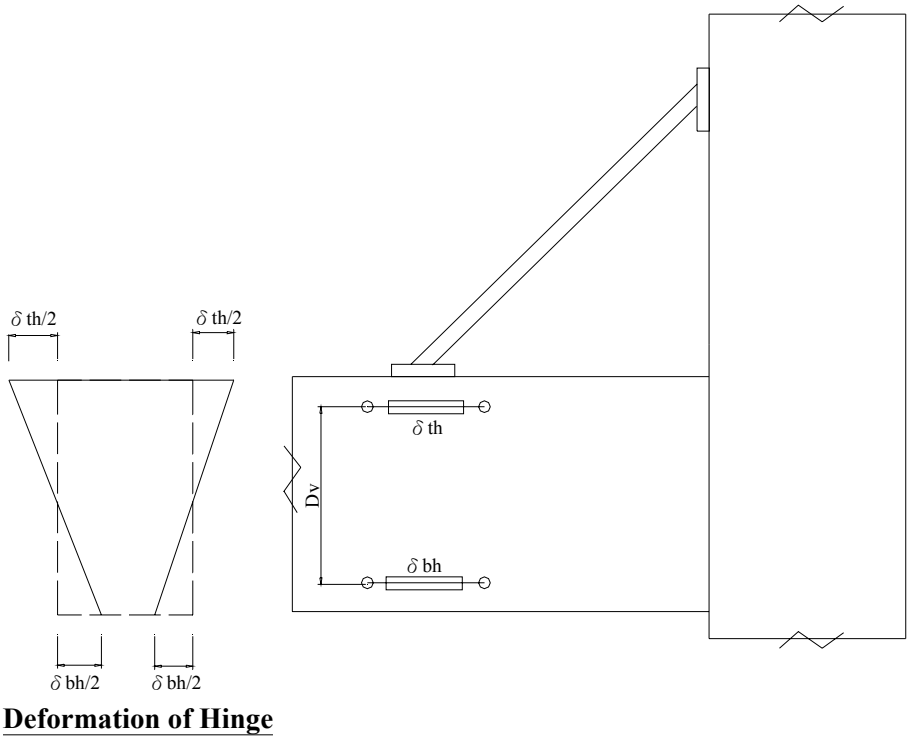

Fig. 4.22 Estimation of hinge rotation of the beam around haunch connected region

6.4.2 Crack Observation

Due to occurrence of plastic hinge in the beam, the critical region of the subassembly was extended to the area around the haunch-connected region. All crack-possible areas around the beam, column and joint were painted in while colour for observing the cracks that were also marked with blue and red colour for the positive and negative loading respectively.

6.5 COMPONENT OF HORIZONTAL DISPLACEMENT

6.5.1 General

The total horizontal displacement Δ_{tot} of the retrofitted subassembly was also composed of the horizontal displacements caused by the deformation of the beam, column and joint .as described in Eq. 4.8. However, the deformation of the plastic hinge in the beam of the retrofitted subassembly would significantly contribute to the deformation of the beam. Therefore, the beam-related deformation θ_{beam}, as well as Δ_{beam} ,need to be modified to consider the contribution of the hinge deformation.

6.5.2 Horizontal Displacement Component of The Beam

By modifying Eq. 4.9, the displacement at the beam end Δ_{end} (Fig. 6.23) was described as the following expression to consider the displacement caused by the plastic hinge:

$$\Delta_{end} = \delta_{b,fle} + \delta_{b,rot} + \delta_{bh,rot} \tag{6.6}$$

Form this equation, the displacement at the beam end Δ_{end} was composed of $\delta_{b,fle}$ (displacements caused by the flexural deformation), $\delta_{b,rot}$ (displacement caused by the fix-end rotation) and $\delta_{bh,rot}$ (displacement caused by the plastic hinge in the beam). To obtain Δ_{tot} by Eq. 4.8, the horizontal contribution of the beam deformation Δ_{beam} had to be estimated first by Eq. 6.7 with obtained Δ_{end} .

$$\Delta_{beam} = \frac{\Delta_{end} H_c}{L_n} \tag{6.7}$$

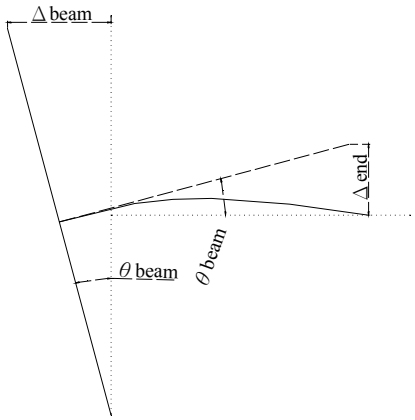

Fig. 6.23 Contribution of the displacement of beam end to the horizontal displacement

CHAPTER 7

EXPERIMENTAL RESULTS OF THE HAUNCH RETROFITTED SPECIMENS

7.1 INTRODUCTION

Since the vulnerability of the joint panel zone was found in the as-built joint tests, the haunch retrofit solutions were proposed to retrofit the beam-column joints and upgrade the performance of the specimens. Following the designed solutions in Chapter 6, this chapter examined the seismic response of retrofitted specimen THR1, THR2, THR3 in 2-D test and THR3D in 3-D test. By relocating the plastic hinge in the beam away from the column surface, the joint panel zone was protected and the effectiveness of the haunch retrofit solutions would be investigated. Due to the use of different types of connections between haunches and specimens, the efficiency of the haunch solutions was experimentally presented and effect of the elastic and elasto-plastic haunch elements on the seismic behaviour was discussed as well. By retrofitting the 3-D corner joint with haunch solutions, the influence of bi-directional loadings on the haunch elements was presented. The experimental results of each test would be summarized and compared with the predicted value in this chapter.

7.2 TEST OF THR1

7.2.1 Specimen

The specimen THR1 was retrofitted with the elastic haunch elements of the hinge connections where the free rotation was allowed. The designed value of the haunch elements (i.e. hinge excluded) was K_d=100000kN/m and the expected axial force to cause the beam hinging was 43kN. The flexural failure of the beam was expected to occur in the location where the haunches were connected to the beam.

7.2.2 General Behaviour

The final crack pattern and the measured global hysteretic loops are illustrated in Fig. 7.1 and Fig. 7.2 respectively. It was observed that minor cracks appeared in the beam and column

surface close to the joint core and the progressive widening of a main flexural crack occurred in the beam around the haunch connection. Due to the decreased column axial load as well as the column capacity in the negative loading direction, the minor cracks observed in the column appeared during the loading in that direction only. The concrete spalling-off was observed in the plastic hinging region of the beam at higher drift level due to the buckling of steel bars between the stirrups in the beam. There was unexpected minor shear crack of outside plastic hinge appearing in the negative loading direction. No joint shear cracks were observed in the joint panel zone due to the seismic behaviour of the perfect beam flexural failure occurred as presented in Fig. 7.2. As a result, a more stable hysteretic response within a weak-beam strong-column mechanism with increased energy dissipation was observed when compared to the as-built specimen response. The experiment was carried out until 2.5% drift level only due to the strength degradation was observed in the negative loading direction. There was unexpected accident occurring during the loading to the –1% drift and it was fixed to continue the experiment. The inter-storey strength to cause the beam flexural failure was about 24kN and the observed strength degradation during the loading to the –2.5% drift was caused by the buckling of the longitudinal bars and crush of the concrete in the plastic hinging region of the beam. Furthermore, strain hardening of the beam bars was initiated in the negative loading direction and was not presented in the positive loading direction.

Fig. 7.1 Final crack of THR1

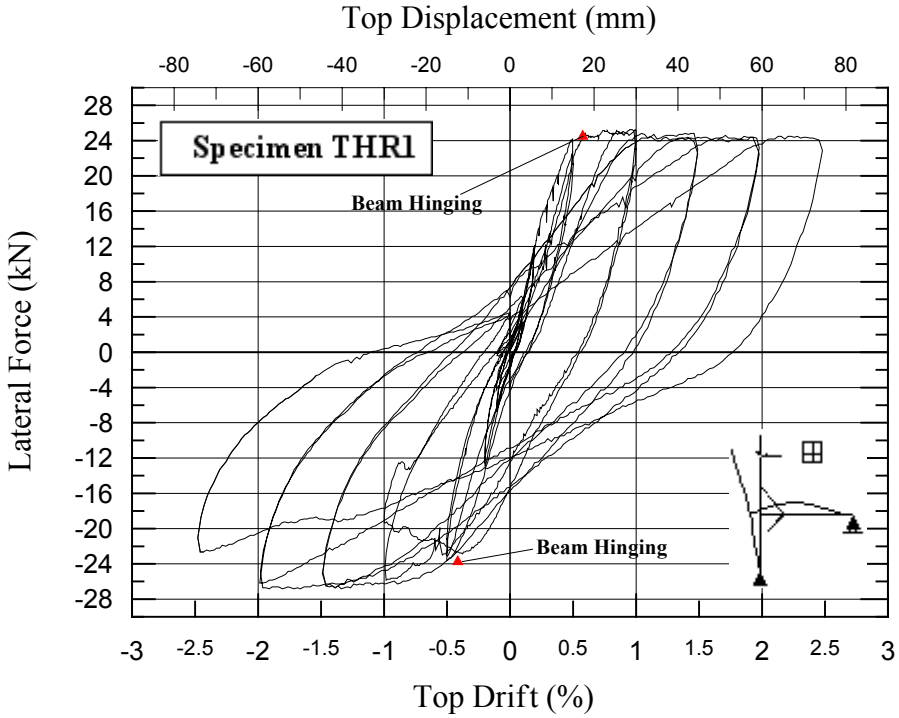

Fig. 7.2 Storey-shear force versus Horizontal Relationship of specimen THR1

7.2.3 Joint Behaviour

The joint behaviour could be investigated in terms of principal tensile stress as illustrated in Fig. 7.3. It was observed that the obtained value of maximum joint principal tensile stress was greater in the negative loading direction than in the positive loading direction since the smaller column axial load was presented during the negative loading. Due to the significantly decreased stiffness of the haunch device (i.e. discussed in the next paragraph), the maximum p_t of the THR1 test was much higher than the expected value of p_t=0.062$\sqrt{f'_c}$. Even if the observed maximum principal tensile stress 0.21$\sqrt{f'_c}$ in the retrofitted subassembly was higher than the critical value 0.2$\sqrt{f'_c}$ of causing joint shear cracks, there were not shear failure of the joint was observed during the test. The possible reason was that, due to the relocation of the plastic hinge away from the joint connection, the longitudinal beam bars could rely on a full development of the anchorage length between the plastic hinge and critical joint area.

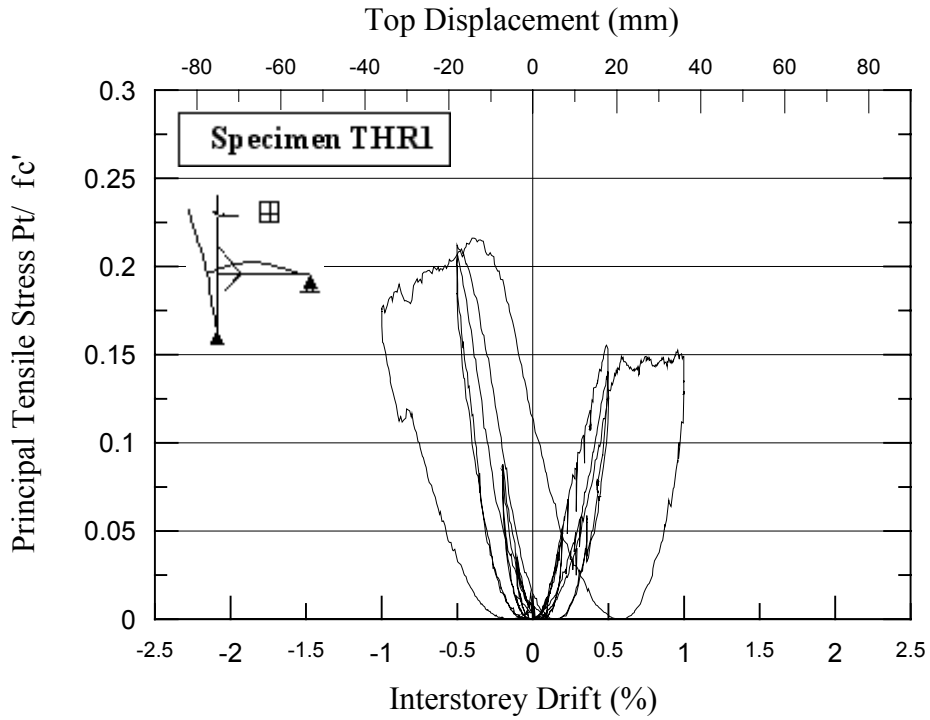

Fig. 7.3 Principal tensile stress versus horizontal relationship

7.2.4 Haunch Behaviour

The hysteretic responses of the top and bottom haunch devices are illustrated in Fig. 7.4 The elastic behaviour as prediction was presented while a little loss of stiffness occurred during the unloading process of the compressive action for both top and bottom haunch devices. The average stiffness of the top and bottom haunch was proposed to be 25000kN/m that was much lower than the designed value of 100000kN/m since the use of hinge connections between haunch elements and the specimen did not provide enough rigidity compared with the stiffness of the haunch element. In addition, the potential gaps existing in the hinge connections caused the slippage between tension and compression activities and thus decrease the stiffness of the haunch devices. It was also observed that the top and bottom devices equally contributed to the total induced axial force of the haunches and the maximum axial force was 25kN for a single haunch only.

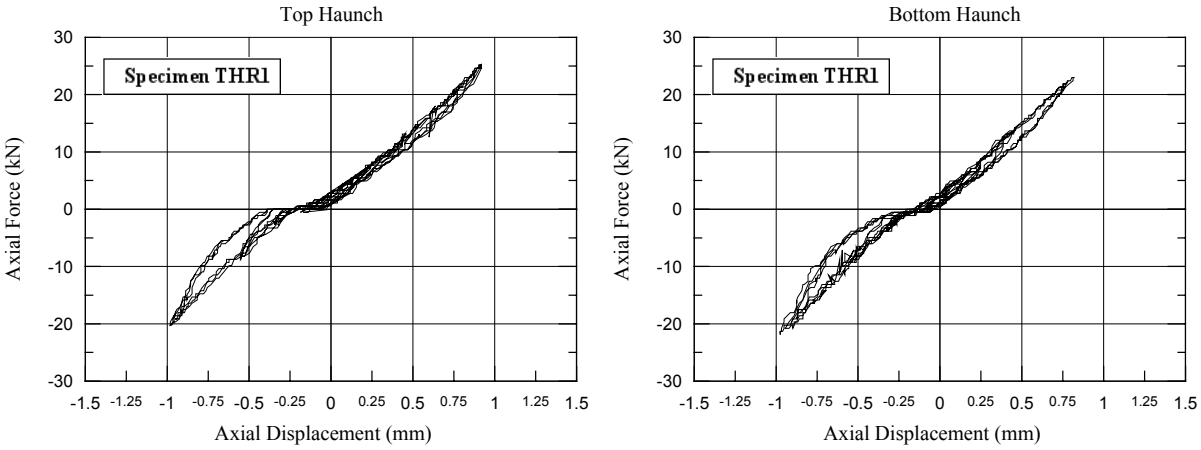

Fig. 7.4 Axial force versus displacement relationship of the haunch

7.2.5 Summary of THR1 Test

Due to the flexible hinge connection of gaps being used, the experimental stiffness of the haunch devices was lower than the designed value. Therefore, the function of haunches was not effectively developed and the maximum principal tensile stress obtained in the joint panel zone was much higher than the expected value for the retrofitted subassembly. However, the joint shear failure was still prevented due to the development of full anchorage length in the longitudinal beam bars even if the maximum moments in the beam and column were not effectively reduced and caused the minor crack observed in the face of the column and beam around the joint. Thanks to the conservative consideration in the designed, the beam flexural mechanism could be activated and performed a desired energy dissipating hysteretic response.

From the respect of component contribution to the total inter-storey drift (Fig. 7.5), the total horizontal displacement in the top of THR1 subassembly mainly came from the rotation of the plastic hinge in the beam in the positive loading direction while the column contributed more to the total displacement in the negative loading direction. The possible reason for this phenomenon was that the beam rotation tended to increase more in the positive loading direction due to the self-weight. In any cases, the retrofitted joint contributed a little to the horizontal drift compared with the as-built joint subassembly.

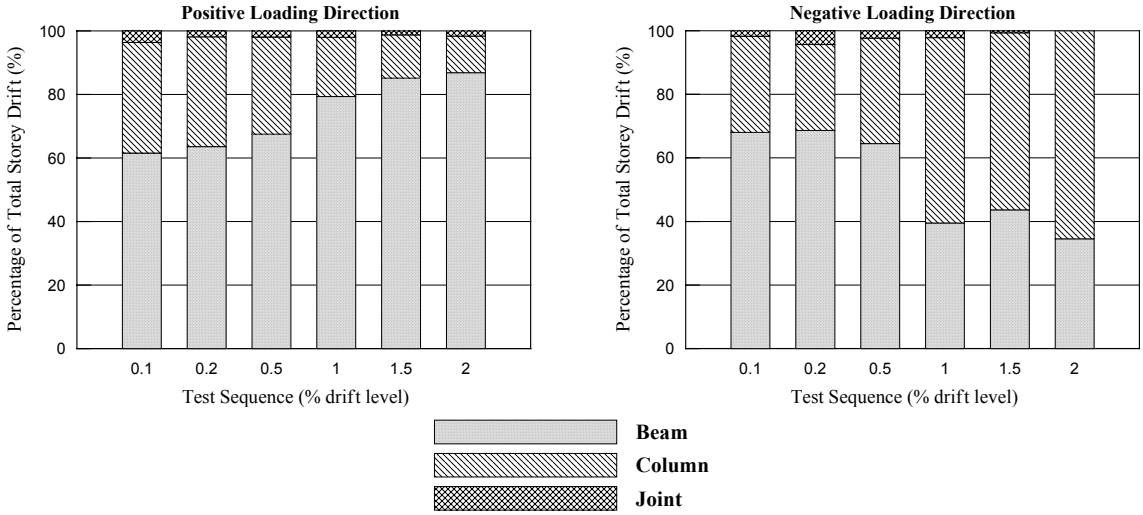

Fig.7.5 Contributions to subassembly drift of beam, column and joint in THR1

7.3 TEST OF THR2

7.3.1 Specimen

The specimen THR2 was retrofitted with the elasto-plastic haunch elements of the hinge connection where the free rotation was allowed. The designed value of the haunch elements (i.e. hinge excluded) was also K_d=100000kN/m. From the analysis of results in THR1 test, the stiffness of the full haunch device was 25000kN/m with the induced maximum axial force 25kN. Therefore, the yielding haunch elements of THR2 were deigned with a yielding strength of 20kN. After yielding the haunch elements, the beam, column and joint elements of THR2 could still remain elastic and internal forces of those elements increased with increasing inter-storey shear force until the beam hinge occurred. The flexural failure of the beam was still expected to located at the point where haunches were connected in the beam

7.3.2 General Behaviour

The final crack pattern and the measured global hysteretic loops are illustrated in Fig. 7.6 and Fig. 7.7 respectively. It was observed that minor cracks also appeared in the beam and column surface close to the joint core due to the under designed stiffness (with hinge connection) of the haunch obtained in THR2 test. The negative loadings decreased the column axial load and

the column capacity as well. As previous THR1 test of lower stiffness, the progressive widening of a main flexural crack also occurred in the beam around the haunch connection. The concrete spalling-off occurred around the plastic hinging region of the beam after 2% drift level and it was caused by the buckling of steel bars between the stirrups in the beam. Due to this phenomenon, the inter-storey strength decreased a little. Unlike the previous test stopping at 2.5% drift level, the experiment was continued to the designed drift level. After concrete crushing, the marked pinching was observed with the wide opening/closing of the main flexural crack at the beam/haunch connection interface and some shear sliding occurred. However, a stable hysteretic response with good energy dissipation was still available in the test. However, compared with the results of THR1, the global hysteretic response of THR2 did not seem to be particularly effective in improving the energy dissipation of the system due to little energy dissipated with only small displacements in the haunches. The unexpected minor shear crack around the plastic hinge in previous THR1 test was not observed in this test and the joint panel zone was also protected from brittle shear failure. The inter-storey strengths were observed as 24kN and 22kN for the positive and negative loading directions respectively. Again, the strain hardening of the beam bars seemed to be initiated in the negative loading direction only.

Fig. 7.6 Final crack of THR2

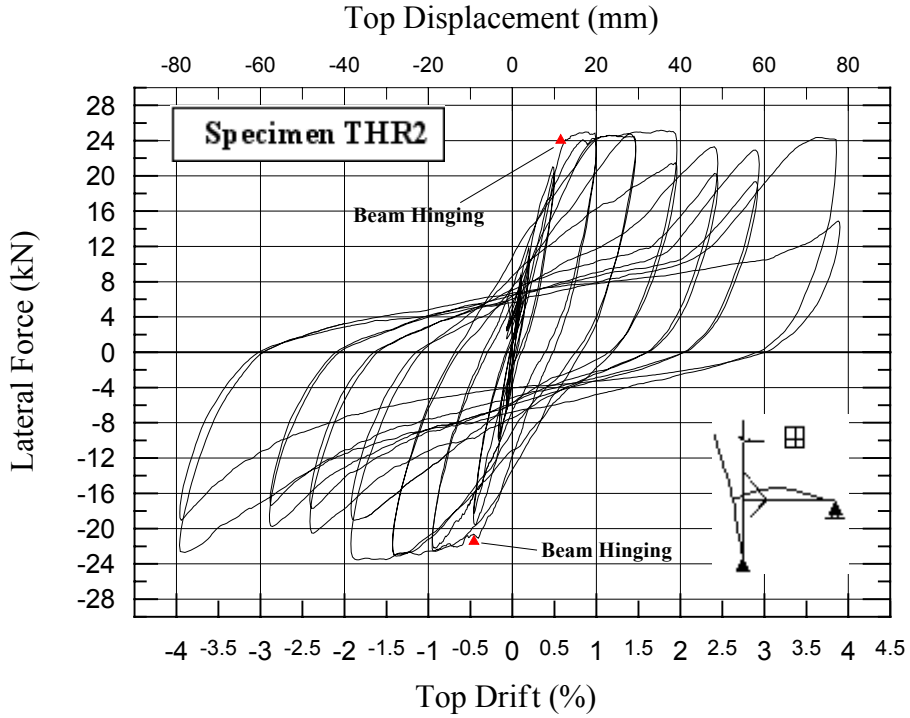

Fig. 7.7 Storey-shear force versus horizontal relationship of specimen THR2

7.3.3 Joint Behaviour

The joint behaviour could be investigated in terms of principal tensile stress as illustrated in Fig. 7.8. The greater maximum value of principal tensile stress in the joint was observed in the negative loading direction than in the positive loading direction. Since the haunch stiffness was expected to be about 2500kN/m that was lower than the designed value as the previous test, maximum p_t was already predicted to be greater than the designed value $0.062\sqrt{f'_c}$ and it had reached $0.19\sqrt{f'_c}$ while the beam flexural strength was achieved in the negative loading direction. It was observed that the principal tensile stress p_t never recovered to be zero after 0.5% drift level. The possible reason was that the haunch element yielded before the occurrence of beam hinging at 0.5% drift level and the haunch residual force, due to the yielding of haunch elements, caused the residual moments existing in the joint even if no force was presented.

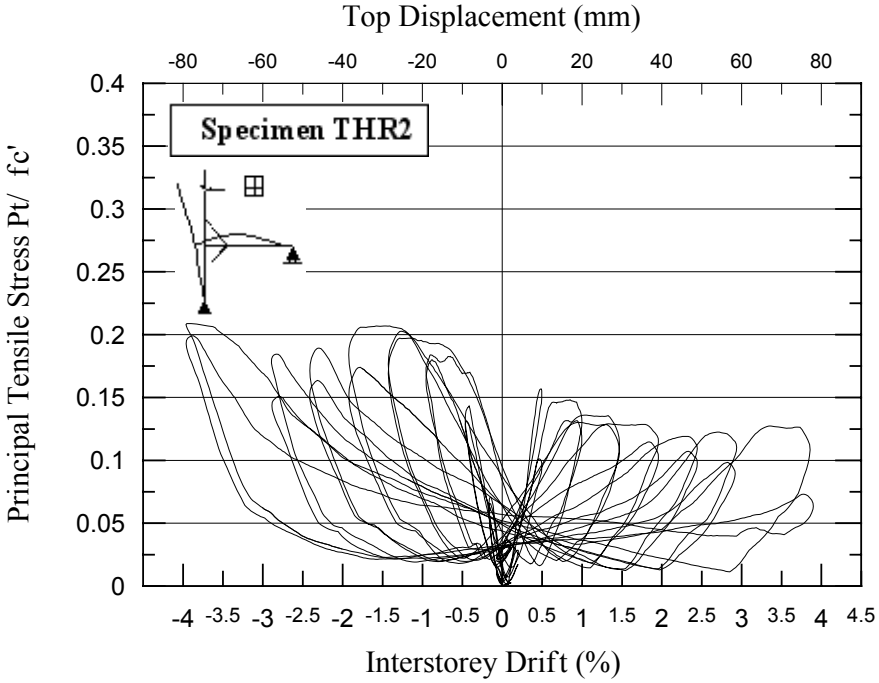

Fig. 7.8 Principal tensile stress versus horizontal relationship

7.3.4 Haunch Behaviour

The hysteretic responses of the top and bottom haunch devices are illustrated in Fig. 7.9. A slight elasto-plastic behaviour was observed since only the small displacement was available in the haunch elements. Compared with the dissipated energy at the global level, the small energy dissipation contributed from the yielding of the haunches could not provide effective improvement of the energy-dissipating pattern. From this experimental study, the use of a dissipating haunch was therefore not a viable solution to improve the energy dissipation. The reduced haunch stiffness of about 22000kN/m was obtained with the hinge connections.

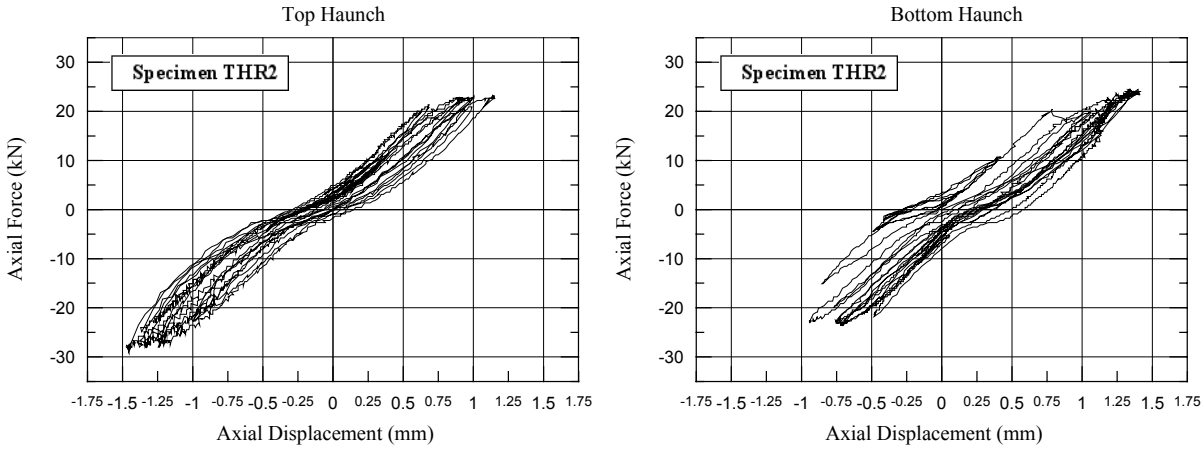

Fig. 7.9 Axial force versus displacement relationship of the haunch

7.3.5 Summary of THR2 Test

As previous THR1 test, use of the hinge connection decreased the haunch stiffness to a much lower value that could significantly reduce the effectiveness in protecting critical joint panel zone. Thanks to introducing the safety factor in the conservative design, the joint shear cracks was still avoided. However, the decreased column capacity in the negative loading direction could risk the failure in the column at the interface of the joint due to under-designed stiffness of the haunch device with inappropriate connections. By using the yielding haunch element, the improved global hysteretic response was expected during the test. However, a little displacement excited in the haunch, compared with the global level, did not provide effective energy-dissipating patterns to the global response. Therefore, the yielding haunch element of low ductility demand did not seem to be an effective solution to retrofit the existing subassembly with a beam flexural hinge forming outside the haunch connection.

As illustrated in Fig. 7.10, the contribution of the beam deformation to the horizontal total displacement was over 50% and increased gradually at higher drift level. The beam deformation had about 90% contribution of horizontal drift at positive 4% drift level and about 70% only after negative 3% drift level. After beam flexural opening, more deformation of the beam required to recover the self-weight of the subassembly in the negative loading direction was the possible reason for this phenomenon. In any cases, the joint deformation was relatively small enough to be ignored in contribution of the horizontal total displacement.

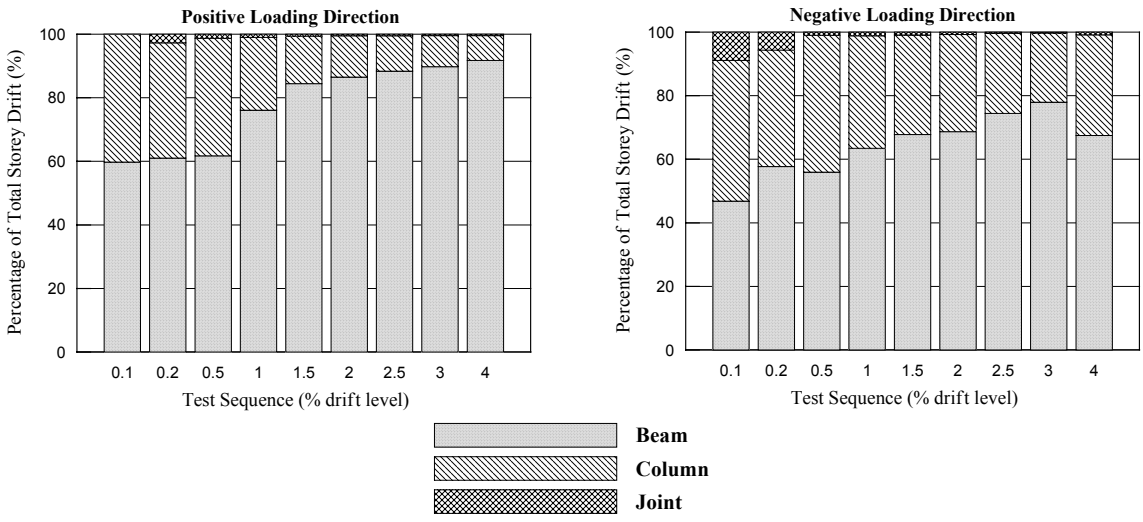

Fig. 7.10 Contributions to subassembly drift of beam, column and joint in THR2

7.4 TEST OF THR3

7.4.1 Specimen

The specimen THR3 was retrofitted with elastic haunch elements welded directly to the plate connections. Due to the small displacement expected in the haunch elements, the bending moments induced at the fix ends of the welded connections were small enough to be ignored. The development of this second generation solution for the haunch elements was aimed to eliminate the uncertainty of connection types in designing full haunch devices. If the haunch stiffness of 100000kN/m was available during the test, the maximum haunch axial force was expected to be 43kN and the flexural failure of the beam was also expected at the location of the haunch/beam connection with more effective protection of the joint panel zone.

7.4.2 General Behaviour

The final crack pattern and the measured global hysteretic loops are illustrated in Fig. 7.11 and Fig. 7.12 respectively. It was observed that two small minor cracks appeared on the back surface of the top column while a small minor crack observed in the beam between column surface and haunch/beam connections. Since the desired haunch stiffness, discussed in the next paragraph, was obtained, the greater axial forces were induced in the haunch devices and had more influence on reducing the column capacity by pushing the joint-closed section of the top column during the negative loading direction. Due to the decreased column axial load combined with the haunch force effect in the negative loading direction, the capacity of the top column between joint and haunch/column connection was significantly decreased below the minimum value required for resisting the flexural crack. The progressive widening of a main flexural crack was still observed in the beam around the haunch connection while the concrete spalling-off was accompanied with the progressive flexural cracks. The perfectly intact joint panel was observed after the test due to the effective protection of designed haunch stiffness. As illustrated in Fig. 7.12, the seismic response similar to THR2 was observed in THR3 test and the inter-storey strength was evaluated as 24kN for both positive and negative loadings. As a result of occurrence of the beam flexural failure without other damages, the desired beam sidesway mechanism was available. There was an accident to the column base during negative loading to 1.0% drift level and it was fixed to continue the experiment. However, imperfect repair leaded to a little slippage observed after 1% drift level

and the earlier strength degradation after 2% drift level in the negative loading direction. Basically, the beam flexural behaviour with some pinching of shear sliding after 2.0% drift level was observed during the test.

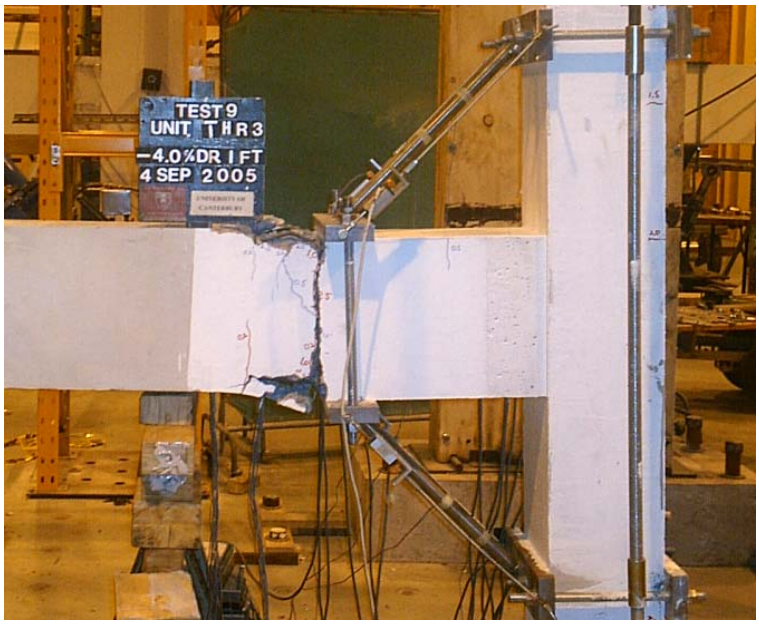

Fig. 7.11 Final crack of THR3

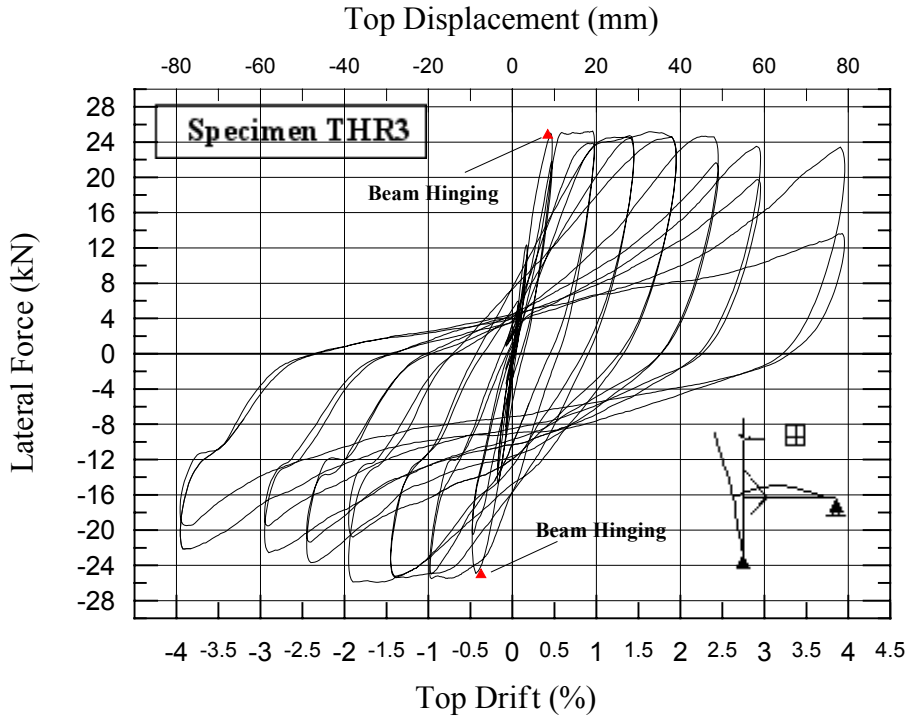

Fig. 7.12 Storey-shear force versus horizontal relationship of specimen THR3

7.4.3 Joint Behaviour

The principal tensile stress of the joint versus the drift level is illustrated in Fig.7.13. Because the accident occurred at the column base and repair was not perfect, the jump of the principal tensile stress could not be avoided during the unloading process in the negative direction. Due to availability of the designed haunch stiffness in the test, the estimated principal tensile stresses were much lower than the values obtained in THR1 and THR2 tests. This demonstrated that the joint panel zone was more effectively protected by the desired haunch stiffness. It was evaluated that the principal tensile stress was $0.11\sqrt{f'_c}$ while the beam flexural failure began in the negative loading direction. Compared with the analytical value, $0.062\sqrt{f'_c}$, for the designed haunch K_d=100000kN/m, it seemed to be still a higher value. However, the obtained p_t=$0.11\sqrt{f'_c}$ had effectively upgraded the joint strength by comparing with the possible critical value $0.2\sqrt{f'_c}$ of causing joint shear cracks in the as-built joint subassembly.

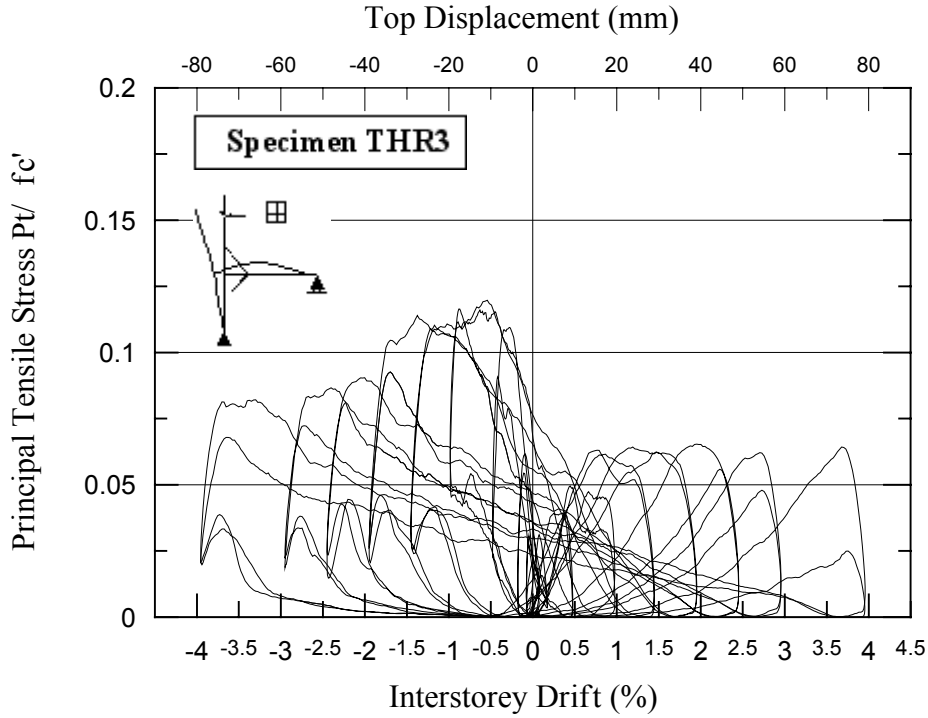

Fig. 7.13 Principal tensile stress versus horizontal relationship

7.4.4 Haunch Behaviour

The hysteretic responses of the top and bottom haunch devices of THR3 test were illustrated in Fig. 7.14. The elastic behaviour without any sliding between connections was observed in

the improved haunch solutions. By welding the haunch elements directly to the steel plate, stiffness losses in the haunch connections were eliminated. Thus, the average stiffness of the top and bottom haunches was evaluated as 110000kN/m that was comparative to the targeted value, 100000kN/m. The haunch axial forces induced by straining the haunch elements could be still treated as being equally distributed of around 47kN that was much greater than the haunch axial forces obtained in THR1 and THR2. However, the greater haunch forces may cause the greater impact on the column and joint capacity by pushing apart the joint-closed section. The small bending moment cased by the small rotation at the fixed end connection could be ignored. Basically, the haunch devices with the weld connection could be an effective and feasible solution for implementing the haunch retrofit strategy

.

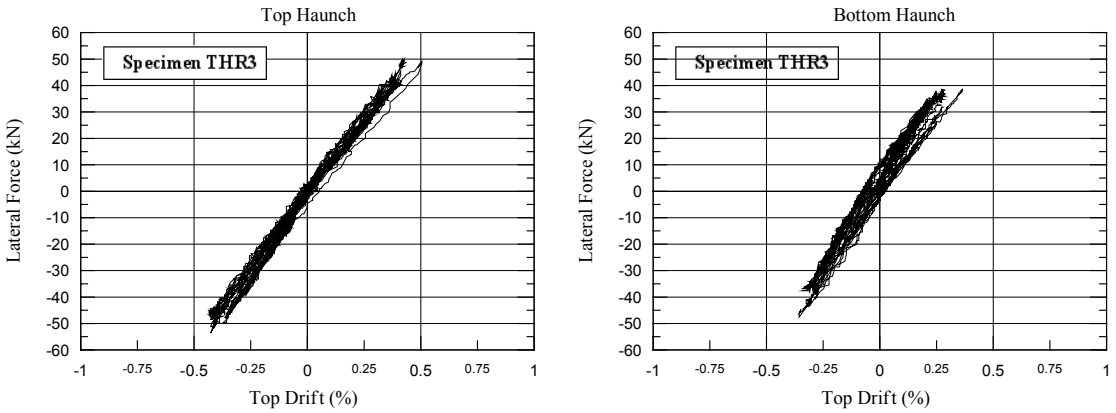

Fig. 7.14 Axial force versus displacement relationship of the haunch

7.4.5 Summary of THR3 Test

By using the weld connections in the haunch devices, the haunch stiffness could achieve the targeted value with pure elastic behaviour and thus the joint panel zone was effectively protected within relatively low principal tensile stress. However, the increased haunch stiffness as well as the increased haunch axial force could possibility decrease the joint/or column capacity through the haunch force pushing against the column axial load. Therefore, the increased column axial load thought applying external tendon force would be the alternative to guarantee the column and joint capacity sufficient for the designed haunch retrofit solution.

As illustrated in Fig.7.15, the joint contribution to the horizontal total displacement was very small compared with the contribution of the beam deformation. As the previous THR1 and

THR2 test, the column contribution of the horizontal displacement was greater in the negative loading direction than in the positive loading direction. This phenomenon may be caused by the self-weight of the beam and/or the lower column stiffness was expected with smaller column axial load in the negative loading direction. At the higher drift level, it is obvious that the column contributed about 10% to 30% of the horizontal total drift and column contributed about 70% to 90% of the horizontal total drift while there was almost no joint deformation observed for the horizontal drift.

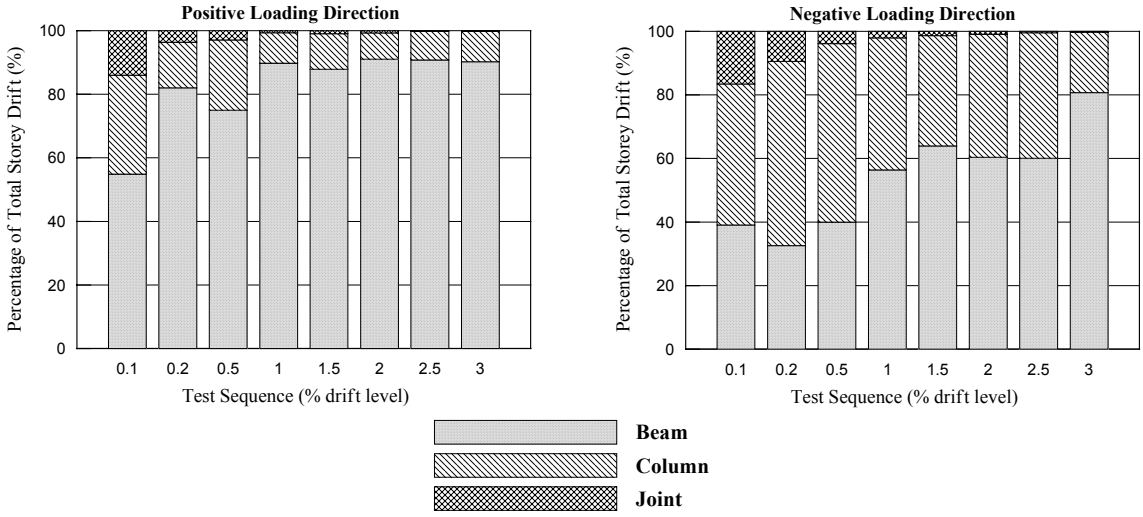

Fig. 7.15 Contributions to subassembly drift of beam, column and joint in THR3

7.5 TEST OF THR3D

7.5.1 Specimen

The specimen THR3D was the existing corner joint retrofitted with the designed haunch elements of weld connection and this experiment was designed to force the plastic hinge occurring. The final crack pattern after testing is illustrated in Fig. 7.16. Compared with the test result of DD2, the joint panel zone was completely saved without joint shear failure and the plastic hinges were formed in both beams where the haunches were connected. Due to bi-directional loadings on the subassembly, there were not only axial loads but lateral forces existing in the haunches and it caused some uncertainties involved in affecting the effectiveness of the haunches. Because the greater total haunch forces were induced on the

column, the simulated dead load that was applied to the column top increased from 75kN to130kN to guarantee the higher capacities of the column and joint.

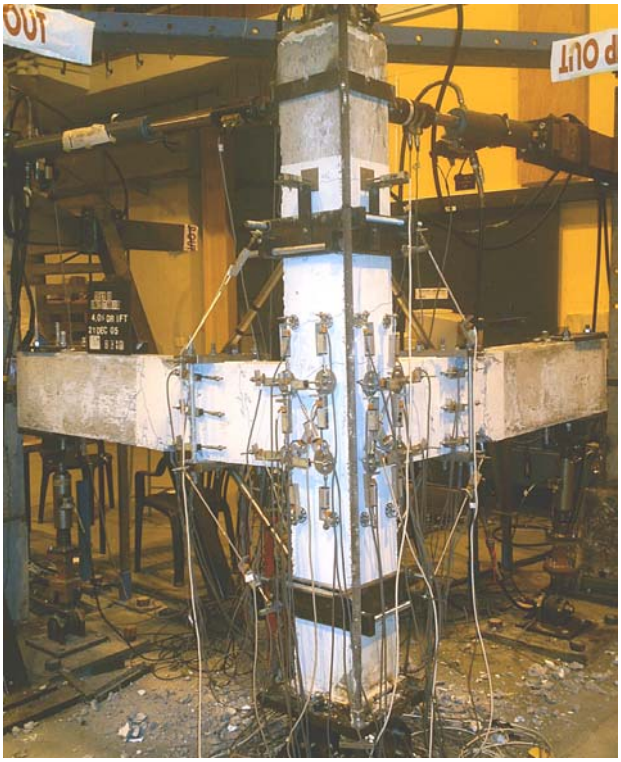

Fig. 7.16 Final crack of THR3D

7.5.2 General Behaviour

Because the joint was intact during the test, the loadings history was completed at 4.0% resultant drift. From Fig. 7.16, the potentiometers were still fixed to the joint panel zone and only cracks around the beam plastic hinges could be observed. Although the major cracks companied with spalling off concrete existed in the beam of haunch locations, the strength of the subassembly did not degrade. A little pinching behaviour occurred only after the serious concrete deterioration of the beam was observed in higher drift level.

7.5.3 The Behaviour of The Retrofitted Corner Joint

X-direction face:

The final crack pattern and the measured global hysteretic loops are illustrated in Fig. 7.17 and Fig .7.18 respectively. Some minor cracks were observed in the top column while the negative loading was applied in the Quadrant 3 where the minimum axial load was applied in the column. However, the beam flexural failure was still observed with widening cracks. Due

to the possible torsion force existing in the beam in bi-directional loading test, the cracks in the beam seemed to be damaged more seriously and propagated not only along a single interface. Therefore, a big crack across through the anchorages that were used to connect the haunch device and the beam was observed. The inter-storey strength obtained during the test was about 25kN and the joint panel zone was still also protected well during whole X-direction loading.

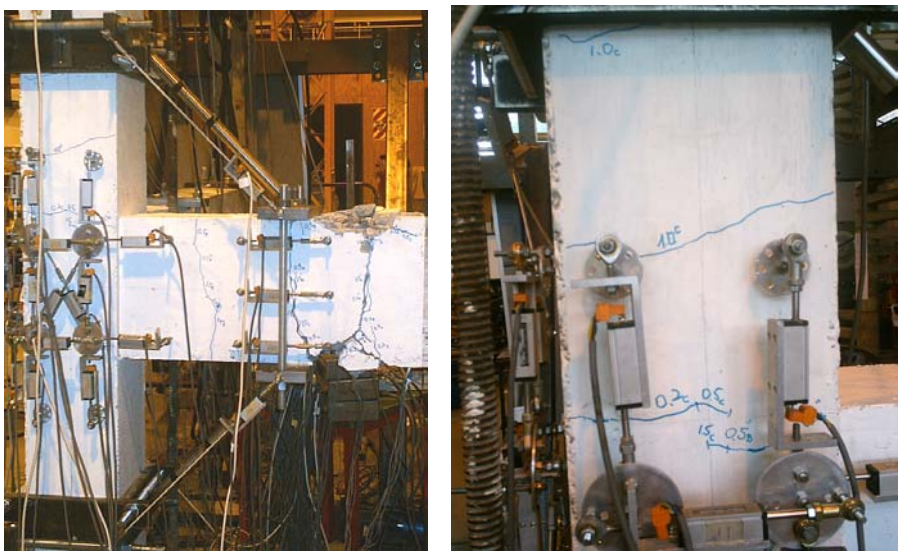

Fig.7.17 Final Crack of THR3D-X dir.

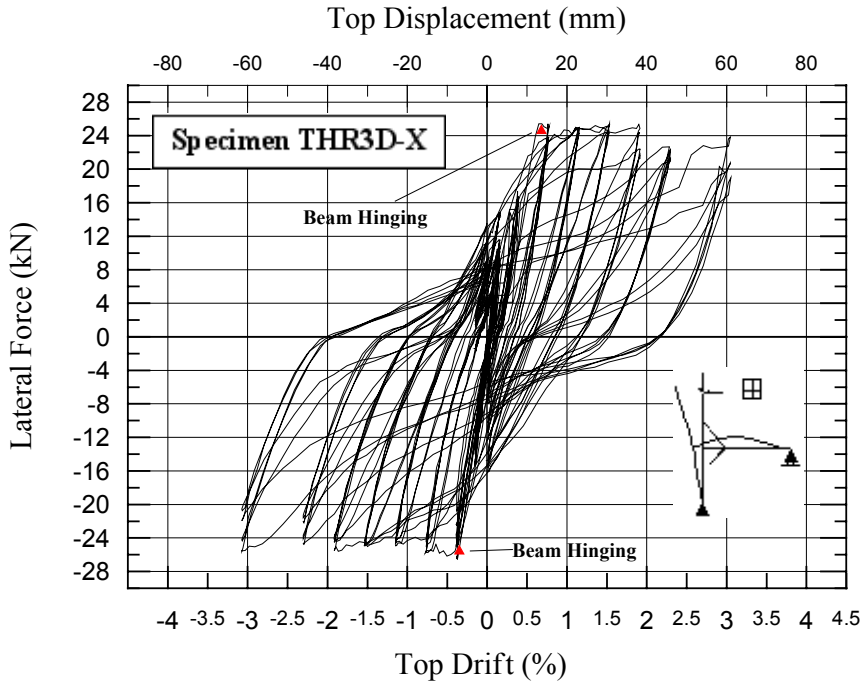

Fig. 7.18 Storey-shear force versus horizontal relationship of specimen THR3D

The principal tensile stress versus the drift level is presented in Fig. 7.19 where the maximum value was $0.095\sqrt{f'_c}$ in the negative loading direction that was close to the value obtained in THR3 test. Therefore, this small principal tensile stress guaranteed that the joint was prevented from the shear failure. Because the lateral forces as well as column axial load were almost constant after plastic hinge occurring, the decreasing principal tensile stress after 1.5% drift in the negative loading direction was not expected. But the almost constant principal tensile stress about $0.024\sqrt{f'_c}$ could be observed in the negative loading direction. And it was much smaller than the value observed in the positive direction. The possible reason was that the principal tensile stress would be smaller if the same horizontal joint shear but greater column axial force were presented in the positive loading direction.

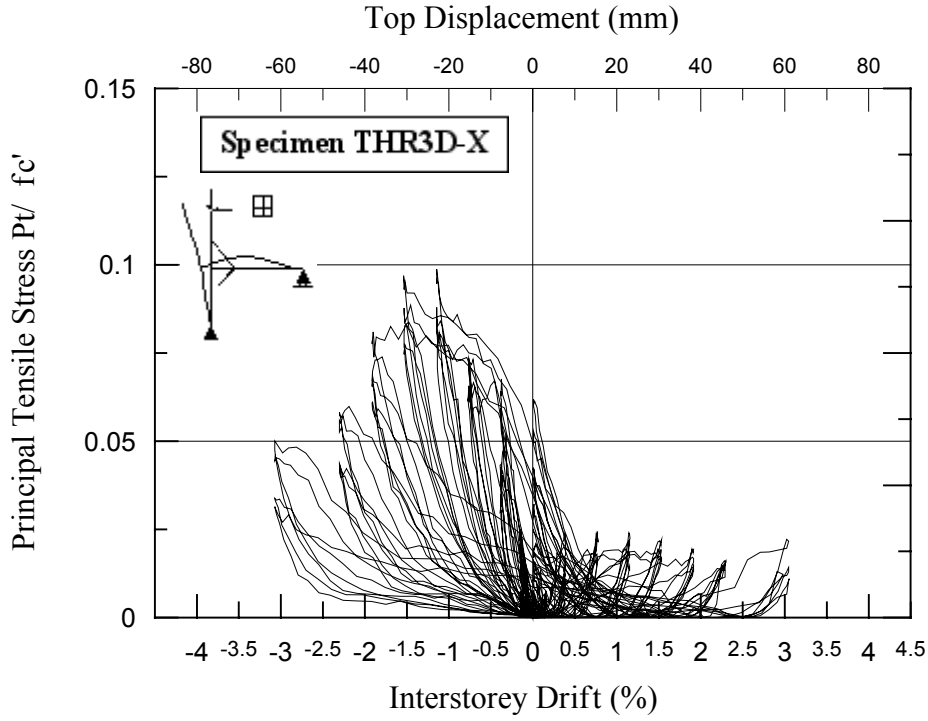

Fig. 7.19 Principal tensile stress versus horizontal relationship for X-direction face

Y-direction face:

The similar crack patterns and seismic response were observed for the Y-direction face (Fig. 7.20 and Fig. 7.21). The column also had minor cracks occurring during loading to the Quadrant 3 where the small column axial load was presented. Due to the varying axial load combined with impact of the haunch axial forces to the column, the top column was always in the weakest situation during loadings to the Quadrant 3. Since an accident occurred during

THR3D set-up, a small pre-crack was observed in the beam/haunch connection. As a result, the beam flexural cracks seemed to be widening along a single interface at the beam/haunch connection. Due to the symmetric set-up of the THR3D subassembly, the inter-storey strength of the Y-direction loading was close to the observed value of X-direction loading and it was about 25kN.

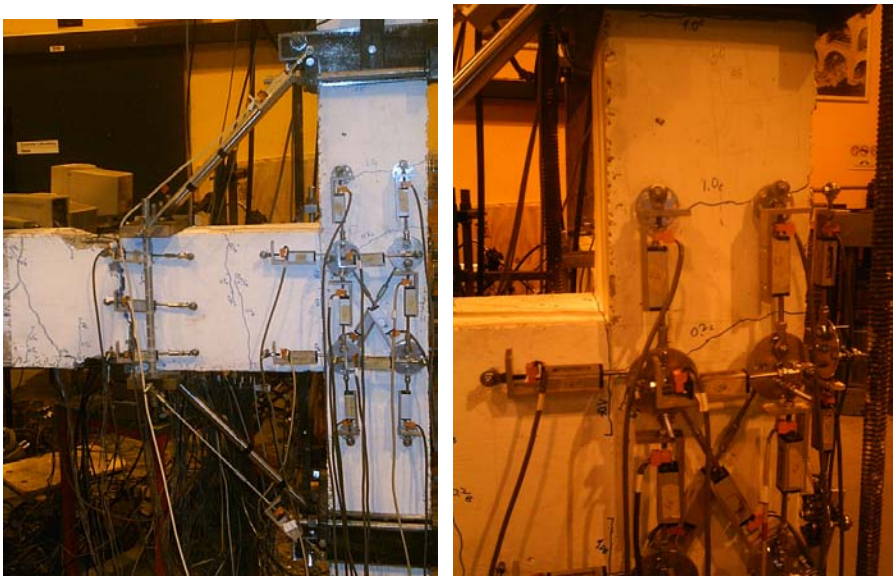

Fig. 7.20 Final Crack of THR3D-Y dir.

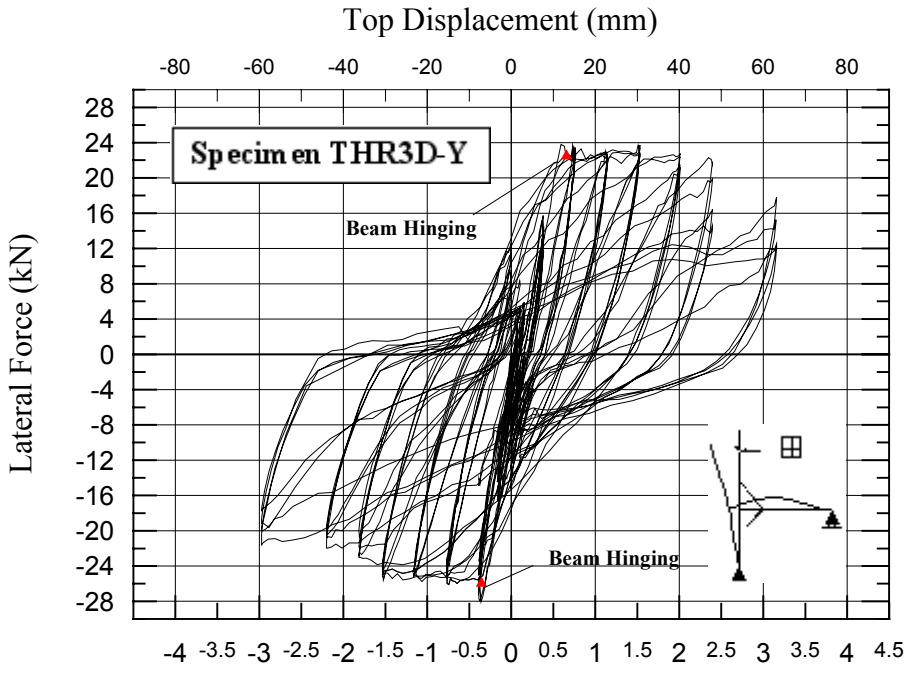

Fig. 7.21 Storey-shear force versus horizontal relationship of specimen THR3D

Since the readings of some instrumentation were not available, the principal tensile stresses were estimated until 1.5% drift level (Fig. 7.22). The maximum principal tensile stress obtained in the Y-direction loading was about $0.085\sqrt{f'_c}$, which was much smaller than the critical value. Hence, the joint shear crack was not observed during the loading history. Again, due to the smaller column axial load in the positive loading direction, the smaller principal tensile stress of $0.085\sqrt{f'_c}$ was observed.

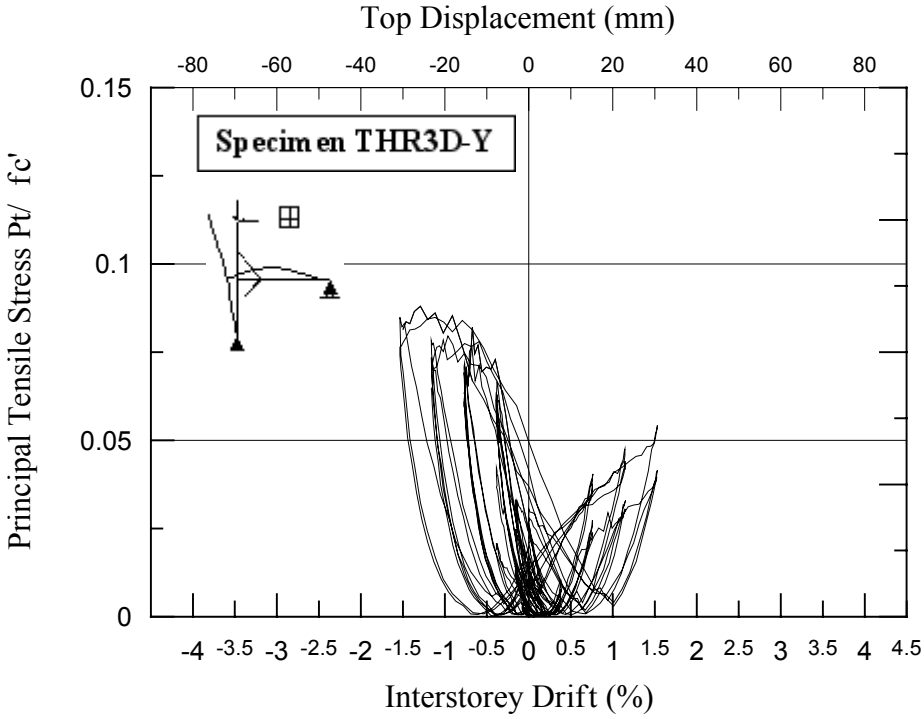

Fig. 7.22 Principal tensile stress versus horizontal relationship for Y-direction face

7.5.4 Haunch Behaviour

X-Direction Face:

The hysteretic responses revealed the more complex behaviour of the haunch was performed in bi-directional loading test. Since the orthogonal displacements were applied to the haunch devices, the bending moments of two orthogonal axes would have a interaction combined with haunch axial force. As illustrated in Fig. 7.23, the presence of the possible moment interaction affected the haunch performance and not a completely linear elastic response was displayed. As a result, the haunch stiffness was more difficult to be determined. Since a big crack was observed close to the anchorage connecting the haunch and the beam, the haunch stiffness was also significantly reduced to an estimated value, 65000kN/m.

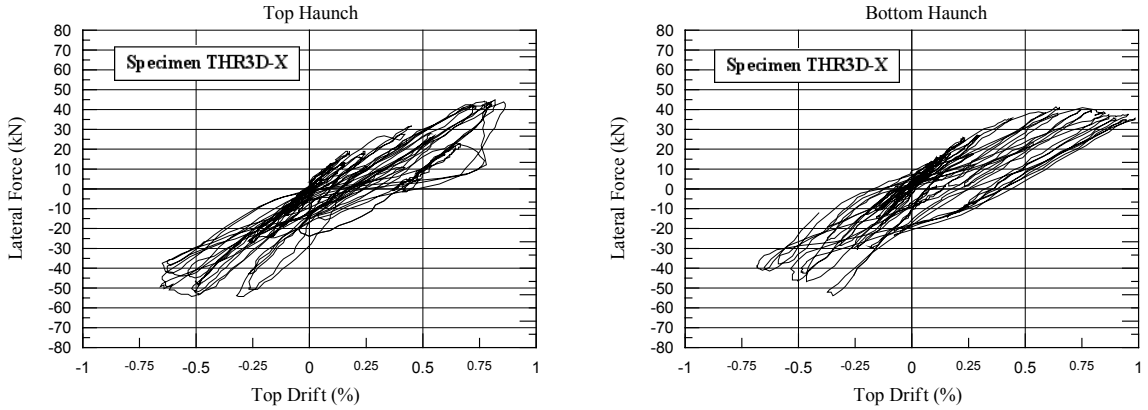

Fig.7.23 Haunch Force-Displacement Relationship-X dir.

Y-Direction Face

Without a cracks across the anchorage, the haunch stiffness was totally developed. The proposed average stiffness of the top and bottom haunches was about 130000kN/m that was higher than the designed value (Fig. 7.24). The possible reason for higher stiffness was that the instrumentation only measured the axial displacement without taking into account the lateral displacement of the haunch which also contributed to the haunch elongation. Again, the moment interaction in the haunch element caused a complex hysteretic response but a linear elastic behaviour.

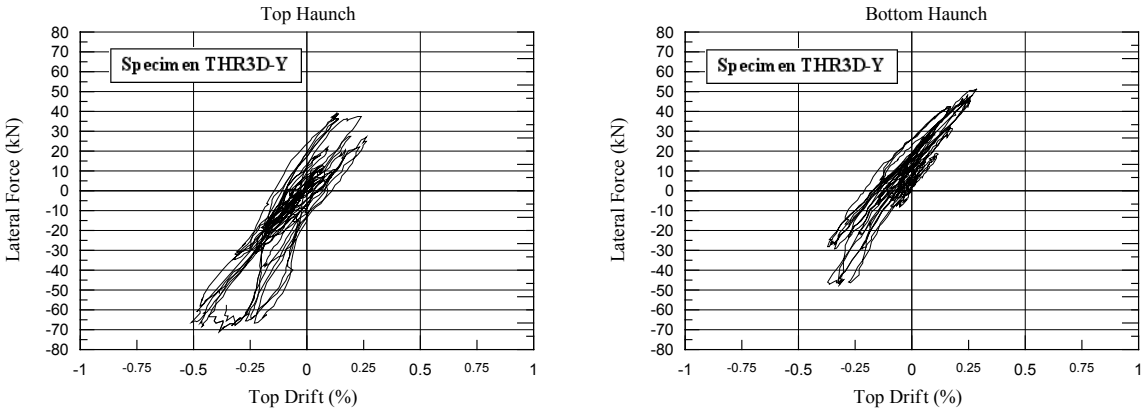

Fig. 7.24 Axial force versus displacement relationship of the haunch

7.5.5 Summary of THR3D Test

Using the weld connection in the haunch devices was still expected to be an effective solution for the 3-D test. However, the interaction of the bending moments along two orthogonal axes would affect the performance of the linear elastic behaviour in the designed haunch. Due to

the potential torsion existing in the beam, flexural crack would not only follow the interface at the haunch/beam connection. Therefore, the possible risk in reducing the designed haunch stiffness would occur while the crack propagated along the anchorages that were used to fix the haunch to the beam. In addition, the significant reduced column axial load combined with the haunch axial force would risk the column and joint capacity during the bi-directional loading. The external tendon force applied to the column could increase the column and joint strength. Generally speaking, the elastic hunch devices with conservative design could still effectively protect the corner joint from the brittle shear failure with bi-directional loadings.

CHAPTER 8

NUMERICAL MODELLING OF THE JOINT BEHAVIOUR AND COMPARISON WITH EXPERIMENTAL RESULTS

8.1 INTRODUCTION

The experimental results in the previous chapters confirmed the significant vulnerability of the joint panel zone that were generally observed in the existing reinforced concrete buildings, designed for gravity-loads-only before the introduction of seismic oriented code in pre-1970. With inadequate reinforcing detail (i.e. lack of transverse reinforcement and deficiencies of the anchorage in the joint region), the brittle shear mechanism of the joint would be developed so that the local as well as the global performances were dramatically affected by the dominant non-linear behaviour of the joint. To assessing the seismic performance of the existing buildings, the effort was essentially given to modelling the inelastic behaviour of the joint panel zone in past several years and several approaches of modelling the RC beam-column joint, ranging from simplified empirical to refined finite elements models, had been developed such as multi-node or multi-spring macro-models. Due to the complexity in requiring the enormous definition of input–parameters and appropriate constitutive laws for the materials, however, these kinds of models were not simply feasible tools for numerical analysis. Furthermore, because of the lack information on the basis of experimental results, appropriate modelling solutions for joint shear behaviour were not available.

A simplified analytical model for joint behaviour, proposed by Pampanin, was treated as a feasible tool to numerically investigate the seismic response of existing frame systems [Pampanin, Magenes and Carr, 2003b]. Following the experimental studies on the under-designed beam-column joint subassemblies and frame systems, the behaviour of joint shear mechanism underlined the characteristic of flexural plastic hinging with particular pinching mechanism at local and global response. Therefore, an equivalent rotational spring, governing the relative rotation of the beams and columns, was introduced to present the peculiar shear mechanism of the joint by a concentrated plasticity approach that required the monotonic moment-rotation characteristics of the spring. By this way, the moment in the joint spring was supposed to be the equivalent value contributed from the bending moments of the adjacent elements (Fig. 8.1). To simulate the joint behaviour, an appropriate hysteretic rule for the

beam-column joint with “pinching” was proposed by Pampanin to take into account both bar slipping mechanisms or shear crack in the joint region in modelling seismic response. In this chapter, this joint hysteresis loop was used to construct the input data of beam-column joints for numerical analysis. Comparisons between the numerical analysis and experimental results of cyclic tests of beam-column subassemblies would be also presented and discussed with the details of joint deformation in different limit states.

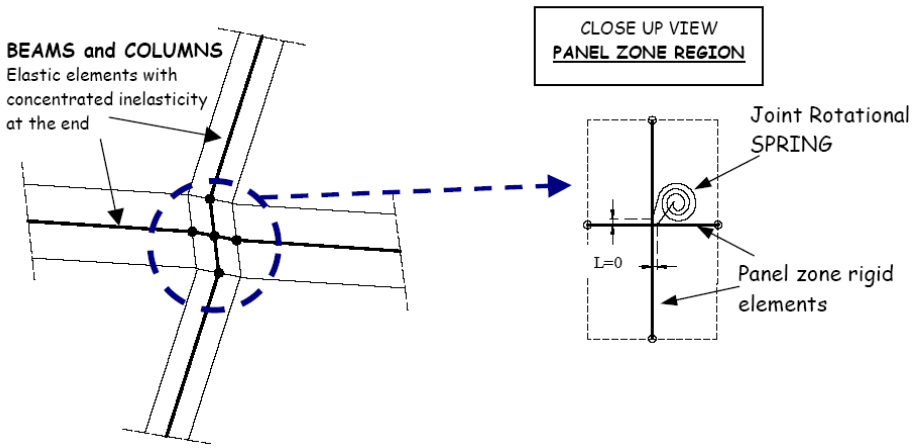

Fig. 8.1 Proposed analytical model for joint behaviour: rotational spring [Pampanin, Magenes and Carr, 2003b]

8.2 REVIEW OF DEVELOPMENT IN NUMERICAL MODELLING

To simulate the behaviour of the beam-column joint considering the bond deterioration and pinching hysteric performance, several numerical methods had been investigated in the past decades. Ranging from simple empirical approaches to the complicated finite element method (FEM), the accuracy and complex of the numerical model were two major issues to be considered in modelling the existing structures and the complex new structure for evaluation purpose. Several different numerical methods are introduced in the following paragraph.

8.2.1 Proposed Beam-Column Joint Model with Springs

A model that consists of elastic elements and spring were proposed by Youssef and Ghobarah [Youssef and Ghobarah, 2001] and took into account the bar slippage by modelling concrete and steel springs that present the stiffness of the effective reinforcing bars and the effective concrete compression. Idealisation of the joint behaviour was achieved in this model by using

twelve concrete springs, twelve steel springs and two shear springs. Three concrete and three steel springs were located at the joint interface with each of the beam and columns framing into the joint as illustrated in Fig. 8.2

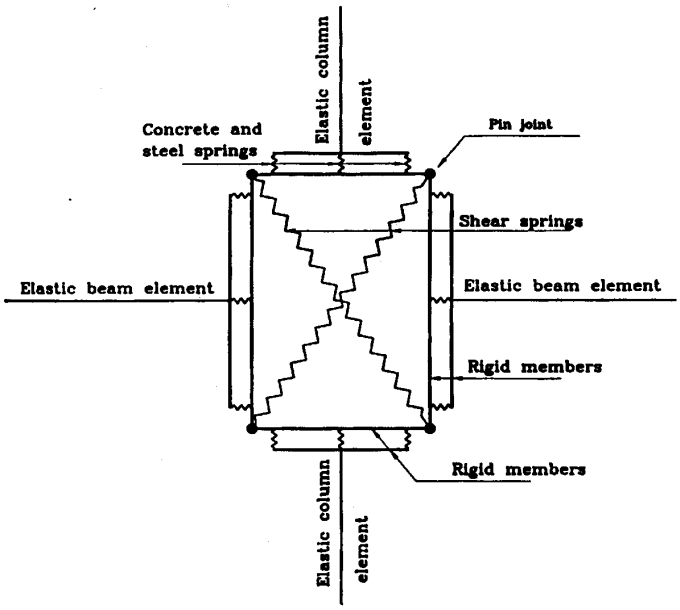

Fig. 8.2 Proposed joint model by Youssef [Youssef and Ghobarah, 2001]

8.2.2 Finite Element Models

In past several years, the Finite Element Method (FEM) had gained attention in practice, as a powerful and reliable tool for modelling and evaluating the structural response. A FEM model composed of the line element and the plane stress finite element (12-node and 10-node) was proposed by Elmorsi [Elmorsi, Kianoush and Tso, 2000] to simulate the joint behaviour under cyclic loading. In addition, the bar slippage in the joint region was model by the truss elements where bond-slip element was proposed to simulate the bond strength between reinforcing bars and concrete. The detail of the proposed model is illustrated in Fig. 8.3

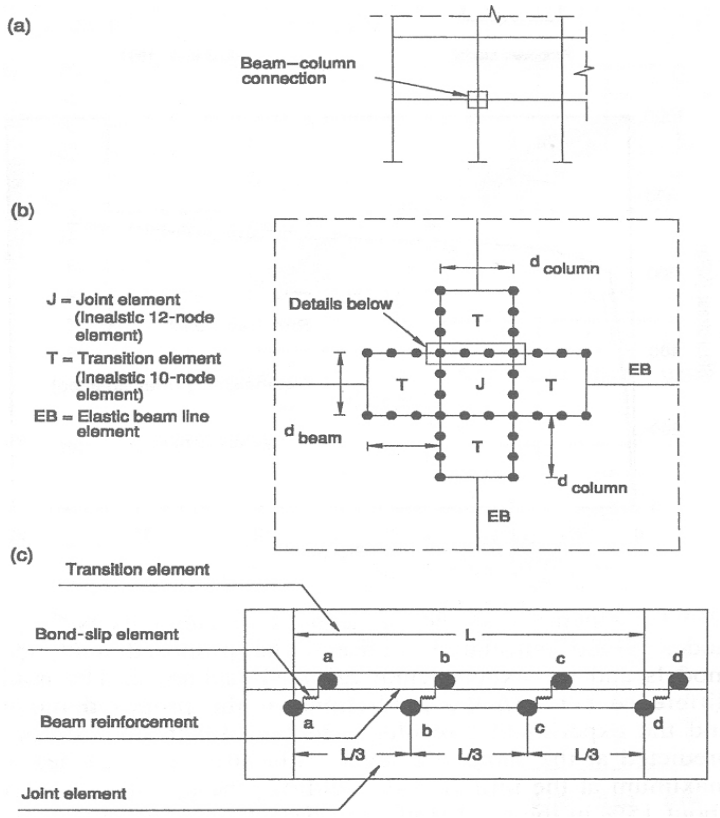

Fig. 8.3 Proposed FEM model by Elmorsi [Elmorsi, Kianoush and Tso, 2000]

8.3 PROPOSED ANALYTICAL MODEL: ROTATIONAL SPRING

A simple model consisting of a non-linear rotational spring was proposed by Pampanin [Pampanin, Magenes and Carr, 2003b] to simulate the joint shear behaviour on the basis of a concentrated plasticity approach that could be implemented using Inelastic Dynamic Analysis Program of RUAUMOKO [Carr, 2003]. The dominant non-linear behaviour of the joint panel zone that had critical contribution of seismic performance in existing buildings was modelled by the rigid panel elements and the joint rotational spring of zero length while the beams and columns were modelled by mono dimensional-elastic element with inelastic behaviour of plastic hinges at the edges (Fig. 8.4). The moment-rotation characteristic of the joint spring could be simply evaluated by considering that the moment of a joint was equilibrium of the moment from the adjacent beam and column. By giving a principal tensile stress corresponding to the joint moment and a derived joint stiffness, the strength degradation curve, p_t-γ (principle tensile stress versus shear deformation) could be obtained. Fig. 8.5 illustrates the basic concept of the equivalent moment-rotation curve to the corresponding p_t-γ.

According to aforementioned results, the principal tensile stress at first crack was defined by typology of the joint (e.g. p_t=0.2$\sqrt{f'_c}$ and p_t=0.42$\sqrt{f'_c}$ for exterior joint (with end-hook and smooth bars) and interior joint respectively). In the model, appropriate stiffness-degradation hysteresis rules for the beams, columns and joints are adopted to simulate the cyclic behaviour of elements in the non-linear range

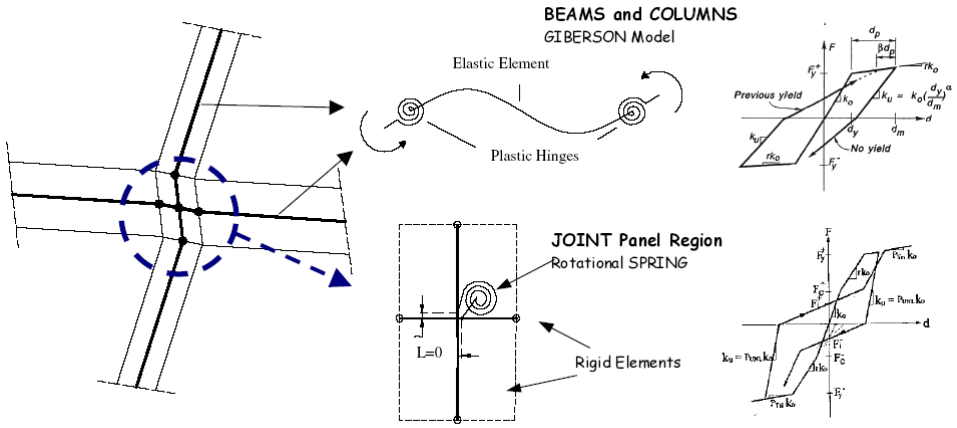

Fig. 8.4 Modelling of structural elements: beam, columns (plastic hinges) and joint panel region (shear hinge) [Magenes and Pampanin, 2004]

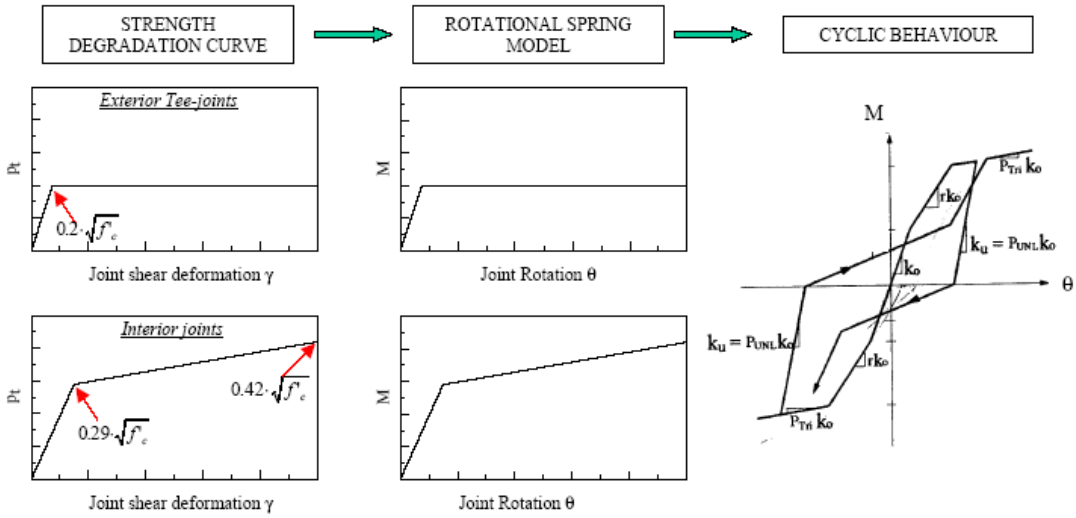

Fig. 8.5 Monotonic and cyclic Behaviour of the shear hinge model [Pampanin, Magenes and Carr, 2003b]

To react the effect of the column axial load on the joint capacity, the modified model with two rotational springs connected between the top/bottom column and the beam was used to

simulate the response of the beam-column joint subassembly (Fig. 8.6). Three rigid elements connected between the beam and column were exploited to form the joint panel zone while the elastic frame elements were used to model the beam and column members. It was noted that the extreme small lengths were applied to the joint rotational spring and the properties of all element were obtained from the preliminary work.

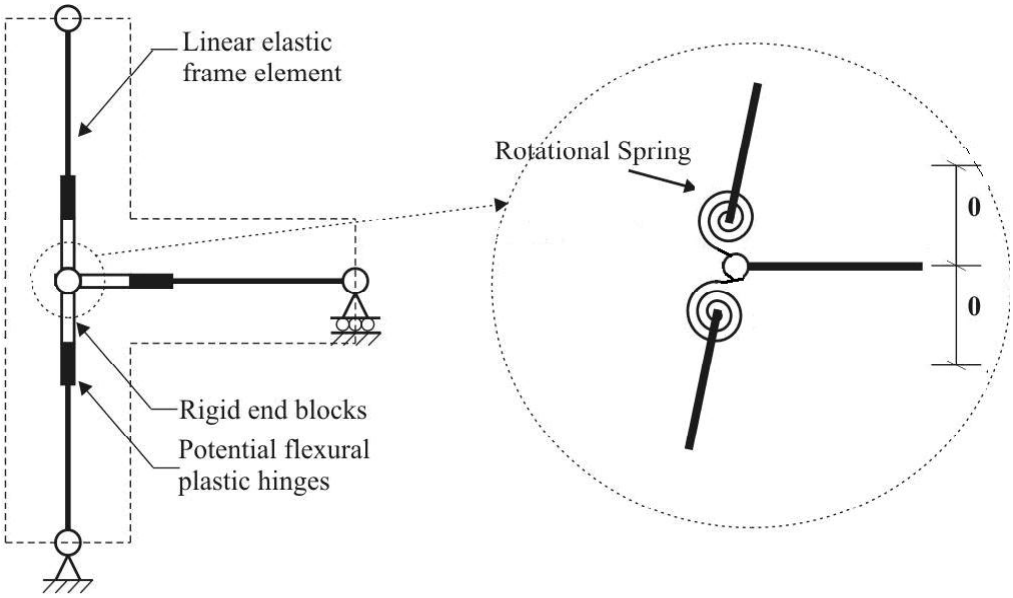

Fig. 8.6 Proposed analytical model for joint behaviour

8.4 INTRODUCTION OF PAMPANIN HYSTERESIS LOOP

A new hysteresis rule that could properly simulate the pinching behaviour of the joint was proposed by Pampanin. The Pampanin Reinforced Concrete Beam-Column Joint Hysteresis presented the joint response, with consideration of the bar slippage, by giving two sets of stiffness for unloading process and another two sets of stiffness for reloading stiffness. According to the investigation on the previous experiment, the derived stiffness could be approximated by the function of initial stiffness and ductility as illustrated in Fig. 8.7 where the unloading stiffness K_{u1}, K_{u2} and reloading stiffness K_{r1}, K_{r2}, could be estimated in terms of initial stiffness K_0 and the coefficients $\alpha_{u1,}$ $\alpha_{u2,}$ α_{r1} and $\alpha_{r2,}$ while these empirical coefficients could be obtained on the basis of the experimental results. Ruaumoko [Carr, 2003] accepted this hysteresis rule to numerically model the beam-column joint behaviour.

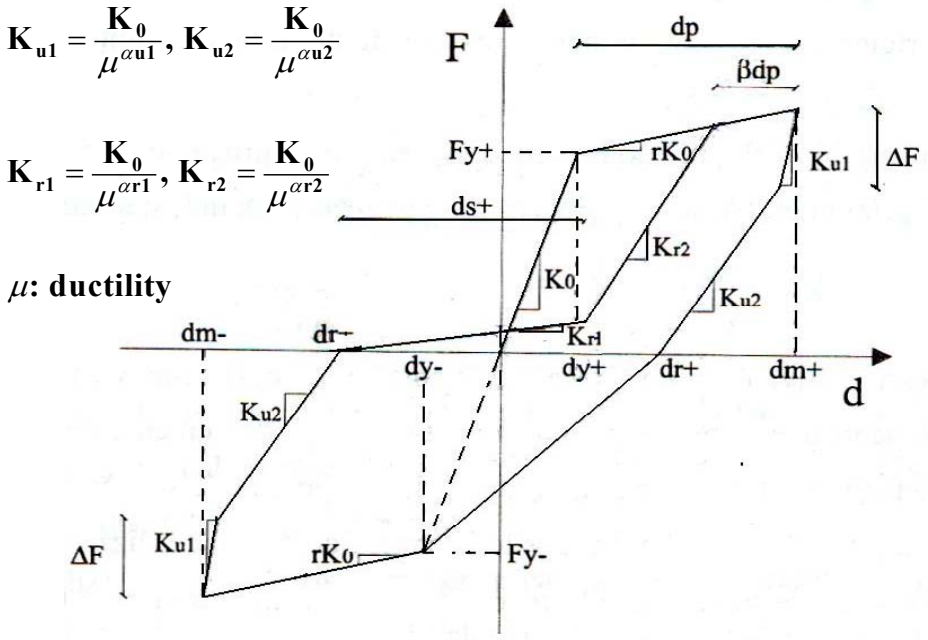

Fig. 8.7 Pampanin reinforced concrete beam-column joint hysteresis [Carr, 2003]

8.5 NUMERICAL VALIDATION OF EXPERIMENTAL RESULTS

To analytically access the seismic behaviour of the beam-column joint subassemblies, the numerical model was constructed with RUAUMOKO and validated by the experimental results. The specific stiffness degradation rules proposed by Pampanin were used to simulate the brittle joint behaviour of pinching performance. Since this rule could only be used to model the joint of failure in both loading directions, the joint spring of TDP1 that maintained elastic in the negative loading direction could not adopt Pampanin hysteresis rule. The basic TAKEDA hysteresis rule was only given in modelling the joint spring of TDP1 and pinched hysteresis rule was used in the joint spring of TDD1, TDP2, TDD2, TSP1, TSD1, DD2, THR1, THR2, THR3 and THR3D. According to the comparison of numerical and experimental results, the coefficients as given in Table 8.1 for Pampanin joint hysteresis were chosen to model the joint springs of all other specimens. And the input data of Ruaumoko for all specimens could also be found in Appendix B.

Table 8.1 Coefficients used for Pampanin joint hysteresis

Option 1	α_1	α_2	ΔF(%)	β
Reloading	1.25	0.9	30	-0.05
Unloading	-1	0.8		

8.5.1 Numerical Results of As-built Beam-column Joints

The numerical results compared with the experimental results were presented in Fig. 8.8 and Fig. 8.9 for the 2-D and 3-D test respectively.

Without modelling the joint with pinched hysteresis, the pinching response of TDP1 was not appropriately presented by TAKEDA hysteresis rule. However, TAKEDA hysteresis rule of the beam could properly present the pure flexural behaviour of the beam in TDD1. In TDP2 and TDD2 of a pure joint shear failure, the numerical results well matched the experimental performance by modelling the joint with Pampanin hysteresis. Although the beam hinging mechanisms were expected and modelled in TSP1 and TSD1, the rare shear cracks at the rear face of the joint caused a joint-like pinching performance and a non-fully developed flexural strength of the beam. Therefore, TAKEDA hysteresis rule could not well present the joint behaviour with a shallow beam that often had a complex shear failure accompanied with a beam flexural mechanism.

In the 3-D model of DD2, the Pampanin hysteresis rule was still valid in modelling the joint spring. Due to the more complex interaction of the bi-directional loadings in the joint, the numerical results did not completely match the experimental result. However, the expected pinching response of the corner joint could be still obtained in the numerical result of DD2.

By estimating the joint shear deformation at each limit state when the defined damage occurred, the comparison between numerical analysis and experimental could be arranged as given Table 8.2. Because the joint shear failures only occurred in the specimen of TDP1, TDP2 and TDD2, they were used to obtain the joint shear deformation of the corresponding failure situation. It was observed that the drift level were quite the same in both analysis but the joint shear deformation showed a much higher value for the first diagonal joint crack by experimental results. However, the numerical analysis and experimental results showed a better-matched value for both drift level and joint shear deformation of extensive damaged situation. The possible reason was that the joint shear deformation was very small before the first diagonal crack and the instrumentation was not sensitive enough to measure it. Therefore, the experimental result was not too reliable for estimating the joint shear deformation at the limit state of first joint shear crack.

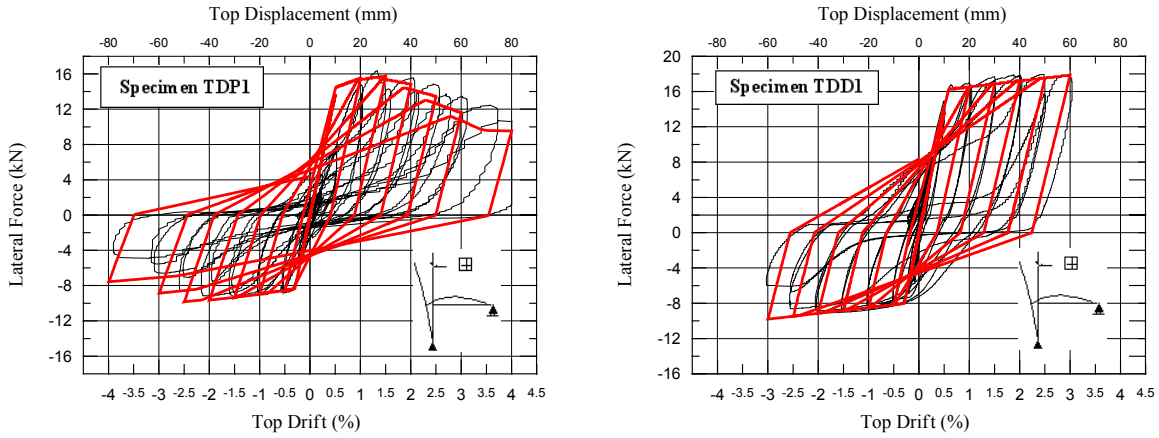

(a) TDP1

(b) TDD1

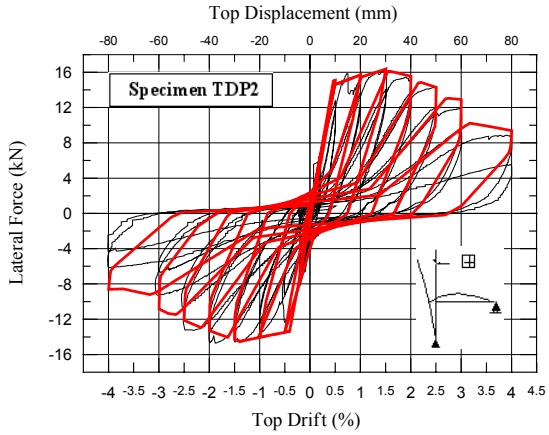

(c) TDP2

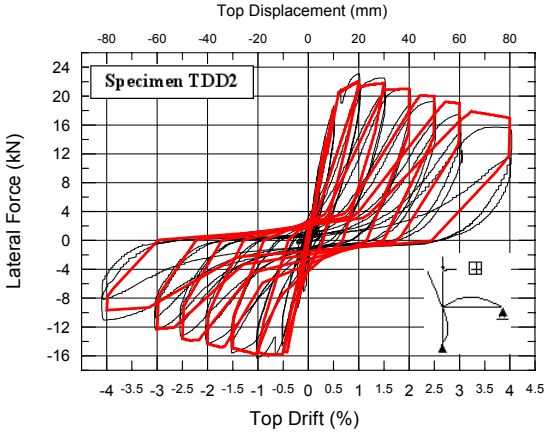

(d) TDD2

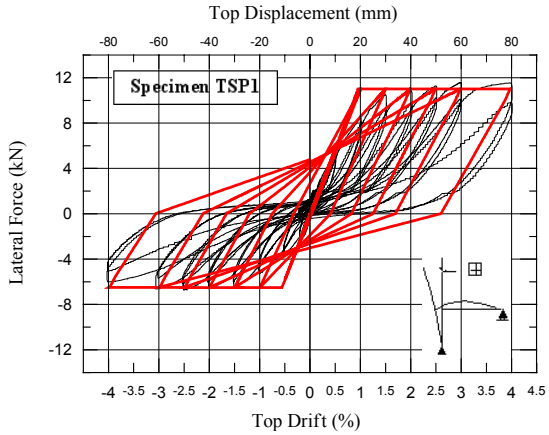

(e) TSP1

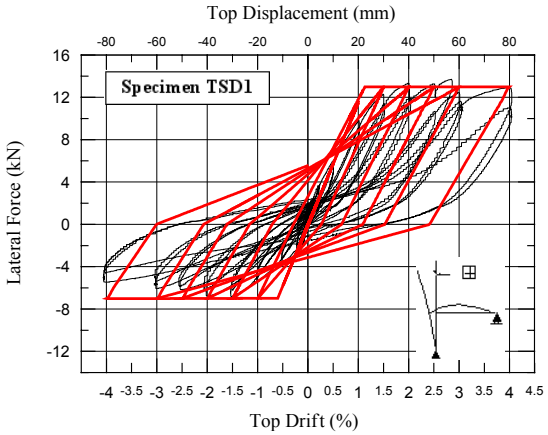

(f) TSD1

Fig. 8.8 Numerical-experimental comparison for as-built specimens of 2-D tests

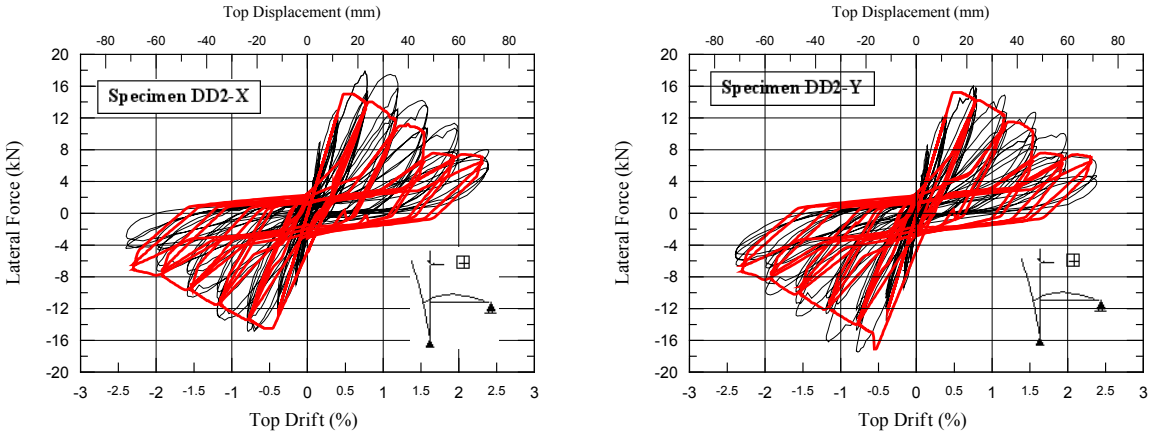

(a) X-direction face (b) Y-direction face

Fig. 8.9 Numerical-experimental comparison for as-built specimens of 3-D tests

Table 8.2 Joint shear deformation at different limit state

Limit State	Numerical Analysis		Experimental Result	
	Subassembly Drift (%)	Joint Shear Deformation (rad)	Subassembly Drift	Joint Shear Deformation (rad)
First Diagonal Crack	0.5% (P) 0.5% (D)	0.00013(P) 0.00014 (D)	0.5~0.75% (P) 0.7% (D)	0.001~0.00136 (P) 0.0025~0.0029 (D)
Extensive Damage	1.0% (D)	0.0026~0.0081 (D)	1.0% (D)	0.0045~0.0065 (D)

Note: P: Plain-round bar with end hook, D: Deformed bar with ends bent into the joint core

8.5.2 Numerical Results of Retrofitted Beam-column Joints

The numerical results of the retrofitted specimens are also illustrated in Fig. 8.10 and Fig. 8.11 for the 2-D and 3-D tests respectively. From the numerical results, the desired hysteresis patterns of the beam flexural failure were presented by the TAKEDA hysteresis rule and matched with the experimental results for all specimens. It was obvious that the haunches successfully relocated the plastic hinge in the beam and saved the joint panel zone from the brittle shear failure. Therefore, the yielding strength of the joint spring with pinched hysteresis rule was not initiated. From the numerical analysis, it was still observed that there was not significant increase in dissipating energy because only little contribution of energy dissipation from the yielding haunches in THR2. In the 3-D model, the numerical results also presented a matched hysteresis loop with experimental result. This could verified that pinched joint hysteresis was also practical in modelling 3-D joint.

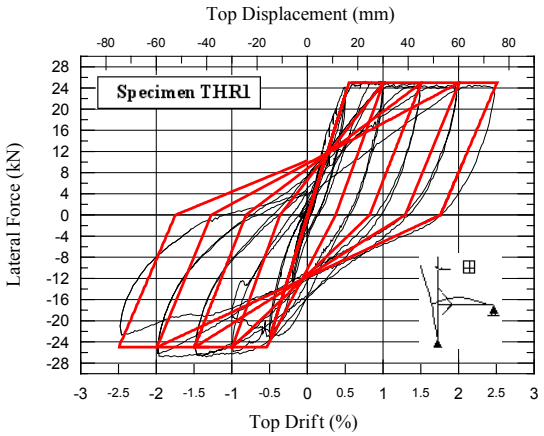

(a) THR1

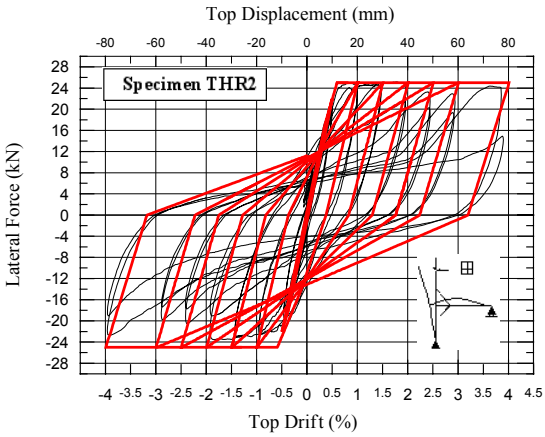

(b) THR2

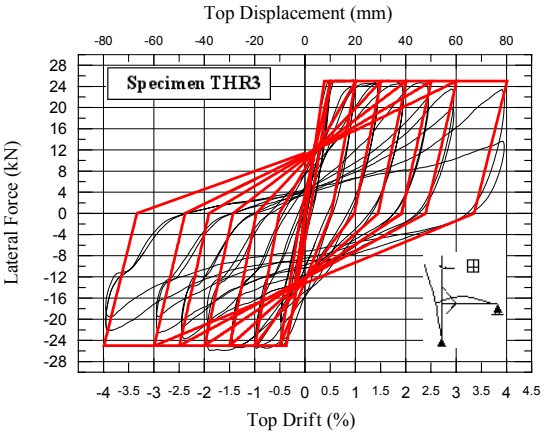

(c) THR3

Fig. 8.10 Numerical-experimental comparison for retrofitted specimen of 2-D Tests

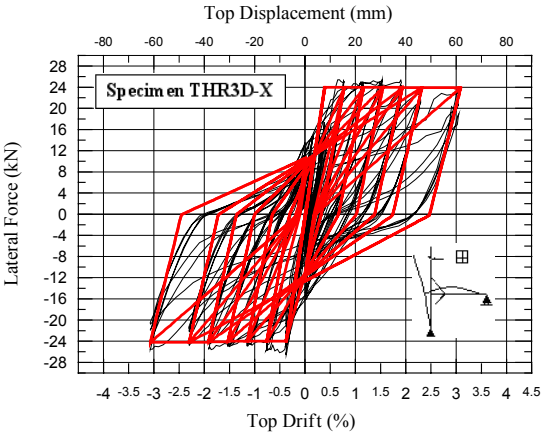

(a) X-direction face

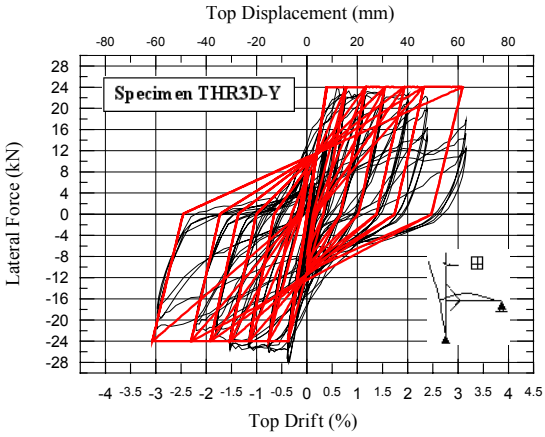

(b) Y-direction face

Fig. 8.11 Numerical-experimental comparison for retrofitted specimen of 3-D Tests

CHAPTER 9

CONCLUSIONS AND RECOMMENDATIONS

9.1 GENERAL

Existing reinforced concrete buildings mainly designed for gravity-loads-only, as typical before the introduction of more advanced seismically-oriented codes in the early-mid 1970s, were expected and shown to have critically brittle failure mechanisms in the joint regions. Due to the lack of capacity design considerations, the shear failure in the joint panel zone can lead to major damage and full collapse to the structure. Experimental test results on pre-1970s as-built beam-column joint subassemblies demonstrated the vulnerability of the existing joint by using plain round bars and inadequate reinforcing detail in the joint core.

A low-invasive low cost retrofit solution base on a metallic diagonal haunch solution has been proposed and investigated through experimental quasi-static cyclic tests on 2-D or 3-D beam-column joint subassemblies, which were representing the older construction practice. The very satisfactory experimental results confirmed the feasibility and efficiency of the haunch devices in retrofitting the joint panel region by relocating the plastic beam hinge away from the joint. Through the well designed haunches protect the beam-column joints, the probability of shear failure or the serious deterioration of the hinge region may increase with the reduced free span of beams and columns. This phenomenon can cause the undesired degradation of strength if it is not designed with further care. A possible solution to prevent the shear failure in this situation is using fibered reinforced polymers, FRP around the potential failure region. Compared to applying FRP to the whole joints region as described in section 2.5.1, the combined method of using haunches and part of FRP can be a more economical solution. The simplified analytical procedure derived for design purposes was also well in agreement with the obtained results. In conclusion, a simplified numerical model based on a lumped plasticity approach well simulated the joint shear brittle behaviour by implementing a recently proposed hysteresis loop to account for pinching and stiffness degradation that were typical in joint shear failure. Thus, it could be proposed as viable tool for more extensive parametric studies on the response of existing buildings prior or after retrofitting.

9.2 SEISMIC PERFORMANCE OF THE EXISTING BEAM COLUMN JOINT SUBASSEMBLY

The experimental results highlighted the likelihood to develop a brittle shear failure mechanism in the existing beam-column joint subassemblies. Due to a general lack of transverse reinforcement in the joint core and no capacity design considerations, diagonal shear cracks were developed followed by extensive damage above the irreparable limit. As shown in previous research, the principal tensile stress related to the occurrence of the first crack in the joint was higher when using deformed bars than when using plain round bars with end hooks. A more pronounced concrete wedge mechanism was similarly observed in the subassembly using the plain round bars with end hook. It was noted that the use of deformed bar with the anchorage bent into the joint core provide more effectiveness in preventing the joint from shear cracks and development of a concrete wedge. Furthermore, the use of a single stirrup in the joint core, even combined with plain round bars, played a major role in delaying the occurrence of a full collapse mechanism and allowed to develop a higher joint strength after the joint first crack. More sudden degradation of strength was observed when no transverse reinforcement was used in the joint region. The response under bi-directional loadings of a 3-D joint specimen confirmed that the interaction of the joint shear demands along the principal axes reduce the overall joint shear capacity during the experimental test. In addition, the wide beam-column joint showed a peculiar shear-torsional crack at the exterior side of the beam instead of a joint shear failure due to the incomplete development of the beam flexural strength.

9.3 SEISMIC RESPONSE OF THE HAUNCH RETROFITTED SUBASSEMBLIES

The retrofit intervention based on the proposed haunch metallic diagonal element, protected the joint panel zone from the shear failure observed in the as-built configuration by relocating the beam plastic hinge away from the critical joint panel zone. The whole set-up of the haunch connection to the beam had revealed critical to activate as desired the haunch devices and thus the effectiveness in protecting the joint region. By using a mechanical type of hinge solution at the haunch-beam-connection, sloppiness and high flexibility of the whole diagonal device could significantly reduce the haunch stiffness. Therefore, a conservative design should be followed by introducing appropriate safety factor to guarantee the desired hierarchy strength

while accounting for the uncertainties associated with practical implementation issues. Alternatively, a second generation of haunch connection was developed, with the intent to favour a simpler and more practical implementation.

It was worth noting that also the possibility of adopting a yielding haunch element had been investigated. However, due to particularly stiff core-region of the "haunched" subassemblies, as well as due to the inherent design criteria (to protect excessive rotational demand in the joint) the efficiency of the dissipating element was impaired by the relatively small rotation allowed between beam and column and was thus not suggested at this stage as a viable solution.

The proposed retrofit solution also demonstrated to be very efficient in upgrading the performance of corner 3-D b-c joints subjected to combined bi-directional lateral loadings. Special attention however was given and should be paid to guarantee that the actual demand of the 3-D frame buildings was accounted for the variation of axial load due to the lateral sway when designing the retrofit intervention into the corner subassemblies. A crude application of the design procedure used in the 2-D joint would lead to un-conservative design and undesirable failure mechanism in the column.

9.4 VALIDATION OF THE DESIGN PROCEDURE

An analytical design procedure was derived and proposed as an effective method to predicting the effects of the haunch solution in protecting the beam-column joint. Simplified charts and formula were provided to evaluate and control the flow of internal forces in the beam-column joint. A simple visualization of the hierarchy strength and sequence of event could be obtained through M-N performance domains.

9.5 RECOMMENDATIONS FOR FUTURE WORK

Further validation of the efficiency of the proposed retrofit solution might require the investigation of practicality when dealing with the presence of floor systems and infills. Similarly special configuration of joint systems (i.e. wide-eccentric-beam combined with deep beam), typical of actual existing building architecture configuration, are worth of attention

and investigation. Simpler and less invasive connections of the haunch device to the existing structure, by using fastener techniques needs to be investigated.

Experimental tests on scaled 2-D or 3-D frame buildings including un-reinforced masonry infills as well as alternative floor configuration could be suggested as ultimate lab validation. Further dynamic tests of as-built and retrofitted frames on shake table could provide insights of the dynamic effects on the whole system

More importantly, while special focus has been herein given on the design methodology and experimental tests on subassemblies, extensive numerical analysis on plane or three-dimensional R.C. concrete buildings representing pre-1970s construction could be carried out as support to design methodology.

At final step within a seismic risk mitigation process for seismic-prone countries, the efficiency of the proposed retrofit solution at a territorial scale (either cities or regions) could be evaluated by means of damage scenario analyses, to define the actual impact assessment of alternative retrofit solution and properly supporting decision makers.

REFERENCES

Aycardi, L. E., Mander, J. B., Reinhom, A. M., 1994 “Seismic Resistance of Reinforced Concrete Frame Structures Designed Only for Gravity Loads: Experimental Performance of Subassemblages”, ACI Structural Journal, Vol. 91, No. 5, pp.552-563

Bolong, Z., Yuzhou, C., 1991 “Behaviour of Exterior Reinforced Concrete Beam-Column Joints Subjected to Bi-Directional Cyclic Loading”, Design of Beam-Column Joints for Seismic Resistance, Special Publication, SP-123-3, 69-96

Bracci, J. M., Reinhorn, A. M., Mander, J. B., 1995 “Seismic Resistance of Reinforced Concrete Frame Structures Designed for Gravity Loads: Performance of Structural System”, ACI Structural Journal, Vol. 92, No. 5, pp. 597-609

Calvi, G. M., 1999 “A Displacement-Based Approach for Vulnerability Evaluation of Classes of Buildings”, Journal of Earthquake Engineering, Vol. 3 No. 3

Carr, A.J., 2003, “Ruaumoko Program for Inelastic Dynamic Analysis-Users Manual”, Department of Civil Engineering, University of Canterbury, Christchurch, Newzealand

Christopoulos, C. and Filiatrault, A., 2000, “Non-invasive Passive Energy Dissipating Devices for the Retrofit of Steel Structures”, Proceedings of the International Conference on the behaviour of steel structures in seismic areas-STESSA 2000, Montreal, Canada, pp.387-394

Elmorsi, M., Kianoush, M. R. and Tso, W. K., 2000, “Modelling bond-slip deformations in reinforced concrete beam-column joints”, Canadian Journal of Civil Engineering, Vol. 27, 490-505

Fib 2006, “Retrofitting of Concrete Structures by Externally Bonded FRPS, with Emphasis on Seismic Application”, fib Bulletin n.35, Lausanne

Furlong, R., 1961, “Ultimate Strength of Square Columns Under Biaxially Eccentric Loads”, Journal of the American Concrete Institute, March

Gentry, T.R., Wight, J.K., 1994 “Wide Beam-Column Connections under Earthquake-Type Loading”, Earthquake Spectra, Vol.10, No.4, 675-703

Gross, J.L., Engelhardt, M.D., Uang, C.-M., Kasai K. & Iwankiw, N.R., 1999 “Modification of Existing Welded Steel Moment Frame Connections of Seismic Resistance”, American Institute of Steel Construction

Hakuto, S., 1995, “Retrofitting of Reinforced Concrete Moment Resisting Frames”, PhD Thesis, Department of Civil Engineering, University of Canterbury, New Zealand

Hakuto, S., Park, R. and Tanaka, H., 2000, “Seismic Load Tests on Interior and Exterior Beam-column Joints with Substandard Reinforcing Details” ACI Structural Journal, V. 97, N.1, pp.11-25

Kwak, H. G., Filippou, F. C., 1990 “Finite Element Analysis of Reinforced Concrete Structures under Monotonic Loading”, Report No. UCB/SEMM-90/14, Structural Engineering, Mechanics and Materials, Department of Civil Engineering, University of California, Berkeley

Leon, R., Jirsa, O., 1986, “Bi-directional Loading of R.C Beam-column Joints”, Earthquake Spectra, Vol. 2, No. 3, 537-564

Liu, A., 2001, “Seismic Assessment and Retrofit of Pre-1970’s Reinforced Concrete Frame Structures”, PhD Thesis, Department of Civil Engineering, University of Canterbury, New Zealand

Magenes, G., Pampanin S., 2004, “Seismic Response of Gravity-load Design Frames with Masonry Infills”, 13th World Conference on Earthquake Engineering, Vancouver, B.C., Canada, No. 4004, August 1-6, 2004

Martinez R., J.E., 1998 “Non-invasive Redesign Technique for RC Framed Buildings Using Energy Dissipation Devices”, Proceedings of the 11th European conference on Earthquake Engineering

Nassi, R., 2002, “Seismic Retrofit Strategy for Under-Designed Beam-Column Subassemblies Using FRP”, Laurea Thesis, Dept. of Structural Mechanics, University of Pavia, Italy.

NZS3101:1995, “The Design of Concrete Structures, NZS3101:1995”, Standards New Zealand, Wellington

N.Z Institution of Engineers, 1953, “Commentary on New Zealand Standard Building Code”, Technical Publications LTD, Wellington

Okada, T., 1997 “Needs to Evaluate Real Seismic Performance of Buildings-Lessons from the 1995 Hyogoken-nambu Earthquake”, INCEDE Report No.15, December 1999, pp.225-231

Owada, Y., 2000 “Three-dimensional Behaviour of Reinforced Concrete Beam-Column Joint Under Seismic Load”, 12th World Conference of Earthquake Engineering, New Zealand

Pampanin, S., Calvi, G.M. & Moratti, M., 2002 “Seismic Behaviour of R.C. Beam-Column Joints Designed for Gravity Loads”, 12th ECEE, Londan, paper n. 726

Pampanin, S., Christopoulos, C., 2003 “Non-invasive Retrofit of Existing RC Frames Designed for Gravity Loads Only”, fib2003 Symp. Concrete Struct. In Seismic Region, Athens

Pampanin, S., Magenes, G., Carr, A., 2003b “Modelling of Shear Hinge Mechanism in Poorly Detailed RC Beam-column Joints” Proceedings of the fib Symposium Concrete Structures in Seismic Regions, Athens, paper n. 171

Pampanin, S., Calvi, G.M., Moratti, M., 2003c “Seismic Response of Reinforced Concrete Buildings Designed for Gravity Loads. Part 1: Experimental Test on Beam-Column Subassemblies”, ASCE Journal of Structural Engineering

Pampanin, S., Magenes G., Calvi, G.M, 2003d "Seismic Response of Reinforced Concrete Buildings Designed for Gravity Loads. Part 2: Experimental Test on a Three Storey Frame", ASCE Journal of Structural Engineering

Pampanin, S., Bolognini, D., Pacese, A., Magenes G., Calvi, G.M, 2004, "Multi-level Seismic Rehabilitation of Existing Frame Systems and Subassemblies Using FRP Composites", Proceedings of the 2nd International Conference on FRP composites in Civil Engineering, CICE, Adelaide Dec 2004

Park, R., 1997, "A Static Force-Based Procedure for the Seismic Assessment of Existing reinforced Concrete Moment Resisting Frames", Bulletin of the New Zealand National society for Earthquake engineering, Vol.30, pp.213-226

Park, R., Paulay, T., 1975 "Reinforced Concrete Structures", Wiley, New York

Priestley, M.J.N., 1997 "Displacement-based seismic assessment of reinforced concrete buildings" Journal of Earthquake Engineering, Vol. 1, No. 1, pp.157-192

Paulay, T., Priestley, M.N.J., 1992, "Seismic Design of Reinforced Concrete and Masonry Buildings", Wiley, New York

Trowland, M., 2004, "Modelling the Shear Hinge in Beam-Column Joints", Report, University of Canterbury, New Zealand

Uang, C.-M., Lee, C.-H., 1997 "Analytical Modelling of Dual Panel Zone in Haunch Repaired Steel MRFs", Journal of Structural Engineering, ASCE, 123(1), pp.20-29

Uang, C.-M., Bondad, D., and Lee, C.-H., 1998 "Cyclic Performance of Haunch Repaired Steel Moment Connections: Experimental Testing and Analytical Modelling", Engineering Structures, 20(4-6), pp.552-561

Uang, C.-M., Yu, Q.-S., Noel, S., and Gross, J., 2000 "Cyclic Testing of Steel Moment Connections Rehabilitated with RBS or Welded Haunch", Journal of Structural Engineering, ASCE, 126(1), pp.57-68

Wilby, C.B., 1991 “Concrete Materials and Structures”, Cambridge University Press

Youssef, M., Ghobarah, A., 2001 “Modelling of RC Beam-Column Joints and Structural Walls”, Journal of Earthquake Engineering, Vol. 5, No. 1

Yu, Q.-S., Uang, C.-M., and Gross, J., 2000 “Seismic Rehabilitation Design of Steel Moment Connection with Welded Haunch”, Journal of Structural Engineering, ASCE, 126(1), pp.69-78

APPENDIX A: CALCULATION PROCEDURE

A1 Theoretical Stiffness of The Joint, K_j

To derive the joint stiffness K_j, the shear strain of the joint is assumed to be equal to the moment-caused rotation. As illustrated in Fig. A.1, Mj is the joint moment caused by the column shear force V_c to the joint core and V_{jh} is the induced joint shear force. Therefore, the equation can be obtained as follow:

$$\frac{M_j}{K_j} = \frac{V_{jh}}{G_c A_e}$$

where G_c is the concrete shear modulus and A_e is the effective area of the joint. Because there are relationships established as bellow:

$$M_j = V_c H_c$$
$$V_{jh} = \frac{M_{bc}}{jd_b} = \frac{V_c(H_c - jd_b)}{jd_b}$$

By substituting M_j and V_{jh} with the above relationships, the first equation can be rearranged to derive K_j as given:

$$K_j = G_c \left(\frac{jd_b H_c}{H_c - jd_b} \right) A_e$$

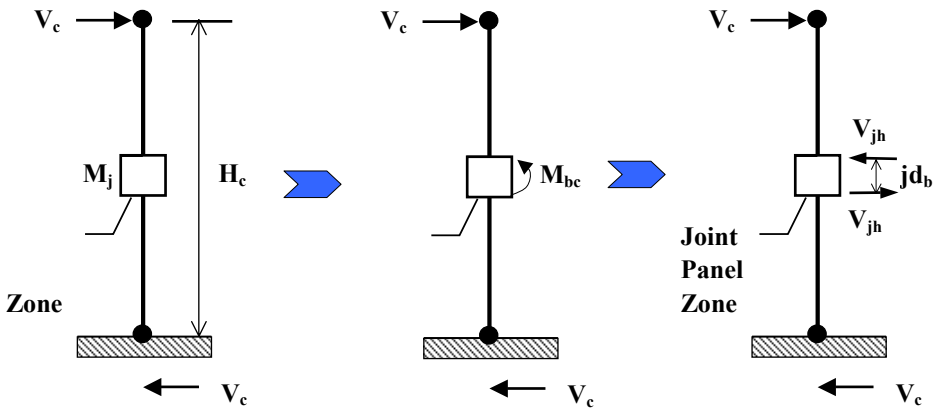

Fig. A.1 The equivalent force in the joint panel zone

A2 Seismic Assessment Example of TDP2

To do the seismic assessment of the subassembly, the basic information is necessary and given as below:

Table A.1 Required information for seismic assessment of TDP2

Concrete shear modulus G	1.37E7 kPa
Simplified lever arm between centres of compression and tension in the beam jd_b	0.28m
Column height H_c	2.0m
Effective joint area A_e	0.0529m^2
Gross joint area A_g	0.0529m^2
Half of beam span length L_b/2	1.525m
Half of clear beam span length L_n/2	1.41m
Compressive column axial load N	75kN
Diameter of longitudinal bar D_b	10mm
Effective depth d	305mm for beam and 205mm for column
Total leg area of transverse reinforcement A_v	56mm^2
Limit state of principal tensile stress p_t=0.2$\sqrt{f_c'}$	1.0MPa
Spacing of transverse reinforcement S	133mm for the beam and 100mm for the column
Yielding strength of longitudinal bar f_y	333MPa
Yielding strength of transverse reinforcement f_{yt}	408MPa
Sum of longitudinal bars reliant on the tie ΣA_b	157mm^2 for the beam and 117.8mm^2 for the column

By giving the section dimension and material properties to the computer program, the flexural strengths of the beam and column are read as 30.1kNm and 22.1kNm respectively and the moment-curvature diagrams are plotted as Fig. A.2. The flexural stiffness can be obtained by estimating the secant slope in the moment-curvature diagram.

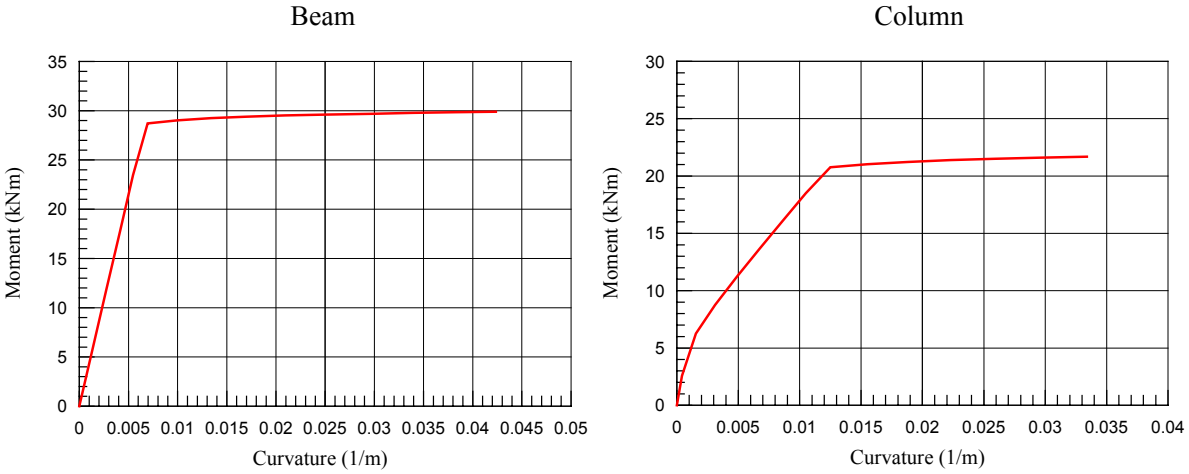

Fig. A.2 Moment-curvature relationship of the beam and column of TDP2

Because the top column and bottom column have the same flexural strength, the capacity ratio is:

$$\frac{\sum M_{column}}{\sum M_{beam}} = \frac{2(22.1)}{30.1} = 1.47$$

From the given formula and information above, the joint stiffness is also estimated as:

$$K_j = 1.37*10^7 \left(\frac{0.28*2}{(2-0.28)} \right) * 0.0529 = 236000 kNm$$

While the flexural hinge occurring in the beam close to the column face, the maximum imposed shear in the beam and column can be estimated by:

$$V_{imposed-beam} = \frac{M_{beam}}{(L_n/2)} = \frac{30.1}{1.41} = 21.3kN$$
$$V_{imposed-column} = \frac{(L_b/2)V_{imposed-beam}}{H_c} = \frac{1.525*21.3}{2} = 16.0kN$$

And the shear capacities of the beam and column are estimated by the code NZS3101:1995 while the joint shear capacity is estimated by Eq. 3.3 (compressive column axial load being in negative sign) as below:

$$V_{capacity-beam} = \frac{A_v f_{yt} d}{S} = \frac{56*408*305}{133} = 52.0kN$$
$$V_{capacity-column} = \frac{A_v f_{yt} d}{S} = \frac{56*408*205}{100} = 46.1kN$$
$$V_{capacity-joint} = A_e \sqrt{p_t^2 - \frac{p_t N}{A_g}} = 0.0529 \sqrt{1.0^2 - \frac{1.0(-0.075)}{0.0529}} = 0.0822MN = 82.2kN$$

The required amount and spacing of the transverse reinforcement can be determined by NZS3101:1995. The estimated value is given for the beam and column as below:

Beam:

$$A_{te} = \frac{\sum A_b f_y}{96 f_{yt}} \frac{S}{D_b} = \frac{157*333*133}{96*408*10} = 17.8mm^2$$

$$S_{\max} = \min(\frac{d}{4}, 6D_b) = \min(\frac{305}{4}, 6*10) = 60mm$$

Column:

$$A_{te} = \frac{\sum A_b f_y}{96 f_{yt}} \frac{S}{D_b} = \frac{117.8*333*100}{96*408*10} = 10mm^2$$

$$S_{\max} = \min(\frac{d}{4}, 6D_b) = \min(\frac{205}{4}, 6*10) = 51mm$$

A3 Procedure of Plotting Hierarchy Strength Diagram

To plot hierarchy diagram, the column interaction diagram will be used. After determining the column interaction curve, the flexural strength of the beam which has the constant value independent from the column axial load can be plotted on the diagram. By giving any inter-storey shear force V_c in the column, the corresponding column axial load N can be determined by Eq. 4.3 (or Eq. 4.4) and the loading demands can be also plotted. With the estimated N, the horizontal joint shear strength V_{jh}^* within a critical value of principal tensile strength can be derived by Eq. 3.3. Because the joint shear strength can be also expressed by Eq. 3.1 as below:

$$V_{jh}^* = \frac{M_{bc}^*}{jd_b} + \overline{V}_{c,joint}$$

where $\overline{V}_{c,joint}$ is the inter-storey shear force to cause the joint shear failure and M_{bc}^* is the equivalent joint moment capacity at this stage. By substituting the critical shear force $\overline{V}_{c,joint}$ in the above equation with the rearranged expression of M_{bc}^* in Eq. 3.4 as given below:

$$\overline{V}_{c,joint} = M_{bc}^* \frac{(1 + d_c / L_n)}{H_c}$$

where $L_n = L_b - d_c$

the equivalent joint moment capacity M_{bc}^* can be derived by rearranged expression as given below:

$$M_{bc}^{*} = \frac{V_{jh}^{*} H_c jd_b}{H_c + jd_b(1 + d_c / L_n)}$$

Therefore, the joint strength curve of equivalent moment capacity corresponding to a given column axial load can be plotted in the diagram by connecting all estimated points. By following the loading demand curve from zero point of the moment to increased value, the first meeting capacity curve can be observed by comparing the sequence of events and it presents the designed failure mechanism of the subassembly. All hierarchy strength diagrams of the testing subassemblies are given in the following figure.

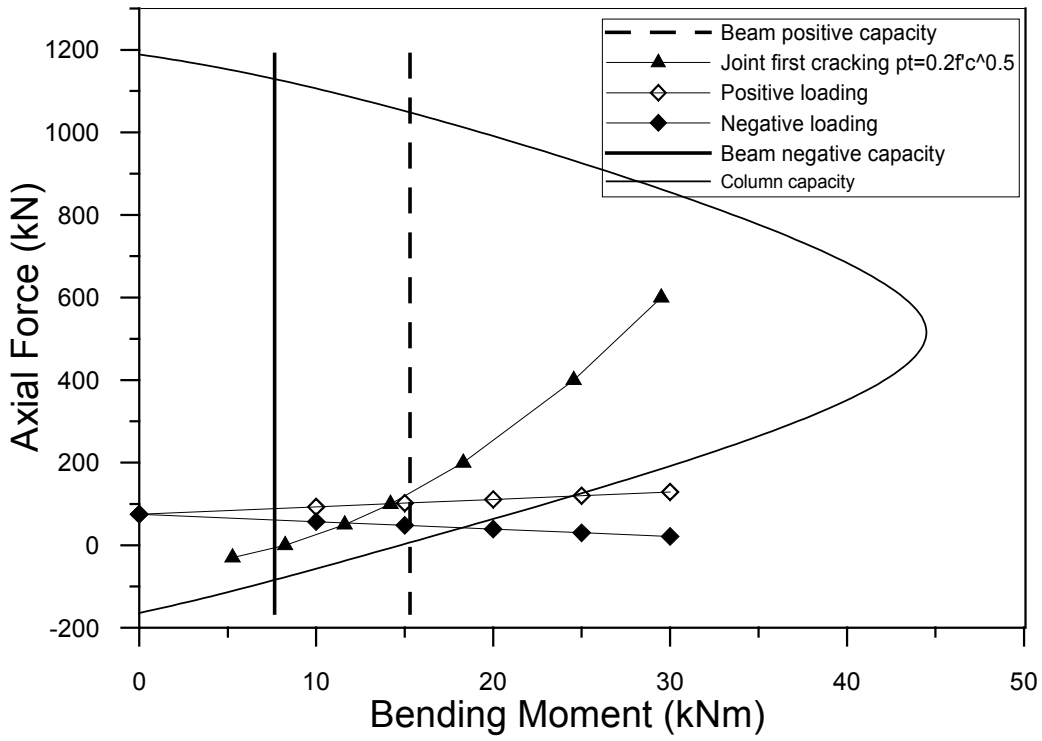

Fig. A.3 Hierarchy strength diagram of TDP1

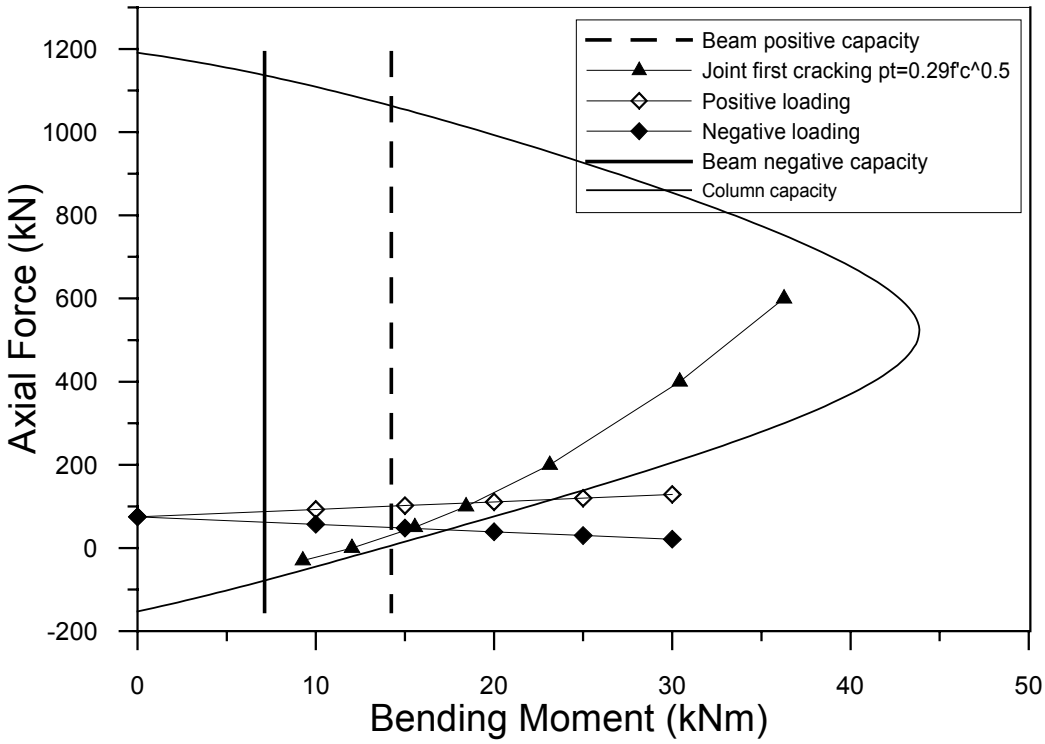

Fig. A.4 Hierarchy strength diagram of TDD1

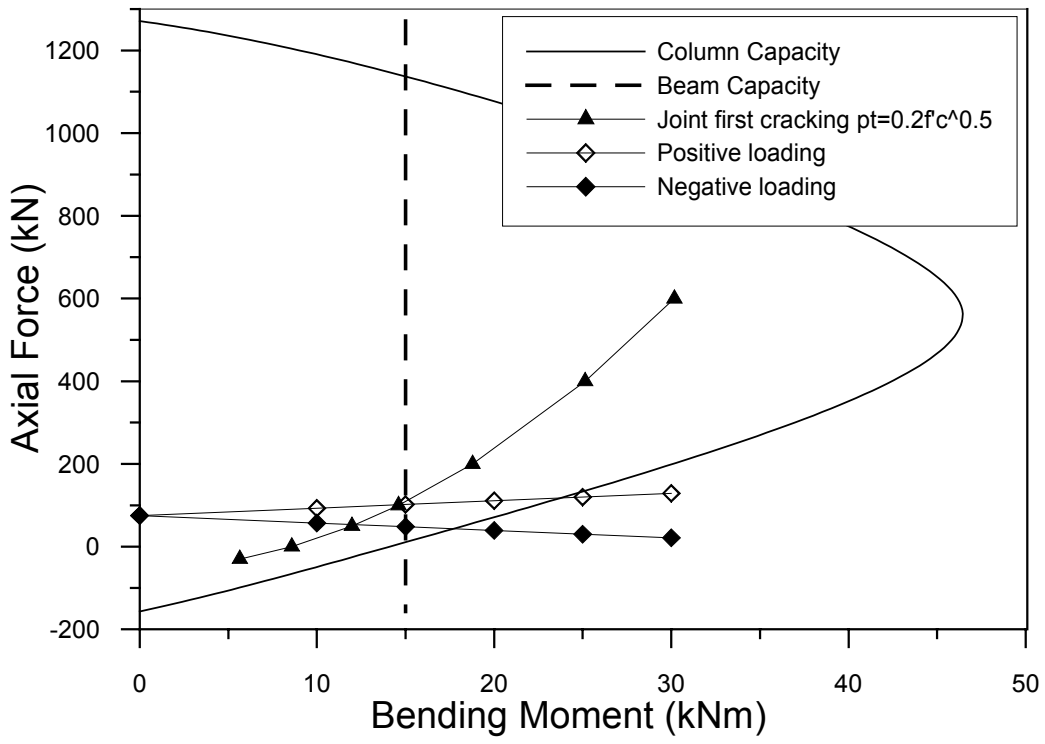

Fig A.5 Hierarchy strength diagram of TDP2

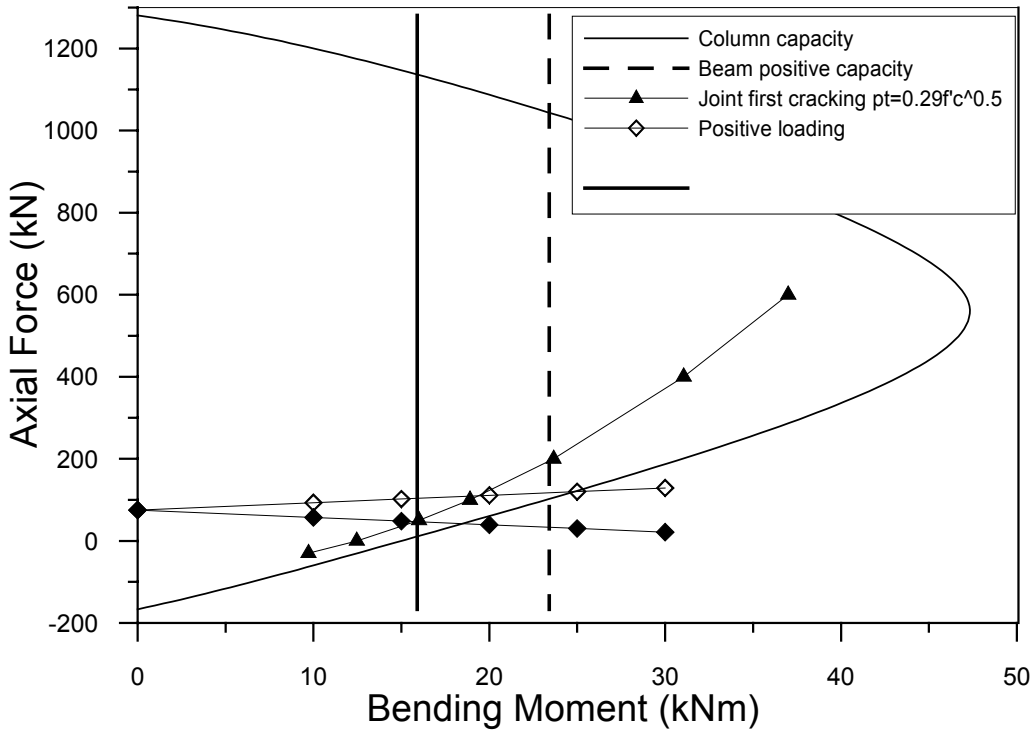

Fig. A.6 Hierarchy strength diagram of TDD2

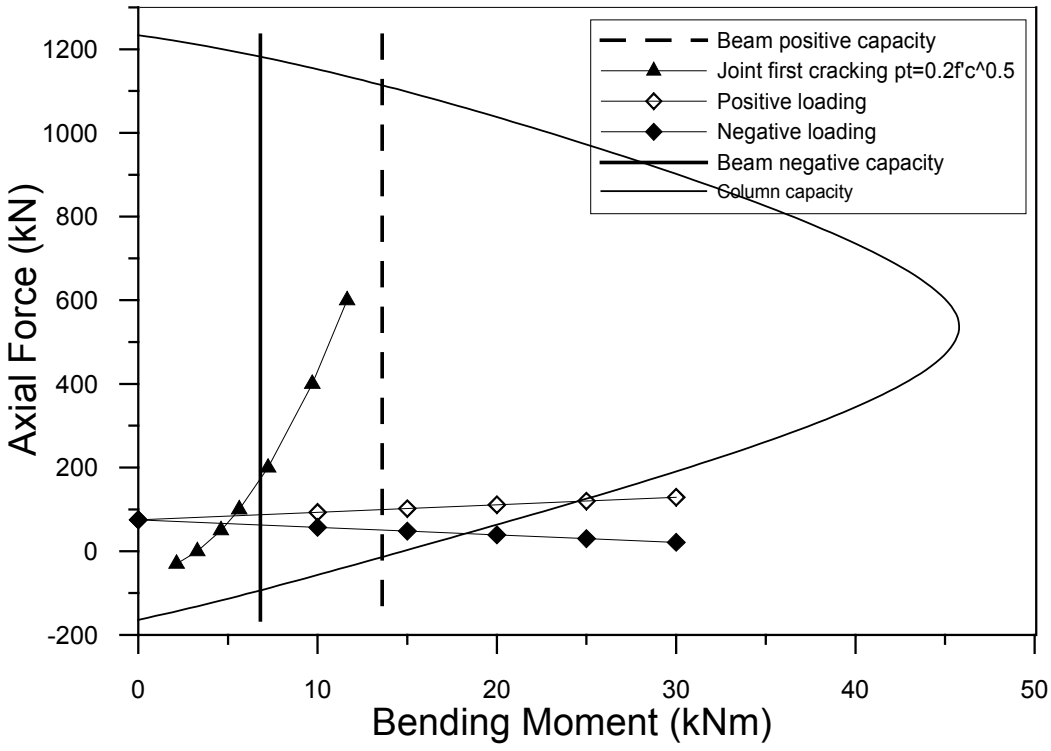

Fig. A.7 Hierarchy strength diagram of TSP1

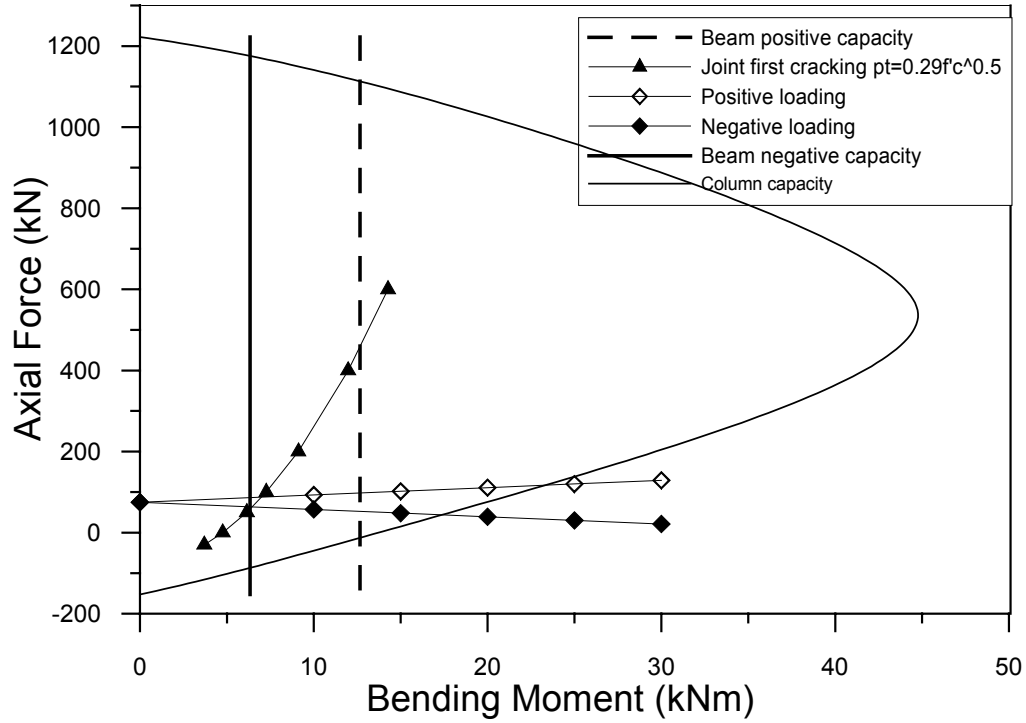

Fig. A.8 Hierarchy strength diagram of TSD1

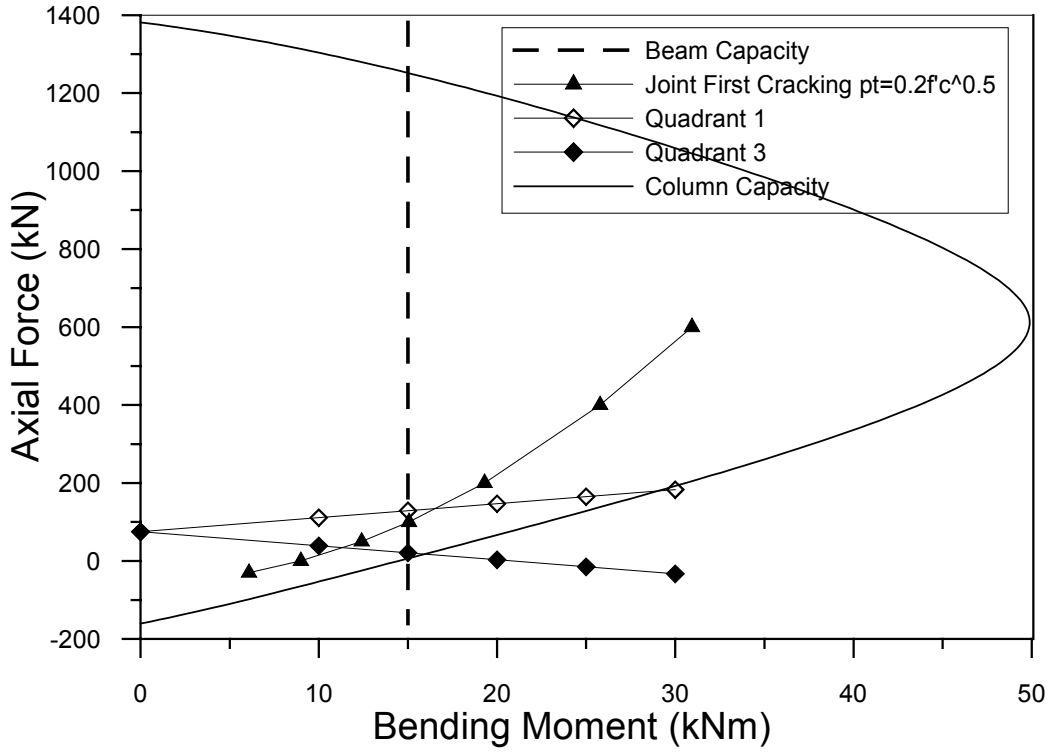

Fig. A.9 Hierarchy strength diagram of DD2

APPENDIX B: RUAUMOKO CODE

TDP1 As-built Deep Beam-column Joint of Unbalanced Reinforcement-Plain Bars:

```
Exterior specimen TDP1  Takeda-joint
8 0 1 0 0 2 0 0 0                                   ! Control Parameters
17 18 9 3 1 3 9.81 5.0 5.0 0.0005 360.0 1.0         ! Frame and Time-history
100 100 100 1 3 10 0.7 0.1                          ! Output and Plotting Options
10 0 0.5                                            ! Iteration Control

NODES
1   0.0    0.0      1 1 0   0 0 0  0
2   0.0    0.835    0 0 0   0 0 0  0
3   0.0    1.0      0 0 0   0 0 0  0
4   0.115  1.0      0 0 0   0 0 0  0
5   1.5    1.0      0 1 0   0 0 0  0
6   0.0    1.001    0 0 0   0 0 0  0
7   0.0    1.165    0 0 0   0 0 0  0
8   0.0    2.0      0 0 0   -1 0 0  0
9   0.0    2.001      1 0 0   0 -2 0  0
10  0.515  1.0      0 0 0   0 0 0  0
11  0.0    1.565    0 0 0   0 0 0  0
12  0.0    0.435    0 0 0   0 0 0  0
13  0.115  1.565    0 0 0   0 0 0  0
14  0.515  1.165    0 0 0   0 0 0  0
15  0.515  0.835    0 0 0   0 0 0  0
16  0.115  0.435    0 0 0   0 0 0  0
17  0.0    0.999    0 0 0   0 0 6  0

ELEMENTS
1  1 1 12
2  1 12 2
3  2 2 17
4  2 6 7
5  1 7 11
6  1 11 8
7  9 3 6
8  3 3 4
9  4 4 10
10 4 10 5
11 6 8 9
12 7 13 14
13 7 15 16
14 8 11 13
15 8 10 14
16 8 10 15
17 8 12 16
18 5 17 3

PROPS
1 FRAME                                             ! column
 2 0 0 4 0 0 0                                      ! Parameters
 3E7 1.37E7 0.0529 0.0529 6.47E-5 1.245             ! Elastic properties
 0.0 0.0026 0.127 0.127                             ! Bi-linear and Hinges
 -1178 -976 19.78 39.2 35.7 12.55 153.1 0           ! Yield Beam Column surface End 2  has the same characteristics
 0.5 0.0 1 2                                        ! Takeda parameters

2 FRAME                                             ! Link joint-column
 1 0 0 0 0 0                                        ! Elastic elements
 3E7 1.37E7 0.0529 0.0529 0.00133 0                 ! Elastic Parameters

3 FRAME                                             ! Link joint-beam
 1 0 0 0 0 0                                        ! Elastic elements
 3E7 1.37E7 0.066 0.066 0.0041 0                    ! Elastic Parameters

4 FRAME                                             ! beam
 1 0 0 4 0 0 0                                      ! Parameters
 3E7 1.37E7 0.066 0.066 1.04E-4 1.553               ! Elastic properties
 0.0 0.005 0.137 0.137                              ! Bi-linear and Hinges
 0.0 0.0 15.4 -31.2 10000 -10000                    ! Yielding properties
 0.4 0.05 1 2                                       ! TAKEDA parameters
```

```
5 SPRING                                                    ! Joint rotational spring
 4 4 3 0 1E12 1E12 236000 0 0 0.0005 0 0 0 0                ! Parameters
 52.9 -452.9 100000000 -100000000 -300 14.6 18.78 14.6 8.59 ! Failure surface
 80 607 0.5 2500
 0.4 0.0 1 2                                                !TAKEDA parameters

6 SPRING                                                    !Vertical spring
 1 0 0 0 75000 0 1E12 0 0 0 0 0 0 0

7 SPRING                                                    !Haunch
 1 1 0 0 0 0 0 0 0 0 0 0 0 0
 1e9 1e9 1e9 1e9 1e9 1e9 1e9

8 FRAME
 1 0 0 0 0 0                                                !Rigid depth spring
 3E7 1.37E7 0.3 0.3 1e9 0

9 SPRING                                                    ! Joint rotational spring
 4 4 3 0 1E12 1E12 236000 0 0 0.0005 0 0 0 0                ! Parameters
 80 -452.9 100000000 -100000000 -300 14.6 18.78 14.6 8.59   ! Failure surface
 169 607 0.5 2500
 0.4 0.0 1 2                                                !TAKEDA parameters

SHAPE
9 1 1 1
8 1 1 1
0 1 1 1

WEIGHTS
1   0.0 0.0 0.0
2   0.0 0.0 0.0
3   0.0 0.0 0.0
4   0.0 0.0 0.0
5   0.0 0.0 0.0
6   0.0 0.0 0.0
7   0.0 0.0 0.0
8   0.0 0.0 0.0
9   0.0 0.0 0.0
10  0.0 0.0 0.0
11  0.0 0.0 0.0
12  0.0 0.0 0.0
13  0.0 0.0 0.0
14  0.0 0.0 0.0
15  0.0 0.0 0.0
16  0.0 0.0 0.0
17  0.0 0.0 0.0

LOADS
1   0.0 0.0 0.0
2   0.0 0.0 0.0
3   0.0 0.0 0.0
4   0.0 0.0 0.0
5   0.0 0.0 0.0
6   0.0 0.0 0.0
7   0.0 0.0 0.0
8   0.0 -75 0.0
9   0.0 0.0 0.0
10  0.0 0.0 0.0
11  0.0 0.0 0.0
12  0.0 0.0 0.0
13  0.0 0.0 0.0
14  0.0 0.0 0.0
15  0.0 0.0 0.0
16  0.0 0.0 0.0
17  0.0 0.0 0.0

EQUAKE c:\temp\c\testh.txt
3  1  0.002  1  -1  0  0  1

EQUAKE c:\temp\c\test1vab.txt
3  1  0.002  1  -1  0  0  1
```

TDD1 As-built Deep Beam-column Joint of Unbalanced Reinforcement-Deformed Bars:

```
Exterior specimen TDD1  Pampanin-joint
8 0 1 0 0 2 0 0 0                                   ! Control Parameters
17 18 9 3 1 3 9.81 5.0 5.0 0.0005 320.0 1.0         ! Frame and Time-history
100 100 100 1 3 10 0.7 0.1                          ! Output and Plotting Options
10 0 0.5                                            ! Iteration Control

NODES
1   0.0    0.0      1 1 0   0 0 0  0
2   0.0    0.835    0 0 0   0 0 0  0
3   0.0    1.0      0 0 0   0 0 0  0
4   0.115  1.0      0 0 0   0 0 0  0
5   1.5    1.0      0 1 0   0 0 0  0
6   0.0   1.001     0 0 0   0 0 0  0
7   0.0    1.165    0 0 0   0 0 0  0
8   0.0    2.0      0 0 0   -1 0 0  0
9   0.0    2.001      1 0 0   0 -2 0  0
10  0.515  1.0      0 0 0   0 0 0  0
11  0.0    1.565    0 0 0   0 0 0  0
12  0.0    0.435    0 0 0   0 0 0  0
13  0.115  1.565      0 0 0   0 0 0  0
14  0.515  1.165      0 0 0   0 0 0  0
15  0.515  0.835      0 0 0   0 0 0  0
16  0.115  0.435      0 0 0   0 0 0  0
17  0.0    0.999      0 0 0   0 0 6  0

ELEMENTS
1  1 1 12
2  1 12 2
3  2 2 17
4  2 6 7
5  1 7 11
6  1 11 8
7  9 3 6
8  3 3 4
9  4 4 10
10 4 10 5
11 6 8 9
12 7 13 14
13 7 15 16
14 8 11 13
15 8 10 14
16 8 10 15
17 8 12 16
18 5 17 3

PROPS
1 FRAME                                             ! column
 2 0 0 4 0 0 0                                      ! Parameters
 3E7 1.37E7 0.0529 0.0529 6.47E-5 1.245             ! Elastic properties
 0.0 0.0026 0.127 0.127                             ! Bi-linear and Hinges
 -1178 -976 19.78 39.2 35.7 12.55 153.1 0           ! Yield Beam Column surface End 2  has the same characteristics
 0.5 0.0 1 2                                        ! Takeda parameters

2 FRAME                                             ! Link joint-column
 1 0 0 0 0 0                                        ! Elastic elements
 3E7 1.37E7 0.0529 0.0529 0.00133 0                 ! Elastic Parameters

3 FRAME                                             ! Link joint-beam
 1 0 0 0 0 0                                        ! Elastic elements
 3E7 1.37E7 0.066 0.066 0.0041 0                    ! Elastic Parameters

4 FRAME                                             ! beam
 1 0 0 4 0 0 0                                      ! Parameters
 3E7 1.37E7 0.066 0.066 1.04E-4 1.553               ! Elastic properties
 0.0 0.005 0.137 0.137                              ! Bi-linear and Hinges
 0.0 0.0 14.8 -30 10000 -10000                      ! Yielding properties
 0.2 0.05 1 2                                       ! TAKEDA parameters
```

```
5 SPRING                                                    ! Joint rotational spring
 4 44 1 0 1E12 1E12 236000 0 0 0.0005 0 0 0 0               ! Parameters
 18.7 -298.7 100000000 -100000000 -210 16.8 22.5 16.8 10.3  ! Failure surface
 60 607 0.5 2500
 1 1.25 0.9 -1.0 0.8 30 -0.05                               !Pampanin
 1 1.25 0.9 -1.0 0.8 30 -0.05
 1 1.25 0.9 -1.0 0.8 30 -0.05

6 SPRING                                                    !Vertical spring
 1 0 0 0 79000 0 1E12 0 0 0 0 0 0 0

7 SPRING                                                    !Haunch
 1 1 0 0 0 0 0 0 0 0 0 0 0 0
 1e9 1e9 1e9 1e9 1e9 1e9

8 FRAME
 1 0 0 0 0 0                                                !Rigid depth spring
 3E7 1.37E7 0.3 0.3 1e9 0

9 SPRING                                                    ! Joint rotational spring
 4 44 1 0 1E12 1E12 236000 0 0 0.0005 0 0 0 0               ! Parameters
 18.7 -298.7 100000000 -100000000 -210 16.8 22.5 16.8 10.3  ! Failure surface
 60 607 0.5 2500
 1 1.25 0.9 -1.0 0.8 30 -0.05                               !Pampanin parameters
 1 1.25 0.9 -1.0 0.8 30 -0.05
 1 1.25 0.9 -1.0 0.8 30 -0.05

SHAPE
9 1 1 1
8 1 1 1
0 1 1 1

WEIGHTS
1   0.0 0.0 0.0
2   0.0 0.0 0.0
3   0.0 0.0 0.0
4   0.0 0.0 0.0
5   0.0 0.0 0.0
6   0.0 0.0 0.0
7   0.0 0.0 0.0
8   0.0 0.0 0.0
9   0.0 0.0 0.0
10  0.0 0.0 0.0
11  0.0 0.0 0.0
12  0.0 0.0 0.0
13  0.0 0.0 0.0
14  0.0 0.0 0.0
15  0.0 0.0 0.0
16  0.0 0.0 0.0
17  0.0 0.0 0.0

LOADS
1   0.0 0.0 0.0
2   0.0 0.0 0.0
3   0.0 0.0 0.0
4   0.0 0.0 0.0
5   0.0 0.0 0.0
6   0.0 0.0 0.0
7   0.0 0.0 0.0
8   0.0 -75 0.0
9   0.0 0.0 0.0
10  0.0 0.0 0.0
11  0.0 0.0 0.0
12  0.0 0.0 0.0
13  0.0 0.0 0.0
14  0.0 0.0 0.0
15  0.0 0.0 0.0
16  0.0 0.0 0.0
17  0.0 0.0 0.0

EQUAKE c:\temp\c\testh.txt
3  1  0.002  1  -1  0  0  1

EQUAKE c:\temp\c\test2vab.txt
3  1  0.002  1  -1  0  0  1
```

TDP2 As-built Deep Beam-column Joint of Balanced Reinforcement-Plain Bars

```
Exterior specimen TDP2  Pampanin-joint
8 0 1 0 0 2 0 0 0                                   ! Control Parameters
17 18 9 3 1 3 9.81 5.0 5.0 0.0005 360.0 1.0         ! Frame and Time-history
100 100 100 1 3 10 0.7 0.1                          ! Output and Plotting Options
10 0 0.5                                            ! Iteration Control

NODES
1   0.0    0.0      1 1 0   0 0 0  0
2   0.0    0.835    0 0 0   0 0 0  0
3   0.0    1.0      0 0 0   0 0 0  0
4   0.115  1.0      0 0 0   0 0 0  0
5   1.5    1.0      0 1 0   0 0 0  0
6   0.0    1.001    0 0 0   0 0 0  0
7   0.0    1.165    0 0 0   0 0 0  0
8   0.0    2.0      0 0 0   -1 0 0  0
9   0.0    2.001    1 0 0   0 -2 0  0
10  0.515  1.0      0 0 0   0 0 0  0
11  0.0    1.565    0 0 0   0 0 0  0
12  0.0    0.435    0 0 0   0 0 0  0
13  0.115  1.565    0 0 0   0 0 0  0
14  0.515  1.165    0 0 0   0 0 0  0
15  0.515  0.835    0 0 0   0 0 0  0
16  0.115  0.435    0 0 0   0 0 0  0
17  0.0    0.999    0 0 0   0 0 6  0

ELEMENTS
1  1 1 12
2  1 12 2
3  2 2 17
4  2 6 7
5  1 7 11
6  1 11 8
7  9 3 6
8  3 3 4
9  4 4 10
10 4 10 5
11 6 8 9
12 7 13 14
13 7 15 16
14 8 11 13
15 8 10 14
16 8 10 15
17 8 12 16
18 5 17 3

PROPS
1 FRAME                                             !  column
 2 0 0 4 0 0 0                                      ! Parameters
 3E7 1.37E7 0.0529 0.0529 6.47E-5 1.245             ! Elastic properties
 0.0 0.0026 0.127 0.127                             ! Bi-linear and Hinges
 -1178 -976 19.78 39.2 35.7 12.55 153.1 0           ! Yield Beam Column surface End 2  has the same characteristics
 0.5 0.0 1 2                                        ! Takeda parameters

2 FRAME                                             ! Link joint-column
 1 0 0 0 0 0                                        ! Elastic elements
 3E7 1.37E7 0.0529 0.0529 0.00133 0                 ! Elastic Parameters

3 FRAME                                             ! Link joint-beam
 1 0 0 0 0 0                                        ! Elastic elements
 3E7 1.37E7 0.066 0.066 0.0041 0                    ! Elastic Parameters

4 FRAME                                             ! beam
 1 0 0 4 0 0 0                                      ! Parameters
 3E7 1.37E7 0.066 0.066 1.36E-4 1.553               ! Elastic properties
 0.0 0.000022 0.137 0.137                           ! Bi-linear and Hinges
 0.0 0.0 30.25 -30.25 10000 -10000                  ! Yielding properties
 0.4 0.0 1 2                                        ! TAKEDA parameters
```

```
5 SPRING                                                    ! Joint rotational spring
 4 44 1 0 1E12 1E12 236000 0 0 0.0005 0 0 0 0               ! Parameters
 52.9 -452.9 100000000 -100000000 -300 14.6 18.78 14.6 8.59 ! Failure surface
 169 607 0.5 2500
 1 1.25 0.9 -1.0 0.8 30 -0.05                               !Pampanin parameters
 1 1.25 0.9 -1.0 0.8 30 -0.05
 1 1.25 0.9 -1.0 0.8 30 -0.05

6 SPRING                                                    !vertical spring
 1 0 0 0 75000 0 1E12 0 0 0 0 0 0 0

7 SPRING                                                    !haunch
 1 1 0 0 0 0 0 0 0 0 0 0 0 0
 1e9 1e9 1e9 1e9 1e9 1e9 1e9

8 FRAME
 1 0 0 0 0 0                                                !rigid depth spring
 3E7 1.37E7 0.3 0.3 1e9 0

9 SPRING                                                    ! Joint rotational spring
 4 44 1 0 1E12 1E12 236000 0 0 0.0005 0 0 0 0               ! Parameters
 52.9 -452.9 100000000 -100000000 -300 14.6 18.78 14.6 8.59 ! Failure surface
 169 607 0.5 2500
 1 1.25 0.9 -1.0 0.8 30 -0.05                               !Pampanin parameters
 1 1.25 0.9 -1.0 0.8 30 -0.05
 1 1.25 0.9 -1.0 0.8 30 -0.05

SHAPE
9 1 1 1
8 1 1 1
0 1 1 1

WEIGHTS
1   0.0 0.0 0.0
2   0.0 0.0 0.0
3   0.0 0.0 0.0
4   0.0 0.0 0.0
5   0.0 0.0 0.0
6   0.0 0.0 0.0
7   0.0 0.0 0.0
8   0.0 0.0 0.0
9   0.0 0.0 0.0
10  0.0 0.0 0.0
11  0.0 0.0 0.0
12  0.0 0.0 0.0
13  0.0 0.0 0.0
14  0.0 0.0 0.0
15  0.0 0.0 0.0
16  0.0 0.0 0.0
17  0.0 0.0 0.0

LOADS
1   0.0 0.0 0.0
2   0.0 0.0 0.0
3   0.0 0.0 0.0
4   0.0 0.0 0.0
5   0.0 0.0 0.0
6   0.0 0.0 0.0
7   0.0 0.0 0.0
8   0.0 -75 0.0
9   0.0 0.0 0.0
10  0.0 0.0 0.0
11  0.0 0.0 0.0
12  0.0 0.0 0.0
13  0.0 0.0 0.0
14  0.0 0.0 0.0
15  0.0 0.0 0.0
16  0.0 0.0 0.0
17  0.0 0.0 0.0

EQUAKE c:\temp\c\testh.txt
3  1  0.002  1  -1  0  0  1

EQUAKE c:\temp\c\test5vab.txt
3  1  0.002  1  -1  0  0  1
```

TDD2 As-built Deep Beam-column Joint of Balanced Reinforcement-Deformed Bars

```
Exterior specimen TDD2  Pampanin-joint
8 0 1 0 0 2 0 0 0                                   ! Control Parameters
17 18 9 3 1 3 9.81 5.0 5.0 0.0005 360.0 1.0         ! Frame and Time-history
100 100 100 1 3 10 0.7 0.1                          ! Output and Plotting Options
10 0 0.5                                            ! Iteration Control

NODES
1   0.0    0.0      1 1 0   0 0 0  0
2   0.0    0.835    0 0 0   0 0 0  0
3   0.0    1.0      0 0 0   0 0 0  0
4   0.115  1.0      0 0 0   0 0 0  0
5   1.5    1.0      0 1 0   0 0 0  0
6   0.0    1.001    0 0 0   0 0 0  0
7   0.0    1.165    0 0 0   0 0 0  0
8   0.0    2.0      0 0 0   -1 0 0  0
9   0.0    2.001    1 0 0   0 -2 0  0
10  0.515  1.0      0 0 0   0 0 0  0
11  0.0    1.565    0 0 0   0 0 0  0
12  0.0    0.435    0 0 0   0 0 0  0
13  0.115  1.565    0 0 0   0 0 0  0
14  0.515  1.165    0 0 0   0 0 0  0
15  0.515  0.835    0 0 0   0 0 0  0
16  0.115  0.435    0 0 0   0 0 0  0
17  0.0    0.999    0 0 0   0 0 6  0

ELEMENTS
1  1 1 12
2  1 12 2
3  2 2 17
4  2 6 7
5  1 7 11
6  1 11 8
7  9 3 6
8  3 3 4
9  4 4 10
10 4 10 5
11 6 8 9
12 7 13 14
13 7 15 16
14 8 11 13
15 8 10 14
16 8 10 15
17 8 12 16
18 5 17 3

PROPS
1 FRAME                                             ! column
 2 0 0 4 0 0 0                                      ! Parameters
 3E7 1.37E7 0.0529 0.0529 6.47E-5 1.245             ! Elastic properties
 0.0 0.0026 0.127 0.127                             ! Bi-linear and Hinges
 -1178 -976 19.78 39.2 35.7 12.55 153.1 0           ! Yield Beam Column surface End 2  has the same characteristics
 0.5 0.0 1 2                                        ! Takeda parameters

2 FRAME                                             ! Link joint-column
 1 0 0 0 0 0                                        ! Elastic elements
 3E7 1.37E7 0.0529 0.0529 0.00133 0                 ! Elastic Parameters

3 FRAME                                             ! Link joint-beam
 1 0 0 0 0 0                                        ! Elastic elements
 3E7 1.37E7 0.066 0.066 0.0041 0                    ! Elastic Parameters

4 FRAME                                             ! beam
 1 0 0 4 0 0 0                                      ! Parameters
 3E7 1.37E7 0.066 0.066 1.64E-4 1.553               ! Elastic properties
 0.0 0.000022 0.137 0.137                           ! Bi-linear and Hinges
 0.0 0.0 31.9 -46.8 10000 -10000                    ! Yielding properties
 0.4 0.0 1 2                                        ! TAKEDA parameters
```

```
5 SPRING                                                    ! Joint rotational spring
 4 44 1 0 1E12 1E12 236000 0 0 0.0005 0 0 0 0               ! Parameters
 18.7 -298.7 100000000 -100000000 -210 16.8 22.5 16.8 10.3  ! Failure surface
 60 607 0.5 2500
 1 1.25 0.9 -1.0 0.8 30 -0.05                               !Pampanin parameters
 1 1.25 0.9 -1.0 0.8 30 -0.05
 1 1.25 0.9 -1.0 0.8 30 -0.05

6 SPRING                                                    !vertical spring
 1 0 0 0 79000 0 1E12 0 0 0 0 0 0 0

7 SPRING                                                    !haunch
 1 1 0 0 0 0 0 0 0 0 0 0 0 0
 1e9 1e9 1e9 1e9 1e9 1e9

8 FRAME
 1 0 0 0 0 0          !rigid depth spring
 3E7 1.37E7 0.3 0.3 1e9 0

9 SPRING                                                    ! Joint rotational spring
 4 44 1 0 1E12 1E12 236000 0 0 0.0005 0 0 0 0               ! Parameters
 18.7 -298.7 100000000 -100000000 -210 16.8 22.5 16.8 10.3  ! Failure surface
 60 607 0.5 2500
 1 1.25 0.9 -1.0 0.8 30 -0.05                               !Pampanin parameters
 1 1.25 0.9 -1.0 0.8 30 -0.05
 1 1.25 0.9 -1.0 0.8 30 -0.05

SHAPE
9 1 1 1
8 1 1 1
0 1 1 1

WEIGHTS
1   0.0 0.0 0.0
2   0.0 0.0 0.0
3   0.0 0.0 0.0
4   0.0 0.0 0.0
5   0.0 0.0 0.0
6   0.0 0.0 0.0
7   0.0 0.0 0.0
8   0.0 0.0 0.0
9   0.0 0.0 0.0
10  0.0 0.0 0.0
11  0.0 0.0 0.0
12  0.0 0.0 0.0
13  0.0 0.0 0.0
14  0.0 0.0 0.0
15  0.0 0.0 0.0
16  0.0 0.0 0.0
17  0.0 0.0 0.0

LOADS
1   0.0 0.0 0.0
2   0.0 0.0 0.0
3   0.0 0.0 0.0
4   0.0 0.0 0.0
5   0.0 0.0 0.0
6   0.0 0.0 0.0
7   0.0 0.0 0.0
8   0.0 -75 0.0
9   0.0 0.0 0.0
10  0.0 0.0 0.0
11  0.0 0.0 0.0
12  0.0 0.0 0.0
13  0.0 0.0 0.0
14  0.0 0.0 0.0
15  0.0 0.0 0.0
16  0.0 0.0 0.0
17  0.0 0.0 0.0

EQUAKE c:\temp\c\testh.txt
3  1  0.002  1  -1  0  0  1

EQUAKE c:\temp\c\test6vab.txt
3  1  0.002  1  -1  0  0  1
```

TSP1 As-built Shallow Beam-column Joint of Balanced Reinforcement-Plain Bars

```
Exterior specimen TSP1  Pampanin-joint
8 0 1 0 0 2 0 0 0                                   ! Control Parameters
17 18 9 3 1 3 9.81 5.0 5.0 0.0005 360.0 1.0         ! Frame and Time-history
100 100 100 1 3 10 0.7 0.1                          ! Output and Plotting Options
10 0 0.5                                            ! Iteration Control

NODES
1   0.0    0.0      1 1 0   0 0 0  0
2   0.0    0.835    0 0 0   0 0 0  0
3   0.0    1.0      0 0 0   0 0 0  0
4   0.115  1.0      0 0 0   0 0 0  0
5   1.5    1.0      0 1 0   0 0 0  0
6   0.0    1.001    0 0 0   0 0 0  0
7   0.0    1.165    0 0 0   0 0 0  0
8   0.0    2.0      0 0 0   -1 0 0  0
9   0.0    2.001      1 0 0   0 0 0  0
10  0.515  1.0        0 0 0   0 0 0  0
11  0.0    1.565      0 0 0   0 0 0  0
12  0.0    0.435      0 0 0   0 0 0  0
13  0.115  1.565      0 0 0   0 0 0  0
14  0.515  1.165      0 0 0   0 0 0  0
15  0.515  0.835      0 0 0   0 0 0  0
16  0.115  0.435      0 0 0   0 0 0  0
17  0.0    0.999      0 0 0   0 0 6  0

ELEMENTS
1  1 1 12
2  1 12 2
3  2 2 17
4  2 6 7
5  1 7 11
6  1 11 8
7  9 3 6
8  3 3 4
9  4 4 10
10 4 10 5
11 6 8 9
12 7 13 14
13 7 15 16
14 8 11 13
15 8 10 14
16 8 10 15
17 8 12 16
18 5 17 3

PROPS
1 FRAME                                             ! bottom column
 2 0 0 4 0 0 0                                      ! Parameters
 3E7 1.37E7 0.0529 0.0529 6.47E-5 1.245             ! Elastic properties
 0.0 0.0026 0.127 0.127                             ! Bi-linear and Hinges
 -1178 -976 19.78 39.2 35.7 12.55 153.1 0           ! Yield Beam Column surface End 2  has the same characteristics
 0.5 0.0 1 2                                        ! Takeda parameters

2 FRAME                                             ! Link joint-column
 1 0 0 0 0 0                                        ! Elastic elements
 3E7 1.37E7 0.0529 0.0529 0.00133 0                 ! Elastic Parameters

3 FRAME                                             ! Link joint-beam
 1 0 0 0 0 0                                        ! Elastic elements
 3E7 1.37E7 0.071 0.071 0.0041 0                    ! Elastic Parameters

4 FRAME                                             ! beam
 1 0 0 4 0 0 0                                      ! Parameters
 3E7 1.37E7 0.071 0.071 0.35E-4 1.553               ! Elastic properties
 0.0 0.000022 0.137 0.137                           ! Bi-linear and Hinges
 0.0 0.0 12 -20.3 10000 -10000                      ! Yielding properties
 0.4 0.0 1 2                                        ! TAKEDA
```

```
5 SPRING                                          ! Joint rotational spring
 4 44 1 0 1E12 1E12 103000 0 0 0.0005 0 0 0 0     ! Parameters
 56.1 -894 100000000 -100000000 -630 56.1 67.5 56.1 31   ! Failure surface
 169 607 0.5 2500
 1 1.25 0.9 -1.0 0.8 30 -0.05                     !Pampanin parameters
 1 1.25 0.9 -1.0 0.8 30 -0.05
 1 1.25 0.9 -1.0 0.8 30 -0.05

6 SPRING                                          !vertical spring
 1 0 0 0 75000 0 1E12 0 0 0 0 0 0 0

7 SPRING                                          !haunch
 1 1 0 0 0 0 0 0 0 0 0 0 0 0
 1e9 1e9 1e9 1e9 1e9 1e9

8 FRAME
 1 0 0 0 0 0                                      !rigid depth spring
 3E7 1.37E7 0.3 0.3 1e9 0

9 SPRING                                          ! Joint rotational spring
 4 44 1 0 1E12 1E12 103000 0 0 0.0005 0 0 0 0     ! Parameters
 56.1 -894 100000000 -100000000 -630 56.1 67.5 56.1 31   ! Failure surface
 169 607 0.5 2500
 1 1.25 0.9 -1.0 0.8 30 -0.05                     !Pampanin parameters
 1 1.25 0.9 -1.0 0.8 30 -0.05
 1 1.25 0.9 -1.0 0.8 30 -0.05

SHAPE
9 1 1 1
8 1 1 1
0 1 1 1

WEIGHTS
1   0.0 0.0 0.0
2   0.0 0.0 0.0
3   0.0 0.0 0.0
4   0.0 0.0 0.0
5   0.0 0.0 0.0
6   0.0 0.0 0.0
7   0.0 0.0 0.0
8   0.0 0.0 0.0
9   0.0 0.0 0.0
10  0.0 0.0 0.0
11  0.0 0.0 0.0
12  0.0 0.0 0.0
13  0.0 0.0 0.0
14  0.0 0.0 0.0
15  0.0 0.0 0.0
16  0.0 0.0 0.0
17  0.0 0.0 0.0

LOADS
1   0.0 0.0 0.0
2   0.0 0.0 0.0
3   0.0 0.0 0.0
4   0.0 0.0 0.0
5   0.0 0.0 0.0
6   0.0 0.0 0.0
7   0.0 0.0 0.0
8   0.0 -110 0.0
9   0.0 0.0 0.0
10  0.0 0.0 0.0
11  0.0 0.0 0.0
12  0.0 0.0 0.0
13  0.0 0.0 0.0
14  0.0 0.0 0.0
15  0.0 0.0 0.0
16  0.0 0.0 0.0
17  0.0 0.0 0.0

EQUAKE c:\temp\c\testh.txt
3  1  0.002  1  -1  0  0  1

EQUAKE c:\temp\c\test5vab.txt
3  1  0.002  1  -1  0  0  1
```

TSD1 As-built Shallow Beam-column Joint of Balanced Reinforcement-Deformed Bars

```
Exterior specimen TSD1  Pampanin-joint
8 0 1 0 0 2 0 0 0                                   ! Control Parameters
17 18 9 3 1 3 9.81 5.0 5.0 0.0005 360.0 1.0         ! Frame and Time-history
100 100 100 1 3 10 0.7 0.1                          ! Output and Plotting Options
10 0 0.5                                            ! Iteration Control

NODES
1   0.0    0.0      1 1 0   0 0 0  0
2   0.0    0.835    0 0 0   0 0 0  0
3   0.0    1.0      0 0 0   0 0 0  0
4   0.115  1.0      0 0 0   0 0 0  0
5   1.5    1.0      0 1 0   0 0 0  0
6   0.0    1.001    0 0 0   0 0 0  0
7   0.0    1.165    0 0 0   0 0 0  0
8   0.0    2.0      0 0 0   -1 0 0  0
9   0.0    2.001    1 0 0   0 0 0  0
10  0.515  1.0      0 0 0   0 0 0  0
11  0.0    1.565    0 0 0   0 0 0  0
12  0.0    0.435    0 0 0   0 0 0  0
13  0.115  1.565    0 0 0   0 0 0  0
14  0.515  1.165    0 0 0   0 0 0  0
15  0.515  0.835    0 0 0   0 0 0  0
16  0.115  0.435    0 0 0   0 0 0  0
17  0.0    0.999    0 0 0   0 0 6  0

ELEMENTS
1  1 1 12
2  1 12 2
3  2 2 17
4  2 6 7
5  1 7 11
6  1 11 8
7  9 3 6
8  3 3 4
9  4 4 10
10 4 10 5
11 6 8 9
12 7 13 14
13 7 15 16
14 8 11 13
15 8 10 14
16 8 10 15
17 8 12 16
18 5 17 3

PROPS
1 FRAME                                             !  column
 2 0 0 4 0 0 0                                      ! Parameters
 3E7 1.37E7 0.0529 0.0529 6.47E-5 1.245             ! Elastic properties
 0.0 0.0026 0.127 0.127                             ! Bi-linear and Hinges
 -1178 -976 19.78 39.2 35.7 12.55 153.1 0           ! Yield Beam Column surface End 2  has the same characteristics
 0.5 0.0 1 2                                        ! Takeda parameters

2 FRAME                                             ! Link joint-column
 1 0 0 0 0 0                                        ! Elastic elements
 3E7 1.37E7 0.0529 0.0529 0.00133 0                 ! Elastic Parameters

3 FRAME                                             ! Link joint-beam
 1 0 0 0 0 0                                        ! Elastic elements
 3E7 1.37E7 0.071 0.071 0.0041 0                    ! Elastic Parameters

4 FRAME                                             ! beam
 1 0 0 4 0 0 0                                      ! Parameters TAKEDA
 3E7 1.37E7 0.071 0.071 0.35E-4 1.553               ! Elastic properties
 0.0 0.000022 0.137 0.137                           ! Bi-linear and Hinges
 0.0 0.0 12.9 -23.9 10000 -10000                    ! Yielding properties
 0.4 0.0 1 2                                        ! TAKEDA
```

```
5 SPRING                                          ! Joint rotational spring
 4 44 1 0 1E12 1E12 103000 0 0 0.0005 0 0 0 0     ! Parameters
 56.1 -894 100000000 -100000000 -630 56.1 67.5 56.1 31   !  Failure surface
 169 607 0.5 2500
 1 1.25 0.9 -1.0 0.8 30 -0.05                     !Pampanin parameters
 1 1.25 0.9 -1.0 0.8 30 -0.05
 1 1.25 0.9 -1.0 0.8 30 -0.05

6 SPRING                                          !vertical spring
 1 0 0 0 75000 0 1E12 0 0 0 0 0 0 0

7 SPRING                                          !haunch
 1 1 0 0 0 0 0 0 0 0 0 0 0 0
 1e9 1e9 1e9 1e9 1e9 1e9

8 FRAME
 1 0 0 0 0 0                                      !rigid depth spring
 3E7 1.37E7 0.3 0.3 1e9 0

9 SPRING                                          ! Joint rotational spring
 4 44 1 0 1E12 1E12 103000 0 0 0.0005 0 0 0 0     ! Parameters
 56.1 -894 100000000 -100000000 -630 56.1 67.5 56.1 31   ! Failure surface
 169 607 0.5 2500
 1 1.25 0.9 -1.0 0.8 30 -0.05                     !Pampanin parameters
 1 1.25 0.9 -1.0 0.8 30 -0.05
 1 1.25 0.9 -1.0 0.8 30 -0.05

SHAPE
9 1 1 1
8 1 1 1
0 1 1 1

WEIGHTS
1   0.0 0.0 0.0
2   0.0 0.0 0.0
3   0.0 0.0 0.0
4   0.0 0.0 0.0
5   0.0 0.0 0.0
6   0.0 0.0 0.0
7   0.0 0.0 0.0
8   0.0 0.0 0.0
9   0.0 0.0 0.0
10  0.0 0.0 0.0
11  0.0 0.0 0.0
12  0.0 0.0 0.0
13  0.0 0.0 0.0
14  0.0 0.0 0.0
15  0.0 0.0 0.0
16  0.0 0.0 0.0
17  0.0 0.0 0.0

LOADS
1   0.0 0.0 0.0
2   0.0 0.0 0.0
3   0.0 0.0 0.0
4   0.0 0.0 0.0
5   0.0 0.0 0.0
6   0.0 0.0 0.0
7   0.0 0.0 0.0
8   0.0 -110 0.0
9   0.0 0.0 0.0
10  0.0 0.0 0.0
11  0.0 0.0 0.0
12  0.0 0.0 0.0
13  0.0 0.0 0.0
14  0.0 0.0 0.0
15  0.0 0.0 0.0
16  0.0 0.0 0.0
17  0.0 0.0 0.0

EQUAKE c:\temp\c\testh.txt
3  1  0.002  1  -1  0  0  1

EQUAKE c:\temp\c\test5vab.txt
3  1  0.002  1  -1  0  0  1
```

DD2 As-built 3-D Corner Joint–Plain Bars

```
Exterior 3-D specimen DD2  Pampanin-joint
8 1 0 0 3 0 0 0                                  ! Control Parameters
25 28 10 1 1 3 9.81 5.0 5.0 0.0005 288 1.0       ! Frame and Time-history
100 100 100 3 0.1 0.1 0.1 0                      ! Output and Plotting Options
0.86603 0 0.866025 0.5 1 -0.5                    ! plot axes transformation
10 0 0.5                                         ! Iteration Control

NODES
1       0       0       0       1       1       1       0       1       0       0
2       0       0.835   0       0       0       0       0       0       0       0
3       0       1.0     0       0       0       0       0       0       0       0
4       0.115   1.0     0       0       0       0       0       0       0       0
5       1.5     1.0     0       0       1       0       0       0       0       0
6       0       1.001   0       0       0       0       0       0       0       0
7       0       1.165   0       0       0       0       0       0       0       0
8   0   2.0     0       -1      0       -2      0       0       0       0       0
9   0   2.001   0   1   -3  1   0   0   0   0
10  0.515   1.0   0  0        0       0       0       0       0       0
11  0.0   1.565   0  0        0       0       0       0       0       0
12  0.0   0.435   0  0        0       0       0       0       0       0
13  0.115   1.565   0        0       0       0       0       0       0       0
14  0.515   1.165   0        0       0       0       0       0       0       0
15  0.515   0.835   0        0       0       0       0       0       0       0
16  0.115   0.435   0   0   0   0   0   0   0   0
17  0   0.999   0        2       2       2       2       2       2       25
18  0   1.0   0.115      0       0       0       0       0       0       0
19  0   1.0   1.5   0    1       0       0       0       0       0
20  0   1.0   0.515      0       0       0       0       0       0       0
21  0   1.565   0.115    0       0       0       0       0       0       0
22  0   1.165   0.515    0       0       0       0       0       0       0
23  0   0.835   0.515    0       0       0       0       0       0       0
24  0   0.435   0.115    0       0       0       0       0       0       0
25  0   1.002   0   0   0   0   0   0   0   0

ELEMENTS
1       1       1       12      0       0       +Z
2       1       12      2       0       0       +Z
3       2       2       17      0       0       +Z
4       2       6       7       0       0       +Z
5       1       7       11      0       0       +Z
6       1       11      8       0       0       +Z
7       9       3       6       0       0       +Z
8   3   3   4   0   0   +Z
9   4   4   10  0   0   +Z
10  4   10  5   0   0   +Z
11  6   8   9   0   0   +Z
12  7   13  14  0   0   +Z
13  7   15  16  0   0   +Z
14  8   11  13  0   0   +Z
15  8   10  14  0   0   +Z
16  8   10  15  0   0   +Z
17  8   12  16  0   0   +Z
18  5   17  3   0   0   +Z
19  3   3   18  0   0   +X
20  4   18  20  0   0   +X
21  4   20  19  0   0   +X
22  7   21  22  0   0   +X
23  7   23  24  0   0   +X
24  8   11  21  0   0   +X
25  8   20  22  0   0   +X
26  8   20  23  0   0   +X
27  8   12  24  0   0   +X
28  10  6   25  0   0   +Z

PROPS
1 FRAME                                                                  ! column
 7 0 0 0 4 0 0                                                           ! Parameters
 2.87E7 1.37E7 0.0529 1e6 6.47E-5 6.47E-5 0.0529 0.0529 0 0 1.245        ! Elastic properties
 0 0 0 0 0 0 0 0                                                         ! Section end properties
 0 0 0.0 0.0                                                             ! bi-linear factors
 0.127 0.127 0.127 0.127                                                 ! plastic hinge lengths
 1e9 -1e9 0 0 0                                                          ! interaction surface parameters
```

```
 -1178 -976 19.78 -976 19.78 12.55 12.55 153.1                    ! Yield Beam Column surface End 2  has the same

characteristics
 0.5 0.0 1 2

2 FRAME                                                           ! Link joint-column
 1 0 0 0 0 0 0                                                    ! Elastic elements
 2.87E7 1.37E7 0.0529 1E6 1e6 1e6 0.0529 0.0529 0 0 0             ! Elastic Parameters
 0.0

3 FRAME                                                           ! Link joint-beam
 1 0 0 0 0 0 0                                                    ! Elastic elements
 2.87E7 1.37E7 0.066 1E6 1e6 1e6 0.066 0.066 0 0 0                ! Elastic Parameters
 0.0

4 FRAME                                                           ! beam
 1 0 0 0 4 0 0                                                    ! Parameters
 2.87E7 1.37E7 0.066 1E6 1.36E-4 0.4E-4 0.066 0.066 0 0 1.553     ! Elastic properties
 0 0 0 0 0 0 0 0                                                  ! section end properties
 0 0 0.000022 0                                                   ! bi-linear factors
 0.137 0.137 0.137 0.137                                          ! plastic hinge lengths
 1e9 1e9 1e9 1e9 0 0                                              ! beam yield axial forces and torques
 31.5 -31.5 31.5 -31.5                                            ! beam yield moments
 0.4 0.0 1 2                                                      ! Takeda hysteresis parameters

5 SPRING                                                          ! Joint rotational spring
 7 44 1 0 0                                                       ! control parameters
 1E12 1E12 1E12 1E12 236000 236000 0 0 0.0                        ! section properties
 1e9 -1e9 1e9 -1e9 1e9 -1e9 0 0                                   ! Yielding forces
 -452.9 -250 81.5 -250 81.5 16.8 16.8 52.9                        ! M-N surface
 20 300 0.5 2000
 1 1.25 0.9 -1.0 0.8 30 -0.05                                     ! Pampanin Parameter
 1 1.25 0.9 -1.0 0.8 30 -0.05

6 SPRING                                                          !vertical spring
 1 0 0 0 0 0
 79000 0 0 1e12 1E12 1e12 0 0 0

7 SPRING                                                          !haunch
 1 1 0 0 0 0
 0 0 0 1e-9 0 0 0 0 0
 1e9 1e9 1e9 1e9 1e9 1e9
 1e9 1e9 1e9 1e9 1e9 1e9

8 FRAME                                                           ! Link joint-beam
 1 0 0 0 0 0 0                                                    ! Elastic elements
 2.87E7 1.37E7 0.3 1E6 1e9 1e9 0.3 0.3 0 0 0
 0.0

9 SPRING                                                          ! Joint rotational spring
 7 44 1 0 0                                                       ! control parameters
 1E12 1E12 1E12 1E12 236000 236000 0 0 0.0                        ! section properties
 1e9 -1e9 1e9 -1e9 1e9 -1e9 0 0                                   ! Yielding forces
 -452.9 -250 81.5 -250 81.5 16.8 16.8 52.9                        ! M-N surface
 20 300 0.5 2000
 1 1.25 0.9 -1.0 0.8 30 -0.05                                     ! Pampanin Parameter
 1 1.25 0.9 -1.0 0.8 30 -0.05

10 SPRING
  1 0 0 0 0 0
  0 0 0 0 1e12 1e12 0 0 0

SHAPE
8 1 1 1 1 1 1
0 1 1 1      1 1 1

WEIGHTS
1 0 0 0 0 0 0
2 0 0 0 0 0 0
3 0 0 0 0 0 0
4 0 0 0 0 0 0
5 0 0 0 0 0 0
6 0 0 0 0 0 0
7 0 0 0 0 0 0
8 0 0 0 0 0 0
9 0 0 0 0 0 0
```

```
10 0 0 0 0 0 0
11 0 0 0 0 0 0
12 0 0 0 0 0 0
13 0 0 0 0 0 0
14 0 0 0 0 0 0
15 0 0 0 0 0 0
16 0 0 0 0 0 0
17 0 0 0 0 0 0
18 0 0 0 0 0 0
19 0 0 0 0 0 0
20 0 0 0 0 0 0
21 0 0 0 0 0 0
22 0 0 0 0 0 0
23 0 0 0 0 0 0
24 0 0 0 0 0 0
25 0 0 0 0 0 0

LOADS
1 0 0 0 0 0 0
2 0 0 0 0 0 0
3 0 0 0 0 0 0
4 0 0 0 0 0 0
5 0 0 0 0 0 0
6 0 0 0 0 0 0
7 0 0 0 0 0 0
8 0 -75 0 0 0 0
9 0 0 0 0 0 0
10 0 0 0 0 0 0
11 0 0 0 0 0 0
12 0 0 0 0 0 0
13 0 0 0 0 0 0
14 0 0 0 0 0 0
15 0 0 0 0 0 0
16 0 0 0 0 0 0
17 0 0 0 0 0 0
18 0 0 0 0 0 0
19 0 0 0 0 0 0
20 0 0 0 0 0 0
21 0 0 0 0 0 0
22 0 0 0 0 0 0
23 0 0 0 0 0 0
24 0 0 0 0 0 0
25 0 0 0 0 0 0

EQUAKE c:\temp\c\e-w.txt                    ! x Displacement control
3  1  0.01  1  -1  0  0  1

EQUAKE c:\temp\c\n-s.txt                    ! x Displacement control
3  1  0.01  1  -1  0  0  1

EQUAKE c:\temp\c\3dv.txt                    ! x Displacement control
1       1  0.01  1  -1  0  0  1
```

THR1 Retrofitted Beam-column Joint-Plain Bars

```
Exterior specimen THR1  Pampanin-joint
8 0 1 0 0 2 0 0 0                                   ! Control Parameters
17 18 9 3 1 3 9.81 5.0 5.0 0.0005 360.0 1.0         ! Frame and Time-history
100 100 100 1 3 10 0.7 0.1                          ! Output and Plotting Options
10 0 0.5                                            ! Iteration Control

NODES
1   0.0    0.0      1 1 0   0 0 0  0
2   0.0    0.835    0 0 0   0 0 0  0
3   0.0    1.0      0 0 0   0 0 0  0
4   0.115  1.0      0 0 0   0 0 0  0
5   1.5    1.0      0 1 0   0 0 0  0
6   0.0    1.001    0 0 0   0 0 0  0
7   0.0    1.165    0 0 0   0 0 0  0
8   0.0    2.0      0 0 0   -1 0 0  0
9   0.0    2.001      1 0 0   0 0 0  0
10  0.515  1.0        0 0 0   0 0 0  0
11  0.0    1.565      0 0 0   0 0 0  0
12  0.0    0.435      0 0 0   0 0 0  0
13  0.115  1.565      0 0 0   0 0 0  0
14  0.515  1.165      0 0 0   0 0 0  0
15  0.515  0.835      0 0 0   0 0 0  0
16  0.115  0.435      0 0 0   0 0 0  0
17  0.0    0.999      0 0 0   0 0 6  0

ELEMENTS
1  1 1 12
2  1 12 2
3  2 2 17
4  2 6 7
5  1 7 11
6  1 11 8
7  9 3 6
8  3 3 4
9  4 4 10
10 4 10 5
11 6 8 9
12 7 13 14
13 7 15 16
14 8 11 13
15 8 10 14
16 8 10 15
17 8 12 16
18 5 17 3

PROPS
1 FRAME                                             ! column
 2 0 0 4 0 0 0                                      ! Parameters
 3E7 1.37E7 0.0529 0.0529 6.47E-5 1.245             ! Elastic properties
 0.0 0.0026 0.127 0.127                             ! Bi-linear and Hinges
 -1178 -976 19.78 39.2 35.7 12.55 153.1 0           ! Yield Beam Column surface End 2  has the same characteristics
 0.5 0.0 1 2                                        ! Takeda paramters

2 FRAME                                             ! Link joint-column
 1 0 0 0 0 0                                        ! Elastic elements
 3E7 1.37E7 0.0529 0.0529 0.00133 0                 ! Elastic Parameters

3 FRAME                                             ! Link joint-beam
 1 0 0 0 0 0                                        ! Elastic elements
 3E7 1.37E7 0.066 0.066 0.0041 0                    ! Elastic Parameters

4 FRAME                                             ! beam
 1 0 0 4 0 0 0                                      ! paramters
 3E7 1.37E7 0.066 0.066 1.36E-4 1.553               ! Elastic properties
 0.0 0.000022 0.137 0.137                           ! Bi-linear and Hinges
 0.0 0.0 32.8 -32.8 10000 -10000                    ! Yielding properties
 0.4 0.0 1 2                                        ! TAKEDA
```

```
5 SPRING                                                    ! Joint rotational spring
 4 44 1 0 1E12 1E12 236000 0 0 0.0005 0 0 0 0               ! properties
 52.9 -452.9 100000000 -100000000 -300 14.6 18.78 14.6 8.59  ! Failure surface
 169 607 0.5 2500
 1 1.25 0.9 -1.0 0.8 30 -0.05                               !Pampanin parameters
 1 1.25 0.9 -1.0 0.8 30 -0.05
 1 1.25 0.9 -1.0 0.8 30 -0.05

6 SPRING                                                    !vertical spring
 1 0 0 0 75000 0 1E12 0 0 0 0 0 0 0

7 SPRING                                                    !haunch
 1 1 0 0 25000 0 0 0 0 0 0 0 0 0
 1e9 1e9 1e9 1e9 1e9 1e9

8 FRAME
 1 0 0 0 0 0                                                !rigid depth spring
 3E7 1.37E7 0.3 0.3 1e9 0

9 SPRING                                                    ! Joint rotational spring
 4 44 1 0 1E12 1E12 236000 0 0 0.0005 0 0 0 0               ! properties
 52.9 -452.9 100000000 -100000000 -300 14.6 18.78 14.6 8.59 ! Failure surface
 169 607 0.5 2500
 1 1.25 0.9 -1.0 0.8 30 -0.05                               !Pampanin parameters
 1 1.25 0.9 -1.0 0.8 30 -0.05
 1 1.25 0.9 -1.0 0.8 30 -0.05

SHAPE
9 1 1 1
8 1 1 1
0 1 1 1

WEIGHTS
1   0.0 0.0 0.0
2   0.0 0.0 0.0
3   0.0 0.0 0.0
4   0.0 0.0 0.0
5   0.0 0.0 0.0
6   0.0 0.0 0.0
7   0.0 0.0 0.0
8   0.0 0.0 0.0
9   0.0 0.0 0.0
10  0.0 0.0 0.0
11  0.0 0.0 0.0
12  0.0 0.0 0.0
13  0.0 0.0 0.0
14  0.0 0.0 0.0
15  0.0 0.0 0.0
16  0.0 0.0 0.0
17  0.0 0.0 0.0

LOADS
1   0.0 0.0 0.0
2   0.0 0.0 0.0
3   0.0 0.0 0.0
4   0.0 0.0 0.0
5   0.0 0.0 0.0
6   0.0 0.0 0.0
7   0.0 0.0 0.0
8   0.0 -120 0.0
9   0.0 0.0 0.0
10  0.0 0.0 0.0
11  0.0 0.0 0.0
12  0.0 0.0 0.0
13  0.0 0.0 0.0
14  0.0 0.0 0.0
15  0.0 0.0 0.0
16  0.0 0.0 0.0
17  0.0 0.0 0.0

EQUAKE c:\temp\c\testh.txt
3  1  0.002  1  -1  0  0  1

EQUAKE c:\temp\c\test5vab.txt
3  1  0.002  1  -1  0  0  1
```

THR2 Retrofitted Beam-column Joint-Plain Bars

```
Exterior specimen THR2  Pampanin-joint
8 0 1 0 0 2 0 0 0                                   ! Control Parameters
17 18 9 3 1 3 9.81 5.0 5.0 0.0005 360.0 1.0         ! Frame and Time-history
100 100 100 1 3 10 0.7 0.1                          ! Output and Plotting Options
10 0 0.5                                            ! Iteration Control

NODES
1   0.0    0.0      1 1 0   0 0 0  0
2   0.0    0.835    0 0 0   0 0 0  0
3   0.0    1.0      0 0 0   0 0 0  0
4   0.115  1.0      0 0 0   0 0 0  0
5   1.5    1.0      0 1 0   0 0 0  0
6   0.0    1.001    0 0 0   0 0 0  0
7   0.0    1.165    0 0 0   0 0 0  0
8   0.0    2.0      0 0 0   -1 0 0  0
9   0.0    2.001      1 0 0   0 0 0  0
10  0.515  1.0        0 0 0   0 0 0  0
11  0.0    1.565      0 0 0   0 0 0  0
12  0.0    0.435      0 0 0   0 0 0  0
13  0.115  1.565        0 0 0   0 0 0  0
14  0.515  1.165        0 0 0   0 0 0  0
15  0.515  0.835        0 0 0   0 0 0  0
16  0.115  0.435        0 0 0   0 0 0  0
17  0.0    0.999        0 0 0   0 0 6  0

ELEMENTS
1  1 1 12
2  1 12 2
3  2 2 17
4  2 6 7
5  1 7 11
6  1 11 8
7  9 3 6
8  3 3 4
9  4 4 10
10 4 10 5
11 6 8 9
12 7 13 14
13 7 15 16
14 8 11 13
15 8 10 14
16 8 10 15
17 8 12 16
18 5 17 3

PROPS
1 FRAME                                             ! column
 2 0 0 4 0 0 0                                      ! Parameters
 3E7 1.37E7 0.0529 0.0529 6.47E-5 1.245             ! Elastic properties
 0.0 0.0026 0.127 0.127                             ! Bi-linear and Hinges
 -1178 -976 19.78 39.2 35.7 12.55 153.1 0           ! Yield Beam Column surface End 2  has the same characteristics
 0.5 0.0 1 2                                        ! Takeda paramters

2 FRAME                                             ! Link joint-column
 1 0 0 0 0 0                                        ! Elastic elements
 3E7 1.37E7 0.0529 0.0529 0.00133 0                 ! Elastic Parameters

3 FRAME                                             ! Link joint-beam
 1 0 0 0 0 0                                        ! Elastic elements
 3E7 1.37E7 0.066 0.066 0.0041 0                    ! Elastic Parameters

4 FRAME                                             ! beam
 1 0 0 4 0 0 0                                      ! paramters
 3E7 1.37E7 0.066 0.066 1.36E-4 1.553               ! Elastic properties
 0.0 0.000022 0.137 0.137                           ! Bi-linear and Hinges
 0.0 0.0 32.8 -32.8 10000 -10000                    ! Yielding properties
 0.4 0.0 1 2                                        ! TAKEDA parameters
```

```
5 SPRING                                                    ! Joint rotational spring
 4 44 1 0 1E12 1E12 236000 0 0 0.0005 0 0 0 0               ! Parameters
 52.9 -452.9 100000000 -100000000 -300 14.6 18.78 14.6 8.59 ! Failure surface
 169 607 0.5 2500
 1 1.25 0.9 -1.0 0.8 30 -0.05                               !Pampanin parameters
 1 1.25 0.9 -1.0 0.8 30 -0.05
 1 1.25 0.9 -1.0 0.8 30 -0.05

6 SPRING                                                    !vertical spring
 1 0 0 0 75000 0 1E12 0 0 0 0 0 0 0

7 SPRING                                                    !haunch
 1 1 0 0 25000 0 0 0 0 0 0 0 0 0
 22 22 1e9 1e9 1e9 1e9

8 FRAME                                                     !rigid depth spring
 1 0 0 0 0 0
 3E7 1.37E7 0.3 0.3 1e9 0

9 SPRING                                                    ! Joint rotational spring
 4 44 1 0 1E12 1E12 236000 0 0 0.0005 0 0 0 0               ! Parameters
 52.9 -452.9 100000000 -100000000 -300 14.6 18.78 14.6 8.59 ! Failure surface
 169 607 0.5 2500
 1 1.25 0.9 -1.0 0.8 30 -0.05                               !Pampanin parameters
 1 1.25 0.9 -1.0 0.8 30 -0.05
 1 1.25 0.9 -1.0 0.8 30 -0.05

SHAPE
9 1 1 1
8 1 1 1
0 1 1 1

WEIGHTS
1   0.0 0.0 0.0
2   0.0 0.0 0.0
3   0.0 0.0 0.0
4   0.0 0.0 0.0
5   0.0 0.0 0.0
6   0.0 0.0 0.0
7   0.0 0.0 0.0
8   0.0 0.0 0.0
9   0.0 0.0 0.0
10  0.0 0.0 0.0
11  0.0 0.0 0.0
12  0.0 0.0 0.0
13  0.0 0.0 0.0
14  0.0 0.0 0.0
15  0.0 0.0 0.0
16  0.0 0.0 0.0
17  0.0 0.0 0.0

LOADS
1   0.0 0.0 0.0
2   0.0 0.0 0.0
3   0.0 0.0 0.0
4   0.0 0.0 0.0
5   0.0 0.0 0.0
6   0.0 0.0 0.0
7   0.0 0.0 0.0
8   0.0 -120 0.0
9   0.0 0.0 0.0
10  0.0 0.0 0.0
11  0.0 0.0 0.0
12  0.0 0.0 0.0
13  0.0 0.0 0.0
14  0.0 0.0 0.0
15  0.0 0.0 0.0
16  0.0 0.0 0.0
17  0.0 0.0 0.0

EQUAKE c:\temp\c\testh.txt
3  1  0.002  1  -1  0  0  1

EQUAKE c:\temp\c\test5vab.txt
3  1  0.002  1  -1  0  0  1
```

THR3 Retrofitted Beam-column Joint-Plain Bars

```
Exterior specimen THR3  Pampanin-joint
8 0 1 0 0 2 0 0 0                                   ! Control Parameters
17 18 9 3 1 3 9.81 5.0 5.0 0.0005 360.0 1.0         ! Frame and Time-history
100 100 100 1 3 10 0.7 0.1                          ! Output and Plotting Options
10 0 0.5                                            ! Iteration Control

NODES
1   0.0    0.0      1 1 0   0 0 0  0
2   0.0    0.835    0 0 0   0 0 0  0
3   0.0    1.0      0 0 0   0 0 0  0
4   0.115  1.0      0 0 0   0 0 0  0
5   1.5    1.0      0 1 0   0 0 0  0
6   0.0    1.001    0 0 0   0 0 0  0
7   0.0    1.165    0 0 0   0 0 0  0
8   0.0    2.0      0 0 0   -1 0 0  0
9   0.0    2.001      1 0 0   0 0 0  0
10  0.515  1.0        0 0 0   0 0 0  0
11  0.0    1.565      0 0 0   0 0 0  0
12  0.0    0.435      0 0 0   0 0 0  0
13  0.115  1.565        0 0 0   0 0 0  0
14  0.515  1.165        0 0 0   0 0 0  0
15  0.515  0.835        0 0 0   0 0 0  0
16  0.115  0.435        0 0 0   0 0 0  0
17  0.0    0.999        0 0 0   0 0 6  0

ELEMENTS
1  1 1 12
2  1 12 2
3  2 2 17
4  2 6 7
5  1 7 11
6  1 11 8
7  9 3 6
8  3 3 4
9  4 4 10
10 4 10 5
11 6 8 9
12 7 13 14
13 7 15 16
14 8 11 13
15 8 10 14
16 8 10 15
17 8 12 16
18 5 17 3

PROPS
1 FRAME                                             !  column
 2 0 0 4 0 0 0                                      ! Parameters
 3E7 1.37E7 0.0529 0.0529 6.47E-5 1.245               ! Elastic properties
 0.0 0.0026 0.127 0.127                             ! Bi-linear and Hinges
 -1178 -976 19.78 39.2 35.7 12.55 153.1 0           ! Yield Beam Column surface End 2  has the same characteristics
 0.5 0.0 1 2                                        ! Takeda paramters

2 FRAME                                             ! Link joint-column
 1 0 0 0 0 0                                        ! Elastic elements
 3E7 1.37E7 0.0529 0.0529 0.00133 0                   ! Elastic Parameters

3 FRAME                                             ! Link joint-beam
 1 0 0 0 0 0                                        ! Elastic elements
 3E7 1.37E7 0.066 0.066 0.0041 0                    ! Elastic Parameters

4 FRAME                                             ! beam
 1 0 0 4 0 0 0                                      ! Parameters
 3E7 1.37E7 0.066 0.066 1.36E-4 1.553                 ! Elastic properties
 0.0 0.000022 0.137 0.137                           ! Bi-linear and Hinges
 0.0 0.0 32.8 -32.8 10000 -10000                    ! Yielding properties
 0.4 0.0 1 2                                        ! TAKEDA
```

```
5 SPRING                                                    ! Joint rotational spring
 4 44 1 0 1E12 1E12 236000 0 0 0.0005 0 0 0 0               ! Parameters
 52.9 -452.9 100000000 -100000000 -300 14.6 18.78 14.6 8.59 ! Failure surface
 169 607 0.5 2500
 1 1.25 0.9 -1.0 0.8 30 -0.05                               !Pampanin parameters
 1 1.25 0.9 -1.0 0.8 30 -0.05
 1 1.25 0.9 -1.0 0.8 30 -0.05

6 SPRING                                                    !vertical spring
 1 0 0 0 75000 0 1E12 0 0 0 0 0 0 0

7 SPRING                                                    !haunch
 1 1 0 0 100000 0 0 0 0 0 0 0 0 0
 1e9 1e9 1e9 1e9 1e9 1e9

8 FRAME
 1 0 0 0 0 0                                                !rigid depth spring
 3E7 1.37E7 0.3 0.3 1e9 0

9 SPRING                                                    ! Joint rotational spring
 4 44 1 0 1E12 1E12 236000 0 0 0.0005 0 0 0 0               ! Parameters
 52.9 -452.9 100000000 -100000000 -300 14.6 18.78 14.6 8.59 ! Failure surface
 169 607 0.5 2500
 1 1.25 0.9 -1.0 0.8 30 -0.05                               !Pampanin parameters
 1 1.25 0.9 -1.0 0.8 30 -0.05
 1 1.25 0.9 -1.0 0.8 30 -0.05

SHAPE
9 1 1 1
8 1 1 1
0 1 1 1

WEIGHTS
1   0.0 0.0 0.0
2   0.0 0.0 0.0
3   0.0 0.0 0.0
4   0.0 0.0 0.0
5   0.0 0.0 0.0
6   0.0 0.0 0.0
7   0.0 0.0 0.0
8   0.0 0.0 0.0
9   0.0 0.0 0.0
10  0.0 0.0 0.0
11  0.0 0.0 0.0
12  0.0 0.0 0.0
13  0.0 0.0 0.0
14  0.0 0.0 0.0
15  0.0 0.0 0.0
16  0.0 0.0 0.0
17  0.0 0.0 0.0

LOADS
1   0.0 0.0 0.0
2   0.0 0.0 0.0
3   0.0 0.0 0.0
4   0.0 0.0 0.0
5   0.0 0.0 0.0
6   0.0 0.0 0.0
7   0.0 0.0 0.0
8   0.0 -120 0.0
9   0.0 0.0 0.0
10  0.0 0.0 0.0
11  0.0 0.0 0.0
12  0.0 0.0 0.0
13  0.0 0.0 0.0
14  0.0 0.0 0.0
15  0.0 0.0 0.0
16  0.0 0.0 0.0
17  0.0 0.0 0.0

EQUAKE c:\temp\c\testh.txt
3  1  0.002  1  -1  0  0  1

EQUAKE c:\temp\c\test5vab.txt
3  1  0.002  1  -1  0  0  1
```

THR3D Retrofitted 3-D Corner Joint–Plain Bars

```
3D deep beam-deep beam one joint stirrup
8 1 0 0 3 0 0 0                                  ! Control Parameters
25 28 10 1 1 3 9.81 5.0 5.0 0.0005 324 1.0  ! Frame and Time-history
100 100 100 3 0.1 0.1 0.1 0                      ! Output and Plotting Options
0.86603 0 0.866025 0.5 1 -0.5                    ! plot axes transformation
10 0 0.5                                          ! Iteration Control

NODES
1       0       0       0       1       1       1       0       1       0       0
2       0       0.835   0       0       0       0       0       0       0       0
3       0       1.0     0       0       0       0       0       0       0       0
4       0.115   1.0     0       0       0       0       0       0       0       0
5       1.5     1.0     0       0       1       0       0       0       0       0
6       0       1.001   0       0       0       0       0       0       0       0
7       0       1.165   0       0       0       0       0       0       0       0
8   0   2.0     0       -1      0       -2      0       0       0       0       0
9   0   2.001   0   1   0   1   0   0   0   0
10  0.515   1.0   0  0        0       0       0       0       0       0
11  0.0   1.565   0  0        0       0       0       0       0       0
12  0.0   0.435   0  0        0       0       0       0       0       0
13  0.115   1.565   0        0       0       0       0       0       0       0
14  0.515   1.165   0        0       0       0       0       0       0       0
15  0.515   0.835   0        0       0       0       0       0       0       0
16  0.115   0.435   0   0   0   0   0   0   0   0
17  0   0.999   0        2       2       2       2       2       2       25
18  0   1.0   0.115      0       0       0       0       0       0       0
19  0   1.0   1.5   0    1       0       0       0       0       0
20  0   1.0   0.515      0       0       0       0       0       0       0
21  0   1.565   0.115    0       0       0       0       0       0       0
22  0   1.165   0.515    0       0       0       0       0       0       0
23  0   0.835   0.515    0       0       0       0       0       0       0
24  0   0.435   0.115    0       0       0       0       0       0       0
25  0   1.002   0   0   0   0   0   0   0   0

ELEMENTS
1       1       1       12      0       0       +Z
2       1       12      2       0       0       +Z
3       2       2       17      0       0       +Z
4       2       6       7       0       0       +Z
5       1       7       11      0       0       +Z
6       1       11      8       0       0       +Z
7       9       3       6       0       0       +Z
8   3   3   4   0   0   +Z
9   4   4   10  0   0   +Z
10  4   10  5   0   0   +Z
11  6   8   9   0   0   +Z
12  7   13  14  0   0   +Z
13  7   15  16  0   0   +Z
14  8   11  13  0   0   +Z
15  8   10  14  0   0   +Z
16  8   10  15  0   0   +Z
17  8   12  16  0   0   +Z
18  5   17  3   0   0   +Z
19  3   3   18  0   0   +X
20  4   18  20  0   0   +X
21  4   20  19  0   0   +X
22  7   21  22  0   0   +X
23  7   23  24  0   0   +X
24  8   11  21  0   0   +X
25  8   20  22  0   0   +X
26  8   20  23  0   0   +X
27  8   12  24  0   0   +X
28  10  6   25  0   0   +Z

PROPS
1 FRAME                                                  ! column
 7 0 0 0 4 0 0                                                                  ! Parameters
 2.87E7 1.37E7 0.0529 1e6 6.47E-5 6.47E-5 0.0529 0.0529 0 0 1.245               ! Elastic properties
 0 0 0 0 0 0 0 0                                                                ! Section end properties
 0 0 0.0 0.0                                                                    ! bi-linear factors
 0.127 0.127 0.127 0.127                                                        ! plastic hinge lengths
 1e9 -1e9 0 0 0                                                                 ! interaction surface parameters
```

```
 -1178 -976 19.78 -976 19.78 12.55 12.55 153.1                    ! Yield Beam Column surface End 2  has the same

characteristics
 0.5 0.0 1 2

2 FRAME                                                           ! Link joint-column
 1 0 0 0 0 0 0                                                    ! Elastic elements
 2.87E7 1.37E7 0.0529 1E6 1e6 1e6 0.0529 0.0529 0 0 0             ! Elastic Parameters
 0.0

3 FRAME                                                           ! Link joint-beam
 1 0 0 0 0 0 0                                                    ! Elastic elements
 2.87E7 1.37E7 0.066 1E6 1e6 1e6 0.066 0.066 0 0 0                ! Elastic Parameters
 0.0

4 FRAME                                                           ! beam
 1 0 0 0 4 0 0                                                    ! Parameters
 2.87E7 1.37E7 0.066 1E6 1.36E-4 0.4E-4 0.066 0.066 0 0 1.553     ! Elastic properties
 0 0 0 0 0 0 0 0                                                  ! section end properties
 0 0 0.000022 0                                                   ! bi-linear factors
 0.137 0.137 0.137 0.137                                          ! plastic hinge lengths
 1e9 1e9 1e9 1e9 0 0                                              ! beam yield axial forces and torques
 31.5 -31.5 31.5 -31.5                                            ! beam yield moments
 0.4 0.0 1 2                                                      ! Takeda hysteresis parameters

5 SPRING                                                          ! Joint rotational spring
 7 44 1 0 0                                                       ! control parameters
 1E12 1E12 1E12 1E12 236000 236000 0 0 0.0                        ! section properties
 1e9 -1e9 1e9 -1e9 1e9 -1e9 0 0                                   ! Yielding forces
 -452.9 -250 81.5 -250 81.5 16.8 16.8 52.9                        ! M-N surface
 20 300 0.5 2000
 1 1.25 0.9 -1.0 0.8 30 -0.05
 1 1.25 0.9 -1.0 0.8 30 -0.05                                     ! Pampanin Parameter

6 SPRING                                                          !vertical spring
 1 0 0 0 0 0
 79000 0 0 1e12 1E12 1e12 0 0 0

7 SPRING                                                          !haunch
 1 1 0 0 0 0
 100000 0 0 1e-9 0 0 0 0 0
 1e9 1e9 1e9 1e9 1e9 1e9
 1e9 1e9 1e9 1e9 1e9 1e9

8 FRAME                                                           ! Link joint-beam
 1 0 0 0 0 0 0                                                    ! Elastic elements
 2.87E7 1.37E7 0.3 1E6 1e9 1e9 0.3 0.3 0 0 0
 0.0

9 SPRING                                                          ! Joint rotational spring
 7 44 1 0 0                                                       ! control parameters
 1E12 1E12 1E12 1E12 236000 236000 0 0 0.0                        ! section properties
 1e9 -1e9 1e9 -1e9 1e9 -1e9 0 0                                   ! Yielding forces
 -452.9 -250 81.5 -250 81.5 16.8 16.8 52.9                        ! M-N surface
 20 300 0.5 2000
 1 1.25 0.9 -1.0 0.8 30 -0.05                                     ! Pampanin Parameter
 1 1.25 0.9 -1.0 0.8 30 -0.05

10 SPRING
  1 0 0 0 0 0
  0 0 0 0 1e12 1e12 0 0 0

SHAPE
8 1 1 1 1 1 1
0 1 1 1      1 1 1

WEIGHTS
1 0 0 0 0 0 0
2 0 0 0 0 0 0
3 0 0 0 0 0 0
4 0 0 0 0 0 0
5 0 0 0 0 0 0
6 0 0 0 0 0 0
7 0 0 0 0 0 0
8 0 0 0 0 0 0
9 0 0 0 0 0 0
```

```
10 0 0 0 0 0 0
11 0 0 0 0 0 0
12 0 0 0 0 0 0
13 0 0 0 0 0 0
14 0 0 0 0 0 0
15 0 0 0 0 0 0
16 0 0 0 0 0 0
17 0 0 0 0 0 0
18 0 0 0 0 0 0
19 0 0 0 0 0 0
20 0 0 0 0 0 0
21 0 0 0 0 0 0
22 0 0 0 0 0 0
23 0 0 0 0 0 0
24 0 0 0 0 0 0
25 0 0 0 0 0 0

LOADS
1 0 0 0 0 0 0
2 0 0 0 0 0 0
3 0 0 0 0 0 0
4 0 0 0 0 0 0
5 0 0 0 0 0 0
6 0 0 0 0 0 0
7 0 0 0 0 0 0
8 0 -200 0 0 0 0
9 0 0 0 0 0 0
10 0 0 0 0 0 0
11 0 0 0 0 0 0
12 0 0 0 0 0 0
13 0 0 0 0 0 0
14 0 0 0 0 0 0
15 0 0 0 0 0 0
16 0 0 0 0 0 0
17 0 0 0 0 0 0
18 0 0 0 0 0 0
19 0 0 0 0 0 0
20 0 0 0 0 0 0
21 0 0 0 0 0 0
22 0 0 0 0 0 0
23 0 0 0 0 0 0
24 0 0 0 0 0 0
25 0 0 0 0 0 0

EQUAKE c:\temp\c\e-w.txt                    ! x Displacement control
3  1  0.01  1  -1  0  0  1

EQUAKE c:\temp\c\n-s.txt                    ! x Displacement control
3  1  0.01  1  -1  0  0  1

EQUAKE c:\temp\c\3dv.txt                    ! x Displacement control
3  1  0.01  1  -1  0  0  1
```